Investigation of continuous-fibre devices based on coupling to high-index planar overlays

A Thesis Submitted to the

Department of Electronic and Electrical Engineering

of the University of Strathclyde for the Degree of

Doctor of Philosophy

by

Kevin J. McCallion, BEng., MSc.

Optoelectronics Division

Dept. of Electronic & Electrical Eng.

Royal College Building

204 George Street, Glasgow

G1 1XW

September 1993

Declaration

Signature Kevin J. McCallion Date 17/9/93

Acknowledgements

I would firstly like to thank Prof. Brian Culshaw and Dr. Walter Johnstone for employing me as a Research Assistant within the Optoelectronics Division and providing the opportunity to study for a PhD. I am also grateful to the Ministry of Defence (RARDE) for providing the financial backing for the Research Assistant post.

On a personal level, many thanks are due to my family, my parents in particular, for unfailing support and encouragement over the course of my PhD study without which nobody would have to read the following two hundred-odd pages. It is difficult to suitably mention all the people within the Optoelectronics Division who helped (or hindered) me over the last few years but several friends/culprits spring immediately to mind: Gordon Fawcett for his considered opinions and "fine" sense of humour, Doug Walsh for being a stout companion, Dave Moodie for being thinner than me (consistently), Iain Mauchline for reaching new heights in grumpiness, Ivan Andonovic for his wall-passing, Graham (Grambo) Thursby for providing the necessary "muscle" when the going got tough, Bob Blue and Scott McCulloch who occasionally snookered me, Craig Michie for his flannel, Aileen Mitchell and Carol Binnie for their helpfulness and ability to turn a blind eye, and the staff of the Scotia and Press Bars (amongst others) for service above and beyond the call of duty. Thanks also to all the other members of the Optoelectronics Division I've encountered over the years for a plethora of opinions, attitudes, religions and countries of origin. Very interesting!

Finally, a "nae luck" award to both Stuart McTavish and Jonnie Burke for their feeble attempts to interrupt my progress by moving to Glasgow.

Abstract

In recent years there has been an increased utilization of optical fibre technology in a variety of fields, telecommunications and signal processing in particular. As a result, the demand for sophisticated optical components has seen a corresponding increase, with devices such as wavelength filters, directional couplers, modulators and switches of particular interest. This thesis describes the design, fabrication and experimental characterisation of a number of continuous-fibre devices whose operation relies on evanescent coupling between the fibre and an overlay planar waveguide. The basic device architecture allows the realisation of several different optical functions, including Bandstop and Bandpass Wavelength Filtering, Intensity Modulation and Directional Switching.

The devices were characterised primarily in terms of their wavelength-transmission response to variation of the overlay waveguide parameters: refractive index and thickness. Filter channel linewidths and spacing have been shown to be directly related to the refractive index and thickness of the overlay waveguide and also the distance between the fibre core and the overlay waveguide. As such, the filtering devices can be designed to given specifications using a variety of optical materials in the role of the overlay waveguide e.g. Glass, Lithium Niobate. Channel spacings and linewidths ranging from 10nm-200nm and 2.4nm-100nm, respectively, have been demonstrated while rejection ratios of >20dB and insertion loss of <0.5dB were recorded. Extensive tuning (>200nm) of the wavelength-transmission response of the bandstop and bandpass filters was achieved by variation of the overlay waveguide superstrate refractive index.

A modulator/switch device which incorporated Lithium Niobate as the overlay was also demonstrated but required unrealistic drive voltages. Application of >300V was required to induce 60% modulation/switching. However, the feasibility of the device geometry for realisation of an intensity modulator/switch was established. Calculations based on materials with larger electro-optic coefficients (e.g. Barium Strontium Niobate) predict 10V drive voltages for >90% modulation/switching.

Table of Contents

CHAPTER 1

Introduction

1.1 Technical Background

In the past two decades the use of glass optical fibre technology has increased significantly in the areas of telecommunications, signal processing and sensing systems. Optical fibres possess several inherent advantages over traditional copper wire based technology including:

(a) large signal bandwidth availability

(b) low signal attenuation

(c) immunity to electro-magnetic interference

(d) synthesised from abundant natural resource i.e. sand

Initially, optical fibres were viewed strictly as a transmission medium with processing of the optical signals performed outwith the fibre. This involved physically breaking the fibre to allow access to the optical signal which was then, in early optical systems, converted to an electrical signal for appropriate processing before being transformed back to the optical domain for further transmission. The desire to maintain the transmitted signal in optical form saw the development of a range of bulk optic and integrated optic components capable of performing the essential optical functions e.g. modulators, filters, switches, etc. These components removed the need for conversion to the electronic domain but had associated problems of high insertion losses (due to diffraction, reflection, mode-mismatch), mechanical and thermal instability, bonding difficulties, etc. This has led to a significant research effort in recent years directed towards the development of components built on the actual optical fibre, with the aim of removing the requirement of physically breaking the fibre to allow device insertion. Such all-fibre or continuous-fibre devices are expected to exhibit high mechanical stability, since the signal is confined to the fibre core at all times, and to display low attenuation.

In addition, compatibility with existing optical fibre networks is guaranteed thus reducing device insertion losses while the extremely small core dimensions of the fibres, single-mode in particular, allow the generation of high power densities for only moderate input powers. This provides the possibility of device behaviour based on non-linear phenomena. The result of this research drive has been the development in recent years of a number of continuous-fibre optical components displaying a range of functions[1][2][3]. These include polarisers, directional couplers, intensity and phase modulators, wavelength filters, frequency shifters, wavelength multiplexers and demultiplexers, and laser sources and amplifiers. This thesis investigates a continuous-fibre device architecture which relies on evanescent contact between a side-polished fibre and a high index, planar, multimode overlay waveguide[4] to realise several optical functions. The device behaves primarily as a tunable wavelength selective element (channel-dropping or bandpass filter) but can also be configured as an intensity or phase modulator or variable ratio directional coupler/switch.

Single channel optical fibre transmission bit rates (10-20Gbits/s) have now reached the stage where electronic component limitations are restricting further progress. As a result, Wavelength Division Multiplexing (WDM) has emerged as a technique capable of enhancing the bandwidth utilization in single-mode optical fibre. The concept of WDM technology was first suggested in 1970 according to published reports[5]. Fundamental research only began in 1977 but since then WDM systems and applications have been the subject of intensive investigation[6][7], with a corresponding emphasis on the development of WDM components. WDM involves the transmission of a number of different peak wavelength optical signals (channels) in parallel on a single optical fibre and was initially directed at upgrading the capacity of installed point-to-point transmission systems i.e. multichannel simultaneous transmission effectively increases the information-carrying capacity of the fibre[8]. Typically, the capacity would be increased by adding several additional wavelengths separated by several tens, or even hundreds of nanometres[7], each having access to the associated signal processing schemes, etc. Recent advances

in single-frequency lasers and narrowband filters have since pushed WDM technology towards applications in optical network architectures. Existing inter-office and subscriber loop services such as computer networking and video distribution, and multi-access facilities in general, which require high bandwidth capability are well suited to implementation using WDM technology[9]. Furthermore, wavelength selection can also be utilized as a means of performing network- and system-orientated functions such as routing, switching and service segregation[9] which are traditionally allocated to the electronic domain. Other advantages include: service channel expendability after installation, simultaneous transmission of different modulation scheme signals and overall system cost reduction.

Current research into WDM technology can generally be divided into three categories specified by channel spacing. These are:

Coarse WDM	-	100-10nm Channel separation
Dense WDM	-	10-1nm Channel separation
Optical FDM	-	1-0.1nm Channel separation

The third category, Optical frequency division multiplexing, uses coherent detection schemes rather than discrete wavelength-selective components at the receiver end of the system and is, therefore, not particularly relevant to this thesis. The research drive is, obviously, towards ever smaller channel spacings to further enhance the multichannel transmission possibilities. However, the corresponding multiplexing and demultiplexing requirements become harder to meet and component tolerances become severe.

WDM networks commonly employ two general architectural forms known as wavelength routing networks and broadcast-and-select networks, respectively[7]. These are illustrated in Figures 1.1a and 1.1b. Wavelength routing networks consist of one or more wavelength-selective elements and the wavelength and input port of each signal precisely determine its path through the network. The essential components required by this architecture are tunable laser sources, a number of WDM elements (the WDM network), and wavelength-independent receivers

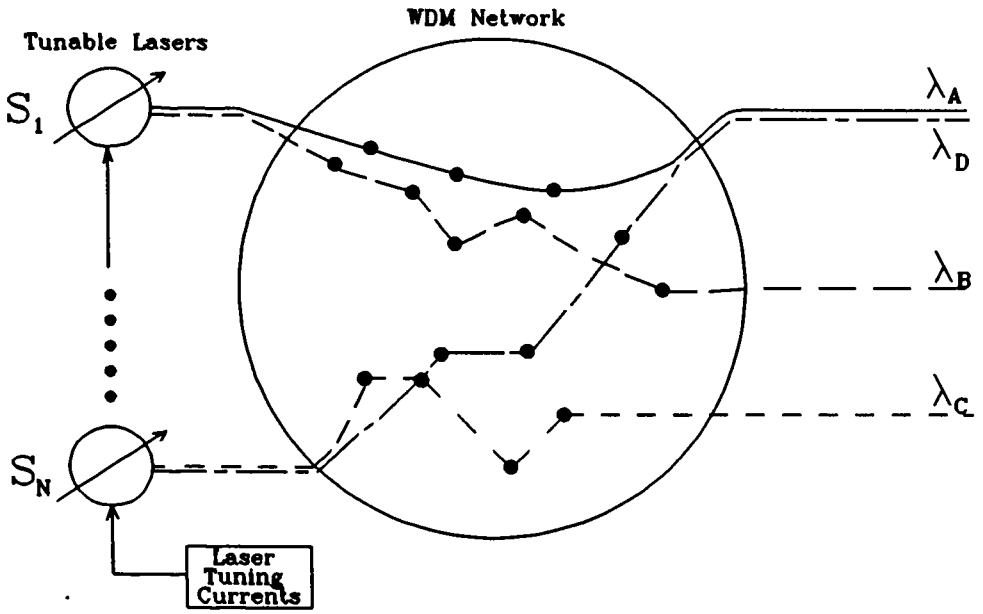

(a) Wavelength Routing Network utilizing non-blocking wavelength addressing

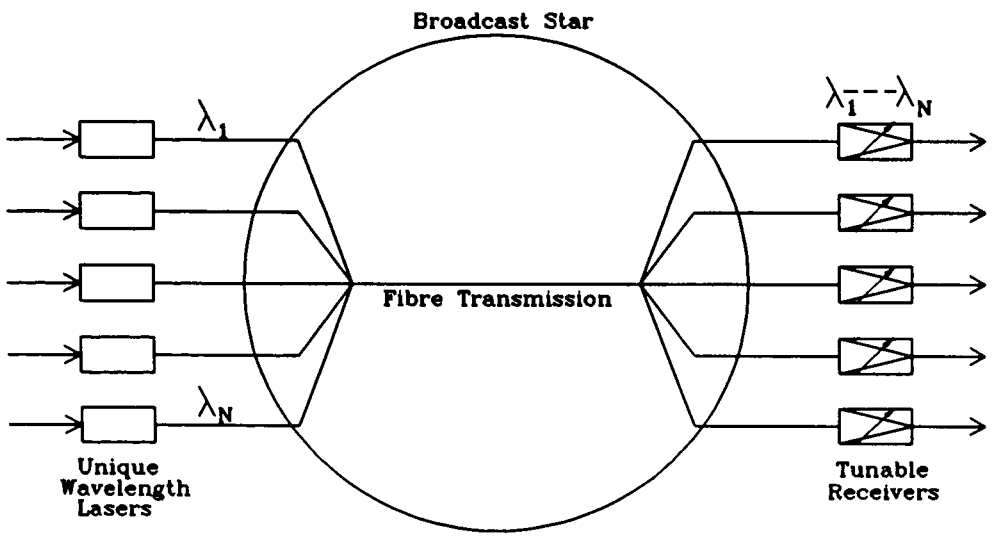

(b) Broadcast-and-Select Network with fixed wavelength lasers and tunable receivers

Figure 1.1 : The two common WDM network architectures

(detectors). Typically tunable filters, diffraction gratings and fibre directional couplers are incorporated in the WDM network. The alternative broadcast-and-select networks are arranged such that all the inputs are combined in a star coupler and made available at all the outputs. A variety of configurations are possible depending on whether the input laser sources, the output receivers, or both, are made tunable. A typical configuration involves splitting the transmitted multiplexed signals and routing them to tunable receivers. The tunable receivers consist of single-wavelength tunable bandpass filters followed by wavelength-independent detectors which allow the selection of a single input signal (channel) from the entire available signal spectrum. This technique is well-suited to Cable Television applications where the subscriber requires access to only one of many available signals at any given time. Drawbacks of this technique are the loss of 1/N of each of the undesired or blocked signals at each output (assuming N outputs). If blocked signal loss in the previous configuration is unacceptable, the wavelength selection scheme could rely on channel-dropping filters. In this case, the de-selected signals are retained while only the desired wavelength channel is extracted from the available spectrum and directed to a particular receiver.

Obviously, with the emergence of WDM technology in recent years, there has been a requirement for appropriate WDM components such as multi/demultiplexers and wavelength filters. A variety of device technologies and fabrication processes have been used with varying success in the attempt to realise these components and a brief review is provided in Chapter 2. The devices investigated in this thesis are envisaged as fulfilling a number of the component requirements of WDM systems, particularly the "broadcast and select" type which rely heavily on tunable filtering at the detection end of the system.

Wavelength-selective elements and other continuous-fibre components are also finding application in fibre laser and amplifier systems. Rare-earth doped fibre lasers and amplifiers are now becoming important components in many areas, particularly in telecommunications, sensing and medical applications. The spectral region covered

by erbium-doped fibres makes them particularly important for telecommunications applications as they operate around 1.55μm and can be pumped by semiconductor laser diodes. Similarly, erbium-fibre amplifiers have important applications in long-haul transmission systems as replacements for electronic signal regeneration stages.

Fibre lasers have a number of advantages over their bulk-glass counterparts. High pump power densities can be achieved for only moderate input power due to the reduced dimensions of the fibre core which confines the light. Additionally, the inherent low loss and waveguiding nature of the fibre allows this power density to be sustained over a long interaction length leading to efficient pumping of the distributed rare-earth ions. A further advantage of the fibre geometry is the large volume-to-surface area ratio which allows efficient heat dissipation and minimises thermal problems commonly encountered in bulk-glass lasers. Consider the typical fibre laser configuration shown in Figure 1.2.

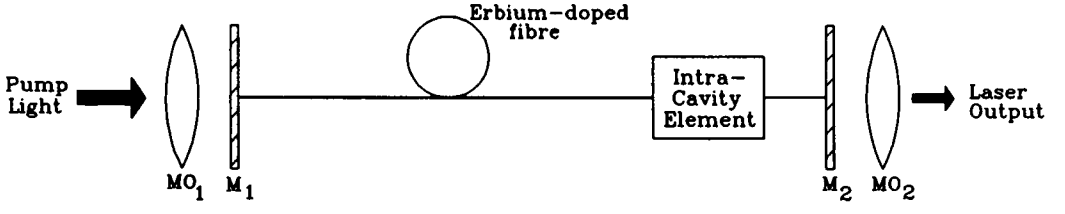

Figure 1.2 : Schematic diagram of basic fibre-laser set-up

Pump light is coupled into the fibre by the microscope objective MO_1 through the mirror M_1, which is butted to the cleaved fibre end. The pump light is then guided along the fibre and the resultant fluorescence is reflected back into the fibre by mirror M_2. This mirror is also butted to the fibre end thus completing the cavity and can behave as an output coupler for the laser light. An intra-cavity element can

typically be included for tuning of the lasing wavelength or for the purposes of linewidth narrowing or mode-locking. Provided the round-trip loss (which includes the insertion loss of the intra-cavity element) is less than the gain of the system, lasing can still occur.

Wavelength tuning of fibre lasers generally requires an intra-cavity wavelength selective element and has been demonstrated using an angle-tuned grating reflector[10] as a replacement for the output mirror in a Neodymium-doped fibre laser to provide a maximum tuning range of 80nm. Similarly, the use of an in-line angle-tuned etalon[11] in an Erbium-doped fibre laser provided 45nm continuous tuning. A fibre grating device[12] utilizing Bragg reflection has also been used in place of the output mirror to produce a significant narrowing in laser linewidth (0.04nm). There are, however, immediate disadvantages of the above techniques. Devices operating in reflection mode are undesirable since output coupling of the laser light is more complicated while angle-tuned, bulk-optic components tend to suffer from mechanical instability. High insertion loss of non-fibre components in the cavity is a further drawback since an increase in pump power is required to attain the lasing threshold and the laser efficiency is reduced. Mode-locking of lasers is a standard technique used to produce a series of ultrashort pulses. This desirable mode-locked situation can be attained in a variety of ways, including the use of amplitude or phase modulation[13] and has been achieved in fibre lasers using both bulk-optic[14] and integrated-optic[15] $LiNbO_3$ modulators. Drawbacks of both implementations are again degradation of laser performance due to increased losses in the cavity while power dissipation problems can occur. Also the possibility of forming subcavities is increased as a result of high reflections produced by the high refractive index mismatch between $LiNbO_3$ and silica.

The use of continuous-fibre components for intra-cavity operation is obviously preferred both from an insertion loss and mechanical stability viewpoint while an increase in laser efficiency can be expected. Each device function described above can, potentially, be provided by appropriate configuration of the device structure

being investigated in this thesis. In particular, the bandpass filter configuration shows much promise as a low-loss intra-cavity wavelength narrowing and tuning device and preliminary results are reported in Chapter 7. Other applications include external modulation of semiconductor lasers and implementation as refractive index sensors appears feasible.

1.2 Fundamental Device Geometry and Operation

The evanescent coupling between a single-mode optical fibre, side-polished close to the core, and a multimode waveguide (of refractive index greater than the fibre mode effective index) in close proximity forms the basis of operation of all devices considered in this thesis. The geometrical arrangement which allows this evanescent contact is depicted in Figure 1.3. The basic principle of operation governing the

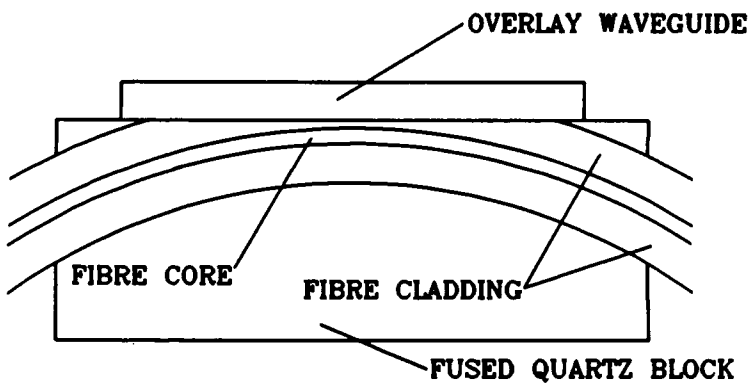

Figure 1.3 : Schematic diagram of basic device structure

behaviour of the above structure relies upon phase-matching of the propagation constant of the single fibre mode and that of a mode supported by the multi-mode overlay waveguide. When this situation is established strong directional coupling of power from the fibre to the overlay waveguide occurs[16]. It has been previously demonstrated[16] that $>90\%$ of the power carried by the fibre can be coupled out under phase-matching conditions. Away from phase-matching the transmission loss of the fibre is <0.5dB. The fibre cladding provides the lower constraint on the

effective refractive index values of the mode(s) in both the optical fibre and the multi-mode overlay waveguide. Since the upper constraint on the fibre mode effective index is that of the fibre core, then the only overlay waveguide mode capable of possessing an effective index value close to that of the fibre mode is the highest order mode when it is close to cut-off. The mode structure (the effective index values of the guided modes) of the asymmetric multimode overlay waveguide can be obtained from its eigenvalue equation (derived in Chapter 3):

$$\frac{2\pi d}{\lambda}\sqrt{n_o^2 - n_{eo}^2} = m\pi + \tan^{-1}\xi_c\sqrt{\frac{n_{eo}^2 - n_c^2}{n_o^2 - n_{eo}^2}} + \tan^{-1}\xi_s\sqrt{\frac{n_{eo}^2 - n_s^2}{n_o^2 - n_{eo}^2}} \qquad (1.1)$$

where λ is the input wavelength, d is the overlay thickness, n_{eo} is the mode effective index, m = 0,1,..,N is the mode order and ξ_c and ξ_s are polarisation dependent constants ($\xi_c,\xi_s=[n_o/n_c,n_s]^2$ for TM, 1 for TE). The cladding index is represented by n_c while n_s is the overlay superstrate index. The guided modes of the overlay waveguide can range in effective index from the fibre cladding index to the waveguide material index. Inspection of the eigenvalue equation indicates that the mode structure of the waveguide can be tuned by varying a number of parameters: wavelength, material index, thickness and superstrate index (to a lesser extent). The most convenient and useful method is wavelength variation. As λ is increased (or material index or guide thickness decreased), the effective index of each successive highest order overlay mode reduces and "scans" past the fibre mode whose effective index value can be considered to be stationary. This causes a transfer of power between the fibre mode and the waveguide mode with the most efficient transfer occurring exactly on phase-matching. The transmission response of the fibre displays a sharp dip as the effective index of the overlay mode approaches, matches and then moves past that of the fibre mode towards "cut off". A sufficient further increase in the wavelength results in another dip in the transmission response as the next overlay mode is scanned across the fibre mode. The transfer of power from fibre to overlay waveguide is approximately periodic in nature with variation of λ, n_o or d,

particularly for highly multi-moded guides (large m) when the effect of the second term on the right-hand-side of equation 1.1 is negligible. Figure 1.4 shows a typical intensity transmission response curve for wavelength variation for a side-polished fibre with a multimode overlay waveguide.

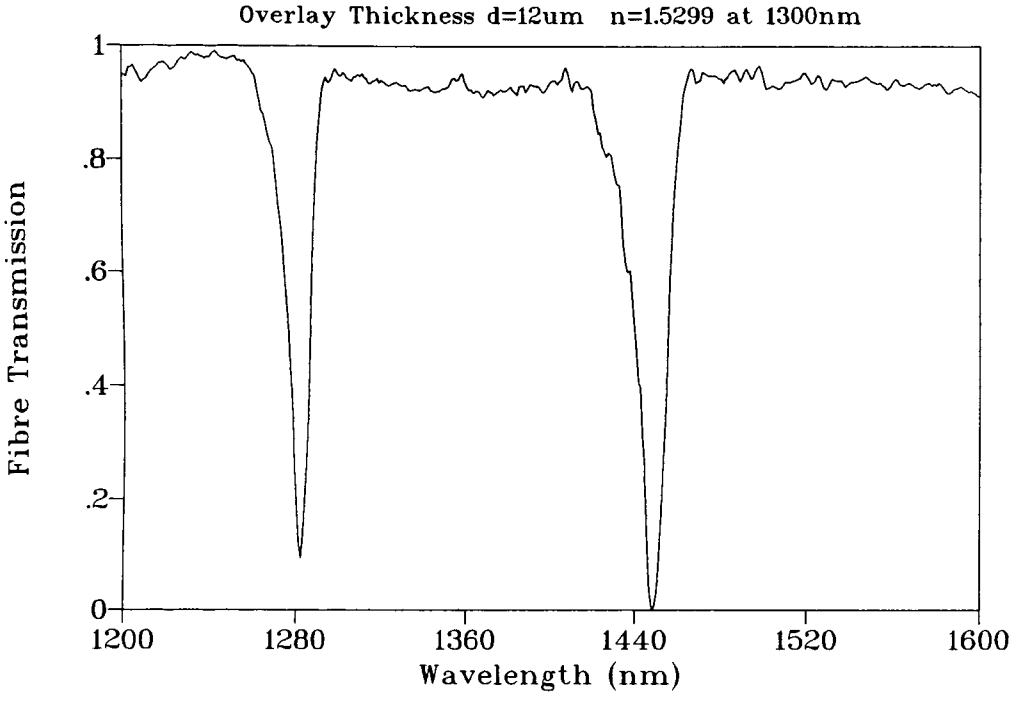

Figure 1.4 : Typical Device Wavelength Response

Similar transmission responses occur for variation of the overlay refractive index and thickness. The possibilities for wavelength filtering are obvious from Figure 1.4 which in its most basic form represents a channel-dropping filter response. Placing an appropriate detector on the overlay surface allows direct detection of the "dropped" channel with the detector "seeing" the inverse of the above response. Wavelength demultiplexing or directional coupling at a fixed wavelength may be obtained by placing a prism-coupler or second fibre half-block in contact with the overlay to collect the power tapped from the input fibre. Alternatively, intensity modulation, via electro-optically or otherwise induced index changes in the overlay, can be achieved with the same device architecture. This requires that the device

wavelength response possesses a resonance dip at a wavelength corresponding to that of the source. In this instance, electro-optic variation of the overlay material index will cause the position of the resonance dip to oscillate about that of the source wavelength with a subsequent modulation of the fibre intensity transmission. In addition, use of either a materially birefringent or very thin overlay permits the operation as a simple polariser. Furthermore, it was found that a slight modification of the polished fibre half-block geometry produced a tunable bandpass wavelength filtering function. This device has a wavelength response function which is, basically, the inverse of that shown in Figure 1.4. Principal advantages of this device structure include those mentioned previously for continuous-fibre devices such as low insertion loss and good mechanical stability. Additionally, they display a large available tuning range, are compatible with a range of material fabrication processes and the device structure allows the implementation of different optical functions without major changes in fabrication procedures.

With regard to Figure 1.4, the important characteristics of the wavelength response are resonance linewidth (FWHM), resonance separation, modulation depth or extinction ratio and off-resonance insertion loss. These "performance parameters" are influenced by the choice of overlay material, thickness and superstrate as well as device input wavelength. As a result significant control of device behaviour can be obtained by appropriate selection of materials and fabrication procedures, thus allowing the realisation of a range of device specifications.

1.3 Objectives of the Project

The preceding sections have introduced the potential applications for the device structure which is the subject of this research project. The primary objectives of the research project were to characterise the response of the basic structure, in a variety of configurations, as a function of the device parameters to enable the design of specific devices. This included:

1. an investigation of the basic building block of the structure - the polished fibre half-block - in terms of fibre radius of curvature and remaining cladding thickness and their effect on device performance

2. determining the effect of material index and thickness of the overlay waveguide on, primarily, device wavelength response in terms of channel linewidth, spacing, modulation depth and insertion loss

3. the production of solid-state wavelength selective devices using a range of materials and processes with a view to optimising the fabrication procedures and performance for particular device functions.

4. an investigation of the various possible tuning techniques and ranges for these wavelength selective devices

5. an assessment of the feasibility of producing an active modulator or switch/filter component

6. a brief theoretical interpretation of the device behaviour

1.4 Thesis Outline

Continuing from here, Chapter 2 provides a review of wavelength sensitive device technologies and applications which are intended for use in WDM systems. Chapter 3 is an account of the theoretical methods which can be used to analyse the device structure and interpret its behaviour. No direct comparison is made with experimental results due to the difficulties in modelling device behaviour absolutely. Rather, predictions on device performance trends are made in a general sense. Chapter 4 details the fabrication and characterisation of the basic component of the device structure, known as the polished fibre half-block. In Chapter 5, refractive index oils are used in the role of the overlay waveguide to gather basic experimental

results on device behaviour while Chapter 6 deals with solid-state device fabrication and characterisation and the potential for passive and active tuning. Experimental results on devices incorporating electro-optic overlay waveguides are also presented in Chapter 6. The implementation of the modified basic device structure as a bandpass filter is introduced in Chapter 7 together with preliminary results on device performance. Incorporation of the filter in an erbium-doped fibre laser system is also discussed. Chapter 8 discusses and draws conclusions about overall device performance, behaviour and applications and suggests possible directions for future work on the device architecture.

References

1. M.J.F. Digonnet and B.Y. Kim,"Single-mode fibre-optic components", J. of Elec. and Radio Eng., **58**, (Supplement), pp566-578, 1988.

2. R.H. Stolen and R. De Paula,"Single-mode fibre components", Proc. IEEE, **75**, pp1498-1511, 1987.

3. J-P Goure, I. Vernier and J-P Meunier,"Linear and non-linear optical fibre devices", J. of Phys. D: Appl. Phys., **22**, pp1791-1805, 1989.

4. C.A. Millar, M.C. Brierley and S.R. Mallinson,"Exposed-core single mode fibre channel-dropping filter using a high index overlay", Opt. Lett., **12**, pp284-286, 1987.

5. O.E. Delange,"Wideband optical communication systems, part II - Frequency division multiplexing", Proc. IEEE, **58**, pp1683-1690, 1970.

6. H. Ishio, J. Minowa and K. Nosu,"Review and status of wavelength division multiplexing technology and its application", J. of Lightwave Technol., **LT-2**, pp448-463, 1984.

7. C.A. Brackett,"Dense wavelength division multiplexing networks: Principles and Applications", IEEE J. on Select. Areas in Comms., **8**, pp948-964, 1990.

8. A.C. Carter,"Wavelength multiplexing for enhanced fibre-optic performance", Telecomm., pp30-36, 1986.

9. M.S. Goodman, H. Kobrinski, M.P. Vecchi, R.M. Bulley and J.L. Gimlett,"The LAMBDANET multiwavelength network: Architecture, applications and demonstrations", IEEE J. on Select. Areas in Comms., **8**, pp995-1004, 1990.

10. L. Reekie, R.J. Mears, S.B. Poole and D.N. Payne,"Tunable single-mode fiber lasers", J. of Lightwave Technol., **LT-4**, pp956-960, 1986.

11. C.Y. Chen, M.M. Choy, M.J. Andrejco, M.A. Saifi and C. Lin,"A widely tunable erbium-doped fiber laser pumped at 532nm", IEEE Photon. Technol. Lett., **2**, pp18-20, 1990.

12. I.M. Jauncey, L. Reekie, R.J Mears, D.N. Payne, C.J. Rowe, D.C.J. Reid, I. Bennion and C. Edge,"Narrow linewidth fibre laser with integral fibre grating", Electon. Lett., **22**, pp987-988, 1986.

13. M.W. Phillips, A.I. Ferguson, D.C. Hanna, M.J. McCarthy and P.J. Suni,"Actively mode-locked fiber lasers", Proc. SPIE, **1171**, pp280-290, 1989.

14. I.P. Alcock, A.I. Ferguson, D.C. Hanna and A.C. Tropper,"Mode-locking of a neodymium-doped monomode fibre laser", Electron. Lett., **22**, pp268-269, 1986.

15. G. Geister and R. Ulrich,"Neodymium-fibre laser with integrated-optic mode locker", Opt. Comm., **68**, pp187-189, 1988.

16. W. Johnstone, S. Murray, M. Gill, A. McDonach, G. Thursby, D. Moodie and B. Culshaw,"Fibre optic modulators using a multi-mode lithium niobate waveguide overlay", Electron. Lett., **27**, pp894-896, 1991.

CHAPTER 2

Wavelength Sensitive Devices for Optical Fibre Systems

2.1 Introduction

The increased utilisation of optical fibres in a variety of technologies has led to a demand for more sophisticated optical components. Subsequently, there has been an increase in the number of components capable of processing optical signals without conversion to the electronic domain e.g. directional couplers, filters, modulators, switches, etc. Devices which display a wavelength dependent/selective function are of particular interest as they are a fundamental requirement of WDM technology. The use of such devices as optical multiplexers and demultiplexers in the wavelength domain allows multichannel transmission on a single-mode fibre and provides vastly increased information capacity. The principal function envisaged for the devices under investigation in this thesis is tunable wavelength division multiplexing, selection and filtering. Therefore, this chapter provides a brief review of device technologies and implementations presently incorporated in optical fibre-based systems which utilize WDM and WDDM technology.

Devices for wavelength multiplexing and demultiplexing are generally based on three wavelength selective mechanisms: angular dispersion, directional coupling of selected wavelengths and spectral filtering based on interferometric techniques. These mechanisms usually result in devices capable of both multiplexing and demultiplexing optical signals due to the reciprocal nature of optical waves.

2.2 Angularly Dispersive Devices

Angularly dispersive techniques for wavelength separation normally rely on prisms[1] or diffraction gratings[2] in which the incident light is spread spatially at the output according to wavelength. Initial devices incorporated glass

prisms but were of only limited use. The material dispersion of the prism material strongly influences the eventual angular dispersion and only a limited range could be achieved with conventional glasses. Material constraints have restricted the development of practical prism WDM devices. Consequently, the major angularly dispersive element employed in WDM devices is the diffraction grating[2], used in reflection mode. The basic diffraction grating consist of a number of grooves or lines formed in a substrate with a constant spacing. Fabrication is by conventional mechanical ruling or the superior technique of anisotropic etching of single crystal silicon[2]. The grating is designed to diffract light at certain angles depending on the grating constant (number of lines per unit length), wavelength of the incident light and angle of incidence. Figure 2.1 illustrates two kinds of grating-based demultiplexing schemes. The demultiplexing mechanism of the device geometries shown in Figure 2.1 can be explained as follows. The incoming multiplexed signal is focussed onto the diffraction grating at a set angle. Each wavelength component of the multiplexed signal is diffracted at an angle which depends on its wavelength and focussed by the same lens into an appropriately aligned output fibre. The GRIN-rod lens configuration in Figure 2.1(b) simplifies alignment and increases device compactness and mechanical stability[3]. A further modification of the device geometry involves the use of a concave grating[4]. This performs both the diffracting and focussing functions and removes the necessity for a lens element.

Grating-based WDM devices have the capability of multiplexing many wavelength channels by appropriate choice of grating constant, blaze angle (angle of the grooves) and fibre types. Typical performance figures for diffraction grating demultiplexers include[5] insertion losses in the range 1-4dB, as many as 20 channels, channel (wavelength) spacings in the range 20-40nm and crosstalk attenuation of 20-30dB. However, a major problem associated with grating-based multiplexers and demultiplexers is that their bandpass characteristics and insertion loss depend on the dimensions of the input and output fibres[6]. This occurs because the spatial location of the diffracted, angularly-dispersed light (and corresponding output coupling efficiency) is sensitive to variations in the input wavelength. To ensure low

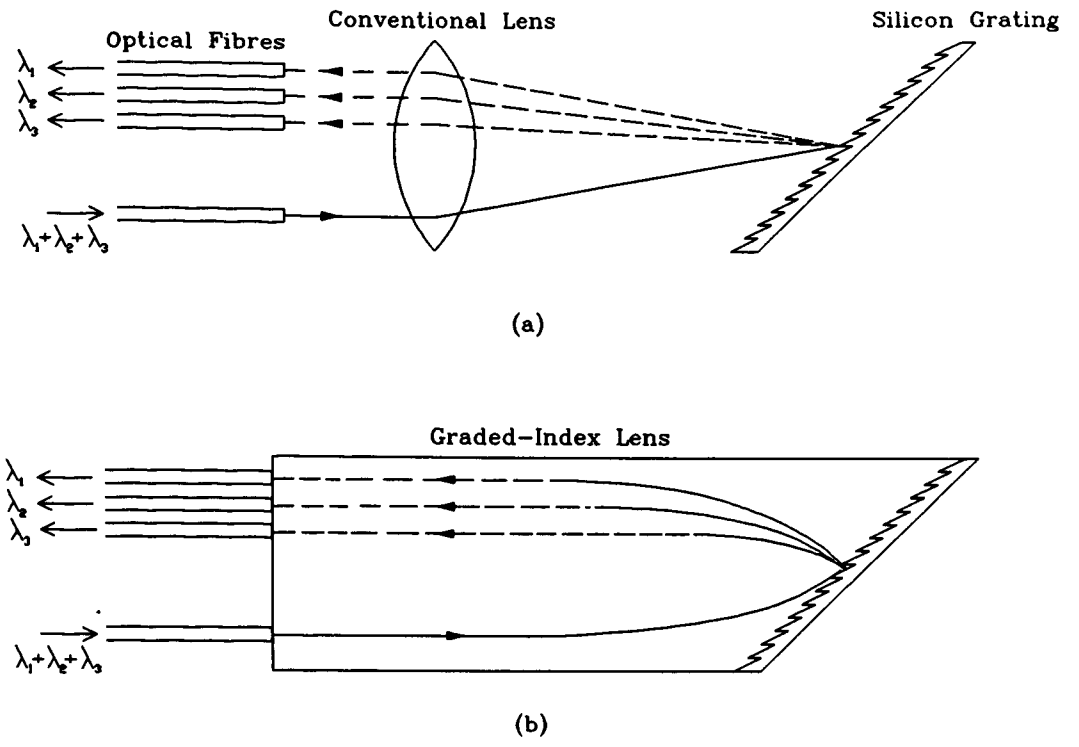

Figure 2.1 : Grating-based demultiplexer using (a) conventional lens (b) Graded-Index lens

insertion loss and specified bandpass response, the grating WDM device requires output fibre(s) possessing larger core diameters than the input fibre(s). This is undesirable when operating the device in a multiplexing configuration with standard single-mode telecomms fibre (core $< 10\mu$m) at the output. Therefore, a bulk or micro-optic grating-based device is unsuitable as a multiplexing element for single-mode fibre systems since the input fibres would require impractically small core diameters i.e. insertion losses would be vastly increased due to source-fibre coupling degradation while any mechanical movement would strongly influence device performance.

Integrated device structures utilizing diffraction mechanisms have been developed in planar Silicon[7] and Lithium Niobate[8]. In these structures, the incoming multiplexed light is guided by a slab waveguide prior to being angularly dispersed

by a concave reflection grating. Reflected light is then guided by the slab waveguide to appropriately placed output fibres. An alternative arrangement[9] uses a series of Bragg gratings to successively deflect the guided input wavelengths to integrated photodetectors. The attraction of these integrated waveguide structures is compactness, improved mechanical stability and the potential for inexpensive mass production. However, fibre-device interfacing problems still remain.

2.3 Wavelength Selective Coupling Devices

Wavelength selective coupling-based multiplexers and demultiplexers generally take the form of directional couplers, devices which usually have two inputs and two outputs (all of which are optical). Directional couplers have become essential components for most optical systems and several different technologies and device geometries have been utilized to date to produce devices with a range of functional complexity. These vary from passive all-fibre device[10][11] to active integrated optics implementations based on Lithium Niobate[12][13] and III-V semiconductor[14][15] technologies. Device operation relies on the coupling of power between modes of adjacent waveguides. The degree of coupling is wavelength dependent, particularly for the case of dissimilar waveguides, and this allows the fabrication of WDM devices.

Single-mode fibre couplers are of particular interest since they alleviate fibre-device insertion loss and are immediately compatible with the standard system fibre. When the core regions of two single-mode fibres are placed in close proximity, they can exchange power via mode-coupling. The evanescent tail of the propagating mode in one fibre extends into and excites the mode of the adjacent fibre, providing the propagation constants of the two modes are similar. As the coupled modes propagate along the fibres, power is periodically exchanged between the fibres. The power distribution after a distance of interaction z is given by[16]:

$$P_1 = P_o \cos^2(cz)$$
$$P_2 = P_o \sin^2(cz) \qquad (2.1)$$

where P_o is the power in the input fibre (fibre 1) at $z=0$, P_1 and P_2 are the powers in fibres 1 and 2 at a distance of propagation z and c is termed the coupling coefficient between the the two coupled fibre modes (assuming identical fibres). The magnitude of c depends on the spatial overlap of the two interacting modes and is strongly related to the fibre core spacing. Full power transfer occurs after a propagation distance $L_c=2\pi/c$, called the coupling length. If the interaction length of the device is matched exactly to the coupling length, then the resulting splitting/coupling ratio will be 100%. A 3dB coupler is produced by arranging that the device interaction length is (N+1/2) times the coupling length. Higher wavelengths result in stronger evanescent fields and enhanced coupling coefficients (provided the input wavelength is still well-guided) since the spatial overlap of the modes is increased. Therefore, the device coupling length is highly wavelength dependent and, for a fixed interaction length, a fibre coupler exhibits a wavelength dependent splitting ratio i.e. cross-coupled power can be vastly different for input light of, say, 1300nm and 1550nm allowing the device to behave as a demultiplexer.

Two distinct approaches have emerged in the fabrication of single-mode fibre couplers: polished fibre techniques and fused biconical tapered fibre techniques. Polished fibre directional couplers are constructed using two side-polished fibres separated by an index-matching fluid. For mechanical stability, the fibres are first bonded into a curved groove which is cut in a glass or fused quartz substrate block (called a half-block). Mechanical lapping and polishing is then performed to reduce the cladding thickness on one side of the fibre to, typically, $<5\mu$m[17]. The two substrates are then mated via an index liquid with the fibres aligned. The geometrical arrangement is shown in Figure 2.2. The critical physical parameters determining the fibre cores spacing and device interaction length are the remaining cladding thickness, δ, on each fibre half-block (with $d=2\delta$ for identical half-blocks) and the

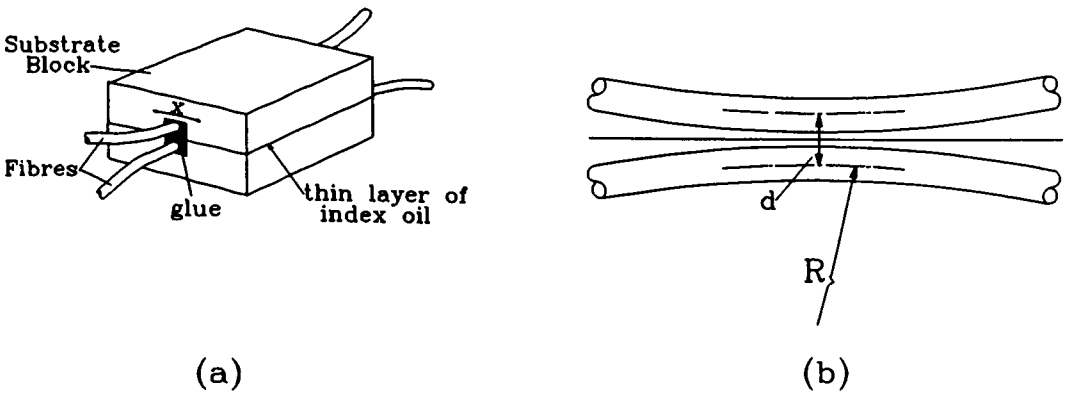

Figure 2.2 : (a) Assembled polished fibre directional coupler
(b) Geometry of polished fibre half-block

groove radii of curvature, R (see Figure 2.2(b)). The coupling ratio of a polished fibre device depends on the mismatch between the device interaction and coupling length, with the coupling length influenced by the wavelength of operation, core spacing, fibre parameters and intervening refractive index. However, polished fibre devices are completely tunable from 0-100%[18] by adjustment of the relative lateral position of the fibre via micrometer screws i.e. movement in the x-direction in Figure 2.2(a). Slight misalignment of the fibres has the effect of varying the fibre cores spacing with corresponding modification of the device coupling length. Therefore, the wavelength multiplexing and demultiplexing functions of the coupler are also tunable. Experimental investigation of a 2 x 2 polished fibre coupler, incorporating two identical, step-index, 2μm core single-mode fibres (R=70cm, d=4.5μm), produced a sinusoidal relationship between coupling ratio and input wavelength[19] i.e. the cross-coupled power varied from 0 -100% depending on wavelength. Two cross-coupled wavelength extinctions in the range 450nm-900nm were recorded with a channel separation of approximately 200nm. The device was capable of multiplexing/demultiplexing two wavelengths (channels) separated by approximately 130nm in the same range although loss and extinction ratio measurements were not given. Insertion loss of <0.1dB and extinction ratios as low

as -50dB[18] have been recorded in similar couplers at fixed wavelengths. Tuning of the spectral characteristics of another polished coupler was performed via lateral offset of the fibre cores. As the offset was increased (effectively increasing core spacing), the response was seen to shift towards higher wavelengths by as much as 400nm, with negligble change in resolution[19]. Further experimental investigation of couplers possessing larger radii of curvature produced narrower channel separations, as low as 35nm for a device with R=8m.

An extension of the initial polished fibre coupler technology has seen the fabrication of devices with dissimilar single-mode fibres[20][21]. For these couplers, the propagation constants of the fibre modes are matched only at a discrete wavelength i.e. at the intersection of the dispersion characteristics of the modes. At this wavelength only, complete power transfer is possible whereas away from this value the transfer of power rapidly decreases. This decrease depends on the difference between the slopes of the respective dispersion curves. Dissimilar fibre couplers are, therefore, much more wavelength selective than identical fibre couplers and show potential for operation as narrow-band WDM devices. A device capable of efficiently separating wavelength channels at 1300nm and 1500nm was demonstrated[21] with <0.6dB insertion loss and extinction ratio of -22dB or better. The fibres had core diameters and core-cladding relative index differences of 1.72μm, $\Delta=0.88\%$ and 3.45μm, $\Delta=0.434\%$, respectively. A 3dB channel linewidth of 50nm was observed. The same workers have also produced a similar WDM device utilizing two different single-mode fibres which displays a channel linewidth (3dB) of 22.5nm[22]. Based on the same principal, a more recent device proposal uses a step-index fibre and a W-index fibre (both single-moded) to form the polished coupler[23]. The parameters of the W-index fibre are selected such that the dominant LP_{01} mode exhibits a non-zero cutoff wavelength. As a result, a significant difference in the slopes of the mode dispersion curves is obtained which can be exploited to produce a narrow-band spectral filter. Channel linewidths on the order of 1nm are predicted for such a device.

Fused fibre couplers can also be designed for use as WDM devices. A typical fused coupler is fabricated by applying heat (> 1500°C for fused silica fibres) and tension to two single-mode fibres which have been twisted together over a fixed length[24]. As the fibre claddings fuse together, the tension causes elongation and a reduction in width of the fused region, resulting in a biconical cross-section (see Figure 2.3).

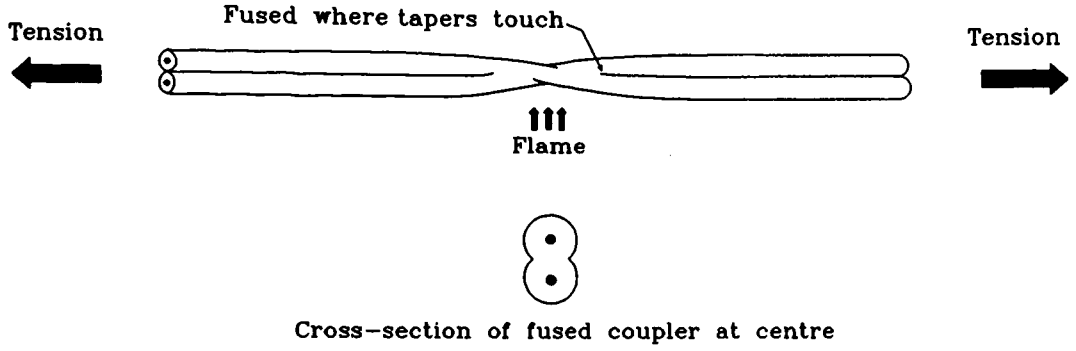

Figure 2.3 : Fused Fibre Directional Coupler

In the fused region the fibre cores are reduced in size and are in close proximity, and power can oscillate between them. The splitting ratio of the fused coupler, for a fixed wavelength, is selected by monitoring the cross-coupled output during the fabrication process, removing the tension when the desired coupling ratio is achieved[25]. As with polished fibre couplers, the coupling ratio of a fused coupler varies sinusoidally with input wavelength. The period of oscillation depends on the dimensions and geometry of the fused (biconical) region but is also related to the refractive index of the surrounding medium[26][27]. (The sensitivity of the splitting ratio to variation in the external cladding index has been used to produce tunable or programmable couplers[26][27] by enclosing the fused region in either index oil followed by heating or an active dye solution which can be laser pumped to induce an index change). In addition, the degree of fusing has an influence since it determines the eventual fibre core spacing. The wavelength channel spacing in fused couplers can be varied by continuing to apply tension during the fabrication after the first complete power transfer is observed. This produces over-coupled

devices possessing long interaction lengths which exhibit many power transfer cycles along their length[28]. Wavelength channel separations ranging from 18nm-25nm (depending on exact fabrication conditions) have been observed with the measured insertion loss and crosstalk (extinction) as low as 0.1dB and -25dB, respectively[26]. However, extending the interaction region of the fused couplers causes the cladding diameter at the centre to become greatly reduced (as low as 10μm) with corresponding handling difficulties. Additionally, in this situation the evanescent field of the guided light can extend into the surrounding environment. As a result the devices can exhibit instabilities in performance (particularly when channel spacing is below 50nm) and require careful control of the surrounding environment.

The single-mode fibre couplers described above are attractive from the point of view of low insertion loss and good extinction ratios. Additionally, the polished type allow extensive tuning of the channel separation and centre wavelength via lateral offsets although this is tempered slightly by undesirable mechanical sensitivity. However, the performance of both coupler types in terms of channel resolution and spacing is limited. The polished fibre half-block structure has also been used in alternative wavelength-dependent device geometries whose operation relies on a coupling mechanism. These devices are known as Fibre Grating filters[29][30] and have the advantages of all-fibre devices discussed earlier. The device geometry consists of a standard polished fibre half-block whose surface is either (i) brought into contact with a periodic grating structure or (ii) imprinted with a periodic grating structure directly on the fibre cladding (termed a surface-relief grating). Figure 2.4 shows a schematic representation of a surface-relief fibre grating filter. Surface-relief grating devices give superior performance when compared with the contact-grating devices and are fabricated using photolithographic and etching techniques to appropriately pattern the polished fibre surface (i.e. form the grating). The polished fibre half-block is produced in the standard manner (polished to within 1-2μm of the core)[17]. A layer of photoresist is then spun onto the polished surface and exposed to a two-beam interference pattern from an Argon-Ion laser. The interference fringe spacing determines the grating period and the photoresist pattern is then transferred

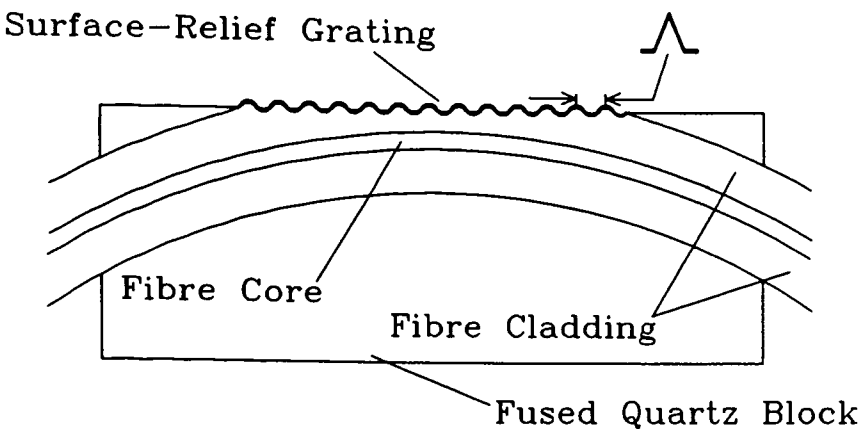

Figure 2.4 : Cross-section of surface-relief grating fibre reflection filter

into the fibre cladding by reactive-ion etching. Deposition of a thin layer of a higher index material (e.g. Al_2O_3) onto the grating surface then helps to increase device efficiency[30].

Fibre grating filters operate in a reflection mode and, depending on the length and efficiency of the grating, can exhibit very narrow filter linewidths. The period of the grating, Λ, is designed such that phase-matching between the forward travelling guided mode and a similar backward travelling guided mode is induced. This causes a transfer of power from the forward to the backward mode. The phase-matching situation is highly wavelength sensitive and given by the first-order Bragg condition, $\Lambda=\lambda_B/2n_e$, where λ_B is the reflected wavelength and n_e is the fibre mode effective index. Reflected linewidths (3dB) as low as 0.8nm with 98% efficiency have been reported[30] using standard polished fibre half-blocks. A reduced linewidth of 0.3nm has been demonstrated for a device with an increased grating (interaction) length where the fibre was held parallel to the grating in a silicon V-groove[31]. Tuning of the reflected centre wavelength is possible by variation of the superstrate refractive index although this also affects the filter linewidth[31]. An alternative tuning method has been demonstrated which allowed variation of the filter centre

wavelength over the range 1460nm to 1540nm[32], although reflection efficiency was low. This was achieved via a novel "fan"-shaped contact grating which was mated to the surface of a polished fibre half-block. Lateral translation of the grating provided a continuous variation in grating period with subsequent variation in reflected wavelength. An improved version of the device[33] yielded 65nm tunability with reflectivities as large as 88%. A disadvantage of the fibre grating filters is the reflection mode of operation which adds to the difficulty in accessing the filtered wavelength. Furthermore, below the reflection wavelength, coupling to radiation modes occurs and the device exhibits high loss which restricts operation as a wavelength selective component.

The implementation of directional couplers in integrated-optical form offers the possibility of high device packing densities and large-scale manufacture, and also the potential for active tuning if appropriate substrate materials are utilized. WDM devices based on directional coupler configurations have been demonstrated in several different substrate materials: Glass[34], Lithium Niobate ($LiNbO_3$)[35], Semiconductors[36], and Silica-on-Silicon[37]. The devices are formed by appropriate patterning of single-mode channel waveguides on the surface of the various substrates (vertically stacked waveguides are also possible in semiconductors). Fabrication techniques include ion-exchange in glass[38], Titanium indiffusion in $LiNbO_3$[39], epitaxial growth with selective etching in semiconductors[40] and flame hydrolysis deposition followed by reactive-ion etching in Silica-on-Silicon[41]. Essentially, these techniques allow the establishment of narrow high index regions surrounded by lower index material which can behave as waveguides. Device geometries comprise adjacent channel waveguides which are in close proximity over a certain length. Wavelength-dependent cross-coupling/filtering occurs in the same manner as described for the symmetrical all-fibre couplers i.e. the splitting ratio has a sinusoidal dependence on wavelength. Production of devices with specified wavelength responses requires precise control of interaction length and waveguide spacing, particularly in passive implementations where fine-tuning is not readily available. Glass and Silica-on-Silicon are inherently passive device

technologies since the substrate material displays no significant optical activity, although doping with active species is a possibility[42][43]. This requires extensive characterisation of the fabrication processes and flexibility in mask design to allow specific wavelength filters to be fabricated. Glass ion-exchange technology is fairly mature and has been well-characterised[36] and a variety of device functions have been realised including multi/demultiplexers. An example of the device performance possible with the symmetrical structure is that of a two-wavelength demultiplexer demonstrated in Ag^+-Na^+ exchanged BK7 glass[44]. The device was a standard I.O. directional coupler configuration in which both wavelengths were launched into the same input arm but emerged from separate output arms. Crosstalk (or extinction ratios) of -30dB and -32dB at wavelengths of 1315nm and 1561nm, respectively, were observed for a 14.5mm long device. A total insertion loss of 1.25dB with propagation loss of 0.15dB/cm was recorded for the same device. A disadvantage of symmetrical directional coupler WDMs is that channel bandwidth is generally fairly wide, with undesirable extension in interaction length required to attain a significant reduction. They are, however, suitable for 2-channel multi/demultiplexing provided the channel separation is wide e.g. 1310nm and 1550nm.

To obtain a narrowing in channel linewidth, the interacting regions of the waveguides can be made dissimilar by modification of the width and/or refractive index of one of the guides. This produces distinct, but intersecting, mode dispersion characteristics for the adjacent waveguides. Significant power transfer then occurs only when the mode propagation constants are closely matched. The device response is that of a channel-dropping/bandpass filter depending on which output arm of the coupler is considered. Such a device has particular application in "broadcast and select" WDM systems as a filtering element prior to signal detection. Asymmetric couplers using different ion-exchange pairs[45] for each arm of the coupler have been proposed in glass I.O. technology. However, a practical demonstration of an asymmetric coupler in $LiNbO_3$ was reported as long ago as 1978[35]. The device possessed different guide widths and indices (related to the amount of deposited

Titanium) such that full cross-coupling only occurred at a discrete wavelength i.e. phase-matching of the mode propagation constants of the adjacent guides only occurred at a specific wavelength. Figure 2.5 shows the device geometry and response. The device had an interaction length of 15mm and was capable of filtering light at λ=600nm with a channel linewidth (3dB) of 20nm. An additional feature of the device was substantial electrical tunability of the filter centre wavelength. The tuning response was achieved via the electro-optic effect in $LiNbO_3$.

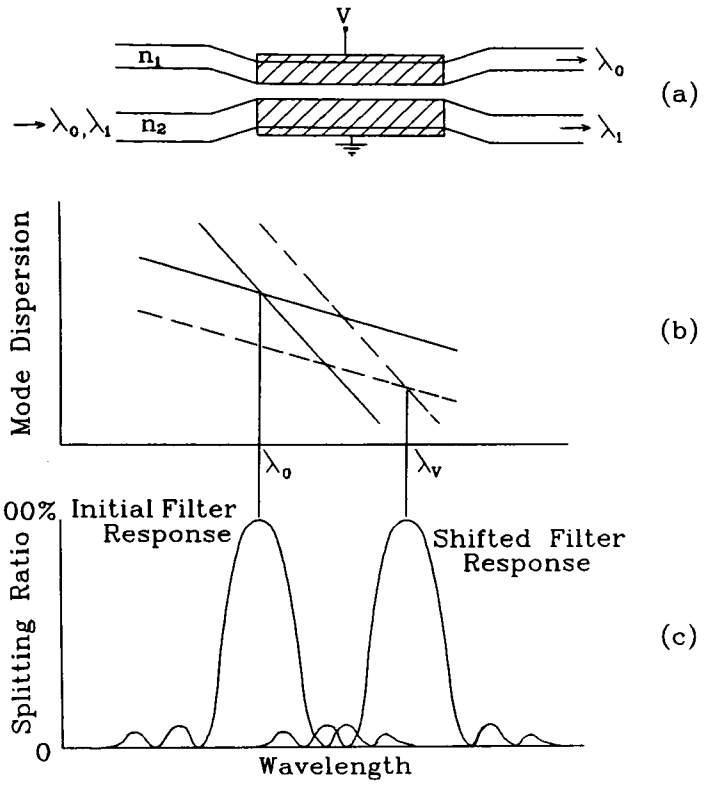

Figure 2.5 : $LiNbO_3$ directional coupler filter
(a) Device Geometry (b) Waveguide Dispersion (c) Filter Response

Application of a voltage, V, to the electrodes (see Figure 2.5) causes a shift in the waveguide refractive indices and a corresponding shift in the corresponding dispersion characteristics. As a result, the phase-matching condition is re-established at a longer wavelength i.e. a higher wavelength is filtered. A tuning range of 60nm was demonstrated, with a centre wavelength shift corresponding to 10nm/V. More recently, a similar device capable of multiplexing light at λ=1320nm and

λ=1550nm was reported[46]. The multiplexing function relies on cross-coupling of only one of the input wavelengths. The different wavelengths are launched into separate input ports of the coupler but only one wavelength is coupled across to the adjacent output arm while the other wavelength remains unaffected and, thus, both wavelengths emerge from the same output port. Channel bandwidth was 75nm, less impressive than the earlier device. An all-optical version of the device geometry shown in Figure 2.5 has also been proposed[47] in which the interacting regions have refractive indices which are intensity dependent. Tuning of the filter/wavelength response would then be possible through control of the input power. As with the asymmetric fibre couplers, the channel bandwidth of the device is dependent on the difference in the slopes of the intersecting dispersion curves.

Active and narrowband filtering using the directional coupler structure is also possible in III-V semiconductor technology. Considerable improvements in filter linewidth response have been reported[36]. In addition, reduced device interaction lengths are available, thus offering the possibility of increased device density while the possibility of integrating sources, detectors, etc. on the same substrate exists. The substrate material is usually Gallium Arsenide (GaAs) or Indium Phosphide (InP), onto which are deposited/grown layers of varying constituency and refractive index (e.g. AlGaAs, InGaAsP) by a variety of processes. Selective etching is then employed to define the waveguide geometry using standard techniques. Directional couplers can be formed in either lateral[14] or vertical[48] dimensions. The filtering mechanism is as described for $LiNbO_3$ devices. Very narrow linewidth filters[49] have been reported using vertical, asymmetrical directional couplers fabricated in AlGaAsP/InP as shown in Figure 2.6. The device consists of two vertically coupled waveguides of dissimilar cross-sections and different material parameters. This produces dramatically different dispersion curves and results in an extremely narrow filter response, $<$0.8nm linewidth (3dB) at a centre wavelength of λ=1265.5nm. Device interaction length was 5mm. However, the power transfer efficiency between the waveguides was low (5%) due to excitation of higher order modes in the lower waveguide which were not coupled to the upper waveguide.

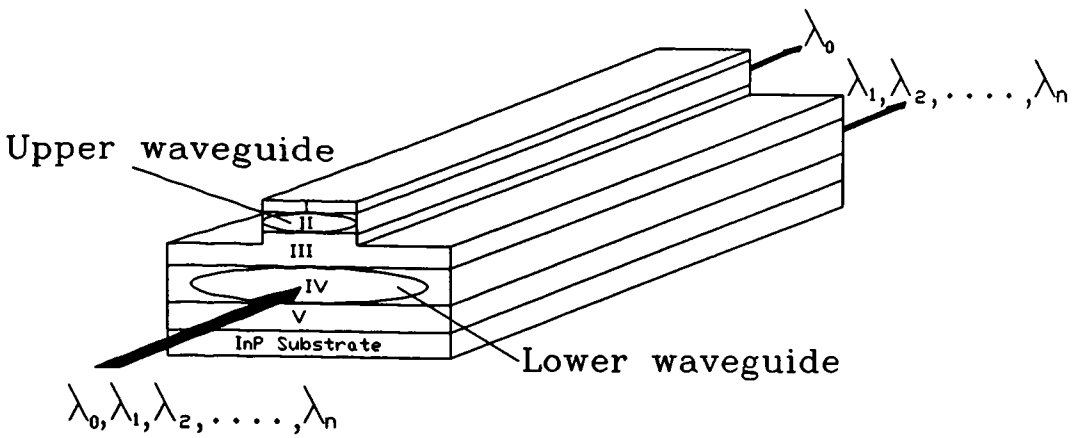

	Thickness	Material
Layer I –	1μm	InP
Layer II –	0.263μm	InGaAsP
Layer III –	1.935μm	InP
Layer IV –	2μm	InGaAsP
Layer V –	1μm	InP

Figure 2.6 : Geometry of Vertical Directional Coupler Filter

Reduction of the lower guide thickness to ensure single-mode operation is required although this will increase fibre-device coupling difficulties. By suitably doping the various material layers of the device, it should be possible to tune the filter response by application of an electric field.

Another category of WDM devices which use a form of wavelength-selective coupling are polarisation converters. These devices rely on wavelength-selective power transfer between orthogonal polarisation states in the same waveguide or bulk-crystal and are the highest performance coupling-based devices available. Both bulk-optic[49] and integrated-optic[50][51] device geometries have been demonstrated. The polarisation conversion can be achieved by either acousto-optic or electro-optic techniques although the acousto-optic approach is preferable in terms of tuning range and multichannel operation.

The basic device geometry consists of a narrowband polarisation converter

sandwiched between two crossed polarisers. An integrated-optic implementation of an acoustically-tunable optical bandpass filter is illustrated in Figure 2.7. Incoming

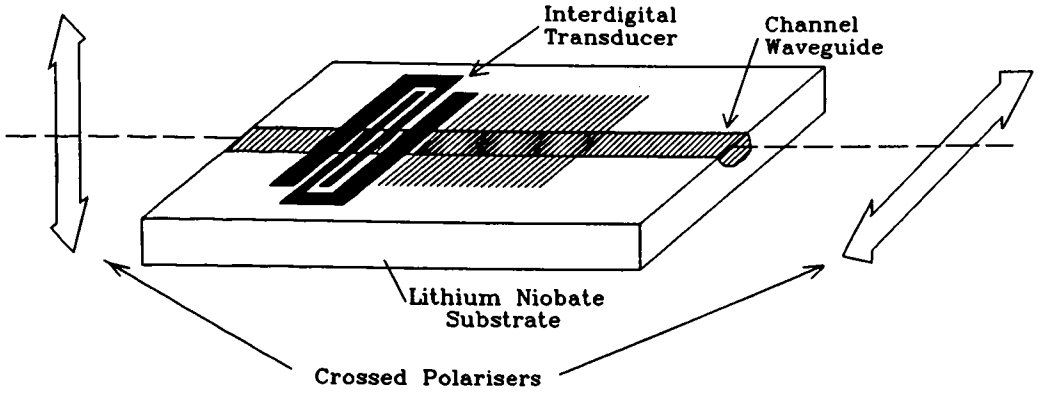

Figure 2.7 : Schematic diagram of I.O. Acoustically-Tunable Optical Filter

light passes through the first polariser and is launched into the $LiNbO_3$ channel waveguide in a particular polarisation state. For wavelengths within the filter passband, conversion to the orthogonal polarisation state occurs as a result of a stress grating formed by an acoustic wave. These wavelengths can then pass through the output polariser for subsequent processing, detection, etc. Wavelengths outwith the filter passband remain in the original polarisation state and cannot pass through the output polariser i.e. the overall device appears as a pair of crossed polarisers to these wavelengths. Filter performance depends on the efficiency of the polarisation conversion which is related to the applied acoustic power density. The mechanism for polarisation or mode conversion in these devices makes use of the high material birefringence present in $LiNbO_3$. TE and TM modes of the channel waveguide possess significantly different propagation constants and a corresponding characteristic beat length given by $L_{beat}=\lambda/\Delta n$, where Δn is the mode birefringence and λ is the optical wavelength (they have equal phase every beat length). If a copropagating acoustic wave is launched along the waveguide, then a refractive index grating is established via the stress-optic effect. Provided the period of the index grating matches the periodic change in the relative phase of the orthogonal

polarisations, then mode (polarisation) conversion can occur and efficient power transfer is possible. This requires that the acoustic wavelength, $\Lambda_{ac}=L_{beat}$, and leads to the relationship between acoustic drive frequency, f_{ac}, and selected/filtered wavelength, λ_f:

$$\lambda_f = \frac{V_s \Delta n}{f_{ac}} \tag{2.2}$$

where V_s is the speed of sound in $LiNbO_3$. The wavelength dependence of the converted polarisation (and thus optical transmission of the filter) is the familiar sinc function obtained from coupled-mode theory (see Figure 2.5). Filter bandwidths of <1nm with insertion loss of <5dB are readily attainable[52] while extinction ratios of <-20dB have been demonstrated by placing neighbouring wavelength channels at transmission nulls[53]. Similar performance has been reported for the electro-optic version of the device[51][54]. The tuning range of the acoustically-tuned device is, in principle, very broad (1200nm-1600nm)[52] and is a result of the dynamic nature of the index grating formed by the acoustic wave. By changing the acoustic frequency, the grating period is changed, and a different wavelength is selected since the phase-matching conditions have also changed. Hence the broad tuning range. However, the fixed nature of the interdigital electrodes required to launch the acoustic waves prevents constant launch efficiencies over the wavelength range mentioned above. As such, in practical devices the tuning range is comprimised by a drop-off in polarisation conversion efficiency and a resulting degradation in device performance. Multiple channel selection is, however, possible, a unique capability, since multiple acoustic waves can be launched simultaneously, the number limited only by the maximum drive power the acoustic transducer can handle. The electro-optic version of the device can be tuned more quickly but has a greatly reduced tuning range due to the static nature of the grating[51].

WDM device implementations in integrated optical form have many attractions including high packing density, narrow bandwidth filtering, good extinction ratio and low voltage active tunability. However, fabrication techniques can be very

complicated, often involving difficult processes and elevated temperatures and device performance is often sensitive to slight fabrication variations. Furthermore, high insertion loss and mechanical/thermal instability with regard to alignment are unavoidable due to the necessity for fibre-device interfacing, although an all-fibre implementation has been reported[55]. A particular difficulty of the acoustically-tunable optical filter is the requirement for precise control of the polarisation state of the light. Since the polarisation state is hard to maintain in an ordinary single-mode fibre, either the polarisation state of the entire system must be controlled or devices with a polarisation-independent function must be developed. Such a device has been reported[56][57] which makes use of two 2 x 2 TE-TM beam splitters, one at the input and one at the output. In this device, the input polarisation state is split into two orthogonal (TE and TM) components by the first TE-TM splitter. Each component then propagates in adjacent (optically de-coupled) waveguides and experiences mode conversion via a common acoustic wave. A second TE-TM splitter at the output then causes the components to recombine and emerge from one arm of the beam splitter while the unfiltered light emerges from the adjacent arm. Similar performance to the polarisation sensitive device is obtained.

2.4 Interferometric-Based Wavelength Filters

A number of optical filters rely on interferometric effects for their operation and display a very wavelength selective response. These include Dielectric Thin Film (DTF) stacks or multilayers, Fabry-Perot Etalons and Mach-Zender Interferometers.

DTF interferometric filters are often constructed from alternating layers of high and low refractive index, each of which has a thickness of one quarter wavelength[58]. Dielectric multilayers are usually fabricated by successive thermal or electron-beam evaporation of high stability materials[59] e.g. Titanium Dioxide (TiO_2) and Silicon Dioxide (SiO_2). A schematic representation of a DTF interference filter is shown in Figure 2.8. When light traverses the dielectric

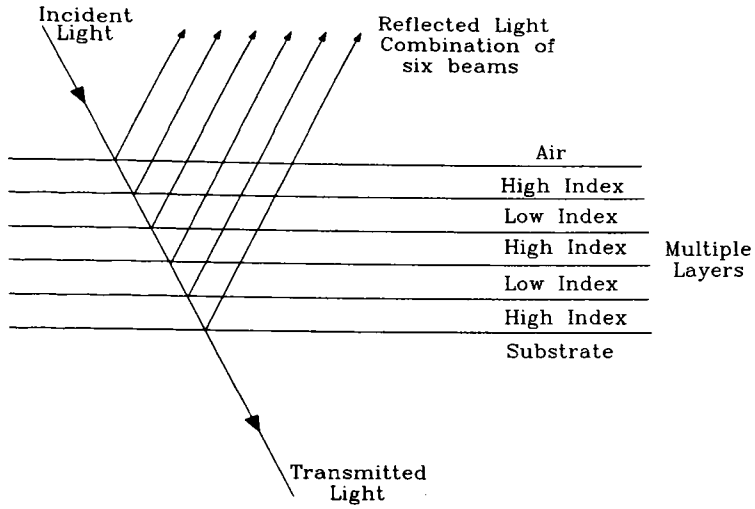

Figure 2.8 : Multiple Layer Interference Filter Structure

stack, it experiences multiple reflections due to the refractive index changes at each layer interface. Light reflected within each of the high index layers does not experience a phase shift while light reflected within the low index layers suffers a phase change of π radians. The thickness of each layer is such that the successive reflected beams emerge from the front surface all in phase and experience constructive interference. Therefore, the effective reflectance of the structure can be made very high, particularly if the number of layers is made large. High reflectance is only observed over a limited wavelength region since constructive interference requires that each layer is a quarter wavelength in thickness, which can obviously only hold exactly for one specific wavelength. Outwith this region, the reflectance changes abruptly to a low value. The response is repeated as the wavelength increases since there are other wavelengths at which the layers are an odd number of quarter wavelengths thick. Consequently, the quarter wave stack or multilayer can operate either as a high pass filter, a low pass filter or a high reflection coating within specified wavelength ranges. Such a filter could be used as a demultiplexing

element which reflects one wavelength channel only. Bandpass filters can be realised by cascading of appropriate dielectric stacks[60] although high insertion losses can result.

A superior interferometric filtering device is the Fabry-Perot Interferometer (FPI)[61] or etalon which consists of a resonant cavity formed by two parallel mirrors (or highly reflective end-faces). The FPI is conceptually a very simple structure and, in principle, a lossless device when on resonance. It works on the principle of partial interference of the input light with itself to produce peaks and troughs in the frequency (wavelength) domain. Figure 2.9 shows the geometry of a Fabry-Perot single-cavity filter.

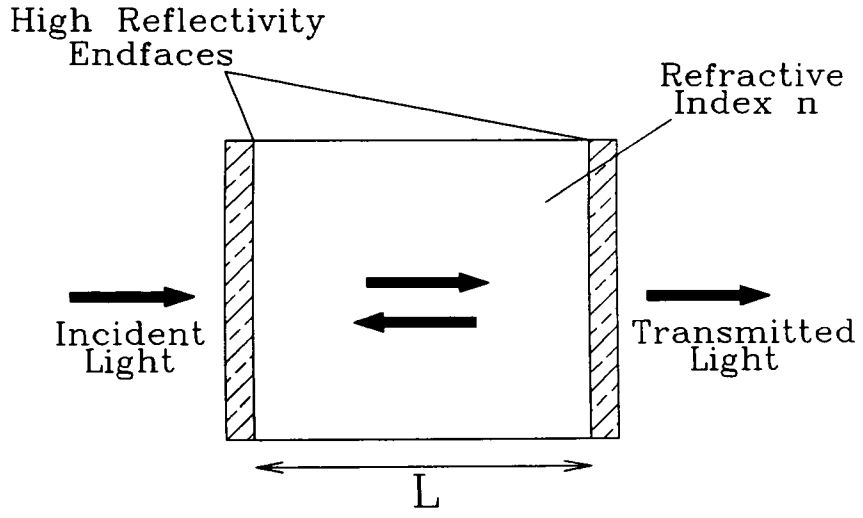

Figure 2.9 : Schematic representation of Fabry-Perot Filter

When a beam of light, e.g. from a fibre, is incident on the front mirror it experiences partial reflection and transmission. Upon reaching the second mirror, the light experiences further reflection and transmission, the extent dependent on the mirror reflectivity. The light which remains in the cavity oscillates between the mirrors, gradually leaking out each end. As a result, the incident beam is split into

many partial beams which mutually interfere. This produces interference fringes and a spectral transmission response which depends on the cavity length, refractive index of cavity material and the mirror reflectivities. Typical spectral transmission responses of Fabry-Perot etalons possessing different mirror reflectivities are shown in Figure 2.10.

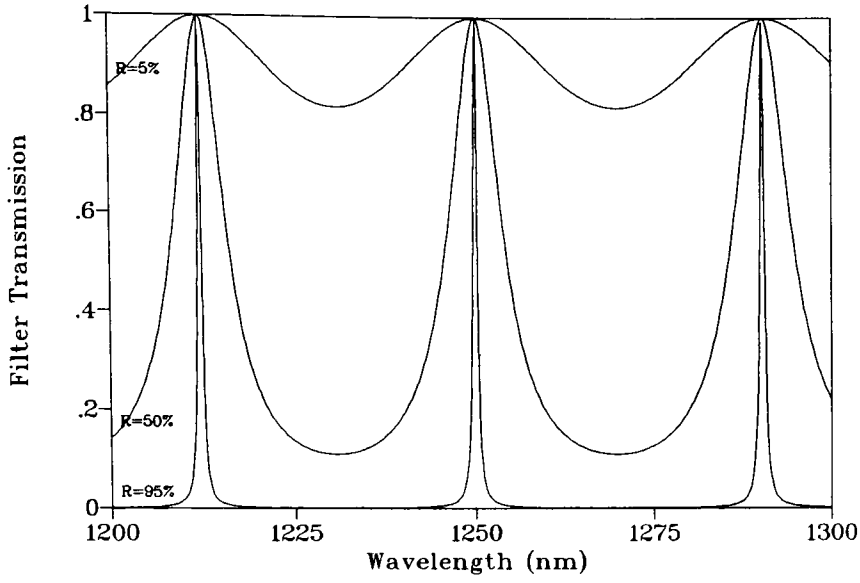

Figure 2.10 : Fabry-Perot Filter Response for Various Mirror Reflectivities

The filter transmission response with wavelength is given by:

$$T(\lambda) = \frac{\left[1 - \frac{A}{1-R}\right]^2}{1 + \frac{4R}{(1-R)^2}\sin^2\left(\frac{2\pi nL}{\lambda}\right)} \qquad (2.3)$$

where A is the mirror absorption, R is the mirror reflectivity, L is the cavity length and n is the refractive index of the cavity material. The spacing between successive transmission peaks is known as the Free Spectral Range (FSR) of the filter. For many applications, including wavelength multi/demultiplexing, the most important

performance parameter of a Fabry-Perot device is the Finesse, F. This parameter is given by the ratio of the FSR to the transmission channel linewidth (FWHM). It determines the number of equally-spaced wavelength channels which can be placed within one FSR. The Finesse is strongly influenced by the mirror reflectivities, R, and is given by:

$$F = \frac{\pi\sqrt{R}}{1 - R} \tag{2.4}$$

Therefore, to achieve high finesse and narrow transmission channels, the mirror reflectivities must be high, as can be interpreted from Figure 2.9. In addition, the mirrors should be as plane and parallel as possible to ensure that the successive reflections add in phase. Normal Fabry-Perot etalons and filters have finesses of up to 200 although precise control of parallelism and mirror reflectivity can increase this significantly[62]. A preferred method of enhancing device finesse is the use of multi-pass or multi-cavity device geometries where either the light is reflected back through the original cavity one or more times or a number of different cavities are cascaded. Finesses of greater than 1000 are readily available[63].

The spectral transmission of a Fabry-Perot filter can be tuned by varying the optical path length of the cavity i.e. nL. Changes in the value of nL can be induced by mechanical, thermal or electro-optic techniques, depending on cavity material and device geometry. A micro-optic device geometry has been reported[64], in which the Fabry-Perot etalon stage was composed of two closely spaced, highly parallel and reflective glass flats. The gap between the glass flats was controlled by a piezoelectric actuator, thus allowing fine-tuning of the optical path length of the cavity. A channel linewidth (FWHM) of approximately 4.7nm and tuning range of about 180nm were recorded, with a finesse of 60 at $\lambda = 1300$nm. The insertion loss was low, measured at 0.8dB. In the device described above, collimating rod lenses were used to couple light from and to the input and output fibres. An all-fibre device based on the same tuning mechanism which dispenses with the requirement for fibre launch optics has also been demonstrated[65]. In this device, the cavity mirrors

were formed directly on the cleaved and/or polished ends of the input and output fibres, with the fibres themselves attached to a piezoelectrically-controlled member. Movement of the supporting member then resulted in variation in cavity length and tunable filtering. Finesses of up to 350 were measured under laboratory conditions and a commercial version of the device is available with a finesse of 150 and an insertion loss of 1-2dB. Tuning across the entire FSR could be readily achieved with a tuning time, allowing for settling at the final position, of a few milliseconds. It is believed that piezoelectrically tuned devices will eventually exhibit tuning times of the order of microseconds. An alternative mechanical tuning method is that of rotating the whole Fabry-Perot cavity with respect to the direction of the incident light, known as angle-tuning[66]. Demultiplexing of up to sixteen wavelength channels with 2nm separation has been demonstrated using an angle-tuned solid Fabry-Perot filter[67].

Problems associated with mechanical tuning techniques include slow response times and potential for device misalignment (since a high degree of parallelism is essential to maintain device performance). Alternative tuning techniques rely on altering the refractive index of the cavity material via the thermo-optic or electro-optic effect. This has a similar effect on the optical path length encountered by the input light as cavity length variation. If the cavity material has a high dn/dT coefficient, then heating the device (in an oven, say) will obviously shift the transmitted spectral response. However, thermal tuning is an inherently slow technique while undesired thermal expansion of the cavity elements can cause complications. Therefore, interest has focussed on the use of electro-optic materials as the cavity element for fast, tunable Fabry-Perot filters. Unfortunately, well-characterised electro-optic materials such as $LiNbO_3$, while possessing a moderately large linear effect (r_{33}=30.8pm/V), would require excessively large applied voltages (assuming the cavity length to be in the region of 10μm) to cause a change of $\lambda/2$ in the optical path length of the cavity, which is the change required to tune over one FSR. At the present time, only liquid crystal materials possess a large enough electro-optic effect to be of practical use in electrically-tunable Fabry-Perot filters implementations. A number of Fabry-

Perot filters using liquid crystals as the cavity material have been reported[64][68]. Figure 2.11 shows the geometry of such a filter[64]. The

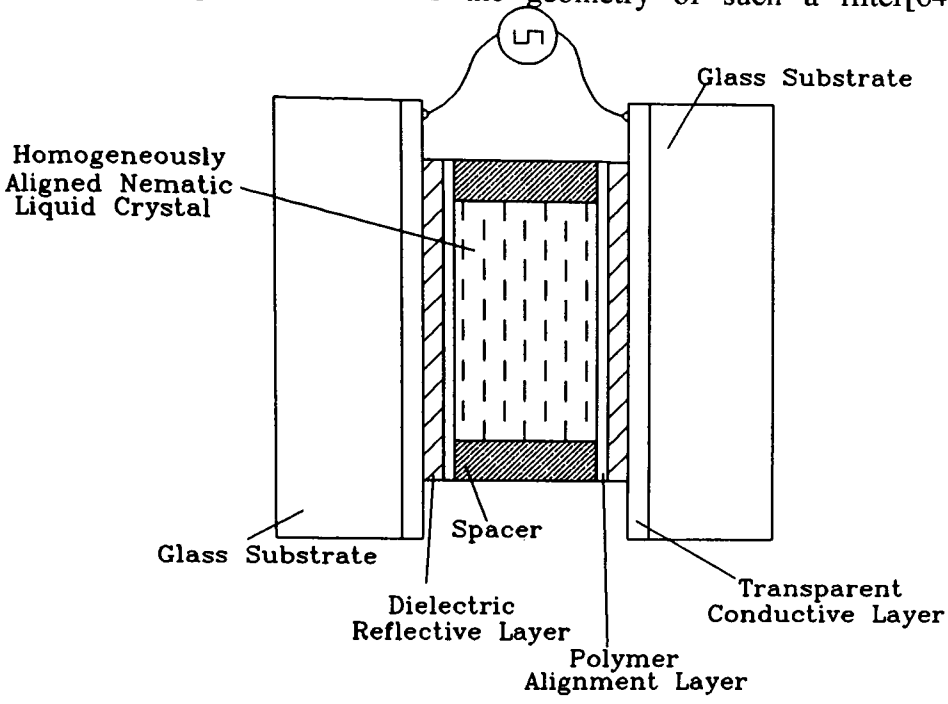

Figure 2.11 : Liquid Crystal Fabry-Perot Filter Implementation

device was constructed by coating two parallel glass plates with (i) an optically transparent electrically conducting layer e.g. Indium Tin Oxide (ii) a multilayer, highly reflective dielectric layer and (iii) a polymer layer for the purpose of suitably aligning the liquid crystal molecules. Spacers were used to define the cavity length and an electro-optic liquid crystal incorporated in the intervening gap. The end-face reflectivities were 90% at λ=1500nm, giving a finesse of approximately 30. However, the measured finesse was only 15 while the insertion loss was 4.2dB. The large discrepancy in measured and calculated finesses was attributed to mirror misalignment (a result of the many different material layers incorporated in the device) and scattering within the cavity. Nevertheless, an impressive spectral shift (tuning range) of thirteen FSRs could be achieved for application of only 25V. The tuning time for this device was not reported but a value of 20msec for tuning over a 175nm range has been reported[68] for a similar liquid crystal Fabry-Perot filter.

The narrow wavelength selectivities offered by Fabry-Perot filters ($<$ 1nm), high

finesses and fairly low insertion loss makes them of particular interest for application in dense WDM systems. They are also attractive for use as intracavity wavelength selective elements in fibre laser systems for mode selection, wavelength tuning and stabilisation purposes. However, fairly stringent mechanical alignment and thermal stability is required to ensure reliable device performance. Tuning of the spectral response of these devices over a considerable range has been demonstrated using piezoelectric or electro-optic techniques, but with only limited speed.

Also of interest for WDM applications are devices based on Mach-Zehnder Interferometer (MZI) elements, particularly in integrated optics form. They are already widely used in existing integrated optical devices such as switches and, by careful design, they can operate as both multiplexers and demultiplexers. A Mach-Zehnder interferometer consists of two 3dB directional couplers in tandem with the connecting waveguide arms of unequal length. The difference in optical path length seen by the light which is split at the first 3dB coupler results in a phase difference in the light which arrives at the second 3dB coupler. Careful control of this phase difference allows the MZI to be used as a WDM device. The layout of such a device is shown in Figure 2.12. A multiplexed signal containing components at λ_1 and λ_2

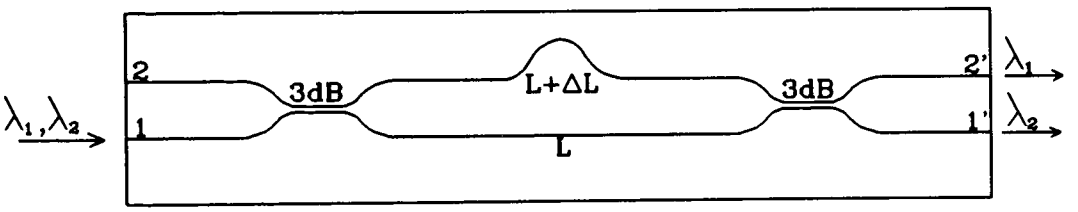

Figure 2.12 : Schematic diagram of single-stage Mach-Zehnder Demultiplexer

is input to port 1, as shown. The transmittance from port 1 to 1' and port 1 to 2' can be written as[69]:

$$T_{1\to 1'} = \cos^2(n_{eff}\pi\Delta L/\lambda)$$
$$T_{1\to 2'} = \sin^2(n_{eff}\pi\Delta L/\lambda) \qquad (2.5)$$

where n_{eff} is the effective refractive index of the waveguides, λ is the input wavelength and ΔL is the difference in length between the two waveguide arms. From eqns.(2.5), when $n_{eff}\pi\Delta L/\lambda=(m+1/2)\pi$, all the light of wavelength λ emerges from port 1'. Similarly, if $n_{eff}\pi\Delta L/\lambda=m\pi$, all the light of wavelength λ emerges form port 2'. Therefore, by appropriate choice of λ_1 and λ_2 and ΔL, complete separation of the two wavelengths can be achieved at the output of the second coupler i.e. the MZI behaves as a demultiplexer. The wavelength spacing required for complete demultiplexing of the input light can be calculated, from eqns.(2.5), as:

$$\Delta\lambda = \lambda_2 - \lambda_1 = \frac{\lambda_1\lambda_2}{2n_{eff}\Delta L} \qquad (2.6)$$

For a ΔL value of 5cm, the corresponding channel spacing is $\Delta\lambda=0.016$nm while $\Delta L=2.7\mu$m gives $\Delta\lambda=250$nm, for $\lambda_1=1550$nm. Wavelength filters based on all-fibre MZIs have been demonstrated[19][70] which avoid the coupling loss problems of I.O. devices but their use requires a relatively large channel spacing (>10nm). For dense WDM applications and Optical FDM attention, in recent years, has been particularly focussed on Silica-on-Silicon technology. The attraction of WDM devices using MZIs in integrated optic form is the ease with which many elements can be cascaded on the same substrate simply by taking advantage of conventional photolithographic techniques. In addition, the small bend radii[43] which is possible in Silica-on-Silicon technology(4mm) allows better use of the space available on the substrate (when compared with other I.O. technologies) to produce many MZI elements with varying ΔL values. Other advantages are low propagation loss (0.1dB/cm) and good matching of channel waveguide mode profiles with those of single-mode fibres (giving low coupling loss). Cascading of several carefully designed MZI elements increases the multi/demultiplexing capability. For a layout such as that shown in Figure 2.13, multiplexing of four equally-spaced wavelengths is possible. The first two parallel MZI elements each combine two of the input

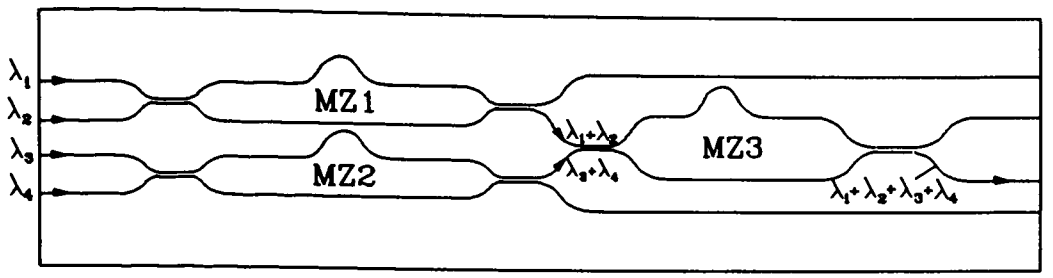

Figure 2.13 : Four Channel Demultiplexer using MZI elements

wavelengths, as shown. The third MZI element is designed so that all the input wavelengths are transmitted out of the same arm. This requires that the periodicity of the first two MZIs is twice that of the third MZI. For multi/demultiplexing of N channels, the device layout requires cascading of $\log_2 N$ MZIs, each with appropriate setting for periodicity. The setting is accomplished by precise fabrication of the two waveguide arms of the interferometers so that their path-length period corresponds to the required period. Both eight and sixteen channel devices have been demonstrated with channel separations ranging from 0.008nm-250nm[71]. Extinction ratios of $<$-15dB were obtained for both devices. Insertion losses are as low as 0.5dB for wide channel-spacing but increase to between 2-5dB for devices designed for Optical FDM applications. The transmission function of each MZI element can be tuned by thermal variation of the path-length difference. This has been demonstrated[72] by placing thin chromium strips above the channel waveguides to act as resistive heating, each with a time constant of about 1msec. Tuning over the complete periodic range of a MZI is possible via $\lambda/2$ variation of the path-length difference. Thermal tuning is fairly slow, however, so there is great interest in finding an electro-optic technique of inducing a phase retardation in silica waveguides.

The major difficulty with Mach-Zehnder WDM devices fabricated in I.O form is the tight fabrication tolerances which require advanced photolithography techniques.

Tuning is also a problem since it requires a multistage control operation and, despite the low fibre coupling loss for devices produced on Silica-on-Silicon substrates, multichannel devices still suffer interfacing problems because multiple fibre connection is required. However, the advantages of narrow channel spacing, large tuning ranges and high packing density remain.

2.5 Development of Fibre-Overlay Device Structure

Initial investigation of the fibre-overlay device structure which is the subject of this thesis was reported in 1987[73]. Refractive index oils, supported by thin spacers and a polished fused-silica superstrate, were employed as the overlay waveguide. A channel-dropping filter response was obtained when the devices were wavelength scanned. Thick (81μm) and thin (1μm) overlay devices were characterised in terms of insertion loss, rejection ratio of dropped-channel and channel spacing. No details about channel linewidth were supplied. For the thin overlay situation, off-resonance insertion loss was approximately 0.5dB while the channel rejection ratio was 25dB. Only one resonance minimum in the fibre transmission was observed for the wavelength scan range (1.2μm-1.6μm). The thick overlay device performance was similar in terms of rejection ratio, a value of 20dB being reported, but insertion loss was significantly higher, ranging between 1 and 4dB. Channel spacing was 13nm with the overall spectral response similar to that of a comb filter. No information was given concerning the coupling strength (remaining cladding thickness) of the polished fibre half-blocks used in the experimental investigation.

The same research group also reported on a switch structure which used a second polished fibre half-block to collect the power coupled into the overlay waveguide[74]. Experimental investigations involved the use of refractive index oils and also an anisotropic nematic liquid crystal as the overlay (interlay) waveguide. Active control of the output power of the adjacent arms of the switch was achieved by piezoelectrically varying the thickness of the oil waveguide layer and electro-optically varying the refractive index of the liquid crystal waveguide

layer, respectively. The best crosstalk observed (ratio of power in top fibre to that in input fibre) was 22dB for the liquid crystal overlay (interlay) device at a drive voltage of 300V. The spectral response of the switch structure with an oil overlay waveguide was also recorded and showed close agreement with a theoretical model. Wavelength-dependent power transfer from input fibre to top fibre was observed which agreed with the earlier results for the single fibre structure. No specific channel spacings or linewidths were quoted. Similarly, insertion loss was not stated but appeared to be in the region of 2dB (off-resonance) for the "straight-through" arm while no details of the coupling strength (remaining cladding thickness) of the polished fibre half-blocks were provided.

The results presented in the two papers mentioned above[73][74] prompted the research work which is described in this thesis. Several improvements in the experimental performance of both the single fibre-overlay device structure and the switch structure have since been demonstrated and are presented and described in the following chapters.

References

1. T. Miki and H. Ishio,"Viabilities of wavelength-division-multiplexing transmission system over an optical fibre cable", IEEE Commun., **COM-31**, pp1095-1102, 1983.

2. Y. Fujii, K. Aoyama and J. Minowa,"Optical demultiplexer using a silicon echelette grating", IEEE J. Quantum Electron., **QE-16**, pp165-169, 1980.

3. R. Erdmann,"Prism gratings for fiber optic multiplexing", Proc. SPIE, Fiber Optics Multiplexing and Modulation, **417**, pp12-17, 1983.

4. R. Watanabe, K. Nosu, T. Harada and T. Kita,"Optical demultiplexer using concave grating in 0.7-0.9 micron wavelength region", Electron. Lett., **16**, pp106-107, 1980.

5. H. Ishio, J. Minowa and K. Nosu,"Review and status of wavelength-division-multiplexing technology and its application", J. Lightwave Technol., **LT-2**, pp448-463, 1984.

6. K. Kobayashi and M. Seki,"Microoptic grating multiplexers and optical isolators for fibre-optic communications", IEEE J. Quantum Electron., **QE-16**, pp11-22, 1980.

7. Y. Fujii and J. Minowa,"Optical demultiplexer using a silicon concave diffraction grating", Appl. Opt., **22**, pp974-978, 1983.

8. J. Lipson, W.J. Minford, E.J. Murphy, T.C. Rice, R.A. Linke and G.T. Harvey,"A six-channel wavelength multiplexer and demultiplexer for single-mode systems", J. Lightwave Technol., **LT-3**, pp1159-1161, 1985.

9. T. Suhura, Y. Handa, H. Nishihara and J. Koyama,"Monolithic integrated micrograting and photodiodes for wavelength demultiplexing", Appl. Phys. lett., **40**, pp120-122, 1982.

10. C.A. Villarruel and R.P. Moeller,"Fused single-mode fibre access couplers", Electron. Lett., **17**, pp243-246, 1981.

11. R.A. Bergh, G. Kotler and H.J. Shaw,"Single-mode fibre-optic directional coupler", Electron. Lett., **16**, pp260-261, 1980.

12. R.V. Schmidt and R.C. Alferness,"Directional coupler switches, modulators and filters using alternating $\Delta\beta$ techniques", IEEE Trans. Circuits Syst., **CAS-26**, pp1099-1108, 1979.

13. A. Neyer,"Electro-optic X-switch using single-mode Ti:$LiNbO_3$ channel waveguides", Electron. Lett., **19**, pp553-554, 1983.

14. H. Takeuchi, K. Nagata, H. Kawaguchi and K. Oe,"GaAs/AlGaAs directional coupler switch with submillimeter device length", Electron. Lett., **22**, pp1241-1243, 1986.

15. A. Carenco and L. Menigaux,"InP electro-optic directional coupler", Appl. Phys. Lett., **40**, pp653-655, 1982.

16. D. Marcuse, *Theory of Dielectric Optical Waveguides*, Academic Press, 2nd Ed., 1991.

17. S-M Tseng and C-L Chen,"Side-polished fibres", Appl. Opt., **31**, pp3438-3447, 1992.

18. M.J.F. Digonnet and H.J. Shaw,"Analysis of a tunable single mode optical fibre coupler", IEEE J. Quantum Electron., **QE-18**, pp746-754, 1982.

19. M.J.F. Digonnet and H.J. Shaw,"Wavelength multiplexing in single-mode fiber couplers", Appl. Opt., **22**, pp484-491, 1983.

20. M.S. Whalen and K.L. Walker,"In-line optical-fibre filter for wavelength multiplexing", Electron. Lett., **21**, pp724-725, 1985.

21. R. Zengerle and O. Leminger,"Wavelength-selective directional coupler made of nonidentical single-mode fibers", J. Lightwave Technol., **LT-4**, pp823-827, 1986.

22. R. Zengerle and O. Leminger,"Narrow-band wavelength selective directional-coupler made of dissimilar optical fibres", J. Lightwave Technol, **LT-5**, pp1196-1198, 1987.

23. C-J Chung and A. Safaai-Jazi,"Narrow-band spectral filter made of W-index and step-index fibres", J. Lightwave Technol., **LT-10**, pp42-45, 1992.

24. B.S. Kawasaki, K.O. Hill and R.G. Lamont,"Biconical-taper single-mode fiber coupler", Opt. Lett., **6**, pp327-328, 1981.

25. T. Bricheno and A. Fielding,"Stable low-loss single-mode couplers", Electron. Lett., **20**, pp230-232, 1984.

26. K.P. Koo and D.C. Tran,"Glass-gel-coated single-mode-fibre coupler with programmable power splitting ratio", Electron. lett., **18**, pp941-942, 1982.

27. T.V. Clapp, T. Bricheno and S. Day,"Low-power, optically switched fibre directional coupler", Electron. Lett., **25**, pp157-159, 1989.

28. M.N. McLandrich, R.J. Orazi and H.R. Marlin,"Polarisation independent narrow channel wavelength division multiplexing fiber couplers for 1.55μm", J. Lightwave Technol., **9**, pp442-447, 1991.

29. I. Bennion, D.C.J. Reid, C.J. Rowe and W.J. Stewart,"High reflectivity monomode-fibre grating filters", Electron. Lett., **22**, pp341-343, 1986.

30. C.J. Rowe, I. Bennion and D.C.J. Reid,"High-Reflectivity surface relief gratings in single-mode optical fibres", IEE Proc. Pt. J., **134**, pp197-202, 1987.

31. C.M. Ragdale, D. Reid, D.J. Robbins, J. Buus and I. Bennion,"Narrowband fiber grating filters", IEEE J. Select. Areas in Communs., **8**, pp1146-1150, 1990.

32. M.S. Whalen, D.M. Tennant, R.C. Alferness, U. Koren and R. Bosworth,"Wavelength-tunable single-mode fibre grating reflector", Electron. Lett., **22**, pp1307-1308, 1986.

33. W.V. Sorin, P. Zorabedian and S.A. Newton,"Tunable single-mode fiber reflective grating filter", J. Lightwave Technol., **LT-5**, pp1199-1202, 1987.

34. S. Iraj-Najafi,"Glass directional coupler wavelength filters", Appl. Opt., **27**, pp1386-1388, 1988.

35. R.C. Alferness and R.V. Schmidt,"Tunable optical waveguide directional coupler filter", Appl. Phys. Lett., **33**, pp161-163, 1978.

36. B. Broberg, B.S. Lindgren, M.G. Oberg and H. Jiang,"A novel integrated optics wavelength filter in InGaAsP-InP", J. Lightwave Technol., **LT-4**, pp196-203, 1986.

37. M. Kawachi,"Silica waveguides on silicon and their application to integrated-optic components", Opt. and Quantum Electron., **22**, pp391-416, 1990.

38. R.V. Ramaswamy,"Ion-exchanged glass waveguides. A review", J. Lightwave Technol., **LT-6**, pp984-1002, 1988.

39. R.R.A. Syms,"Advances in channel waveguide lithium niobate integrated optics", Opt. and Quantum Electron., **20**, pp189-213, 1988.

40. E. Garmire,"Semiconductor components for monolithic applications", in *Integrated Optics*, T. Tamir, Ed., Springer-Verlag, pp243-304, 1985.

41. N. Takato and A. Sugita,"Silica-based single-mode waveguides and their applications to integrated-optic devices", Mat. Res. Soc. Symp. Proc., **172**, pp253-264, 1990.

42. S. Iraj-Najafi, W.J. Wang, J.F. Currie, R. Leonelli and J.L. Brebner,"Fabrication and characterisation of neodymium-doped glass waveguides", IEEE Photon. Technol. Lett., **1**, pp109-110, 1989.

43. T. Kitagawa, K. Hattori, M. Shimizu, Y. Ohmori and M. Kobayashi,"Guided-wave laser based on erbium-doped silica planar lightwave circuit", Electron. Lett., **27**, pp334-335, 1991.

44. H.C. Cheng and R.V. Ramaswamy,"Symmetrical directional coupler as a wavelength multiplexer-demultiplexer: Theory and experiment", IEEE J. Quantum Electron., **QE-27**, pp567-574, 1991.

45. F. Xiang and G.L. Yip,"A new Y-branch wavelength multi/demultiplexer by K and Ag ion-exchange for $\lambda=1.31\mu m$ and $\lambda=1.55\mu m$", Tech. Digest GRIN '92 (University of Santiago de Compostela, Spain), pp56-59, 1992.

46. R.C. Alferness and J.J. Veselka,"Simultaneous modulation and wavelength multiplexing with a Ti:$LiNbO_3$ directional coupler filter", Electron Lett. **21**, pp466-467, 1985.

47. F. Farjady and M.G.F. Wilson,"New application for nonlinear directional coupler: intensity controlled tunable optical filter", Electron. Lett., **27**, pp2218-2219, 1991.

48. C. Wu, C. Rolland, N. Puetz, R. Bruce, K.D. Chik and J.M. Xu,"A vertically coupled InGaAsP/InP directional coupler filter of ultranarrow bandwidth", IEEE Photon. Technol. Lett., **3**, pp519-521, 1991.

49. S. Harris, S. Nieh and R. Feigelson,"$CaMoO_4$ electronically tunable optical filter", Appl. Phys. Lett., **17**, pp223-225, 1970.

50. B.L. Heffner, D.A. Smith, J.E. Baran, A. Yi-Yan and K.W. Cheung,"Integrated-optic acoustically tunable infrared optical filter", Electron. Lett., **24**, pp1562-1563, 1988.

51. F. Heismann, L. Buhl and R.C. Alferness,"Electro-optically tunable narrowband Ti:$LiNbO_3$ wavelength filter", Electron. Lett., **23**, pp572-574, 1987.

52. K-W Cheung,"Acoustooptic tunable filters in narrowband WDM networks; systems issues and network applications", IEEE J. on Select. Areas in Comms., **8**, pp1015-1025, 1990.

53. D.A. Smith, J.E. Baran, J.J. Johnson and K-W Cheung,"Integrated-optic acoustically-tunable filters for WDM networks", IEEE J. on Select. Areas in Comms., **8**, pp1151-1159, 1990.

54. R.C. Alferness,"Efficient waveguide electro-optic TE-TM mode converter/wavelength filter", Appl. Phys. Lett., **36**, pp513-515, 1980.

55. W.P. Risk, G.S. Kino and B.T. Khuri-Yakuk,"Tunable optical filter in fiber optic form", Opt. Lett., **11**, pp578-580, 1986.

56. W. Warzanskyj, F. Heismann and R.C. Alferness,"Polarisation-independent electro-optically tunable narrow-band wavelength filter", Appl. Phys. Lett., **53**, pp13-15, 1988.

57. D.A. Smith, J.E. Baran, K.W. Cheung and J.J. Johnson,"Polarisation-independent acoustically-tunable optical filter", Appl. Phys. Lett., **56**, pp209-211, 1990.

58. H.A. McLeod, *Thin film optical filters*, Adam Hilger Ltd, 1986.

59. J. Minowa and Y. Fujii,"Dielectric multilayer thin film filters for WDM transmission systems", J. Lightwave Technol., **LT-1**, pp116-121, 1983.

60. J. Minowa and Y. Fujii,"High performance bandpass filter for WDM transmission", Appl. Opt., **23**, pp193-194, 1984.

61. J.M. Vaughan, *The Fabry-Perot Interferometer: history, theory, practice and applications*, Adam-Hilger, 1989.

62. H.R. Hicks, N.K. Reay and P.D. Atherton,"The application of capacitance micrometry to the control of Fabry-Perot etalons", J. Phys E, Sci. Instrum., **17**, pp49-55, 1984.

63. A.A.M. Saleh and J. Stone,"Two-stage Fabry-Perot filters as demultiplexers in optical FDMA LANs", J. Lightwave Technol., **LT-7**, pp323-330, 1989.

64. S.R. Mallinson,"Wavelength-selective filters for single-mode fiber WDM systems using Fabry-Perot interferometers", Appl, Opt., **26**, pp430-436, 1989.

65. J. Stone and L.W. Stulz,"Pigtailed high-finesse tunable fiber Fabry-Perot interferometers with large, medium and small free spectral range", Electron. Lett., **23**, pp781-783, 1987.

66. A. Frenkel and C. Lin,"In-line tunable etalon filter for optical channel selection in high density wavelength division multiplexed fiber systems", Electron. Lett., **24**, pp159-161, 1988.

67. C. Lin, H. Kobrinski, A. Frenkel and C.A. Brackett,"Wavelength tunable 16 optical channel transmission experiment at 2Gb/s and 600Mb/s for broadband subscriber distribution", Electron. Lett., **24**, pp1215-1217, 1988.

68. J.S. Patel, M.A. Saifi, D.W. Berreman, C. Lin, N. Andreadakis and S.D. Lee,"Electrically tunable optical filter for infrared wavelength using liquid crystals in a Fabry-Perot etalon", Appl. Phys. Lett., **57**, pp1718-1720, 1990.

69. N. Takato, T. Kominato, A. Sugita, K. Jinguji, H. Toba, and M. Kawachi,"Silica-based integrated optic Mach-Zehnder multi/demultiplexer family with channel spacing 0.01-250nm", IEEE J. on Select. Areas in Comms., **8**, pp1120-1127, 1990.

70. A.C. Boucouvalas and G. Georgiou,"Fiber optic interferometric electrically tunable filter using the thermo-optic effect", Proc. SPIE, **585**, pp132-135, 1985.

71. K. Oda, N. Takato, T. Kominato, and H. Toba,"A 16-channel frequency selection switch for optical FDM distribution systems", IEEE J. on Select. Areas in Comms., **8**, pp1132-1140, 1990.

72. H. Toba, K. Oda, K. Nosu and N. takato,"Factors affecting the design of optical FDM information distribution systems", IEEE J. on Select. Areas in Comms., **8**, pp965-972, 1990.

73. C.A. Millar, M.C. Brierley and S.R. Mallinson,"Exposed-core single-mode-fiber channel-dropping filter using a high-index overlay waveguide", Opt. Lett., **12**, pp284-286, 1987.

74. J.V. Wright, S.R. Mallinson and C.A. Millar,"A fiber-based crosspoint switch using high-index refractive index interlay materials", IEEE J. on Select. Areas in Comms., **6**, pp1160-1167, 1988.

CHAPTER 3

Device Operation - Analytical Methods

3.1 Introduction

This chapter introduces some fundamental waveguide theory and gives a description of two methods of analysing the device structure shown schematically in Figure 1.3. An exact theoretical model of the device is very difficult to achieve and outwith the objectives of this thesis. The aim of this chapter is to analyse the basic fibre-overlay structure in a general sense and identify trends in device behaviour, with respect to the overlay parameters, which can be utilised in the design of practical devices.

Several important design parameters can be identified by treating the device geometry as:

(i) two parallel slab waveguides in close proximity
(ii) a multilayer waveguide system

In both cases the fibre is replaced by an equivalent single-mode slab waveguide possessing the same propagation constant and transverse optical field distribution, perpendicular to the plane of the overlay waveguide. Case (i) can be analysed using coupled-mode theory[1], although this technique, which relies on a perturbation approach, is most accurate for identical waveguides in a weak coupling situation. The advantage of analysis by coupled-mode theory is that for weakly coupled waveguides, significant power transfer occurs only on phase-matching of adjacent waveguide propagation constants. As a result, a great deal of information concerning device behaviour can be obtained by simple manipulation of the overlay waveguide parameters via equation 1.1. This approach was preferred in this thesis since it allowed discussion of device behaviour in a more simplified fashion. Case (ii)

requires that the normal or compound modes of propagation of the multilayer system are obtained. A matrix method[2] can be used which relates the Fresnel reflection and transmission coefficients at each layer interface and calculates the corresponding normal mode field distributions numerically. The input power is distributed among these normal modes which possess different propagation constants and this causes beating of the power between different waveguide layers.

3.2 Slab Waveguide Analysis

It was mentioned in Chapter 1 that the operation of the fibre-overlay device is highly dependent on response of the overlay waveguide to variations in index, thickness and input wavelength. It is, therefore, useful at this point to include an analysis of a simple slab (or planar) waveguide in terms of these parameters, prior to analysing the entire structure. The overlay slab waveguide in Figure 1.3 is capable of supporting a discrete number of guided waves or modes of propagation (mode structure) for a given parameter set. Device operation can be related to the behaviour of the mode structure when the parameters are varied. The guided modes of the waveguide in question are obtained from the solution of the eigenvalue equation, which is derived from Maxwell's equations subject to the boundary conditions imposed by the waveguide geometry.

3.2.1 Guided Modes and the Eigenvalue Equation

Figure 3.1 shows a typical example of an asymmetric slab waveguide, consisting of a thin dielectric layer sandwiched between two semi-infinite bounding media. The structure is unbounded in the y-direction. In general, for the geometry shown in Figure 3.1 to function as a waveguide, the refractive index of the guiding layer (or core) must exceed those of the surrounding media. Additionally, the thickness of the guiding layer, d, should be on the order of the wavelength of the input light. To obtain the guided modes of the waveguide, it is then necessary to apply Maxwell's equations to each segment of the structure and match the boundary conditions at each dielectric interface.

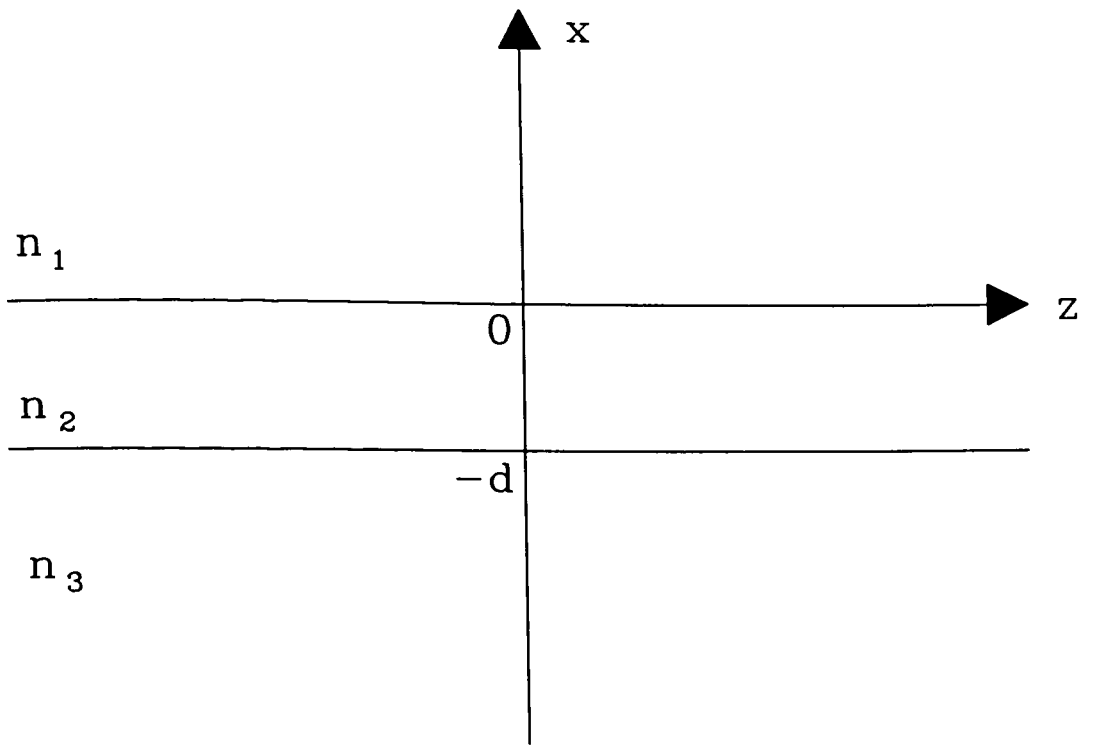

Figure 3.1 : Schematic representation of an asymmetric slab waveguide

The refractive index of the asymmetric slab waveguide can be written as:

$$n(x) = n_1 , \qquad 0 \leq x$$

$$n(x) = n_2 , \quad -d \leq x \leq 0 \tag{3.1}$$

$$n(x) = n_3 , \qquad x \leq -d$$

and it is assumed that $n_1 < n_3 < n_2$. Maxwell's equations can be written in the form

$$\nabla \times H = i\omega \epsilon_o n^2 E \quad , \quad \nabla \times E = -i\omega \mu H \tag{3.2}$$

where ω is the angular frequency and n is the refractive index profile of the medium,

in this case given by eqn.(3.1). The electric and magnetic field vectors are E and H, respectively, ϵ_o is the dielectric permittivity of free space, μ is the permeability of the medium. For this analysis, the permeability is taken to be that of free space since the materials are assumed to be non-magnetic while the relative permittivity is taken as $\epsilon_r=n^2$. The entire structure is homogeneous in the z-direction and, thus, the solutions to the wave eqns.(3.2) can be written as:

$$E(x,t) = E_m(x)\exp[i(\omega t - \beta_m z)] \tag{3.3}$$

$$H(x,t) = H_m(x)\exp[i(\omega t - \beta_m z)] \tag{3.4}$$

where $E_m(x)$ and $H_m(x)$ are the wavefunctions of the guided modes, t is time, β_m is the z-component of the wavefunctions and called the propagation constant and m is an integer designating the mode number. The general wave equation for the structure can be obtained by eliminating H from eqns.(3.2) via substitution. i.e.

$$\nabla \times (\nabla \times E) = \omega^2 \mu \epsilon_o n^2 E \tag{3.5}$$

Then using the vector identity

$$\nabla \times (\nabla \times E) = \nabla(\nabla.E) - \nabla^2 E \tag{3.6}$$

and noting $\nabla.\mathbf{E} = 0$ for source-free, homogeneous media yields:

$$\nabla^2 E + \omega^2 \mu \epsilon_o n^2 E = 0 \tag{3.7}$$

Completing the differentiation leaves:

$$\frac{\partial^2 E_m(x)}{\partial x^2} + [(\frac{\omega}{c} n)^2 - \beta^2] E_m(x) = 0 \tag{3.8}$$

where $c=(\mu_o\epsilon_o)^{1/2}$ is the speed of light and $\mu=\mu_o\mu_r$ with $\mu_r=1$. Eqn.(3.8) is in

standard second-order differential equation form with solutions which vary either exponentially or sinusoidally depending on the value of β (since ω, c and n in each region are fixed).

The relevant boundary conditions require that the tangential components of both the E and H fields are continuous at the dielectric interfaces. In addition, for confined modes, the field amplitude must decay exponentially to zero outwith the guiding region, thus indicating the required nature of the field in regions 1 and 3. For continuity of the field, the solution in region 2 must, therefore, be sinusoidal. These conditions impose a restriction on the values β can assume:

$$\beta < \frac{\omega}{c} n_2 \quad , \quad \beta > \frac{\omega}{c} n_3 \tag{3.9}$$

recognising that $n_3 > n_1$. The polarisation of the modes of the waveguide can be either Transverse Electric (TE) or Transverse Magnetic (TM). The TE modes have their electric field normal to the x-z plane and possess only the field components, E_y, H_x and H_z. The TM modes possess the field components H_y, E_x and E_z.

3.2.2 Guided TE Modes

The electric field amplitude of the TE modes can be obtained by substituting $E_m(x)$ into eqn.(3.8), subject to the restrictions on β, and noting that the field amplitude must decay to zero at $x = \pm\infty$. This yields the general solution:

$$\begin{aligned} E_m(x) &= A\exp(-ax) \quad , \quad x \geq 0 \\ E_m(x) &= B\cos(hx + \gamma) \quad , \quad -d \leq x \leq 0 \\ E_m(x) &= C\exp(b[x + d]) \quad , \quad x \leq -d \end{aligned} \tag{3.10}$$

where

$$h = \left[\left(\frac{\omega}{c}n_2\right)^2 - \beta^2\right]^{1/2}$$

$$a = \left[\beta^2 - \left(\frac{\omega}{c}n_1\right)^2\right]^{1/2} \quad , \quad b = \left[\beta^2 - \left(\frac{\omega}{c}n_3\right)^2\right]^{1/2}$$

and A, B and C are related constants while γ indicates that the solutions are, in general, neither exact even or odd functions (unlike a symmetric waveguide). To be acceptable solutions, the tangential components of the electric and magnetic fields, E_y and H_z, must be continous across the dielectric interfaces. H_z can be related to E_y by manipulation of eqn.(3.2) to give $H_z=(i/\omega\mu)^{-1}\partial E_y/\partial x$. Therefore, both the magnitude and gradient of $E_m(x)$ must be matched (since $\omega\mu$ is constant) at the interfaces, x=0 and x=-d. Combining the resultant equations relating the constants A, B, C and γ yields:

$$\tan\gamma = \frac{a}{h} \quad , \quad \tan(hd - \gamma) = \frac{b}{h} \qquad \textbf{(3.11)}$$

which can be referred to as the mode condition. Noting that

$$\tan(\theta) = \tan(\theta \pm n\pi)$$

allows eqns.(3.11) to be written as:

$$\gamma = \tan^{-1}\left(\frac{a}{h}\right) \mp p\pi \qquad \textbf{(3.12)}$$

$$hd - \gamma = \tan^{-1}\left(\frac{b}{h}\right) \mp q\pi \qquad \textbf{(3.13)}$$

Recognising that the propagation constant $\beta_m=k_0n_{em}$, where n_{em} is called the effective index of the mode and $k_0=\omega/c$, simple addition then yields the familiar form of the

eigenvalue equation for an asymmetric slab waveguide:

$$k_o d\sqrt{n_2^2 - n_{e_m}^2} = m\pi + \phi_1^{TE} + \phi_3^{TE} \quad , \quad m = 0,1,.. \qquad (3.14)$$

where

$$\phi_1^{TE} = \tan^{-1}\sqrt{\frac{n_{e_m}^2 - n_1^2}{n_2^2 - n_{e_m}^2}} \quad , \quad \phi_3^{TE} = \tan^{-1}\sqrt{\frac{n_{e_m}^2 - n_3^2}{n_2^2 - n_{e_m}^2}} \qquad (3.15)$$

The eigenvalue equation is an important tool in predicting device behaviour and can be solved either graphically or numerically to give the effective indices of the guided modes. The resulting TE mode fields can then be obtained by substituting the corresponding propagation constants back into eqns.(3.10) giving:

$$E_y(x,z,t) = B\cos(\gamma)\exp(-ax)\exp(\omega t - \beta z) \quad , \quad x \geq 0$$

$$E_y(x,z,t) = B\cos(hx + \gamma)\exp(\omega t - \beta z) \quad , \quad -d \leq x \leq 0$$

$$E_y(x,z,t) = B\cos(hd - \gamma)\exp(b[x + d])\exp(\omega t - \beta z) \quad , \quad x \leq -d$$

where γ is obtained from eqn.(3.12) or (3.13).

3.2.3 Guided TM Modes

The TM polarised guided modes are derived in a similar manner to the TE case, the significant difference arising when the boundary conditions are imposed. For TM modes the tangential field components are H_y and E_z. From eqn.(3.2):

$$E_z = \frac{-i}{\omega \epsilon_o n^2}\frac{\partial H_y}{\partial x} \qquad (3.16)$$

Inspection of eqn.(3.16) indicates that the refractive index of the layer on each side of an interface plays a part in establishing continuity conditions. The resulting mode condition, derived as before and analogous to eqns.(3.11), then becomes:

$$\tan\gamma' = \left(\frac{n_2^2}{n_1^2}\right)\frac{a}{h} \quad , \quad \tan(ht - \gamma') = \left(\frac{n_2^2}{n_3^2}\right)\frac{b}{h} \qquad (3.17)$$

Note the dependence of the mode condition on the ratio of the index of the surrounding layers to the index of the guiding region. This becomes a significant factor in terms of device behaviour when the overlay waveguide is very thin ($<3\mu$m), typically fabricated by vacuum deposition. The field distribution of the TM modes is of an identical form to the TE case except that γ is replaced by γ'. The corresponding eigenvalue equation for TM polarised guided modes is then:

$$k_o d\sqrt{n_2^2 - n_e^2} = m\pi + \phi_1^{TM} + \phi_3^{TM} \qquad (3.18)$$

where

$$\phi_1^{TM} = \tan^{-1}\left(\frac{n_2^2}{n_1^2}\right)\sqrt{\frac{n_{e_m}^2 - n_1^2}{n_2^2 - n_{e_m}^2}} \quad , \quad \phi_3^{TM} = \tan^{-1}\left(\frac{n_2^2}{n_3^2}\right)\sqrt{\frac{n_{e_m}^2 - n_3^2}{n_2^2 - n_{e_m}^2}} \qquad (3.19)$$

3.2.4 Slab Waveguide Mode Structure

The mode structure of a slab waveguide is a term which encompasses both the effective indices and field profiles of each guided (or supported) mode for a particular parameter set. Any variation of the waveguide parameters results in a corresponding change in the mode structure the waveguide supports.

The effective indices of a waveguide provide a simple, straightforward way in which to investigate the behaviour of the mode structure when subject to parameter

variation. Each mode effective index, n_{em}, can be obtained from the waveguide eigenvalue equation and is related to the corresponding mode propagation constant β_m, i.e. $n_{em}=\beta_m/k_o$. The value of n_{em} is the index "seen" by the light contained in mode m as it propagates along the waveguide. A computer program which solves the eigenvalue equation in a numerical fashion was developed to allow the effective indices of any slab waveguide to be found. The values of n_{em} for a typical waveguide are shown below:

Waveguide Details - Core Index $n_2=1.6$ Thickness $d=5\mu m$

Superstrate $n_1=1$ (Air) Substrate $n_3=1.447$ (Silica)

$\lambda=1.3\mu m$

TE Polarisation	TM Polarisation
$n_{e0} = 1.5956$	$n_{e0} = 1.5953$
$n_{e1} = 1.5823$	$n_{e1} = 1.5813$
$n_{e2} = 1.5600$	$n_{e2} = 1.5577$
$n_{e3} = 1.5287$	$n_{e3} = 1.5248$
$n_{e4} = 1.4885$	$n_{e4} = 1.4831$

For the waveguide being investigated, 5 modes (i.e.m=0-4) are supported for both polarisations. Inspection of the values confirms that all the effective indices lie within the range $n_3 < n_{em} < n_2$, as complying with conditions (3.9). Notice also that there is a slight difference between the values of corresponding TE and TM mode indices (known as waveguide birefringence). The number of modes the waveguide supports can be quite simply altered by varying an appropriate parameter. e.g. wavelength. With the same waveguide geometry as detailed above but with $\lambda=1.6\mu m$, the effective index values are (assuming all material indices remain fixed):

TE Polarisation	TM Polarisation
$n_{e0} = 1.5936$	$n_{e0} = 1.5931$
$n_{e1} = 1.5742$	$n_{e1} = 1.5724$
$n_{e2} = 1.5418$	$n_{e2} = 1.5378$
$n_{e3} = 1.4965$	$n_{e3} = 1.4902$

It can be observed that by increasing the input wavelength, the mode with m=4 can no longer be supported for the particular waveguide geometry in question. Effectively, the mode can be defined as having "cut-off", i.e. above a certain wavelength the guidance conditions for mode m=4 are no longer satisfied. Increasing the wavelength still further will, eventually, cause mode m=3 to become cut-off. Alternatively, decreasing the wavelength by a sufficient amount below $\lambda=1.3\mu m$ will cause the mode with m=5 to become supported i.e. it can be said to have "cut-on". Figure 3.2 shows how the mode structure of this particular waveguide behaves as the input wavelength is increased from $\lambda=1.0\mu m$ to $\lambda=1.8\mu m$, for both TE and TM polarisations. Essentially, the entire waveguide mode structure experiences a shift as λ is varied, with the degree of movement of the individual modes depending on the mode number, m.

The cut-off wavelength for mode m=4 can be obtained by substituting $n_{e4}=n_3$ into the eigenvalue equation (since this is the lower restriction on effective index) and solving for λ. The subsequent values are:

m=4 Cut-Off $\lambda^{TE} = 1.582\mu m$ $\lambda^{TM} = 1.545\mu m$

Note that the TM mode cuts-off at a lower wavelength and a further increase of 37nm would be required to remove the TE m=4 mode. The general condition for the cut-off wavelength of mode m is given by (assuming $n_3 > n_1$):

$$\lambda_m^{TE} = \frac{2\pi d\sqrt{n_2^2 - n_3^2}}{m\pi + \tan^{-1}\sqrt{\frac{n_3^2 - n_1^2}{n_2^2 - n_3^2}}} \qquad (3.20)$$

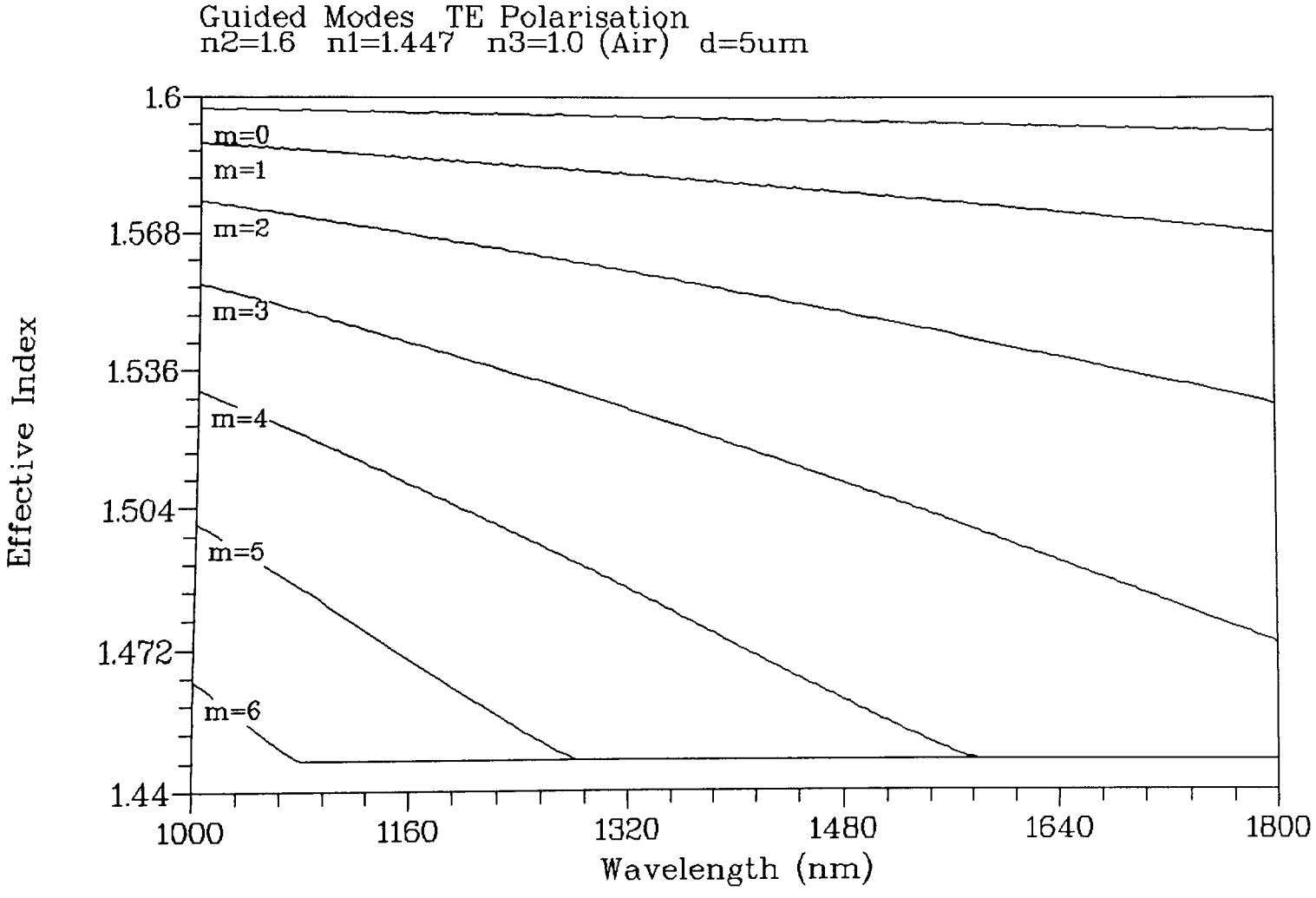

Figure 3.2 : Mode Dispersion with Wavelength

$$\lambda_m^{TM} = \frac{2\pi d\sqrt{n_2^2 - n_3^2}}{m\pi + \tan^{-1}\left(\frac{n_2^2}{n_1^2}\right)\sqrt{\frac{n_3^2 - n_1^2}{n_2^2 - n_3^2}}} \qquad (3.21)$$

For a symmetrical waveguide ($n_1=n_3$), the cut-off wavelength is the same for both polarisations. This is obvious from inspection of eqns.(3.20) and (3.21). The mode structure for the same device geometry but with $n_1=n_3=1.447$ (i.e. symmetric) and $\lambda=1.3\mu$m is shown below:

Waveguide Details -	Core Index	$n_2=1.6$	Thickness $d=5\mu$m
	Superstrate	$n_1=1.447$	Substrate $n_3=1.447$
	$\lambda=1.3\mu$m		
	TE Polarisation		TM Polarisation
	$n_{e0} = 1.5958$		$n_{e0} = 1.5956$
	$n_{e1} = 1.5832$		$n_{e1} = 1.5825$
	$n_{e2} = 1.5621$		$n_{e2} = 1.5608$
	$n_{e3} = 1.5328$		$n_{e3} = 1.5306$
	$n_{e4} = 1.4956$		$n_{e4} = 1.4931$
	$n_{e5} = 1.4541$		$n_{e5} = 1.4531$

Increasing the index of the superstrate, n_1, has resulted in a 6th mode being supported by the modified structure. The mode structure has been shifted upwards and mode m=5 has "cut-on". The shift is not consistent for each mode, being greater for the higher-order modes. Furthermore, the waveguide birefringence has decreased significantly. Additionally, mode m=4 will have a different cut-off wavelength in response to the change in n_1. The shifted cut-off wavelength is now:

m=4 Cut-Off $\lambda^{TE} = \lambda^{TM} = 1.707\mu$m

and the general cut-off condition for a symmetric guide is given by:

$$\lambda_m = \frac{2d}{m}\sqrt{n_2^2 - n_3^2} \qquad (3.22)$$

which is valid for both polarisations. The significance of the above results is that the cut-off wavelengths of the TE and TM modes converge as the waveguide becomes more symmetric. Notice that the m=0 mode is never cut-off i.e. $\lambda_0 = \infty$. Figure 3.3 illustrates this effect. Similar variation of the waveguide parameters d and n_2 also causes shifting of the mode structure. Increasing either of these parameters sufficiently results in an additional mode being supported. Figures 3.4 and 3.5 show the effect on the mode structure of increasing d and n_2, respectively. The waveguide has a guiding layer $n_2=1.6$ (value at $\lambda=1.3\mu$m), substrate $n_3=1.447$ and superstrate $n_1=1.0$ and thickness $d=5\mu$m. It can be seen from Figures 3.4 and 3.5 that increasing the wavelength or decreasing the material index causes the higher order modes to move towards cut-off i.e. the effective index of each successive highest order mode decreases until it reaches the substrate index and guiding ceases. This movement of the highest order mode towards cut-off has a major effect on the fibre-overlay device performance (in terms of resonance linewidth). The effective index of the fibre mode is essentially fixed relative to the overlay modes whose effective indices move due to parameter variation (particularly for index or thickness variation) and has a value slightly above that of fibre cladding/overlay substrate. Therefore, as each overlay mode is tuned towards cut-off it will approach the fibre mode value and become phase-matched to it at some value of wavelength or material index (resulting in power transfer) before cutting off. The spacing between resonances can be obtained by observing the wavelength or index at which the overlay mode effective indices equal that of the fibre mode using the equivalent wavelength or index response for the overlay under investigation. It is clear from the dispersion curves for the overlay mode effective indices, shown in Figures 3.2, 3.4 and 3.5 for wavelength, index and thickness variation, that the rate at which each overlay mode "scans" the fibre mode is not constant and depends on mode order. Therefore, it would be expected that the wavelength (index, thickness) range in which significant power transfer between fibre and overlay occurs will be related to

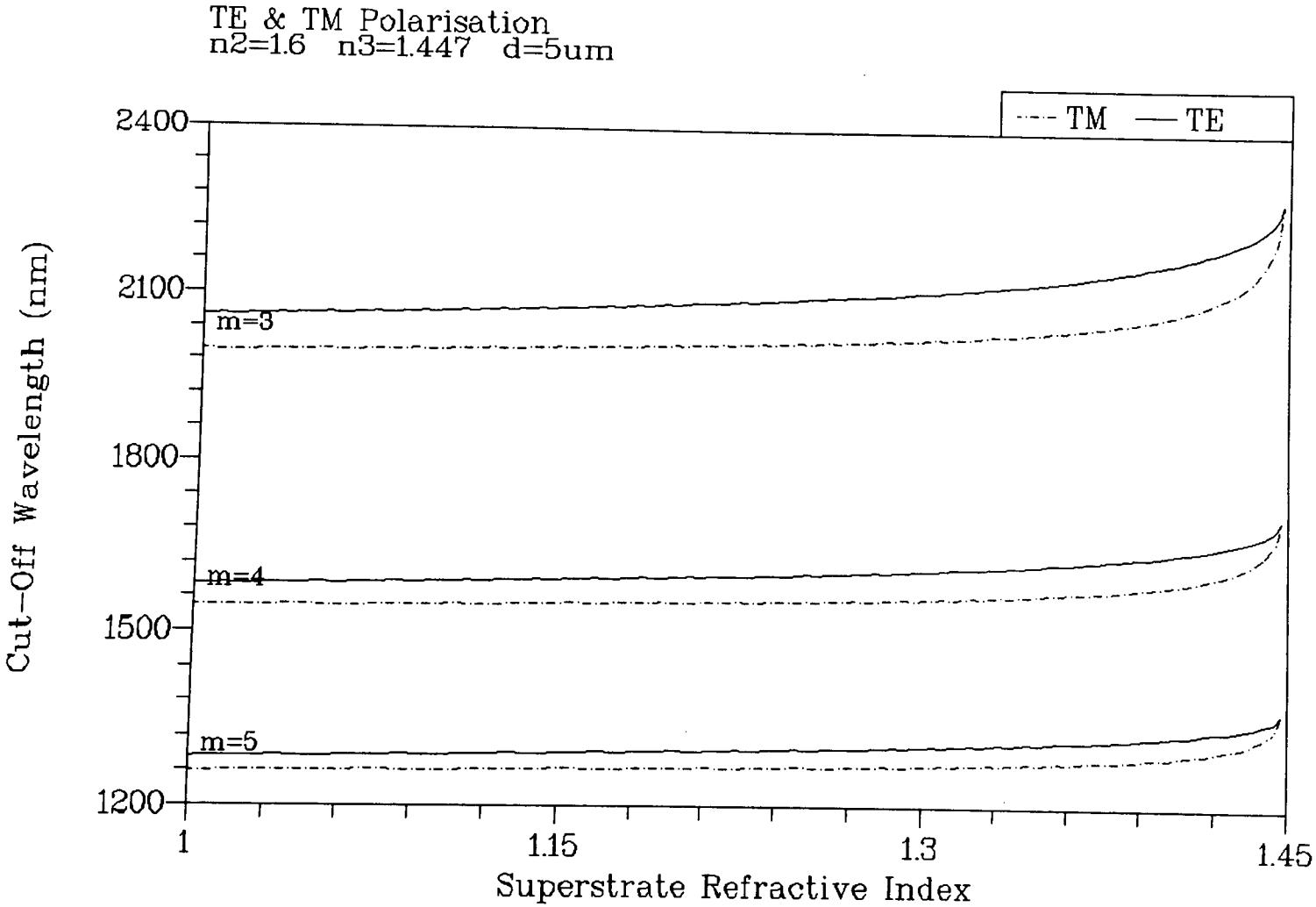

Figure 3.3 : Cut-Off Wavelength Variation

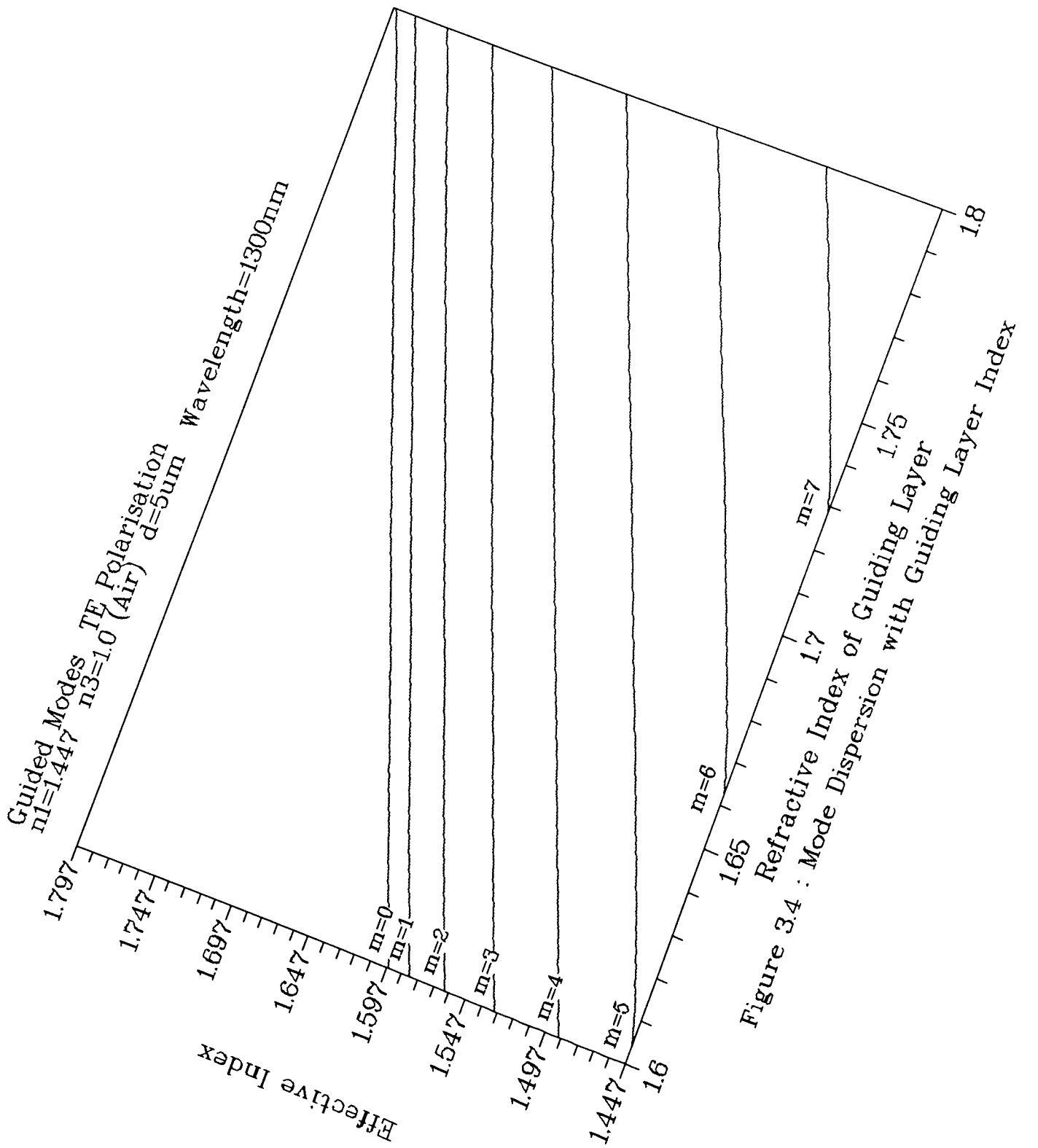

Figure 3.4 : Mode Dispersion with G

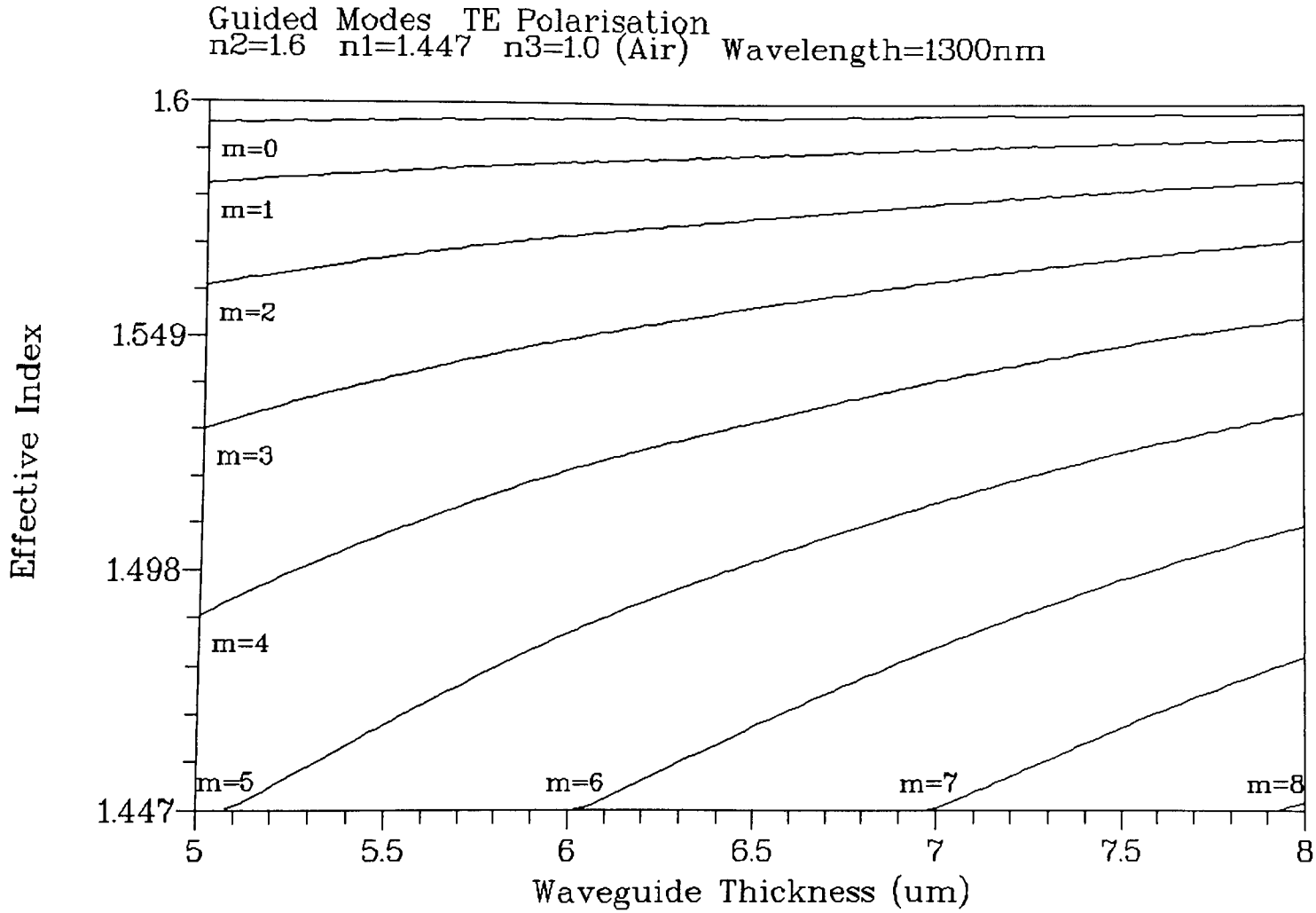

Figure 3.5 : Mode Dispersion with Waveguide Thickness

the gradient of the mode dispersion curves and, thus, mode order of the overlay waveguide. This suggests that the linewidth of the resonance dips in the transmission response of a fibre-overlay device will be influenced by the overlay dispersion. Further theoretical investigation of this effect is presented in section 3.3.2.

3.3 Coupled-Mode Theory

When two or more waveguides are in close proximity, the optical field distibution possessed by each (when in isolation) is perturbed by the presence of the other waveguides. This situation can be analysed using a mathematical technique known as coupled-mode theory[1][3]. This technique is most accurate when the individual waveguides are similar and are only weakly perturbed by (or coupled to) the adjacent guide(s)[4]. In this case it is possible to express the overall optical field distribution of the multi-waveguide system as a superposition of the simpler, known field distributions of the individual isolated waveguides. The structure displayed in Figure 1.3 is basically a single-mode waveguide separated from a multimode waveguide by a small amount of lower index dielectric material (fibre cladding). Although the structure is not ideally suited to analysis by coupled-mode theory (significant index differences), some meaningful information concerning device behaviour can be obtained through its use.

The modes of adjacent waveguides can become coupled as a result of the overlap (or penetration) of the evanescent tail of the field distribution on each waveguide. The evanescent tail of a guided mode is that part which extends into the cladding/substrate section of the waveguide, decaying exponentially with distance (laterally). For ease of analysis it is useful to assume a case where only two parallel waveguides are present. When energy is launched into guide 1 (assume single-mode in isolation) it is carried by the optical field distribution of the waveguide mode with a certain velocity and corresponding mode effective index. If the spacing between the two waveguides is small enough, the evanescent tail of the mode of guide 1 will overlap guide 2. If guide 2 is capable of supporting a guided mode with a phase

velocity (effective index) similar to that of the mode of guide 1, then power can couple between the two guides. The energy initially carried by guide 1 then oscillates between the two guides with distance along the propagation direction. It is appropriate at this stage to develop the solution to the field distribution for the situation where two single-mode slab waveguides (referred to as guide 1 and guide 2) are in close proximity, as shown in Figure 3.6.

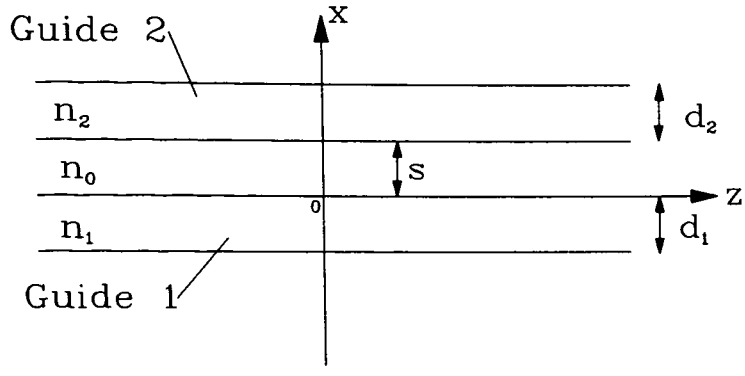

Figure 3.6 : Two parallel slab waveguides with separation s

The electric field distibution, E(x,z), for the two-waveguide system can be approximately represented as a combination of the isolated waveguide modes, $E_1(x)$ and $E_2(x)$ (possessing propagation constants β_1 and β_2, respectively) i.e.

$$E(x,z) = A_1(z)E_1(x)\, e^{-j\beta_1 z} + A_2(z)E_2(x)\, e^{-j\beta_2 z} \qquad (3.23)$$

where the coefficients $A_{1,2}(z)$ describe the contribution of each normalised isolated mode field to the overall field and $\beta_{1,2}$ are the isolated mode propagation constants. The coupled-mode equations relating the $A_{1,2}(z)$ coefficients can, after manipulation, be written in compact form as[5]:

$$\frac{dA_1}{dz} = -jC_{21}e^{j2\delta z}A_2$$
$$\frac{dA_2}{dz} = -jC_{12}e^{-j2\delta z}A_1 \qquad (3.24)$$

where

$$2\delta = (\beta_1 + M_{11}) - (\beta_2 + M_{22})$$

is called the phase mismatch. The quantities C_{12} and C_{21} are termed the coupling coefficients and are related to the overlap of the optical fields of the modes of guides 1 and 2. They are strongly influenced by the guide separation, s, and also the index difference between the guiding regions and the surrounding media. C_{12} and C_{21} are given by[5]:

$$C_{12} = \frac{\omega\epsilon_o(n_1^2 - n_o^2)}{4}\int_{d_1} E_1(x)\,E_2(x)\,dx$$
$$C_{21} = \frac{\omega\epsilon_o(n_2^2 - n_o^2)}{4}\int_{d_2} E_2(x)\,E_1(x)\,dx \qquad (3.25)$$

with d_1 and d_2 denoting the widths of guides 1 and 2 while ϵ_o is the free-space permittivity and $\omega=2\pi/k_o$ is the angular frequency. M_{11} and M_{22} represent a small correction to the propagation constants β_1 and β_2 , respectively, due to the presence of the adjacent guide and are given by:

$$M_{11} = \frac{\omega\epsilon_o(n_2^2 - n_o^2)}{4}\int_{d_2} [E_1(x)]^2\,dx$$
$$M_{22} = \frac{\omega\epsilon_o(n_1^2 - n_o^2)}{4}\int_{d_1} [E_2(x)]^2\,dx \qquad (3.26)$$

The differential equations eqns. (3.24) can be easily solved, and with the power P_1 and P_2 carried by guides 1 and 2 being proportional to the magnitude squared of the

coefficients $A_{1,2}(z)$, it can be shown that for $A_1(0)=A_1$ and $A_2(0)=0$ the power transfer between guides is given by:

$$P_1(z) = P_o - P_2(z)$$

$$P_2(z) = P_o \frac{C_{12}^2}{C_{12}C_{21} + \delta^2} \sin^2[(C_{12}C_{21} + \delta^2)^{1/2} z] \qquad (3.27)$$

where $P_o=A_1^2$. For the case of identical guides, the phase mismatch $2\delta=0$ and $C_{21}=C_{12}=C$. This results in 100% power transfer between the guides as illustrated in Figure 3.7. The propagation distance required for complete power transfer is known as the coupling length and given by $L_c= \pi/2C$. In a practical device such as a directional coupler, the number of coupling lengths contained within the device interaction length determines the power splitting ratio. It can be shown that the coupling coefficients decrease in an exponential-like manner with distance between the guides and this gives rise to a corresponding non-linear increase in coupling length. Figure 3.8 shows the effect of guide separation on the coupling coefficients at several wavelengths. For the structure shown in Figure 1.3, the two guides between which power transfer occurs (fibre and overlay) are obviously not identical. Therefore, although phase-matching can be achieved the coupling coefficients will always differ to some extent. From eqns. (3.27), the maximum power transfer occurs when $z=\pi/[2(C_{12}C_{21})^{1/2}]$ (assuming $\delta=0$) and this distance is termed the coupling length. At this condition, the maximum power that can be transferred is dependent upon the relationship between the coupling coefficients, reaching 100% when the coupling coefficients (and, therefore, waveguides) are identical.

3.3.1 Coupled-Mode Approach to Fibre-Overlay Device Behaviour

An attempt was made to qualitatively interpret the behaviour of the device structure shown in Figure 1.3 with the basis of coupled-mode theory outlined above. It was assumed that coupling was only ever significant between the highest order overlay mode and the single mode of the fibre and, therefore, only the coupling coefficients between these two modes required to be calculated. The optical fibre was replaced

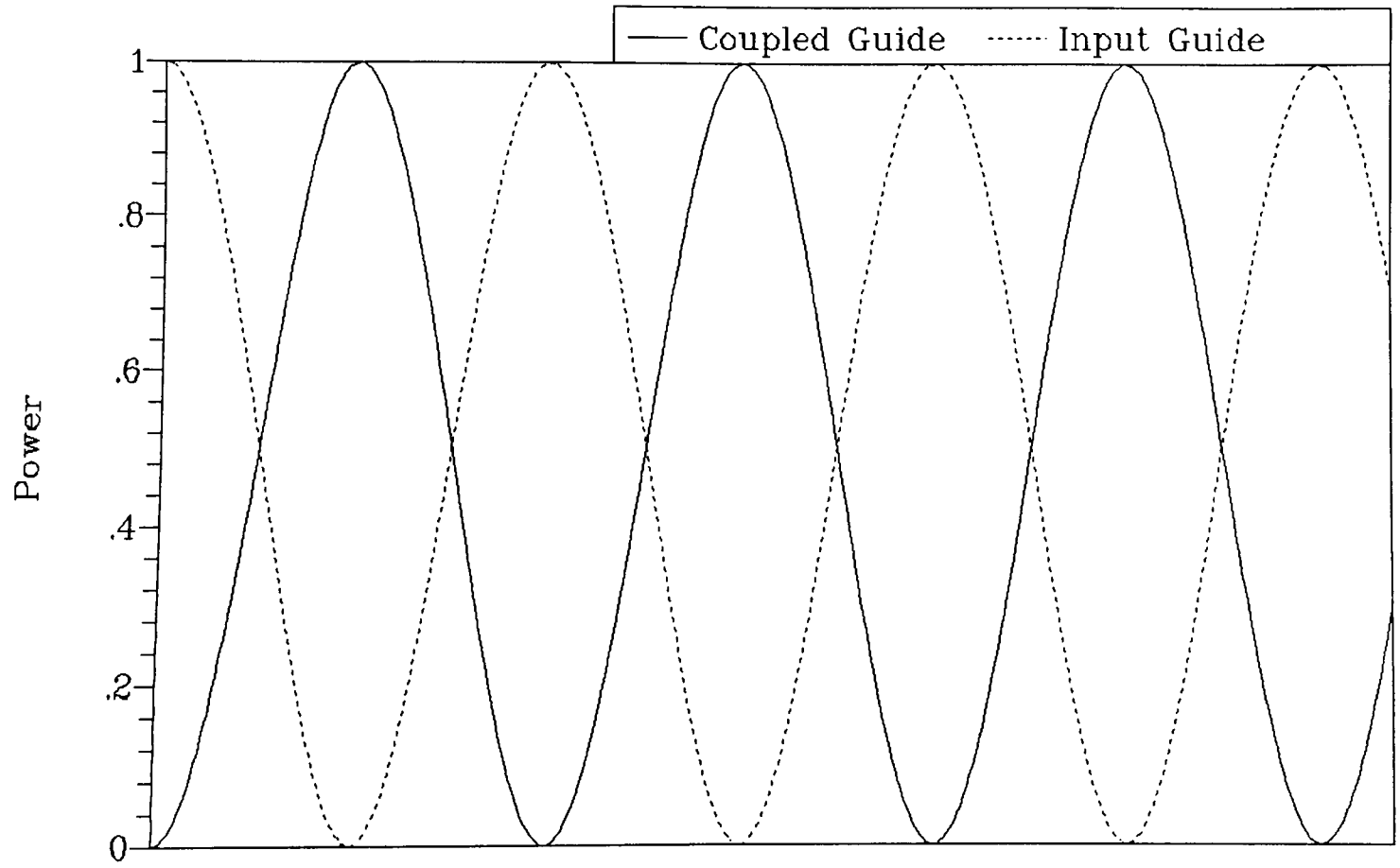

Figure 3.7 : Power transfer between identical guides

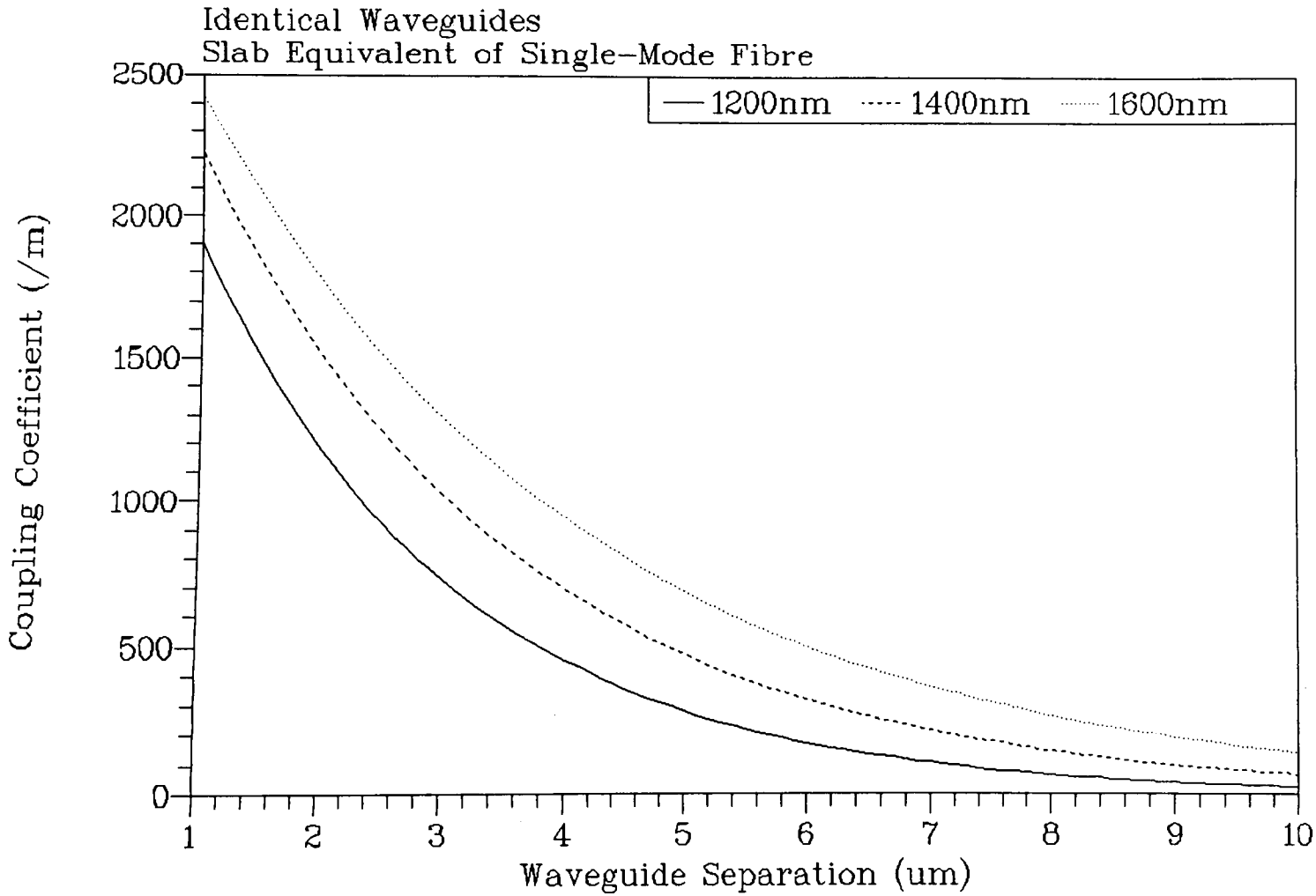

Figure 3.8 : Effect of guide separation on coupling coefficients

by an equivalent single-mode slab waveguide which possessed approximately the same propagation constant and transverse optical field distribution perpendicular to the plane of the overlay[6]. The resulting device geometry is a multimode slab waveguide in close proximity to a single-mode slab waveguide. From the analysis of a multimode slab waveguide performed earlier, the only mode capable of possessing a propagation constant close to that of the fibre mode is the highest order mode of the overlay. Based on this fact, it was assumed that coupling was only ever significant between the highest order overlay mode and the single mode of the fibre and, therefore, only the coupling coefficients between these two modes required calculation. The highly dissimilar nature of the two adjacent waveguides and mode field profiles suggests that the coupling coefficients C_{12} and C_{21} will be dissimilar. Figure 3.9 shows an example of the field profiles of the fibre mode and the highest order overlay mode below the phase-matching wavelength, at the phase-matching wavelength, and very close to cutoff (above the phase-matching wavelength). The field profiles were generated for a symmetrical overlay of 10μm thickness and refractive index 1.6 while the slab-equivalent model of the fibre was approximately 7μm thick. Separation between waveguides was taken as 5μm. Note that the penetration into the fibre region of the evanescent tail of the overlay mode is much greater at the phase-matching and cutoff wavelengths. This suggests that the corresponding overlap integrals and coupling coefficients will be highly dependent on the input wavelength. The values of C_{12} and C_{21} were calculated in a numerical manner using the computer model of the device structure, for several waveguide separations, as the wavelength was varied such that the overlay mode moved from a tightly confined situation, through phase-matching, to approximately cutoff. Figure 3.10 shows the results. A simple explanation for the behaviour of the coupling coefficients can be obtained by considering the mode field profiles shown in Figure 3.9. Away from phase-matching or cutoff, the strength of the evanescent tail of the overlay mode is small across the width of the fibre i.e. the overlay mode is tightly confined to the guiding region. As the wavelength is increased, the amplitude of the evanescent tail increases while the field amplitude in the guiding region decreases and the mode "spreads out". The corresponding overlap integral across the fibre

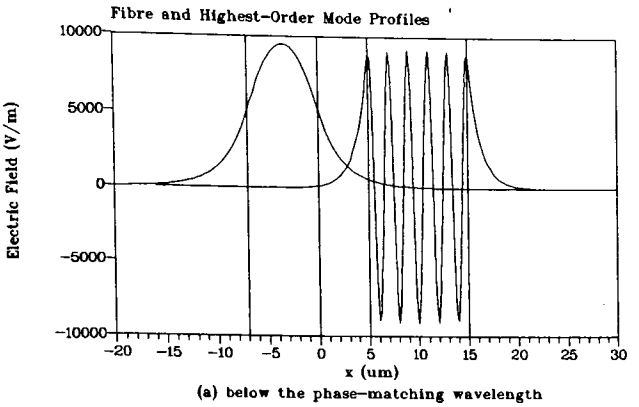

(a) below the phase-matching wavelength

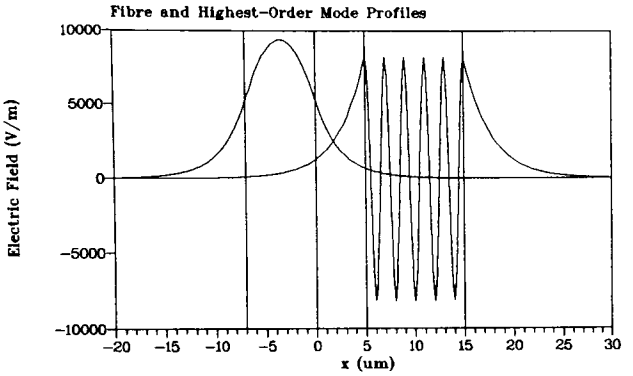

(b) at the phase-matching wavelength

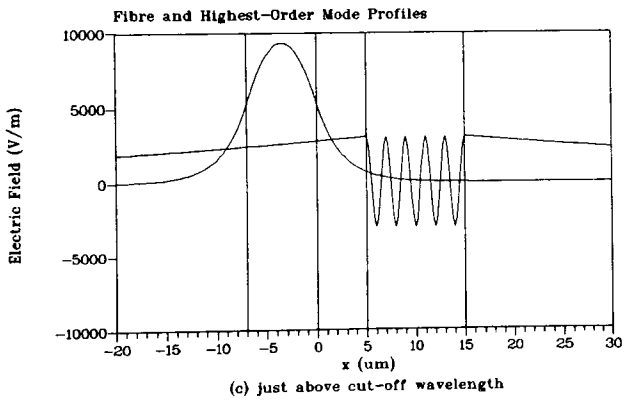

(c) just above cut-off wavelength

Figure 3.9 : Field Profiles of adjacent fibre and highest-order overlay modes

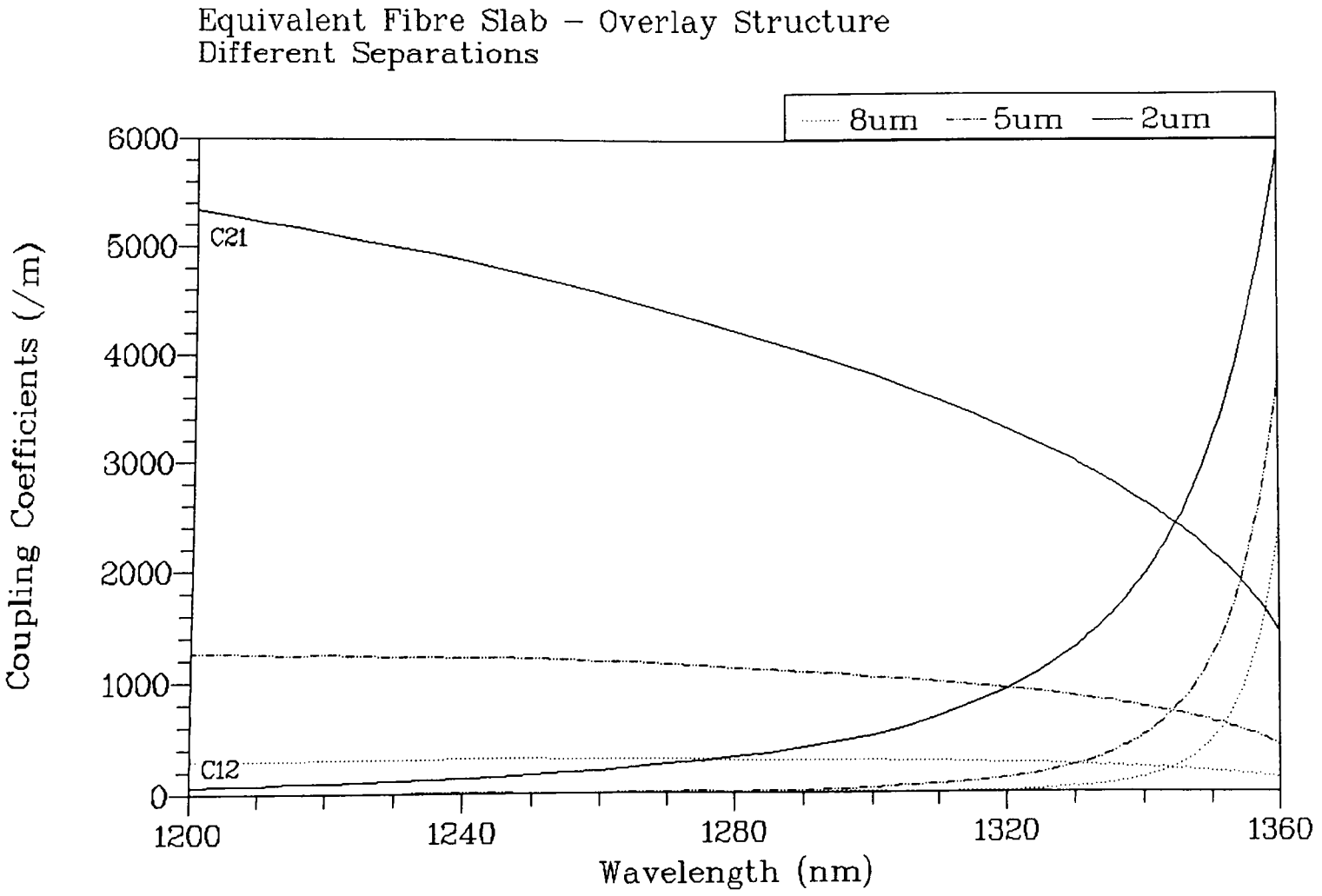

Figure 3.10 : Wavelength Response of Coupling Coefficients

region will, therefore, also increase since it depends on the product of the fibre field and overlay field in that region. Thus, the value of C_{12} will also increase until a maximum is reached prior to reducing again just before cutoff when the overlay mode has "spread out" to such an extent that the proportion of the power carried by the evanescent tail of the overlay mode in the region of the fibre has decreased. The C_{21} coupling coefficient gradually reduces as the amplitude of the overlay mode in the guiding region decreases since the amplitude of the fibre mode evanescent tail is not significantly altered by varying the input wavelength. Although the calculated values of C_{12} and C_{21} close to cutoff of the overlay mode are correct from a mathematical standpoint, the original coupled-mode theory from which they were derived is not really applicable in this regime i.e. substituting the calculated values of C_{12} and C_{21} into eqns. (3.27) leads to power transfers of $>100\%$, a physical impossibility. The condition of weak coupling cannot be applied in this instance due to the field of the overlay mode not being well confined to the overlay guiding region. However, it is reasonable to assume that the coupling coefficients decrease as the separation between fibre and overlay is increased i.e. similar to the case of identical waveguides. Bearing this in mind, the wavelength range in which significant power transfer occurs would be expected to similarly decrease as the guide separation is increased i.e. low values of coupling coefficients would be expected to result in a more rapid reduction in the maximum transferred power since the phase mismatch, 2δ, will quickly dominate the equation. A corresponding narrowing of the wavelength range (linewidth) over which power is transferred will result.

3.3.2. Influence of Overlay Dispersion on Resonance Linewidth

The above section suggested that the strength of the coupling and, thus power transfer, between the fibre and overlay modes will be affected by the guide separation. For a fixed separation, intuitively, the linewidth of the resonances in the transmitted intensity for each device can also be related to the change in material index or wavelength required to shift the overlay effective index across the fibre mode index. It is interesting to investigate the rate of change of overlay effective index with wavelength, material index or overlay thickness (gradient of dispersion

curves) and relate it to the degree of phase-matching between the highest order overlay and fibre mode. It is difficult to obtain a precise analytical expression for any of these quantities by differentiation of the eigenvalue equation. Instead, a computer program was developed which solves eqn. (1.1) by a numerical method and the values of $\delta n_e/\delta\lambda$, $\delta n_e/\delta n_o$ and $\delta n_e/\delta d$ were recorded for different waveguide geometries. However, wavelength variation was the preferred parameter since comparison with trends in experimental results was possible. Tables 3.1 and 3.2 show the value of $\delta n_e/\delta\lambda$ and mode order for a range of waveguide indices and two thicknesses. Similarly, Tables 3.3 and 3.4 show the value of $\delta n_e/\delta\lambda$ and mode order for a range of overlay thicknesses and two overlay indices.

The index and thicknesses of the waveguides (for Tables 3.1 and 3.2) were chosen to correspond to actual experimental values to allow comparison with results given in Chapter 5. Superstrate and cladding indices were 1.447. Each waveguide was investigated in the wavelength range 1.2-1.6μm and the effective index of the mode which cut-off nearest to $\lambda=1.3\mu$m was recorded. Inspection of Tables 3.1 - 3.4 indicates that the sensitivity (gradient) of the effective index to wavelength increases quite substantially as both overlay waveguide index and thickness (and, therefore, mode order) are increased. Figures 3.11 and 3.12 show the relationship between $(\delta n_e/\delta\lambda)^{-1}$ and (i) overlay index for two thicknesses and (ii) overlay thickness for two refractive indices, respectively. The actual linewidth response of a practical device can be expected to behave in a similar manner to Figures 3.11 and 3.12 although the coupling strength of the polished fibre half-block (and, therefore, coupling coefficients between the fibre and overlay) will determine the actual linewidth values. It is believed that the sensitivity of the mode effective indices to wavelength variation and, thus, the behaviour of 2δ, dominate the overall device behaviour, particularly in the weak-coupling regime. This is a result of the dependence of $\delta n_e/\delta\lambda$ on thickness and index being stronger than that of the coupling coefficients. Note also that the phase mismatch is a stronger function of wavelength for highly-multi-moded waveguides as observed from Tables 3.1 - 3.4. Narrow linewidth fibre-overlay devices are, therefore, expected from devices which possess thick, high index

Refractive Index	$dn_e/d\lambda$ (x 10^6)	Mode Number, *m*
1.470	0.0108	3
1.494	0.03	5
1.548	0.0875	9
1.598	0.132	11
1.650	0.184	13
1.698	0.24	15

Table 3.1 WavelengthSensitivity of Mode Effective Index
Waveguide Thickness 12μm

Refractive Index	$dn_e/d\lambda$ (x 10^6)	Mode Number, *m*
1.470	0.0131	6
1.494	0.0415	11
1.548	0.101	17
1.598	0.164	22
1.650	0.228	26
1.698	0.286	29

Table 3.2 Wavelength Sensitivity of Mode Effective Index
Waveguide Thickness 23μm

Overlay Thickness	$dn_e/d\lambda$ (x 10^6)	Mode Number, *m*
2.5μm	0.02051	1
5μm	0.04030	3
10μm	0.05300	6
15μm	0.05970	9
20μm	0.06350	12
25μm	0.06614	15
30μm	0.06826	20

Table 3.3 Wavelength Sensitivity of Mode Effective Index
Overlay Index n=1.5

Overlay Thickness	$dn_e/d\lambda$ (x 10^6)	Mode Number, *m*
2.5μm	0.09390	3
5μm	0.20462	7
10μm	0.27259	14
15μm	0.29336	20
20μm	0.32280	27
25μm	0.33468	34
30μm	0.35182	41

Table 3.4 Wavelength Sensitivity of Mode Effective Index
Overlay Index n=1.7

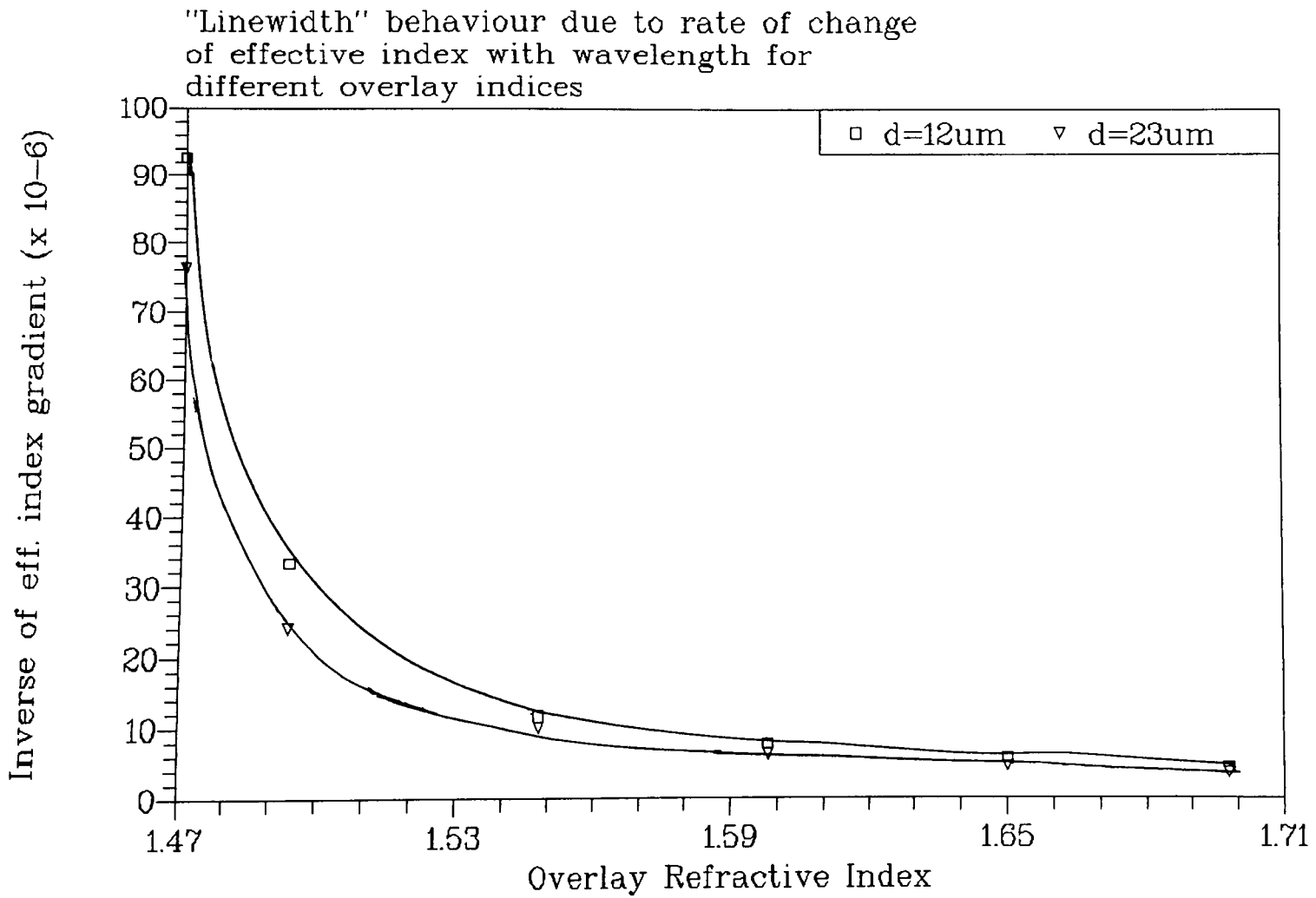

Figure 3.11 : "Linewidth" versus Overlay Index

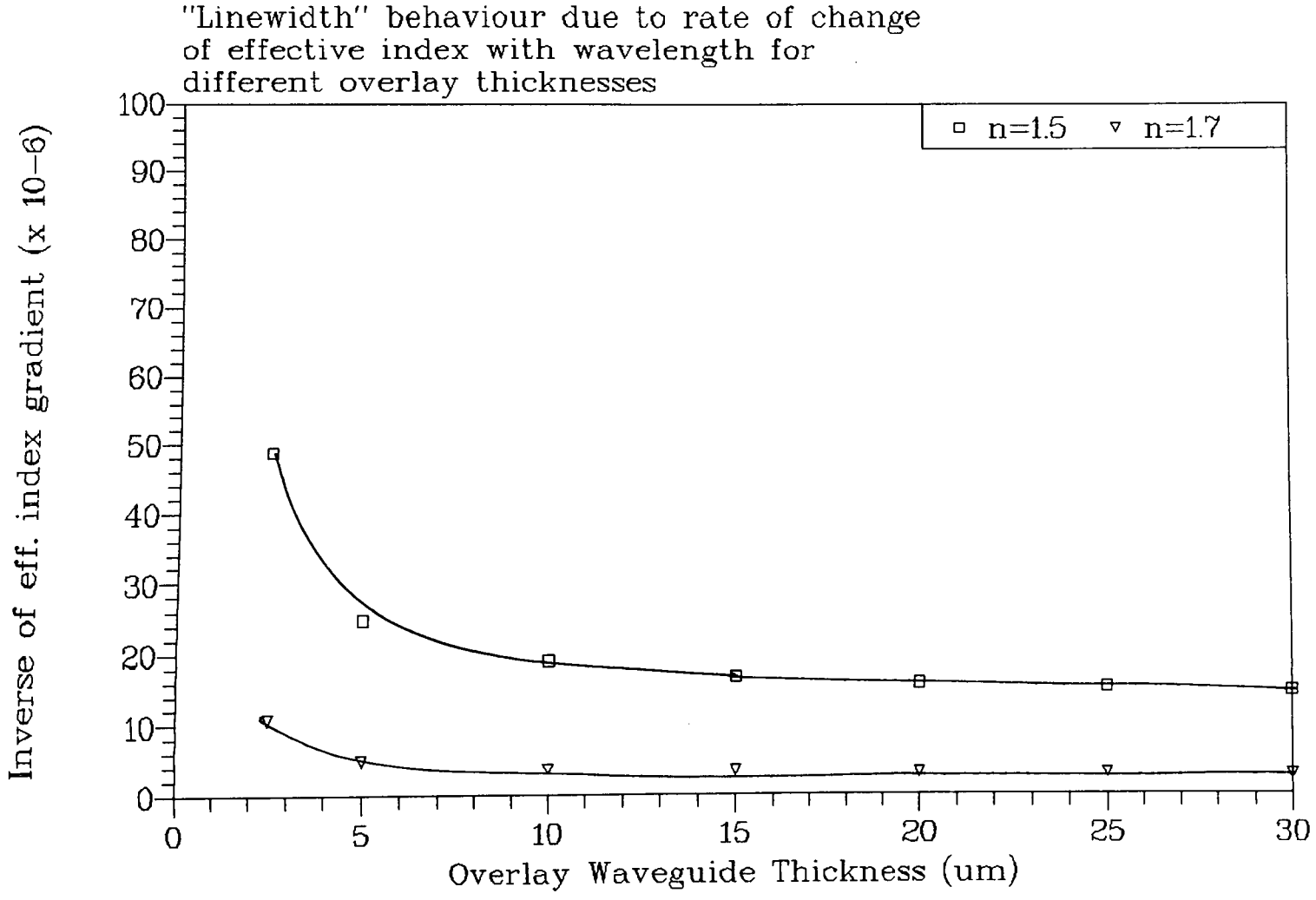

Figure 3.12 : "Linewidth" versus Overlay Waveguide Thickness

overlays which are only weakly coupled to the fibre i.e. when the coupling coefficients are small due to large separation.

3.4 Multi-Layer Analysis of Device Structure

The previous sections treated the device structure shown in Figure 1.3 as two coupled waveguides with the fibre replaced by an equivalent slabguide. If the fibre equivalent slab is retained, then the structure can also be viewed as consisting of a number of adjacent, parallel layers of different refractive index. A matrix method[2] can then be used to successively calculate the electric field distribution across each layer of the structure and, thus, provide the super or normal modes of the entire guiding structure. The interference or beating of these supermodes causes oscillation of the input power between the guiding layers (fibre and overlay "core") of the structure with the beat length depending on the difference in propagation constants of the supermodes.

The matrix method referred to above involves the multiplication of 2 x 2 matrices from which the real and imaginary parts of the supermode propagation constants as well as the mode field distributions can be readily obtained. The derivation of the method is fairly simple and is based on the layered structure shown in Figure 3.13. An incoming plane wave is incident at the first interface at an angle θ_1 and, assuming y-direction invariance, the electric field in each layer can be written in the form:

$$\begin{aligned}\overline{E_m} = {} & e_m^+ E_m^+ \exp(i\Delta_m)\exp[i(\omega t - k_m \cos\theta_m x - \beta z)] \\ & + e_m^- E_m^- \exp(-i\Delta_m)\exp[i(\omega t + k_m \cos\theta_m x - \beta z)]\end{aligned} \qquad (3.28)$$

where

$$\Delta_1 = \Delta_2 = 0 \quad , \quad \Delta_3 = k_3 d_2 \cos\theta_3 \quad , \quad \Delta_4 = k_4 \cos\theta_4 (d_2 + d_3) \qquad (3.29)$$

The quantity β is an invariant of the system while e_m^+ and e_m^- represent the unit vectors in the direction of the field and E_m^+ and E_m^- are the field amplitudes for the

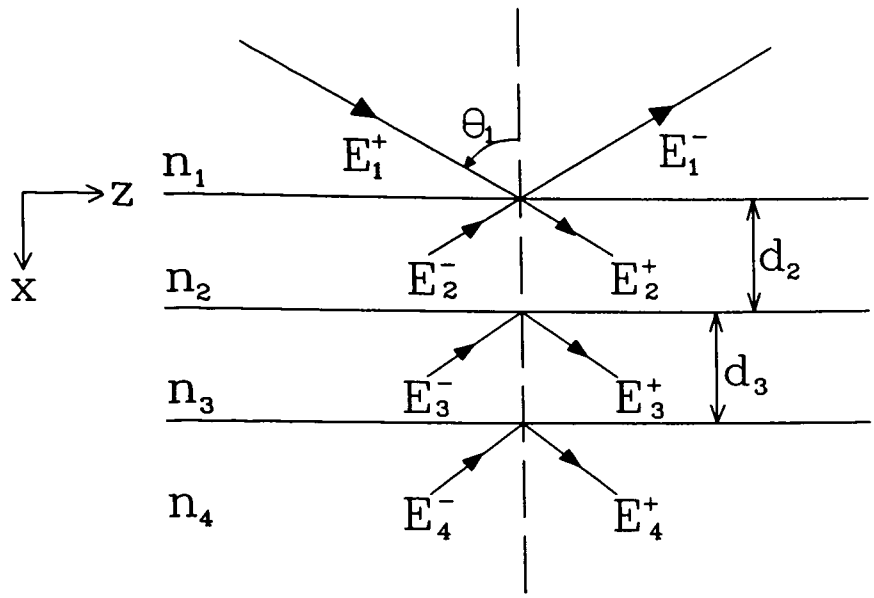

Figure 3.13 : Plane Wave incident on a multilayer structure

$$k_m = k_0 n_m = \frac{\omega}{c} n_m$$

$$\beta = k_1 \sin\theta_1 = k_2 \sin\theta_2 = ... = k_m \sin\theta_m \qquad (3.30)$$

downward and upward waves, respectively. Applying the usual boundary conditions for an electric field across a dielectric interface leads to the following expression[2]:

$$\begin{pmatrix} E_1^+ \\ E_1^- \end{pmatrix} = S_1 \begin{pmatrix} E_2^+ \\ E_2^- \end{pmatrix} = ... = S_1 S_2 S_3 ... S_{m-1} \begin{pmatrix} E_m^+ \\ E_m^- \end{pmatrix} \qquad (3.31)$$

where

$$S_m = \frac{1}{t_m} \begin{pmatrix} e^{i\delta_m} & r_m e^{i\delta m} \\ r_m e^{-i\delta_m} & e^{-i\delta_m} \end{pmatrix} \qquad (3.34)$$

and r_m and t_m represent,respectively, the amplitude reflection and transmission

coefficients at the mth layer interface while $\delta_m = k_m d_m \cos\theta_m$. The values of r_m and t_m are related to the refractive indices of the adjacent layers at each interface and also the angle of incidence of the incoming light. For TE polarisation

$$r_m = \frac{n_m \cos\theta_m - n_{m+1}\cos\theta_{m+1}}{n_m \cos\theta_m + n_{m+1}\cos\theta_{m+1}} \qquad \textbf{(3.33a)}$$

$$t_m = \frac{2n_m \cos\theta_m}{n_m \cos\theta_m + n_{m+1}\cos\theta_{m+1}} \qquad \textbf{(3.33b)}$$

while for TM polarisation

$$r_m = \frac{n_{m+1} \cos\theta_m - n_m \cos\theta_{m+1}}{n_{m+1} \cos\theta_m + n_m \cos\theta_{m+1}} \qquad \textbf{(3.34a)}$$

$$t_m = \frac{2n_m \cos\theta_m}{n_{m+1} \cos\theta_m + n_m \cos\theta_{m+1}} \qquad \textbf{(3.34b)}$$

For a wave incident from the first layer, there is no upward propagating wave in the last layer and, therefore, for the structure shown in Figure 3.13, $E_4^- = 0$. This condition, used in conjunction with eqns. (3.31) and (3.32), allows the electric field at each interface to be calculated in terms of E_1^+. The normal or super modes of a multilayer structure can be obtained using this approach by evaluating the excitation efficiency of the wave in the guiding regions as a function of β (variation of β can be achieved by changing the angle of incidence, θ). Resonance peaks[2] in the excitation efficiency occur when the value of β corresponds to a guided mode. For the structure shown in Figure 3.13, if layer 3 is selected as the guiding layer then the excitation efficiency is given by $\eta(\beta) = |E_3^+/E_1^+|^2$ or $|E_3^-/E_1^+|^2$. The value of β can then be used to calculate the corresponding mode field distribution across the entire structure.

3.4.1 Application to Fibre-Overlay Device

A computer program was developed which allowed the matrix method outlined above to be applied to the basic fibre-overlay device structure. Again the fibre was replaced

with an equivalent slab waveguide[6] to leave a fundamental five layer structure. Replacing the optical fibre by an equivalent slab waveguide in the above discussions has two important consequences: the device interaction length is no longer defined by the fibre curvature and remaining cladding thickness and the device, in principal, exhibits no loss. Obviously, an appropriate interaction length can easily be chosen but the effect of loss is more complicated and discussed in the next section. The program was designed to vary the propagation constant β until resonance peaks in the excitation efficiency of the field in the overlay region were detected. The β values at these peaks correspond to the propagation constants of guided modes of the structure as suggested earlier. The excitation and propagation of these normal modes of the structure then determines the behaviour of the fibre-overlay device structure. At the start of the interaction region, the fibre mode excites normal modes of the structure which then interfere as they propagate along the interaction region. The power contained by each normal mode depends on the excitation efficiency which is primarily related to the overlap of the fibre field and the normal mode field[7]. In general, a large number of normal modes can be supported by the multilayer structure. However, the excitation efficiency of most of the normal modes is negligible except for those possessing a β value close to that of the fibre mode (in isolation). It is found that significant excitation only occurs when the fibre mode is close to phase-matching with the highest-order overlay mode. In this situation, two normal modes known as the symmetric and anti-symmetric modes are significantly excited i.e. each normal mode possesses a significant fraction of the input power. When exact phase-matching of the fibre mode and the highest-order overlay mode occurs, the two resultant normal modes are equally excited (approx.) and each possesses half the input power. Figure 3.14 shows the field distribution for the symmetric and anti-symmetric normal modes of a typical structure at the phase-matching wavelength.

The β values of the symmetric (β_s) and anti-symmetric (β_a) normal modes are slightly above and slightly below that of the fibre mode, respectively. The difference in the normal mode β values provides the coupling length via the relationship

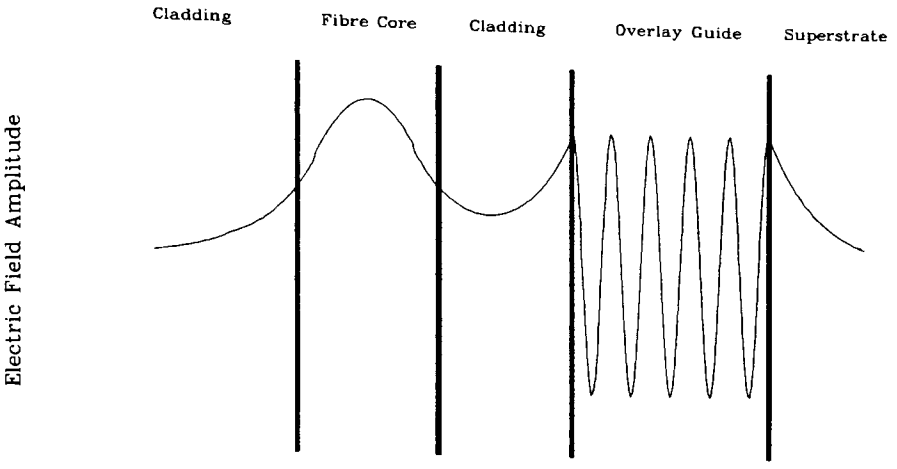

(a)

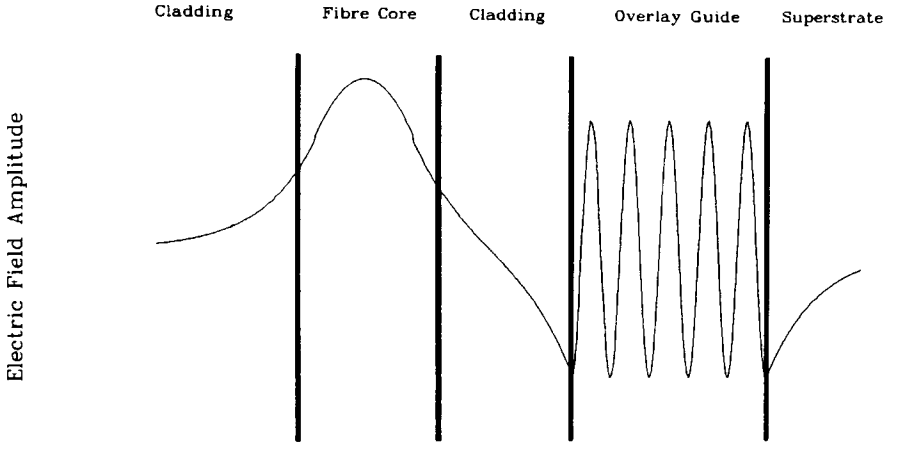

(b)

Figure 3.14 : **Normal Modes of Structure at Phase-Matching (a) Symmetric Mode (b) Anti-symmetric Mode Overlay Waveguide : n=1.6, d=10μm Guide Separation 8μm**

$L_c=\pi/|\beta_s-\beta_a|$ i.e. the length required for power to transfer from the fibre region to the overlay region. At the output of the interaction region the resulting overall field distribution, obtained from the addition of the normal mode fields at that point, re-excites the fibre mode. The power in the fibre mode depends on the location of the power carried by the normal modes at the end of the interaction region. If the interaction length is exactly equal to the coupling length, then there will be negligble power in the fibre region at the output. However, this situation can only occur when the excitation of the normal modes, in terms of power, is equal and this requires phase-matching of the fibre mode with an overlay mode. Below the phase-matching wavelength, the power in each normal mode is highly dissimilar with the symmetric mode containing the majority. In this instance, only a small fraction of the power can oscillate between the guiding regions (fibre and overlay) and as a result almost all the power is located in the fibre at the output. As the wavelength approaches the phase-matching value, the power in each normal mode moves towards 50% and a greater amount of power can oscillate between the adjacent guides. Full power transfer can only occur at phase-matching of the fibre and highest-order overlay mode. Correspondingly, the power in the fibre at the output decreases, reaching a minimum on phase-matching (assuming the interaction length and coupling lengths are closely matched). Further increasing the wavelength causes the current highest-order overlay mode to cutoff and then the above situation is repeated when the next highest-order mode enters the phase-matching regime. The result is resonance minima in the fibre output power. This is the basic mechanism upon which the operation of the fibre-overlay device relies. Again, as in the coupled-mode theory approach, phase-matching of the fibre mode and the highest-order overlay mode is the critical issue.

No device modelling results are presented here but instead the effect of the different parameters are discussed qualitatively. The width of the resonance minimums mentioned above are obviously of great interest as regards device performance. Since phase-matching is critical in establishing equally-excited normal modes and subsequent efficient fibre-overlay power transfer, the dispersion of the overlay

modes, as with the coupled-modes approach, is obviously again an important factor with regard to resonance linewidth i.e. the wavelength range over which the overlay mode is in the vicinity of phase-matching is directly related to the wavelength dispersion. Therefore, the discussion given in section 3.3.2 concerning the influence of overlay dispersion with respect to wavelength, index and guide thickness is applicable here also.

The other important parameter which contributes strongly to resonance linewidth is the spacing between the fibre and the overlay i.e. the remaining cladding thickness. This spacing has an influence on the excitation of, and thus the power contained in, both the symmetric and anti-symmetric normal modes. Figures 3.15(a) and (b) show the effect of increasing fibre-overlay spacing on the excitation of the normal modes, for the same degree of phase mismatch (same structure as for Figure 3.14). It is clear that the smaller fibre-overlay spacing (3μm) results, in this instance, in greater excitation of both the anti-symmetric normal mode and the symmetric normal mode and, for a set interaction length, the possibility of a substantial fraction of the total power being located in the overlay region is increased. When the fibre-overlay spacing is increased (8μm), the excitation of the symmetric normal mode is very small (power in anti-symmetric normal mode almost 100%) and, irrespective of the interaction length, virtually all the power will be located in the fibre region at the device output. In addition, power located in the overlay region is subject to a lateral loss mechanism which further reduces total power available at the device output. This loss mechanism is considered in the next section. When the fibre-overlay spacing is large, the power contained in the symmetric normal mode is very small except in the close vicinity of the phase-matching condition. Subsequently, the fraction of power located in the overlay region at the end of the interaction region will be very small except close to phase-matching and the resultant power re-excited in the fibre will be high. However, when the fibre-overlay spacing is small, the power in the symmetric mode is significant over a greater wavelength range (in the vicinity of phase-matching). Therefore, the amount of power located in the overlay region at the end of the interaction region will be significant over this same

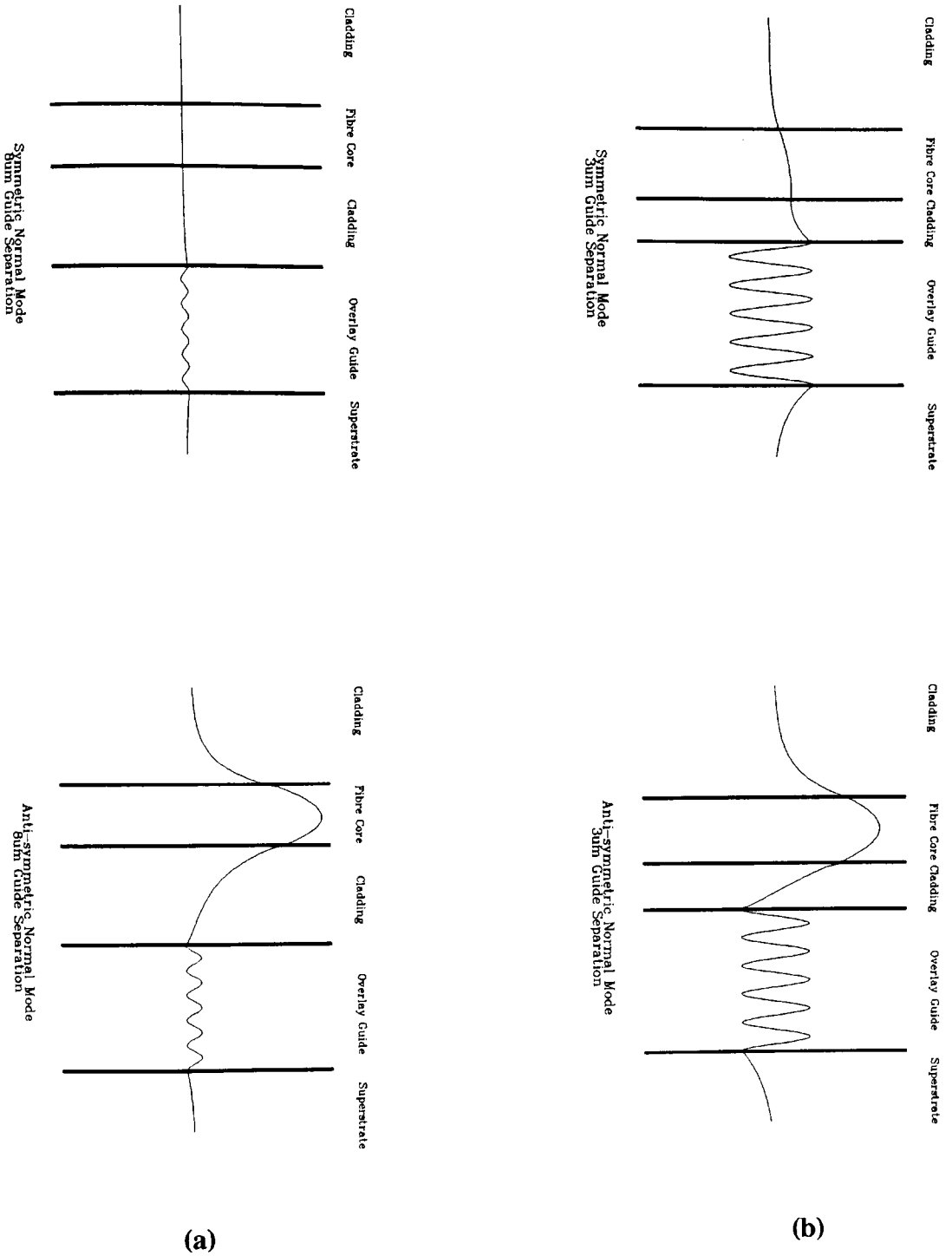

(a) (b)

Figure 3.15 : Effect of guide separation on excitation of normal modes

(a) 8μm Separation (b) 3μm Separation

wavelength range and power re-excited in the fibre will, correspondingly, be reduced. From the above explanation, devices which are identical apart from fibre-overlay spacing will, for the same degree of phase mismatch (slightly below the resonance wavelength), possess different resonance linewidths i.e. power coupled out of the fibre will be significant over a broader wavelength range for small fibre-overlay spacing devices.

3.5 Influence of Lateral Loss

Intuitively, a practical fibre-overlay device would be expected to suffer lateral loss of power (diffraction losses) due to the difference in geometries of the fibre and overlay waveguides i.e. the overlay only confines light in two dimensions. The lateral loss mentioned above will obviously have a strong influence on the overall device behaviour and is, therefore, worthy of discussion. A theoretical analysis of this loss mechanism has been made using a coupled-mode approach[8]. In this analysis, it was indicated that the combined structure of fibre and overlay supports compound modes, some of which form ridge modes that are bound, in the plane of the overlay, to the vicinity of the fibre. Light initially launched into the fibre is redistributed among these compound modes, many of which are not confined to the fibre region. This results in power being carried away from the vicinity of the fibre and a numerical expression for the attenuation is developed which is related to the coupling of the fibre and overlay modes.

An alternative analysis of the fibre-overlay coupling situation[9] represents the fibre as an equivalent square waveguide in close proximity to a slab waveguide. In this case, the equivalent index method[10] is used to split the overall structure into x and y slabs for separate analysis. A perturbation approach is then used to determine the influence of the slab on the power guided by the fibre. A loss term was derived in the subsequent analysis which was related to the modal field distributions and fibre parameters and represented as an imaginary part of the propagation constant of the normal modes of the structure[8]. This loss term is

compatible with the matrix method described above and can be incorporated in the calculation of the power remaining in the fibre at the end of the interaction region of the device.

For both approaches, the result is that the power in the fibre at the device output at the phase-matching wavelength will always be attenuated to some extent even if the coupling length and the interaction length are mismatched. In terms of device response, this will lead to high resonance modulation depths (extinction ratios), particularly if the interaction length is much longer than the coupling length. The experimental results given in Chapters 5 and 6 confirm this point. Therefore, the lateral loss has an important effect on device behaviour.

An additional loss mechanism can also be identified by considering again the eigenvalue equation of the overlay waveguide. The complete solution of this equation results in a degenerate mode structure i.e. solutions exist at an infinite number of angles in the plane of the waveguide. Coupling of power to these off-axis modes would obviously result in attenuation of the input power. This loss mechanism is considered in more detail in Chapter 5.

3.6 Conclusions

The coupled-mode approach to analysing the fibre-overlay device structure, with the assumption of weak-coupling, allows the behaviour of the overlay waveguide mode structure to be considered the dominant factor in device performance. As a result, a great deal of information concerning device behaviour can be obtained by observing the effect of varying the various overlay waveguide parameters. Subsequent performance of practical devices can then be considered as having a significant dependence on the overlay waveguide, which can be fabricated accordingly.

Considering the fibre-overlay device as a multilayer structure allows a simple, but

powerful, matrix method to be adopted in the calculation of mode electric field profiles and propagation constants and resultant spectral transmission responses. More precise modelling of the device performance, in terms of channel linewidths, spacing and modulation depth (extinction ratio), is possible with this approach. Extensive modelling of the device structure using this technique has recently been carried out in the Optoelectronics Group at University of Strathclyde. The modelling results show encouraging similarity to experimental results and are presented elsewhere[11]. Again, design of practical devices can be based on modelling results and adjusted to provide the desired device response.

References

1. A. Hardy and W. Streifer,"Coupled mode theory of parallel waveguides", J. Lightwave technol., **LT-3**, pp1135-1146, 1985.

2. A.K. Ghatak, K. Thyagarajan and M.R. Shenoy,"Numerical analysis of planar optical waveguides using matrix method", J. Lightwave Technol., **LT-5**, pp660-667, 1987.

3. A. Hardy, S. Shakir and W. Streifer,"Coupled-mode equations for two weakly guiding single-mode fibers", Opt. Lett., **11**, pp324-326, 1986.

4. Y. Shama, A.A. Hardy and E. Maron,"Multimode coupling of unidentical waveguides", J. Lightwave Technol., **LT-7**, pp420-425, 1989.

5. A. Yariv, *Optical Electronics*, Holt-Saunders, 3rd Ed., 1985.

6. A. Sharma, J. Kompella and P.K. Mishra,"Analysis of fiber directional couplers and coupler half-blocks using a new simple model for single-mode fibers", J. Lightwave Technol., **LT-8**, pp143-151, 1990.

7. R.V. Ramaswamy and R. Srivastava,"Ion-exchanged glass waveguides: a review", J. Lightwave Technol., **LT-6**, pp984-1002, 1988.

8. D. Marcuse,"Investigation of coupling between a fiber and an infinite slab", J. Lightwave Technol., **LT-7**, pp122-130, 1989.

9. J.V. Wright, S.R. Mallinson and C.A. Millar,"A fiber-based crosspoint switch using high-refractive index interlay materials", IEEE J. on Select. Areas in Comms., **6**, pp1160-1167, 1988.

10. K.S. Chiang,"Effective-index method for the analysis of optical waveguide couplers and arrays: an asymptotic theory", J. Lightwave Technol., **LT-9**, pp62-72, 1991.

11. Gordon Fawcett, *Fibre Optic Components utilizing Passive and Active Polymeric Overlays*, PhD Thesis, University of Strathclyde, 1993.

CHAPTER 4

Polished Fibre Half Block - Basic Component

4.1 Introduction

The devices investigated within this thesis rely upon external interaction with the optical field of a single-mode step-index optical fibre. This interaction occurs via the evanescent tail of the modal field distribution which extends beyond the core region of the optical fibre. In order to achieve the necessary interaction a basic device geometry facilitating exposure of the evanescent field is required. To produce this requires several fabrication steps, the resulting structure being termed a polished fibre half-coupler or half-block. This component is an integral part of all the subsequent device structures studied in this thesis. Hence, this chapter describes the geometry, fabrication and characterisation of this basic component and introduces the important parameters it possesses.

The devices investigated in this thesis incorporate low-loss (0.36dB/km) standard step-index, single-mode telecommunications optical fibre (supplied by Optical Fibres). The optical field distribution and refractive index profile across the fibre are shown in Figures 4.1(a) and 4.1(b), respectively. The fibre is fabricated from fused silica with the core germanium-doped to cause a slight increase in its index. Outside diameter is 125μm while the core has a diameter of 8μm. The dimensions and core-cladding index difference (approx. 0.0044) are designed so that the fibre is single-moded above a wavelength of 1200nm.

4.2 Fabrication Procedures

The basic geometry of a standard polished fibre half block is shown in Figure 4.2. The device consists of a single-mode optical fibre, of the type described in section 4.1, bonded into a groove which has been formed in a fused silica substrate block.

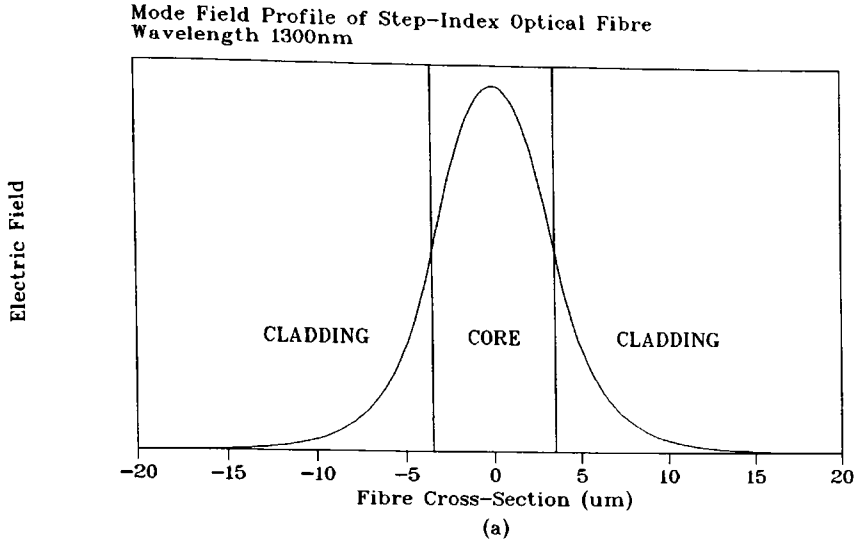

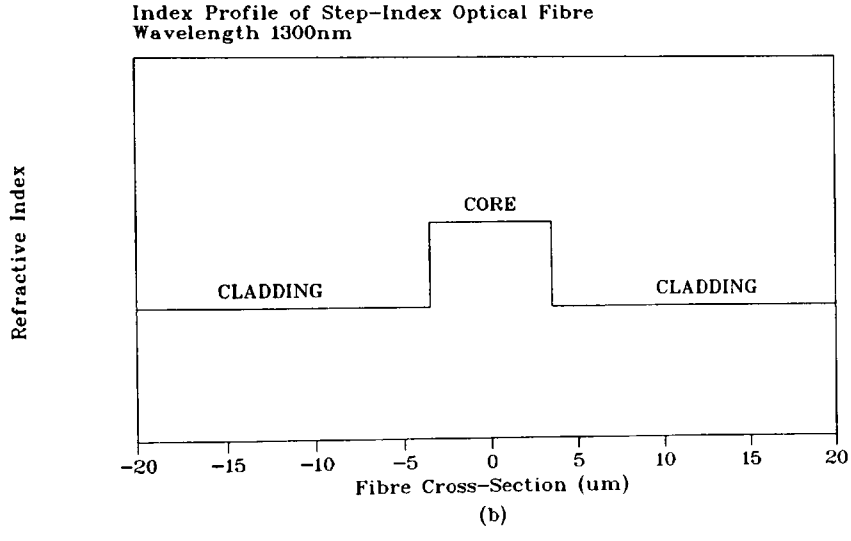

Figure 4.1 : (a) Fibre Mode Field Profile
(b) Fibre Refractive Index Profile

Lapping and polishing of the top surface of the composite structure is performed to leave an appropriate amount of fibre cladding between the core and the top surface (typically 2-5μm). The block which holds the optical fibre is generally 30mm x 15mm x 10mm and and cut from slabs of fused quartz, thus allowing the same lap/polish rate as the fibre. The groove is cut in the substrate block using a diamond-impregnated wire saw which can be angled and tensioned such that a range of radius of curvature grooves (7.5cm to 50cm) can be obtained. Two thicknesses of wire were used to form the grooves, 130μm and 200μm. Typical radii of curvature for polished fibre half-couplers (half-blocks) fabricated for investigation in this thesis are 11cm and 22cm. Once the groove has been cleaned and any debris left as a result of the sawing process removed, a length of fibre equal to the groove length (generally 30mm) is immersed in DiChloroMethane, an organic solvent. This causes the plastic buffer coating on the fibre, used to provide mechanical strength and to act as a radiation mode stripper, to soften and detach from the fibre cladding. Next, a low viscosity two-part epoxy is introduced into the groove via capillary action. The exposed fibre is then cleaned and inserted into the groove while lateral and vertical tension is applied to it to cause it to conform to the shape of the groove. A heat gun is then used to slowly cure the epoxy and secure the fibre. Ultra-Violet cured glue, brand name NORLAND 63, is then applied to the fibre at each end of the groove to provide support to the unbuffered fibre at these points. A number of adhesives were tested for use in bonding the fibre along the length of the groove to assess their response to the lapping/polishing processes and reaction to various solvents used in cleaning optical surfaces, e.g. Isopropyl alcohol, acetone, etc. Problems encountered included a tendency for the adhesive/glue to lap/polish at a different rate from the fused quartz resulting in a slight variation from complete optical flatness across the entire surface of the substrate block. Best results were obtained for a two part heat-curing epoxy, brand name EPOTEK 353ND.

The half-block is then mounted on a standard LOGITECH polishing jig using a low melting point (56°C) paraffin-based wax. A photograph of a standard polishing jig and polishing machine are shown overleaf. The polishing jig is shown with a fibre

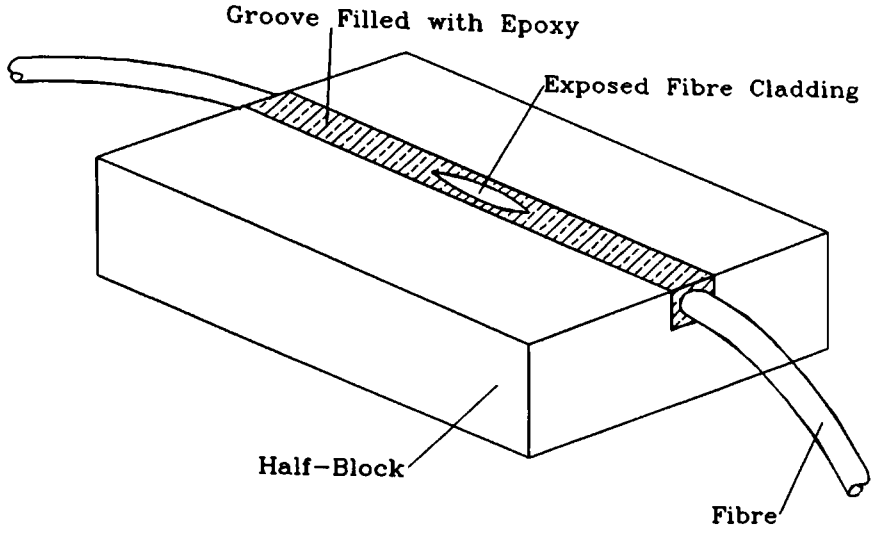

Figure 4.2 : Polished Fibre Half-Block Geometry

half-block mounted in the correct position for polishing. A 3-stage process of mechanical/chemical lapping and polishing is used to remove the desired amount of fibre cladding and produce a good optical quality surface on the half-block. The lapping stages of the process were performed on a LOGITECH PM2 precision polishing machine. Initial material removal is obtained by lapping the half-block surface on a cast-iron or glass plate with a slurry containing 9μm particles of calcined Aluminium Oxide powder in de-ionised water. The lapping action is obtained by placing the jig upside down with its drive-ring in contact with the surface of the selected plate. The sample is then lowered until it also contacts the plate surface, the pressure of the sample on the plate being controlled by an adjustable screw. Material removal then occurs as the plate is rotated with the jig confined to one spot. A micrometer spring gauge is attached to the polishing jig which allows a coarse measurement of the amount of material which has been removed (accurate to 2μm). Distance from the half-block surface to the fibre core (taking the outside diameter of the fibre as 125μm) can be calculated, using the depth of the groove at the centre, and this value indicates the thickness of material to be removed. Generally the depth of the groove is made substantially larger than the

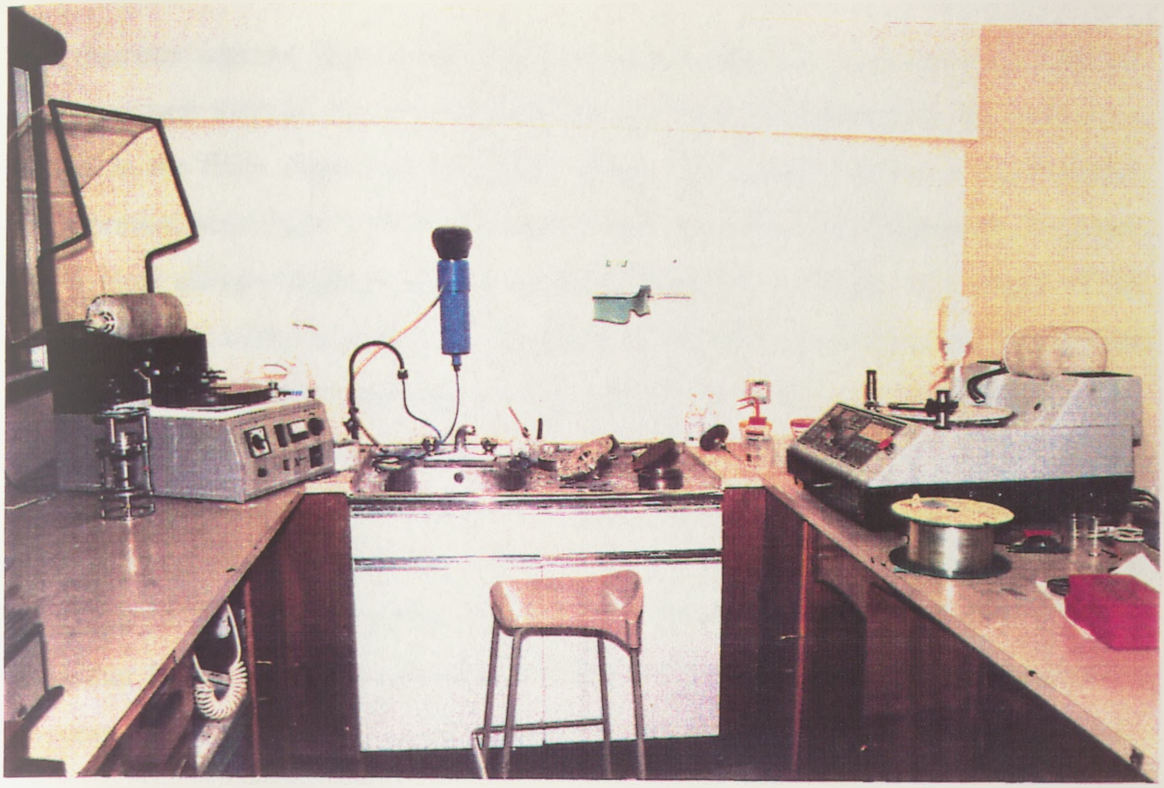

Logitech Lapping/Polishing Machines

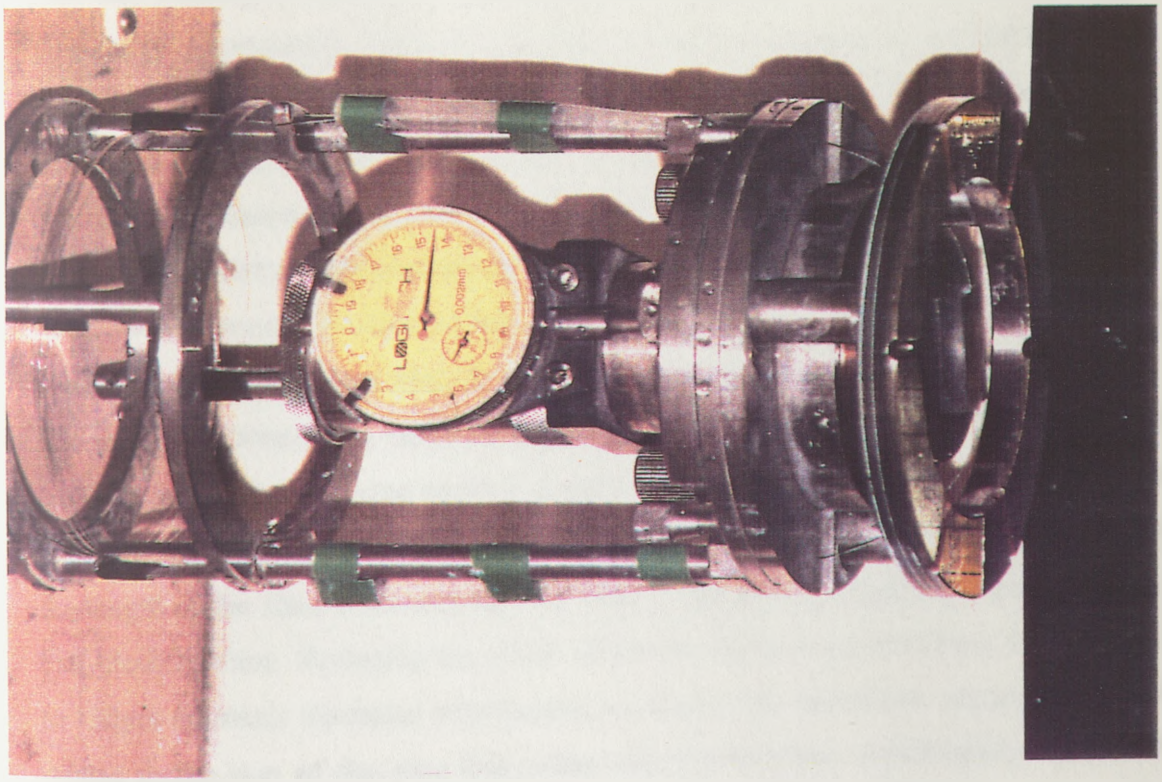

Logitech Polishing Jig with half-block mounted

fibre diameter and the 9μm lapping procedure is performed until the fibre cladding is just exposed through the surrounding epoxy. Visual inspection of the half-block surface in the fibre region at this point using a microscope shows a small ellipse shape present with major axis in the same direction as the fibre alignment. A section of a typical ellipse shape is shown in the photograph overleaf. The length of the ellipse together with the radius of curvature of the groove can be used to calculate the precise thickness of cladding material which has been removed. Once the fibre cladding has been reached the 9μm lapping slurry is replaced with a 3μm particle solution and further cladding removed until the fibre core to half-block surface distance is approximately 12μm. The 3μm slurry has a significantly slower lapping rate than the 9μm case, therefore giving more precise control, and also produces a smoother finish which reduces the polishing time required in the next stage of the process.

Polishing of the half-block surface is carried out using an expanded polyeurathane plate and a slurry containing 0.5μm particles of Cerium Oxide in de-ionised water. This slurry is commonly referred to as OPALINE. A prototype LOGITECH PS2000 precision polishing machine was used for the polishing stage of the process since it allowed some adjustment of the shape of the polyeurathane plate and thus better control of the flatness of the half-block surface. Inspection of the half-block surface quality and flatness was performed periodically during the polishing stage of the fabrication process. A microscope was used to check the half-block surface, in particular the fibre ellipse area, for mechanical damage such as scratches, pits, etc. The surface flatness was determined by placing an optical flat in contact with the half-block surface in the presence of a monochromatic light source and observing the resulting interference fringe pattern. Slight distortion of the interference fringes along the length of the fibre indicates that the fibre is not exactly flush with the rest of the half-block surface. Reducing the width of the saw groove by switching from 200μm to 130μm diameter diamond wire helped to reduce this distortion, suggesting it was related to the size of the glue line either side of the fibre. Additionally, slivers of fused silica were lapped to a thickness of 125-130μm and inserted vertically into the

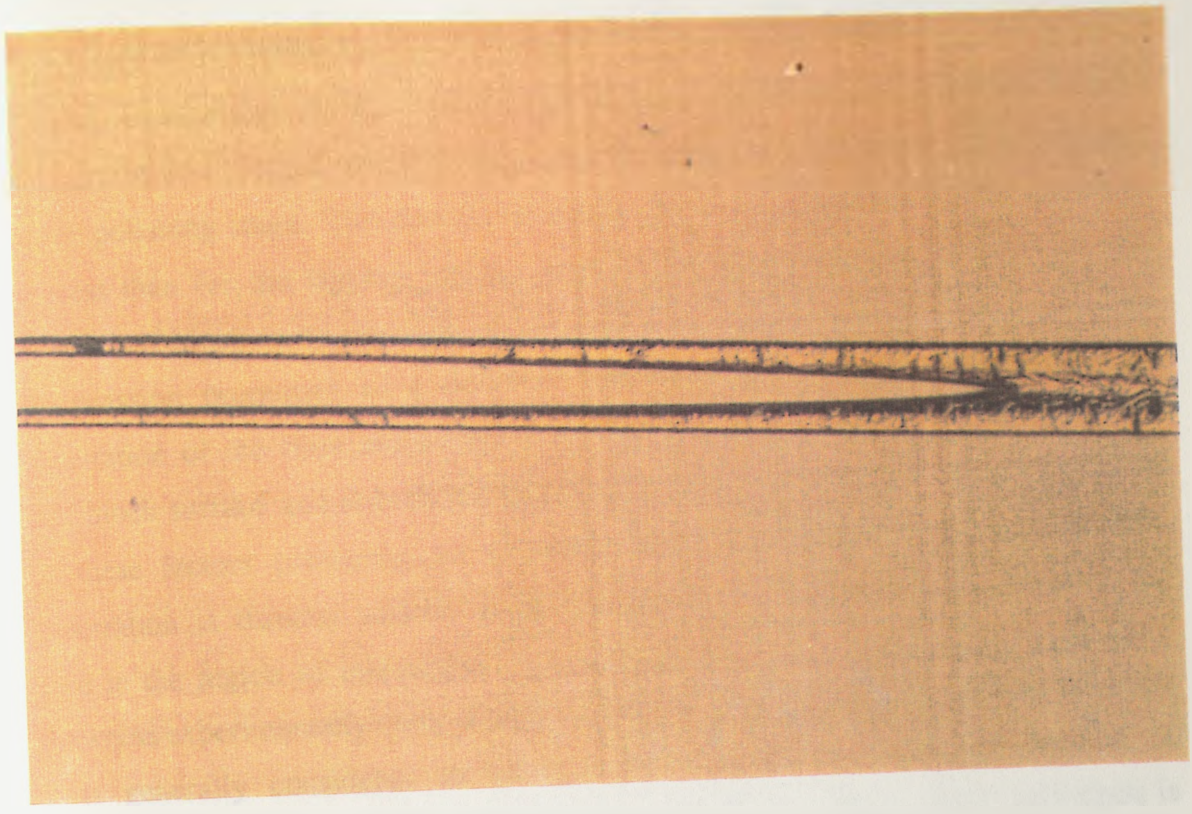

Section of ellipse shape on polished fibre cladding

groove above the fibre thus reducing the total surface area of glue required to bond the fibre in place. Further steps taken to improve flatness included reducing the jig pressure whilst polishing and also controlled adjustments of the sample surface alignment relative to the jig drive-ring.

4.3 Characterisation of Polished Fibre Half-blocks

Careful monitoring of the remaining cladding thickness is essential in the characterisation of each polished fibre half-block with particular care being required at the polishing stage. The material removal rate is much slower for the polishing process than for the lapping process and is quite time-consuming. However, this allows half-block to be regularly tested during the process which is desirable. The transmission properties of a polished fibre half-block are dependent upon the penetration of the fibre evanescent field into whichever material is placed on the half-block surface and also on the radius of curvature of the fibre, the combination of these factors producing an effective interaction length. The extent of this penetration is directly related to the remaining cladding thickness[1] above the core in the region of interaction. It is difficult to measure the remaining cladding thickness experimentally using standard optical and mechanical instruments, although it is generally considered to be less than 5μm[2], so a simpler method of calibrating the polished fibre half-block is used in this thesis. Each half-block is categorised in terms of a notional "coupling strength" which is defined as the percentage drop in transmitted intensity incurred when an oil of refractive index n_D=1.600 is applied in bulk form to the surface of the half-block (operation at λ=1.3μm). (The refractive index of the oils is generally quoted for the Sodium D-line wavelength and for a temperature of 25°C. They display significant dispersion with both wavelength and temperature). The above method is known as the liquid-drop method[3] and has the advantage that the interface between the oil and the polished fibre is always as good as the polished fibre surface. Thus, there is no need to treat the oil/fibre boundary in any special way. Once an optical quality finish has been produced on the half-block surface by polishing, the surface is carefully cleaned

and light from a 1300nm diode laser launched into the fibre. The transmission response of the half-block is most sensitive to a bulk overlay material possessing a refractive index value close to that of the fibre effective index (i.e. the refractive index "seen" by the fibre mode). Therefore, initial transmission measurements are performed using an oil of index $n_D \approx 1.456$ as the bulk overlay to detect the earliest sign of the fibre interacting with the external medium. Once this point has been reached the half-block is subjected to a number of short periods on the polishing machine (typically 2-5mins in duration) with transmission measurements being made using oil of $n_D = 1.600$ after each period of polishing. It should be noted that the optical field strength in the cladding region decays exponentially with distance and that the material removal rate should be adjusted accordingly. The radius of curvature of the fibre further complicates this part of the process. Repeated polishing and testing is continued until the polished fibre half-block displays the desired "coupling strength" (as defined earlier).

Two radii of curvature were selected for the design of polished fibre half-blocks, 11cm and 22cm approx. Three half-blocks with each radius were fabricated possessing coupling strengths of approximately 10%, 55% and 90%. The liquid drop method was then employed to characterise the half-blocks over a range of bulk oil overlay indices. Figures 4.3 and 4.4 show the transmission response of the half-blocks for bulk indices 1.0 (air) to $n_D = 1.698$, the input wavelength being 1300nm. The response of each half-block displays a minimum in transmission corresponding to an oil index of $n_D = 1.456$, which is approximately equal to that of the fibre mode when wavelength dispersion is considered. The transmission responses compare well with similar experimental results[4], although coupling strengths of less than 90% are generally not examined. Simple waveguide theory can be used to interpret the transmission responses. While the bulk index in contact with the reduced cladding side of the fibre is less than or equal to the fibre cladding no light will be lost i.e. the fibre will guide as normal. For oil indices in the vicinity of the effective index of the single fibre mode, the propagation constants of the bulk optical wave and the guided fibre mode are almost matched, and strong coupling of the light out of the

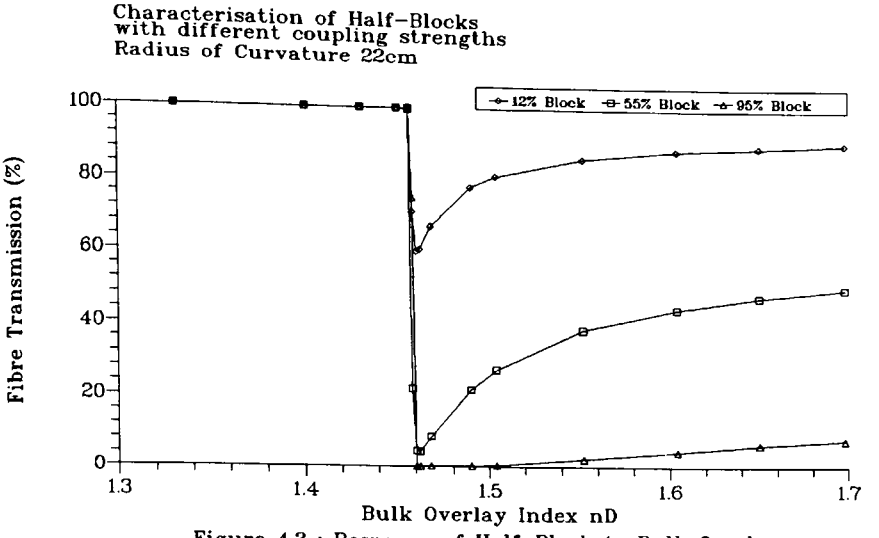

Figure 4.3 : Response of Half-Block to Bulk Overlay

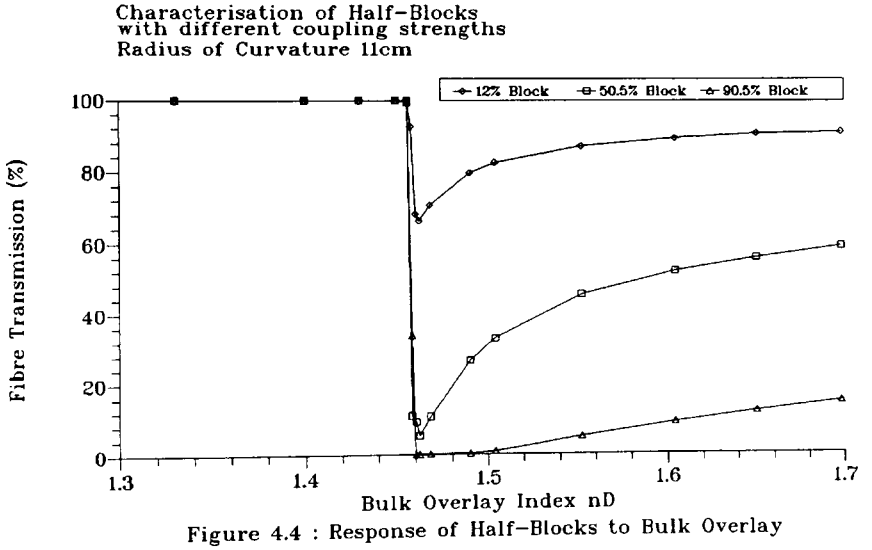

Figure 4.4 : Response of Half-Blocks to Bulk Overlay

fibre occurs[7] i.e. the fibre becomes leaky. Increasing the oil index still causes coupling of light from the fibre but with a corresponding decrease in efficiency. Reducing the cladding thickness further increases the strength of the coupling and, thus, reduces the fibre transmission.

The difference in radii of curvature appears to have only a small effect on the fibre transmission properties, the recovery rate of the fibre transmission on the high index side of the minimum being slower for the low radius half-blocks. However, it is probably inappropriate to compare the different radius of curvature half-blocks via their respective coupling strengths since, intuitively, the interaction lengths will be different i.e. it is very unlikely that the remaining cladding thickness is identical for the different radius of curvature half-blocks although they may possess the same coupling strength. It would be expected that the longer r.o.c. half-blocks possess thicker remaining cladding but also a longer interaction length than their shorter r.o.c. counterparts. In each case, however, the combination of remaining cladding and interaction length gives rise to similar coupling strengths. Chapter 5 reports on the effect of fibre radius of curvature on the behaviour of the fibre-overlay devices.

Once each polished fibre half-block displays the desired coupling strength, it is ready for incorporation into fibre-overlay device structures. Typically, such devices are formed with index oils, vacuum-deposited films, optical crystals or optical glass in the role of the overlay. The following chapters report on the experimental investigation of a variety of these devices.

References

1. O.G. Leminger and R. Zengerle,"Determination of single-mode fiber coupler design parameters from loss measurements", J. of Lightwave Technol., **LT-3**, pp864-867, 1985.

2. M.J.F. Digonnet and H.J. Shaw,"Analysis of a tunable single mode optical fiber coupler", IEEE J. Quantum Electron., **QE-18**, pp746-754, 1982.

3. M.J.F. Digonnet, J.R. Feth, L.F. Stokes and H.J. Shaw,"Measurement of the core proximity in polished fibre substrates and couplers", Opt. Lett., **10**, pp463-465, 1985.

4. S-M Tseng and C-L Chen,"Side-polished fibres", Appl. Opt., **31**, pp3438-3447, 1992.

CHAPTER 5

Oil Overlay Devices

5.1 Introduction

This chapter investigates device structures incorporating Cargille refractive index oils[1] in the role of the high index overlay waveguide. The advantages of using oil overlays were twofold. Firstly, the device fabrication process was rapid and relatively simple. Secondly, each polished fibre half-block could be tested with a range of overlay thicknesses and refractive indices since the oil could be easily removed from the half-block surface. Thus, extensive characterisation of the device structure could be achieved while difficult, time-consuming fabrication processes were avoided, the aim being to establish a general understanding of device behaviour. Initial investigation centres on the index response (via the thermo-optic effect) of the devices while a more detailed study of the wavelength response is reported in the later part of the chapter.

5.2 Device Geometry and Fabrication

Initial experiments were performed on devices which incorporated Cargille refractive index oils, supported by Mylar polyester spacers of known thickness, sandwiched between a polished fibre half-block and a superstrate of polished fused silica. Two thicknesses of spacer were used, 12μm and 23μm and the oils ranged in refractive index from $n_D = 1.47$ to $n_D = 1.698$. Several different coupling strength polished fibre half-blocks were employed. A specially designed jig, possessing spring-loaded clamps to prevent thickness variations due to temperature changes, was used to hold the structure. A significant degree of clamp pressure was required to ensure the waveguide thickness was approximately equivalent to that of the Mylar spacers and cleanliness of the adjacent polished surfaces and the Mylar spacers was essential.

The device was constructed by sandwiching the spacers between the half-block and fused silica superstrate prior to introducing the Cargille oil via capillary action to form the overlay waveguide. The overlay waveguide was then of a symmetric nature and displayed negligible waveguide birefringence. A switch structure was constructed in a similar fashion by substituting the fused silica superstrate for a second polished fibre half-block. Precise lateral location of the second half-block was required to achieve alignment of the fibre cores.

5.3 Experimental Techniques

Methods of tuning the overlay mode structure, in the case of a fixed superstrate index, are via modification of the overlay thickness and/or refractive index or variation of the input wavelength to the device. Dynamic variation of the overlay thickness could, in principle, be achieved by adjusting the spacer thicknesses via the piezoelectric effect but practical implementation is difficult. Experimental investigation of the oil overlay devices was, therefore, restricted to the two remaining overlay parameters, refractive index and input wavelength. However, it should be noted that variation of any of the parameters has the same basic effect of shifting the mode structure of the overlay waveguide, and this is the basic mechanism upon which device operation relies.

Simple variation of the overlay refractive index was possible for the oil devices. All the Cargille oils possessed a significant, negative dn/dT (rate of change of index with temperature), in the range 3-5 x 10^{-4}/°C. Therefore, using this thermo-optic effect, the refractive index of the overlay could be "scanned" with the subsequent device transmission response being recorded. Light from a pig-tailed internally modulated (2KHz) 1300nm wavelength semiconductor laser diode was launched into a 9:1 fused fibre coupler. The 90% output arm was then connected to the input lead of the oil overlay test device via a mechanical splice while the 10% arm was fed to a Germanium photodetector for use as a monitor signal. The output lead of the test device was fed to a second Germanium photodetector (measurand signal). Both

photodetector outputs were connected to a lock-in amplifier and the signals recorded during the thermal scan. The temperature of the oil overlay was raised by placing the device and supporting jig inside an oven. A temperature scan range in the region of 60-70°C above room temperature was generally used. Transmitted intensity readings were recorded as the device cooled slowly to room temperature, thereby minimising the effect of thermal fluctuations. The oil temperature was measured by placing a thermocouple as close as possible and in contact with the half-block or superstrate. The cooling cycle was initiated after the thermocouple reading had reached a steady-state value and performed slowly (1.5hrs) to reduce the effect of fluctuations. The recorded temperature values could then be converted into corresponding index changes using the appropriate value of dn/dT and graphed against the normalised transmitted intensity readings (measurand/monitor). No polariser or polarisation controller was included in the set-up because the oils are isotropic and the waveguides symmetrical and multi-moded thus causing negligible waveguide birefringence and corresponding polarisation sensitivity.

The mode structure of all waveguides is also sensitive to variation of the input wavelength. This provides a simple way of modulating the transmission response of a device. This method of device interrogation was easier, quicker to use and more reliable than thermal scanning and was, therefore, widely utilised throughout this project. The main component was a Bentham Instruments scanning monochromator configured for use with optical fibre. The output from a 100W (Halogen) white light source was chopped and focused onto the input slit of the monochromator. Light passing through the slit is filtered and is then incident on a grating, the angle of which can be adjusted by servo-motor control. The grating angle is calibrated such that a discrete wavelength, within a wavelength range, can be selected to emerge from the output slit. The light from the output slit was then polarised and launched into the input lead of the test device via a polarisation controller and mechanical splice. The device transmitted intensity was fed to an InGaAs photodetector which was connected to a lock-in amplifier. Figure 5.1 illustrates the experimental set-up. The set-up was controlled from a suitably configured IBM personal computer. The

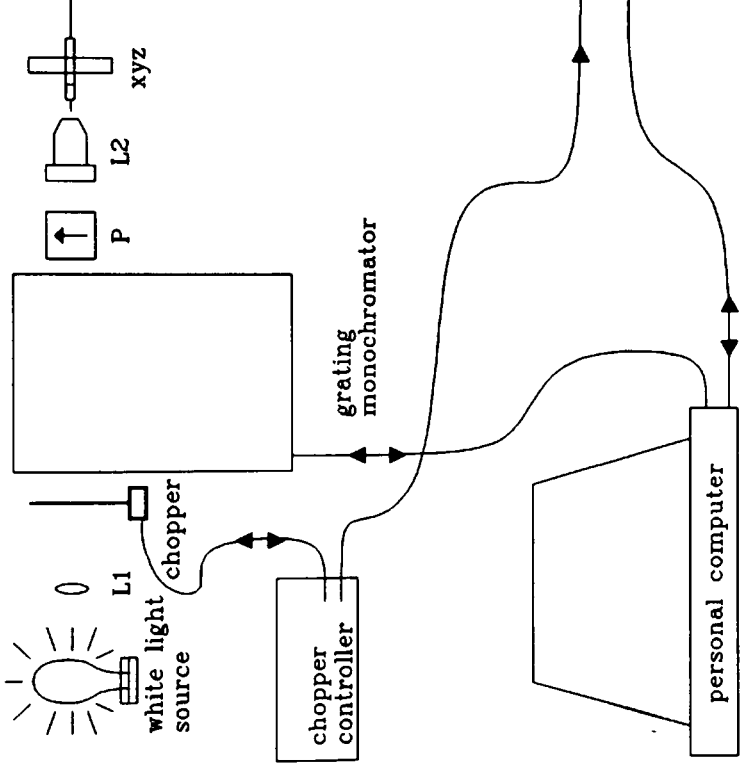

Figure 5.1 : Schematic Diagram of Wavelength Scanning Set-Up

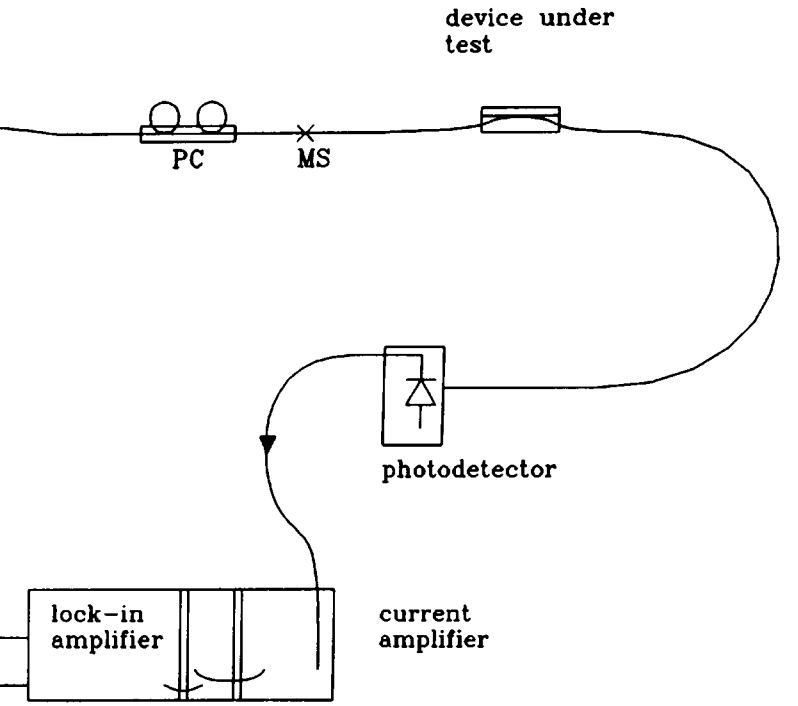
device under
test
PC
MS
photodetector
lock–in
amplifier
current
amplifier

components denoted by P and PC represent a polariser and polarisation controller, respectively, L1 and L2 are lenses, and MS is a mechanical splice. The usual scan range was between 1200nm and 1600nm with the step intervals generally 1-2nm, depending on desired accuracy. Wavelength resolution was determined by the width of input and output slits of the monochromator, usually 0.5mm giving 1.8nm resolution. The signal-to-noise ratio (and, thus, dynamic range) of the system was reduced when high wavelength resolution (limit < 1nm) was required because this significantly cut the amount of power available at the output slit of the monochromator. A typical intensity versus wavelength scan is shown in Chapter 1, Figure 1.4.

5.4 Device Characterisation by Overlay Index Variation

Initial oil device experiments made use of the thermo-optic effect since the wavelength scanning equipment was not available at that time. This characterisation technique was time-consuming and not of high accuracy but allowed some basic knowledge of device behaviour to be gathered. Results are presented here for eight test devices. The devices incorporated two different coupling strength polished fibre half-blocks (12% and 90%) with radius of curvature approximately 22cm. Two different Cargille refractive index oils ($n_D = 1.494$ and 1.548) were used as the overlay material, supported by two thicknesses of spacer (12μm and 23μm). Each device was index scanned over a range which allowed at least two resonances dips to be observed in the transmitted intensity (typically 60-70°C). The transmitted intensity versus overlay index (dispersion-corrected to $\lambda = 1.3\mu$m) was recorded for each combination of half-block and overlay parameters. The resulting graphs of transmitted intensity versus overlay index were all of a similar form but the width of the resonances and modulation depths were strongly dependent upon the coupling strength of the half-blocks. Figures 5.2 and 5.3 are typical examples and demonstrate this effect. The resonance spacing increased as both the index and waveguide thickness were reduced. This effect is expected from simple waveguide theory and is discussed in more detail in section 5.5.1. The resonance linewidth and modulation

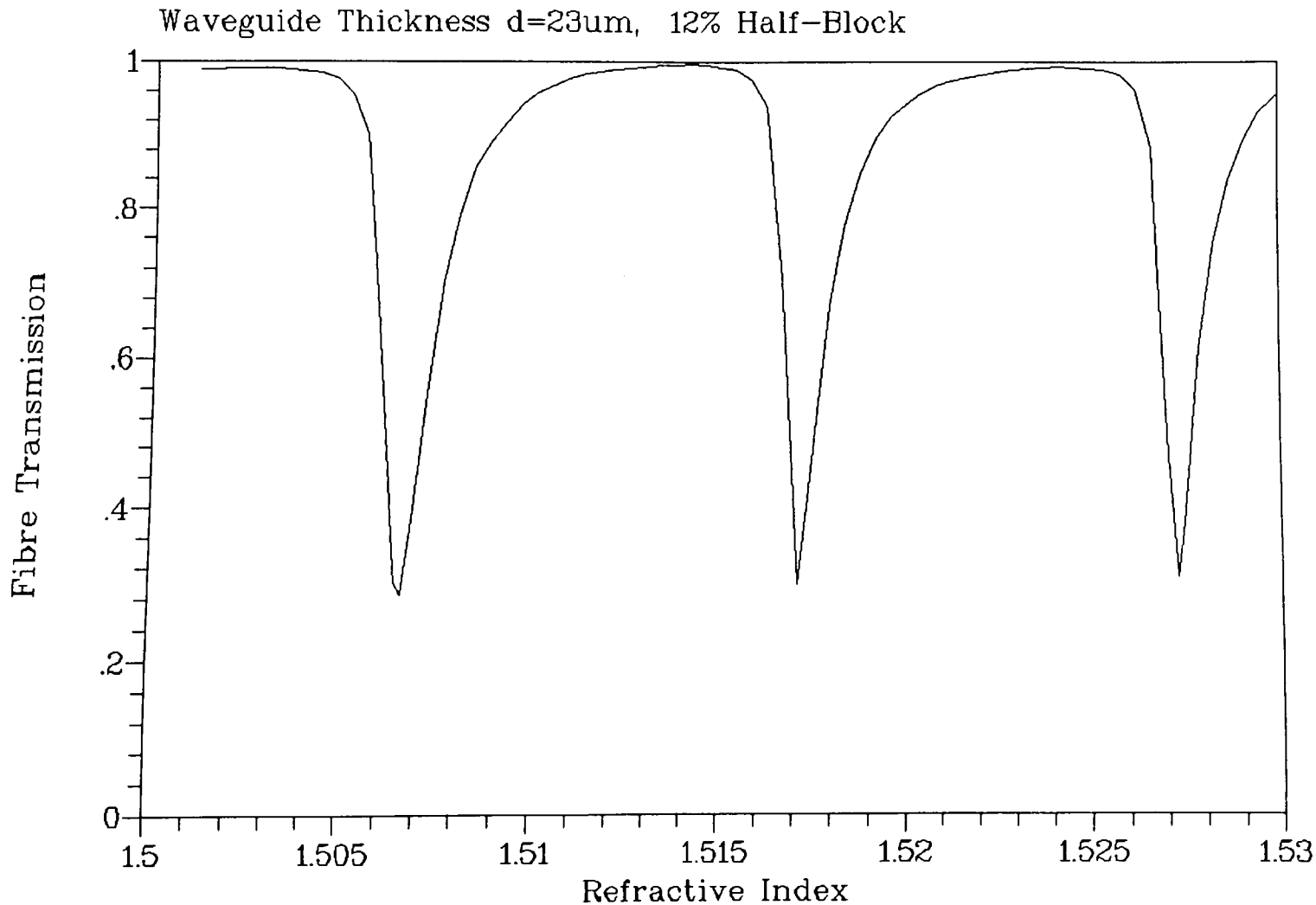

Figure 5.2 : Index Response of Oil Overlay

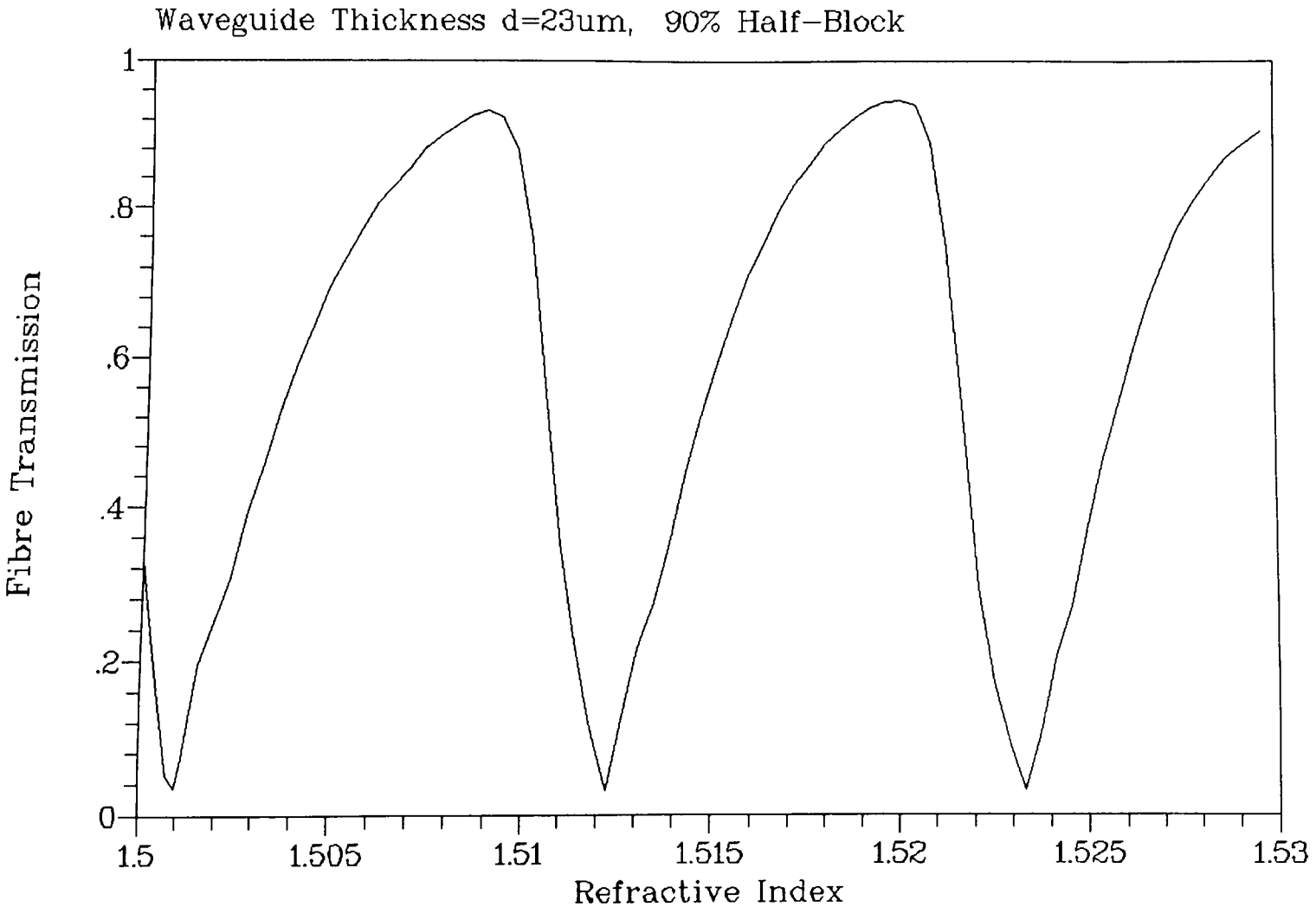

Figure 5.3 : Index Response of Oil Overlay

depth and of the device transmission responses for the different overlay indices n_D and thicknesses, d, are shown in Tables 5.1 and 5.2 for the 12% and 90% coupling strength half-blocks, respectively. The modulation depth is a measure of the percentage of the power coupled out of the fibre at a resonance position. From Tables 5.1 and 5.2, it is clear that the lower coupling strength half-block produces devices with narrower resonance linewidths. It also appears that the low index, thicker overlays, for each coupling strength, produce narrower resonance widths. This does not agree with simple waveguide theory which indicates that high index, thicker overlays will give higher dispersion and, therefore, the narrowest linewidths. The discrepancy is thought to be due to inaccuracies in the experimental procedure and reflects the unreliability of this method of device characterisation. A more detailed experimental analysis of the effect on linewidth of the overlay parameters was conducted via wavelength variation and is given in section 5.5.2. The modulation depth shows an increase for the 90% coupling strength results but there is no clear trend as regards overlay parameters from inspection of the data in Tables 5.1 and 5.2. Again, a more detailed discussion of modulation depth (or channel rejection ratio from a filter viewpoint) is given in section 5.5.3. An advantage of the index variation experimental technique is that loss measurements are easier to make due to better signal to noise ratios when compared with the wavelength variation approach. The off-resonance loss (comparison of with/without overlay throughput) of the devices was higher for the 90% coupling strength devices. The thinner, low index overlays caused the highest loss, 0.12dB (12% half-block) and 1.6dB (90% half-block). Particularly low loss values appear possible with the 12% coupling strength half-block, 0.018dB being recorded for $n_D=1.548$, $d=23\mu m$.

With regard to intensity modulator and switch configurations using the basic fibre-overlay geometry, the sharper side of the resonances observed in an index scan are crucial. At these points on the index response, a significant shift in the transmitted intensity can be induced by a relatively small variation of the overlay index. A switch structure is envisaged as possessing a cross-coupled intensity response which is the inverse of the typical transmitted intensity responses shown, for example, in

Overlay Index	Linewidth (FWHM)		Modulation Depth	
	d=12μm	d=23μm	d=12μm	d=23μm
n_D=1.494	0.00126	0.00087	96.1%	78.1%
n_D=1.548	0.00113	0.00102	83.3%	69%

Table 5.1 : 12% Coupling Strength Half-Block Results

Overlay Index	Linewidth (FWHM)		Modulation Depth	
	d=12μm	d=23μm	d=12μm	d=23μm
n_D=1.494	0.00337	0.00256	85.7%	94.3%
n_D=1.548	0.00482	0.00381	97.9%	96.8%

Table 5.2 : 90% Coupling Strength Half-Block Results

Figures 5.2 and 5.3. Therefore, a similar shift in overlay index should produce an intensity change in the cross-coupled output. Intensity modulation or switching could be achieved by utilising the linear electro-optic effect (Pockels) in a suitable overlay material ($LiNbO_3$) to produce the necessary change in material index. The smallest index change to induce a 10%-90% intensity variation for the devices tested was 0.721×10^{-3}. The overlay details were n_D=1.494, t=12μm. The reduced modulation depth of the higher index, thicker oil overlay devices meant that a 10%-90% intensity change was not attained. However, improved figures can be expected from other devices. Assuming, a similar index response in a $LiNbO_3$ overlay device, then the corresponding required drive or switching voltage can be attained from the following equation[2]:

$$\Delta n = \frac{n^3}{2} r_{33} \frac{V}{d} \qquad (5.1)$$

where r_{33}=30.8pm/V is the appropriate electro-optic coefficient, n is the material index (approx. 2.15 at λ=1300nm), d is the overlay thickness and V is the applied transverse voltage. Using the value of Δn obtained from the oil response, the corresponding voltage required to induce 10%-90% intensity modulation is 57.3V or 4.78V/μm. It is not unreasonable to expect better results for practical devices incorporating $LiNbO_3$ since theoretical calculations indicate that sharper resonances should be produced by higher index overlays. By manipulating the waveguide eigenvalue equation (1.1), wavelength scans detailed in the following sections can be converted to equivalent index scans. This allows further calculations concerning drive voltages to be made.

5.4.1 Index Response of Oil Overlay Switch

An initial assessment of the feasibility of the switch structure was made using the technique of index scanning via the thermo-optic effect. The experimental set-up was the same as before apart from the superstrate being replaced with a second half-block. A number of difficulties in experimental procedure were immediately encountered. Obviously, the jig must be set up at room temperature and then placed in the oven for thermal/index scanning. Therefore, it was essential that alignment of the two half-blocks was achieved at room temperature. However, significant power transfer was the only method of determining when the half-blocks were correctly aligned and significant power transfer can only occur when the device transmission response is on a resonance. The likelihood of a resonance occurring at room temperature was small. Additionally, whenever the second half-block was translated laterally, a small change in the waveguide thickness tended to occur because of the liquid nature of the oil. This meant that the device resonance positions would shift making good alignment with strong power transfer almost impossible to achieve. It was found that no power could be transferred using low coupling strength half-

blocks. When higher coupling strength blocks were used (both 85%) some power transfer could be achieved. Figures 5.4 - 5.6 show the response of each arm of the switch structure for different overlay parameter combinations. The intensity transmission responses of the "straight through" arm and the "cross-coupled" arm are the inverse of each other and of a basically periodic nature. This indicated that the structure was behaving as a routing switch i.e. light tapped from the input fibre was collected by the second fibre. It was possible to couple light between the fibres using the higher coupling strength blocks because of the wider resonances they produce. This means that light can still be coupled out of the input fibre even when there is a significant phase mismatch and therefore a greatly increased chance of aligning the blocks such that some power transfer occurs at room temperature. The need for lateral alignment of the second half-blocks and thus continual small thickness variation of the oil waveguide meant that switch structure was unlikely to ever perform efficiently without the aid of complicated mechanical alignment jigs. However, the results displayed in Figure 5.4 - 5.6 indicate that the switch structure is feasible, with good alignment of the second half-block being critical. Further investigation of the switch structure was carried out using solid-state devices with characterisation via wavelength variation. The results of this investigation are presented in Chapter 6.

5.5 Device Characterisation by Wavelength Variation

To assess the wavelength response of the device structure to variations in the overlay material index and thickness, spacer thicknesses of 12μm and 23μm were used with five different oil indices. The oils ranged from $n_D=1.47$ to $n_D=1.698$ and three different coupling strength polished fibre half-blocks (12%, 55%, 95%) were used in the experiments. Each half-block was associated with each combination of overlay index and thickness. The intensity versus wavelength response for each device was then obtained using the set-up described earlier. The polarisation sensitivity of the devices was very small and, therefore, not recorded. Every wavelength response was of a similar nature to that shown in Figure 1.4 although the resonance spacing and

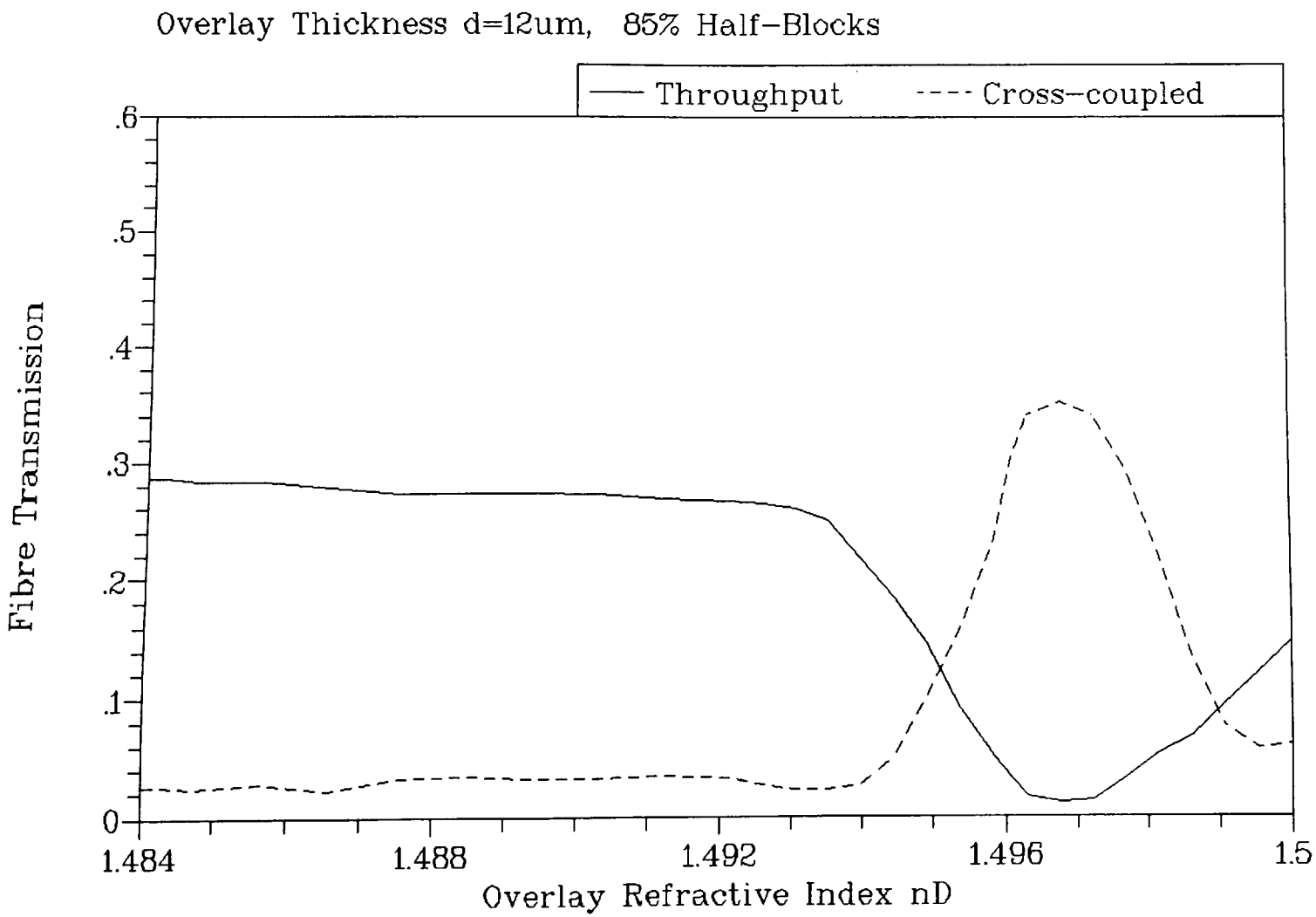

Figure 5.4 : Index Response of Oil Overlay Switch

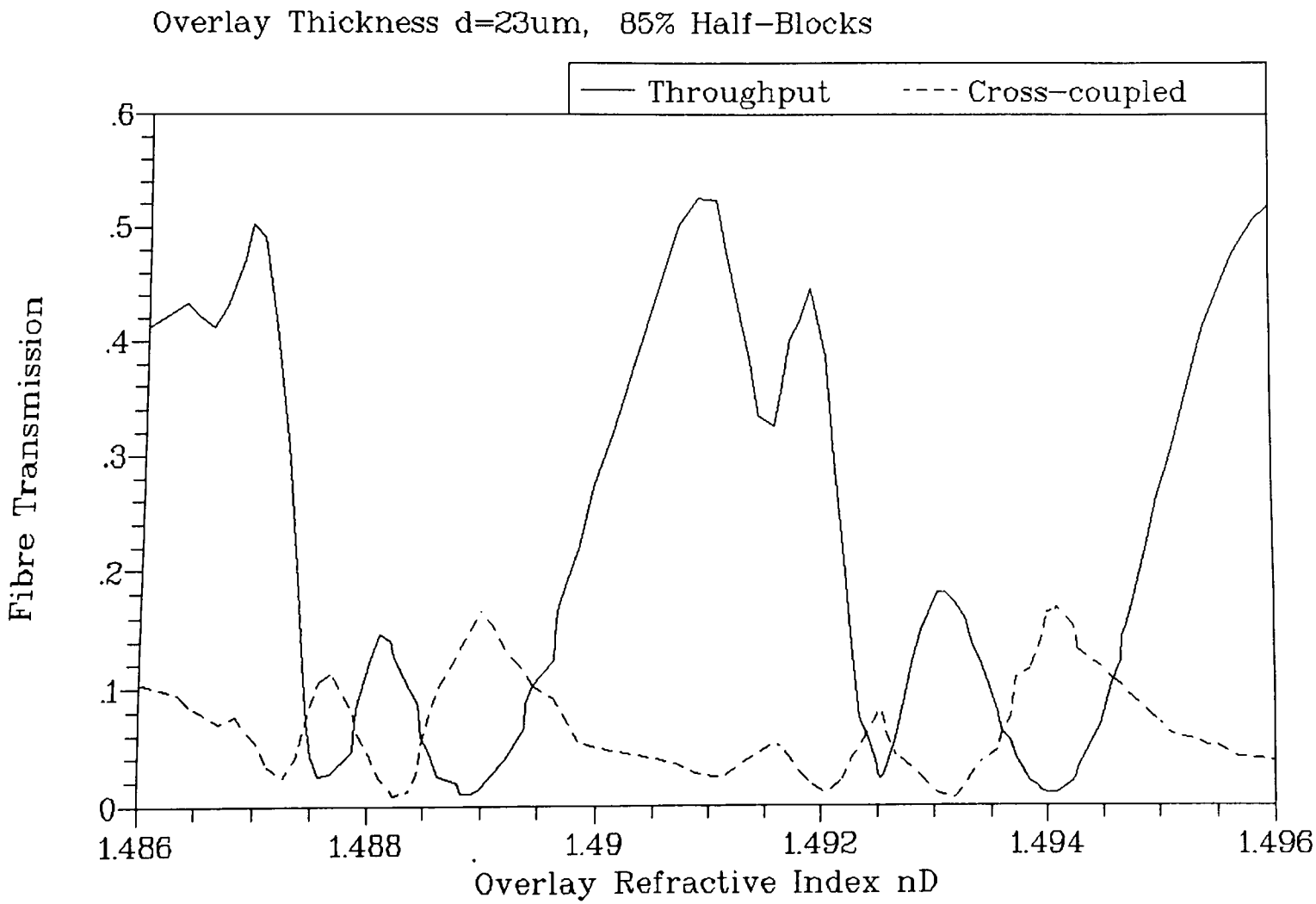

Figure 5.5 : Index Response of Oil Overlay Switch

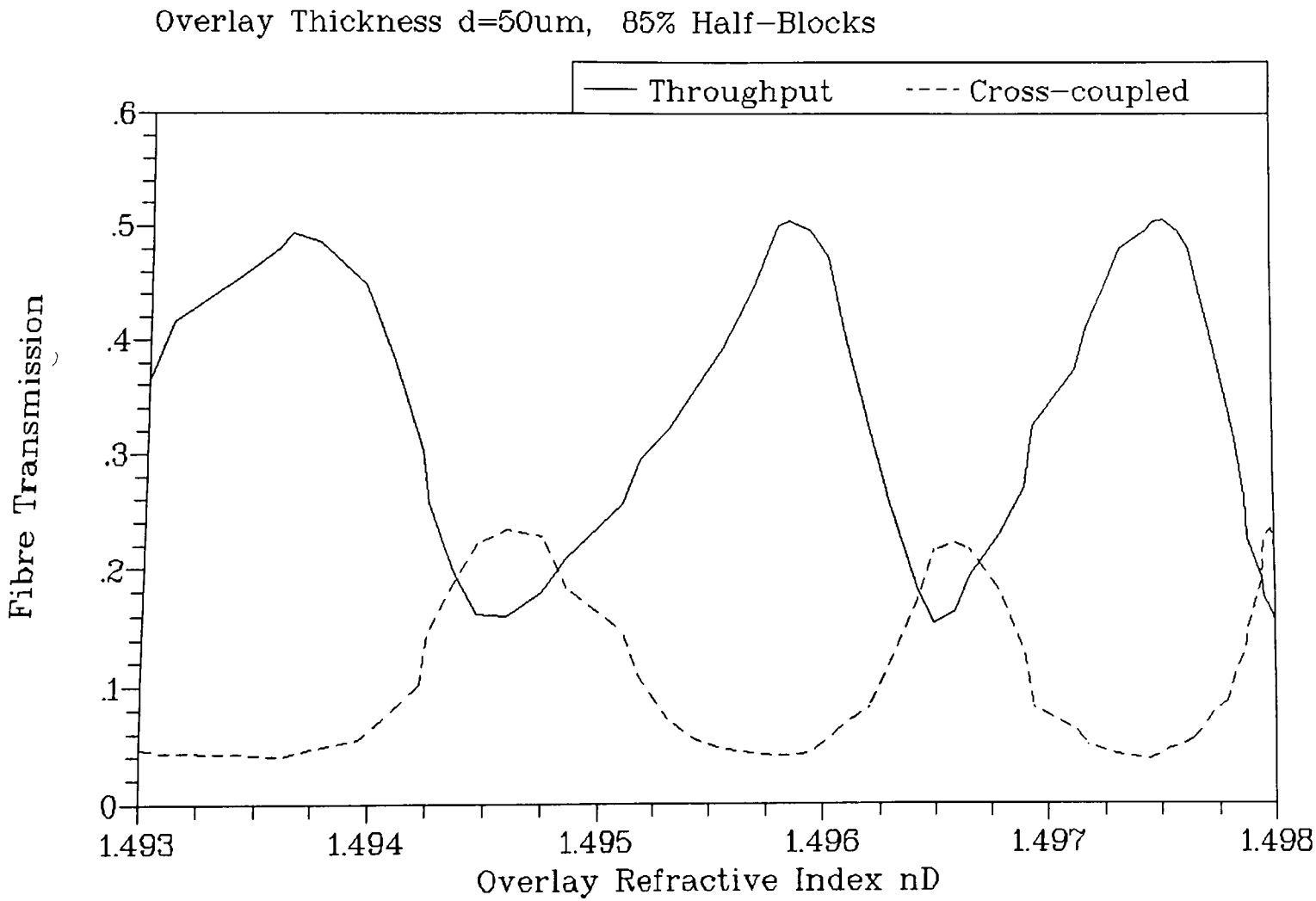

Figure 5.6 : Index Response of Oil Overlay Switch

linewidth varied considerably for different parameter combinations. Figures 5.7 and 5.8 highlight this effect. Tables 5.3 - 5.8 show the difference in resonance linewidths and spacing for the different polished fibre half-blocks and overlay parameters.

All values were taken from the resonance closest to $\lambda = 1300$nm for each scan. The resonance linewidth and spacing and also the corresponding modulation depth (the term "modulation depth" will be retained to be consistent with its earlier use although rejection ratio is technically more correct) are of primary importance with regard to device performance. Inspection of Tables 5.3 - 5.8 indicates that these device performance parameters are closely linked to the overlay waveguide parameters, n_D and d. The coupling strength of the polished fibre half-blocks also appears to be significant. Similar experimental investigation was performed for devices in which the polished fibre half-blocks possessed approximately 11cm radii of curvature. No major differences were observed with regard to device behaviour and for this reason the results are not presented. However, the modulation depth values were, in general, slightly reduced and this aspect is discussed in section 5.5.3.

5.5.1 Resonance Spacing

The recorded data on resonance spacing displays a clear dependence on the overlay index, the spacing decreasing as the index is raised. In addition, the overlay thickness causes a further spacing decrease as it is increased from 12μm to 23μm. The relationship between the resonance spacing and the overlay parameters is similar for each half-block, particularly for the higher indices. This is expected and can be explained from simple waveguide theory. Assuming the weakly-coupled guides approach to the device structure, then the overlay waveguide is virtually unperturbed by the presence of the fibre. In this case, the resonance spacing for each waveguide will depend on the waveguide parameters and can be obtained from the eigenvalue equation. The resonance positions correspond to the overlay highest order mode index matching that of the fibre mode. Simple substitution into the eigenvalue equation produces the resonance wavelength values, the difference being the resonance spacing. Assuming that remaining cladding thickness on each half block

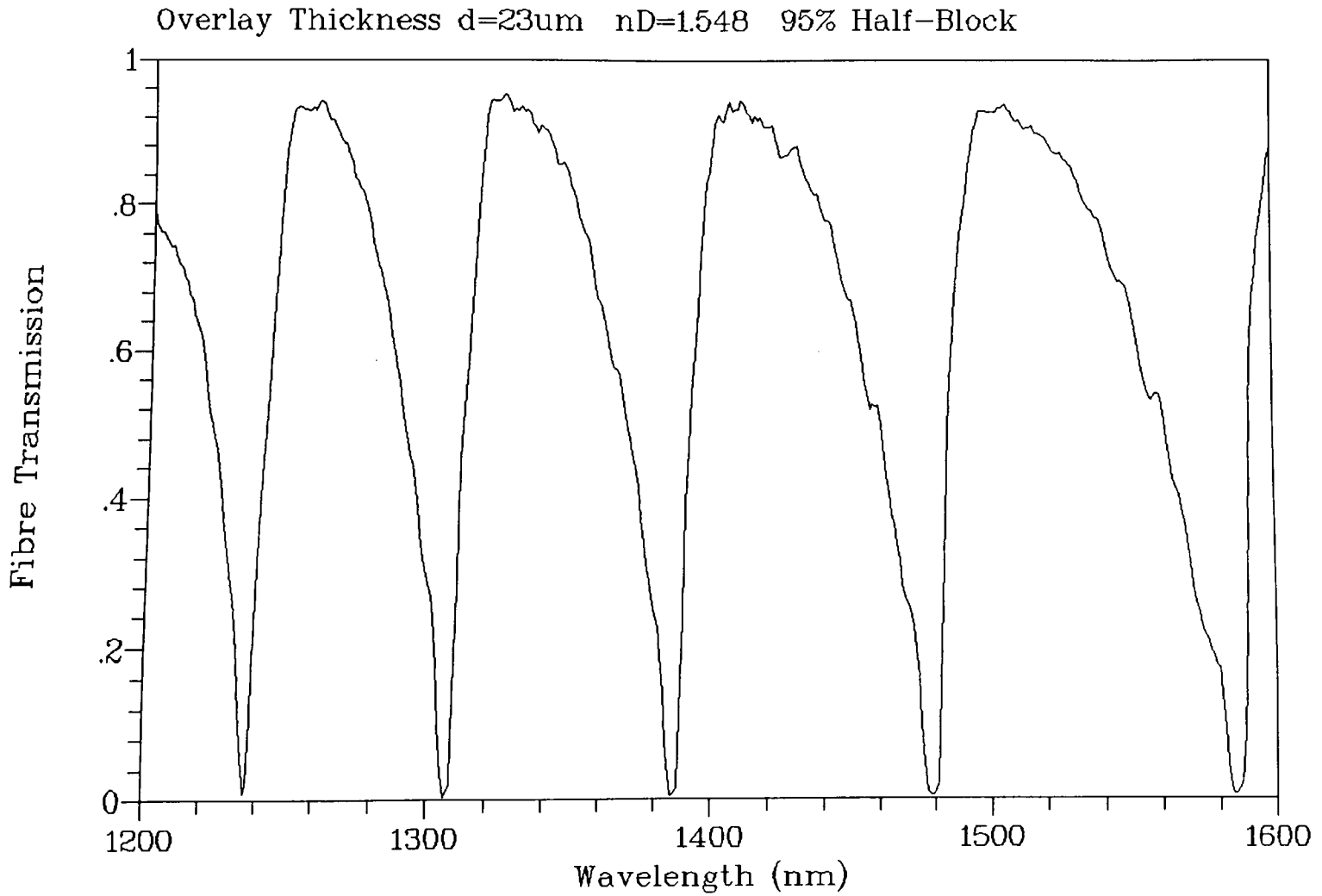

Figure 5.7 : Wavelength Response of Oil Overlay

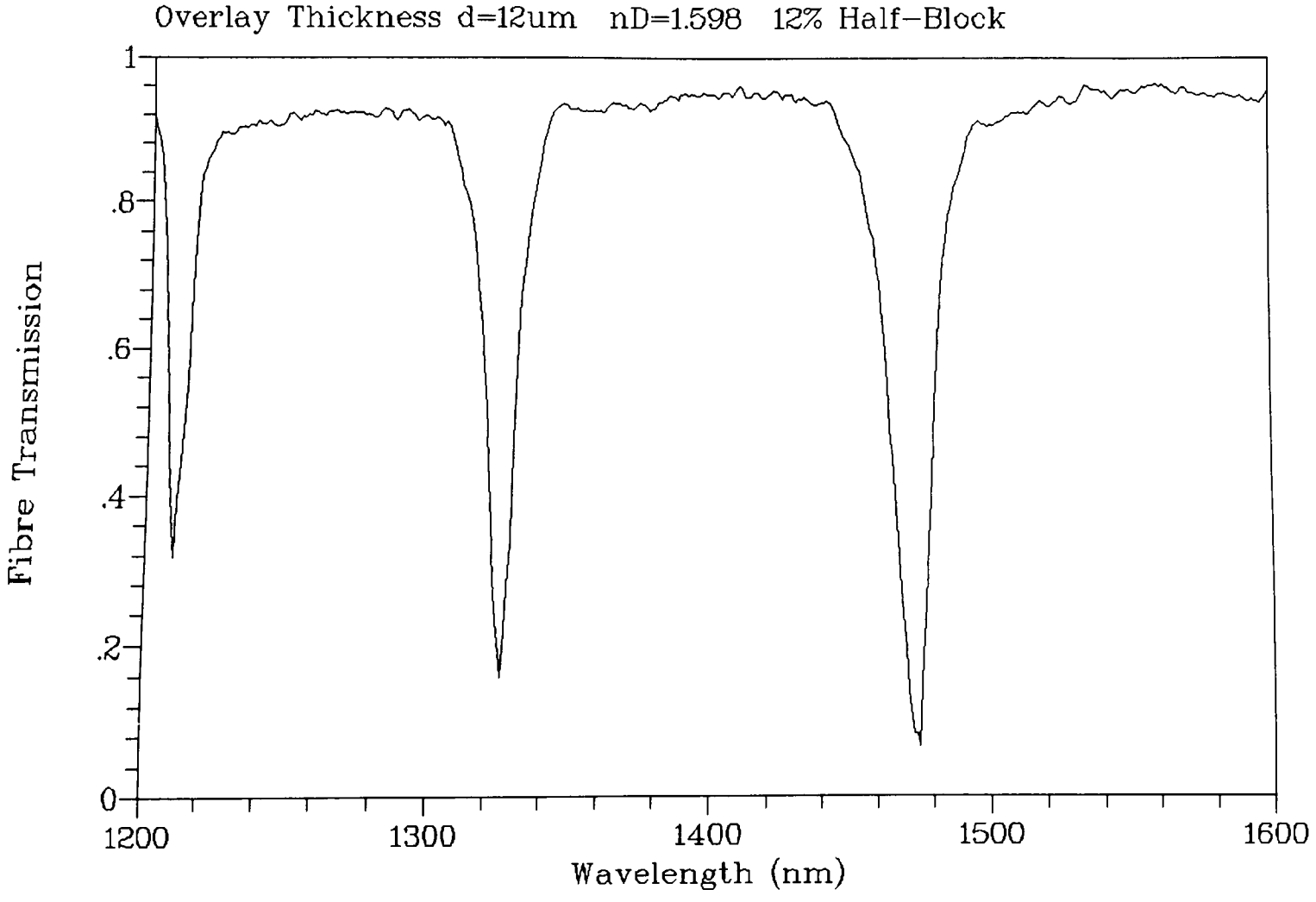

Figure 5.8 : Wavelength Response of Oil Overlay

Oil Index, n_D	Linewidth (FWHM)	Resonance Spacing	Modulation Depth
1.470	31nm	----	79.4%
1.494	15.8nm	132nm	90.8%
1.548	7.4nm	70nm	93.3%
1.598	5nm	55nm	78.0%
1.650	3.7nm	50nm	71.8%
1.698	3.1nm	45nm	81.7%

Table 5.3 : 12% Coupling Strength Half-Block, roc=22cm
Spacer Thickness 23μm

Oil Index, n_D	Linewidth (FWHM)	Resonance Spacing	Modulation Depth
1.470	56nm	----	94.8%
1.494	21.7nm	254nm	90.0%
1.548	8.6nm	166nm	91.6%
1.598	7nm	116nm	92.9%
1.650	5.6nm	97nm	84.9%
1.698	4.65nm	89nm	90.6%

Table 5.4 : 12% Coupling Strength Half-Block, roc=22cm
Spacer Thickness 12μm

Oil Index, n_D	Linewidth (FWHM)	Resonance Spacing	Modulation Depth
1.470	84nm	----	88.3%
1.494	31.7nm	125nm	82.6%
1.548	12nm	74nm	82.8%
1.598	8.6nm	59nm	84.3%
1.650	5.7nm	47nm	82.6%
1.698	4.7nm	43nm	82.6%

Table 5.5 : 55% Coupling Strength Half-Block, roc=22cm
Spacer Thickness 23μm

Oil Index, n_D	Linewidth (FWHM)	Resonance Spacing	Modulation Depth
1.470	103.3nm	----	87.6%
1.494	71.4nm	284nm	99.8%
1.548	20.8nm	166nm	99.1%
1.598	11.4nm	124nm	98.4%
1.650	10.7nm	95nm	97.8%
1.698	9.1nm	90nm	83.3%

Table 5.6 : 55% Coupling Strength Half-Block, roc=22cm
Spacer Thickness 12μm

Oil Index, n_D	Linewidth (FWHM)	Resonance Spacing	Modulation Depth
1.470	144nm	----	77.3%
1.494	55.6nm	126nm	88.2%
1.548	19.2nm	68nm	90.6%
1.598	15.2nm	51nm	89.0%
1.650	11.3nm	48nm	90.5%
1.698	9.8nm	44nm	88.3%

Table 5.7 : 95% Coupling Strength Half-Block, roc=22cm
Spacer Thickness 23μm

Oil Index, n_D	Linewidth (FWHM)	Resonance Spacing	Modulation Depth
1.470	205nm	----	92.0%
1.494	109.9nm	274nm	99.8%
1.548	26.1nm	162nm	99.0%
1.598	18.1nm	109nm	95.7%
1.650	13.8nm	106nm	94.2%
1.698	13.6nm	89nm	93.5%

Table 5.8 : 95% Coupling Strength Half-Block, roc=22cm
Spacer Thickness 12μm

is sufficient to ensure weak coupling, then the overlay resonance spacings should not be affected by the coupling strengths of the half-blocks and the resonance spacings for each half-block should be the same. The differences can be accounted for by discrepancies in the overlay thickness between experiments caused by dust particles, etc. The eigenvalue equation can be simply manipulated, for highly multi-moded waveguides (large *m*), to give:

$$\Delta\lambda = \frac{\lambda_r^2}{2d\sqrt{n_2^2 - n_{ef}^2} - \lambda_r} \qquad (5.2)$$

where λ_r is a resonance wavelength, n_{ef} is the fibre mode index, n_2 is the overlay index and d is the thickness. Notice the inverse dependence on both d and n_2. Equation 5.2 indicates that resonance spacing will be very small for a high index, thick overlay, particularly at lower wavelengths. Table 5.9 shows the calculated spacing values for the overlays used in the experiments (resonances adjacent to λ=1300nm).

Oil Index, n_D	Thickness 12μm	Thickness 23μm
1.470	372nm	202nm
1.494	244nm	130nm
1.548	160nm	84nm
1.598	110nm	68nm
1.650	96nm	54nm
1.698	82nm	49nm

Table 5.9 : Calculated Resonance Spacings

The calculated values show reasonable agreement with the experimental data as

would be expected. The major differences occur at the lower index values when slight thickness variations in the experimental overlays have a greater effect on mode spacing, and, hence, resonance spacing. Figure 5.9 compares theoretical and experimental resonance spacing.

5.5.2 Resonance Linewidth

From Tables 5.3 - 5.8, it is apparent that high index, thick overlays (large *m*) produce the narrowest linewidth (FWHM) values. The coupling strength of the polished fibre half-block incorporated in each test device also appears to be related to the width of the resonance, with low coupling strength (large remaining cladding thickness) giving the narrowest results.

Figure 5.10 - 5.12 show linewidth versus overlay index in graphical form for both a 23μm and 12μm overlay thickness using the data contained in Tables 5.3 - 5.8. The relationship in each instance is similar and displays a strong inverse nonlinear dependence on overlay index, suggesting that the use of higher index overlays (e.g. Zinc Sulphide, Lithium Niobate, Silicon) may produce very narrow (<2nm) linewidths. It is possible to compare Figures 5.10 - 5.12 with Figure 3.11 which relates the theoretical resonance linewidth with the overlay parameters. The similar relationship indicates that the value of $dn_e/d\lambda$ for an overlay mode close to phase-matching is the dominant factor in the device wavelength response. Tables 3.1 and 3.2 indicate that overlays with high mode orders produce narrowest linewidths and this agrees with the experimental results. The mode order increases with increasing index and thickness of the waveguide.

From Tables 5.3 - 5.8, the coupling strength of the particular polished fibre half-block incorporated in each test device is significant. The width of the device transmission resonances are dramatically increased when the 95% coupling strength half-block device responses are compared with the lower coupling strength half-block device responses (particularly the 12% half-block). As outlined in Chapter 3, the half-block coupling strength is a measure of the remaining cladding thickness on the

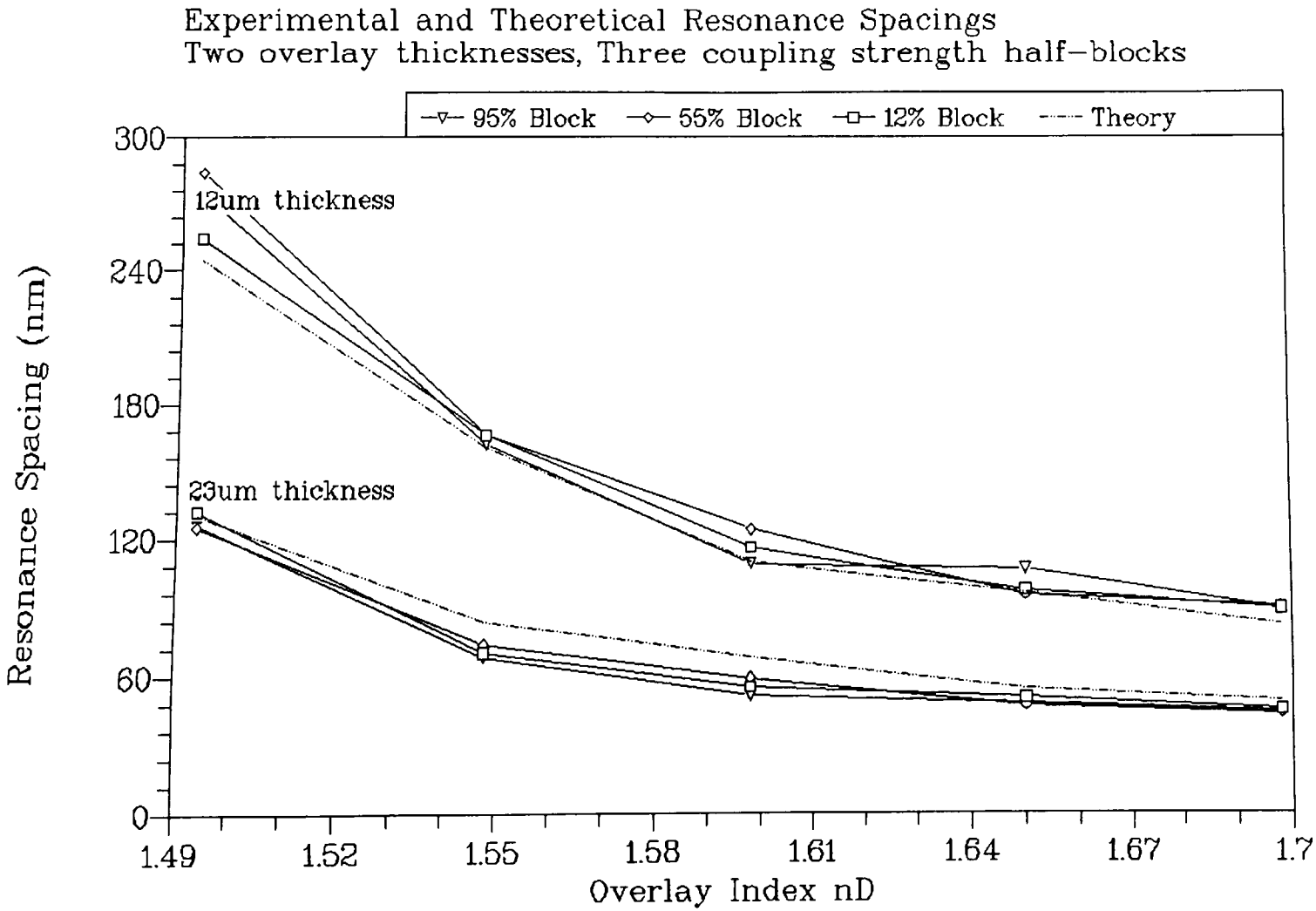

Figure 5.9 : Resonance Spacing versus Overlay Index

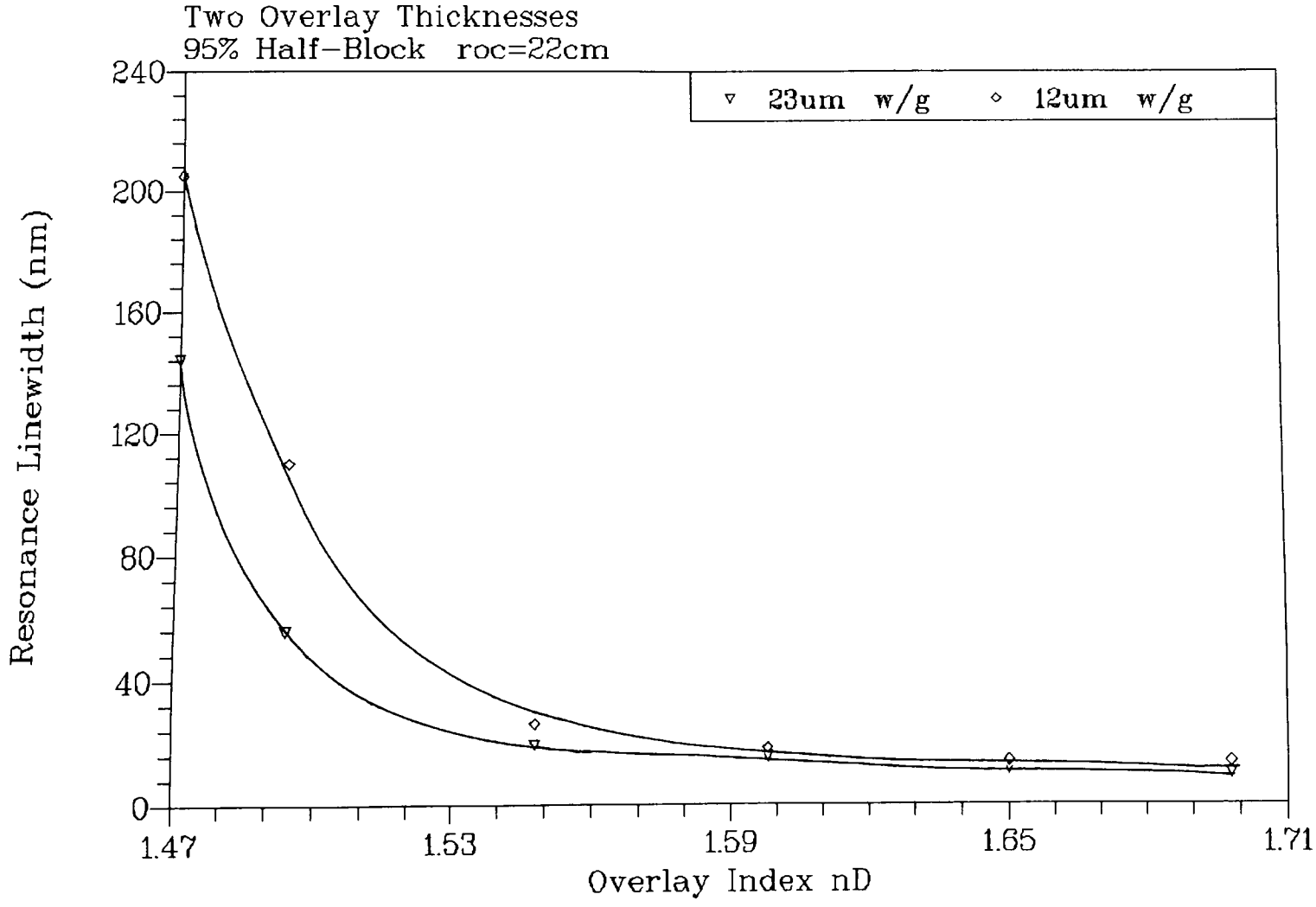

Figure 5.10 : Resonance Linewidth versus Overlay Index

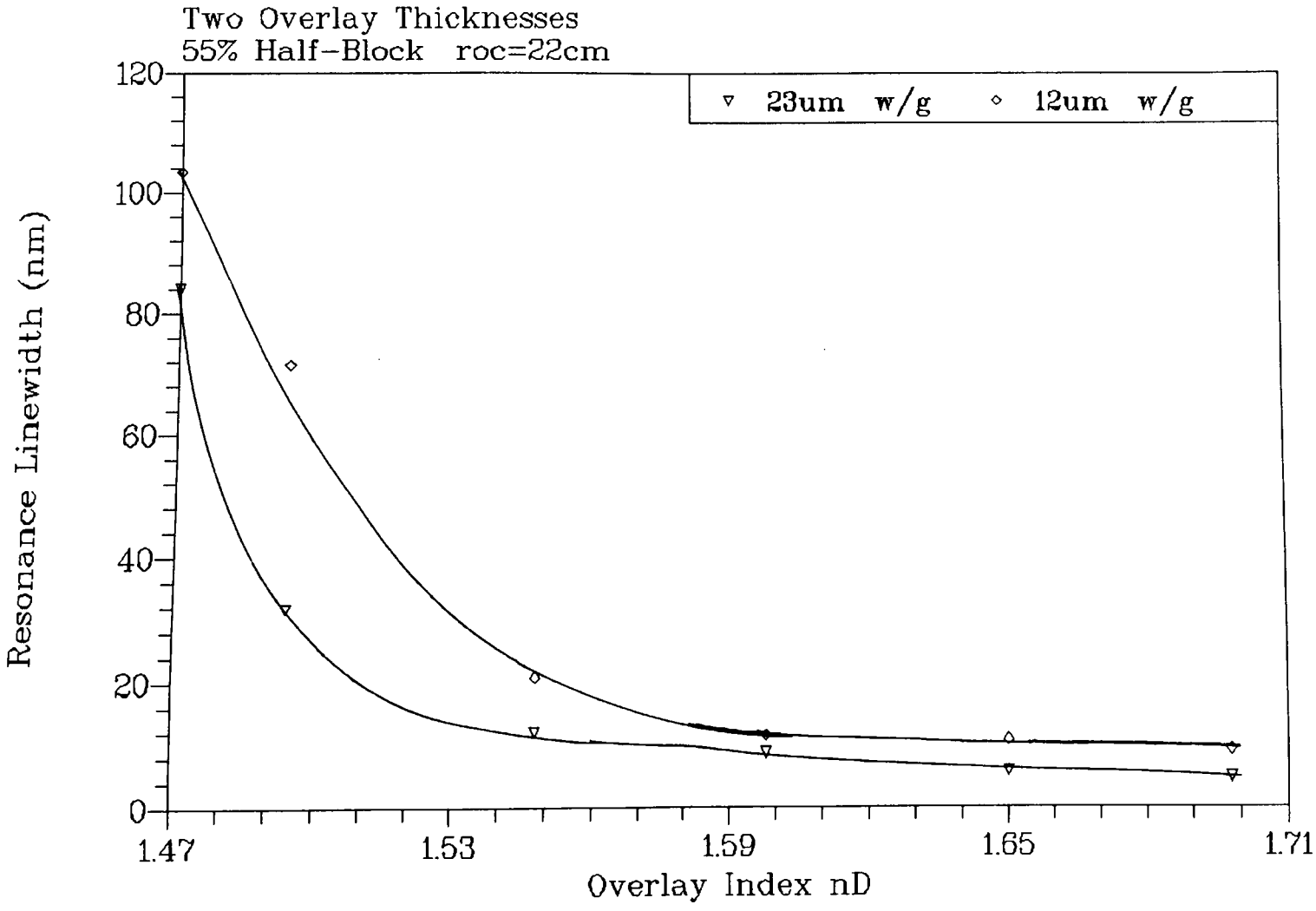

Figure 5.11 : Resonance Linewidth versus Overlay Index

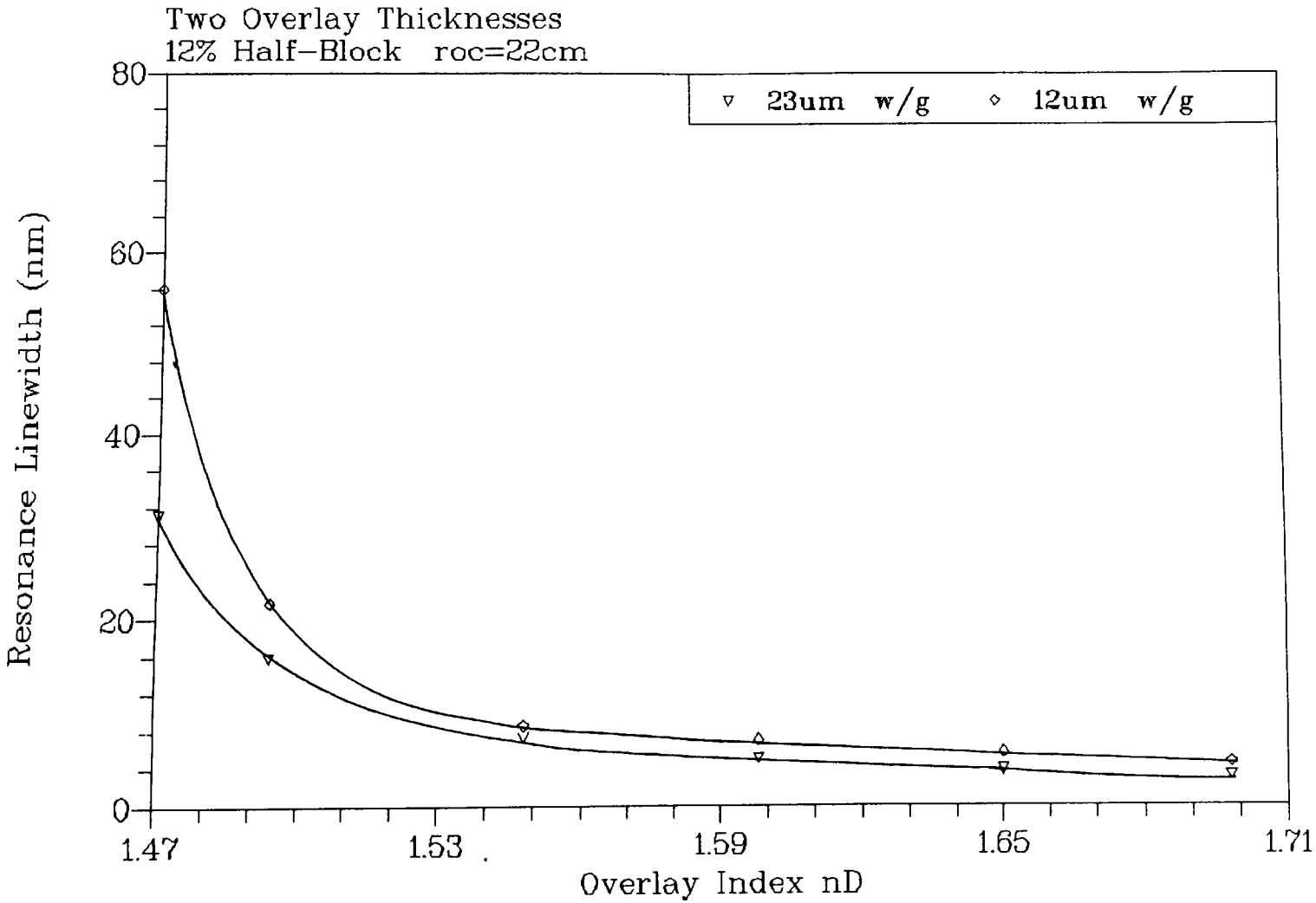

Figure 5.12 : Resonance Linewidth versus Overlay Index

polished side of the optical fibre. Since the data in Tables 5.3 - 5.8 is for half-blocks with the same radius of curvature, it is possible to relate the resonance linewidths to the remaining cladding thickness i.e. to the separation between the fibre core and the overlay. The result is that large remaining cladding thickness (or separation) produces much narrower linewidths. This agrees with the brief theory developed, qualitatively, in Chapter 3 which suggested that well-separated waveguides are weakly coupled (small coupling coefficients) and exchange significant power only on or very close to a phase-matching condition. This corresponds to the 12% coupling strength test devices. When the guide separation is small (95% coupling strength), significant power exchange can still occur when the guides are phase mismatched (to a certain extent) because the coupling coefficients between the guides are large i.e. a strongly coupled situation (as described in Chapter 3). This explains the wider resonances present in the transmission responses of the 95% coupling strength test devices. The 55% half block devices produce results which lie between the two extremes.

5.5.3 Modulation Depth

There is no obvious trend to the values of modulation depth displayed by the test devices with respect to the overlay index, but, in general, it appears higher for lower indices. However, although the resonance modulation depth for each device is consistently high ($>70\%$), there appears to be a more significant increase in modulation depth when the half-block coupling strength is increased and also when the overlay thickness is reduced from 23μm to 12μm. Relating the modulation depth to coupled-mode theory, the maximum value should occur (100% for identical guides) when the device interaction length is equal to or a multiple of the coupling length between the fibre and overlay (assuming no losses)[3]. Less than maximum values will result if the coupling length is either less than (power remaining in fibre) or greater than (power coupled back into fibre) the device interaction length. With the range of overlay parameters incorporated in the test devices, a wider spread of modulation depths would be expected than was recorded. It is believed that some of the initial power radiates sideways in the overlay region and never returns to the

fibre. This is probably due to a diffraction-type effect which occurs when light initially confined in two dimensions (fibre) enters a region in which there is only one-dimensional confinement (overlay). Therefore, whenever power couples into the overlay, a fraction of this power is lost and cannot re-couple into the fibre. The result is that any device possessing an interaction length considerably longer than the coupling length (and therefore undergoing many power oscillations) will display a loss-enhanced resonance modulation depth. Low coupling strength half-blocks will, therefore, be more likely to possess a lower value of modulation depth since they exhibit longer fibre-overlay coupling lengths (small coupling-coefficients). This appears to hold true from the experimental data. Since low coupling strength half-blocks are desirable in that they produce the narrowest resonance linewidths, practical device implementations will have to compromise between these two performance parameters. It has been shown[4], for two identical guides, that the coupling coefficients are inversely related to the guide thickness. This provides a possible explanation for the dependence of the modulation depth on the overlay thickness since this will cause a greater number of power oscillations to occur within the device interaction length and, therefore, result in greater loss and subsequent modulation depth.

Similar trends in modulation depth were recorded for the test devices incorporating the smaller (11cm) radius of curvature half-blocks with regard to coupling strength and overlay parameters. This was expected. Tables 5.10 and 5.11 show the recorded modulation depths for the various combination of overlay parameters and coupling strengths. Comparison of the corresponding modulation depths for the different radius of curvature half-blocks reveals that there is a slight reduction for the tighter radius devices. A possible explanation may be a decrease in effective interaction length for the tighter radius of curvature half-blocks and subsequent reduction in power oscillations i.e. the effect of radiative loss is slightly reduced.

5.5.4 Effect of Loss on Device Behaviour

As was noted above (and is also apparent from Tables 5.3 - 5.8), the modulation

Oil Index, n_D	Modulation Depth		
	12% Block	50.5% Block	90.5% Block
1.494	79.6%	73.5%	88.2%
1.548	66.2%	73.4%	90.6%
1.598	67.4%	80.6%	89%
1.650	65.3%	75.9%	90.5%
1.698	68.5%	94.7%	88.3%

Table 5.10 : Modulation Depth for Devices with roc=11cm Spacer Thickness 23μm

Oil Index, n_D	Modulation Depth		
	12% Block	50.5% Block	90.5% Block
1.494	79.8%	72.2%	99.8%
1.548	83.8%	84.5%	99%
1.598	86.7%	85%	95.7%
1.650	83.8%	88.3%	94.2%
1.698	77.2%	83.7%	93.5%

Table 5.11 : Modulation Depth for Devices with roc=11cm Spacer Thickness 12μm

depth recorded for the oil overlay devices is always large, an unexpected result when coupled-mode theory is considered. This suggests that a loss mechanism is present which reduces the effect of any mismatch between coupling length and device interaction length. Diffraction-type effects at the interface of the fibre and overlay waveguide, due to the difference in waveguiding geometries, was identified as the probable source of this loss. The consequence of this loss mechanism is an enhancement of the resonance modulation depths displayed by the devices which is a desirable effect.

A second loss mechanism, coupling of power to off-axis overlay modes[5], is also believed to have an effect on device behaviour. It is believed that this loss mechanism is related to the fact that the overlay slab waveguide supports modes which are angularly degenerate i.e. an infinite number of modes with the same absolute propagation constant but different propagation direction can be solutions of the overlay eigenvalue equation. Consider the case where the highest order overlay mode has a propagation constant slightly above the phase-matching value (assume that only the highest order mode is ever significantly involved in the mechanism). In this situation, the z-component of an angularly degenerate highest-order overlay mode will satisfy the phase-matching condition and the possibility of power transfer to this mode exists. Power leakage in the lateral direction would then result. Intuitively, the extent of this power leakage will be related to the angle of the coupling mode of the overlay. The greater the angle, the smaller the subsequent coupling coefficients and the longer the coupling length. As was suggested earlier, long coupling lengths decrease the number of power oscillations and, for the case of coupling to an angularly degenerate overlay mode, this will reduce power leakage. This suggests that the dispersion of the mode will strongly influence the extent of off-axis power leakage. For devices with low index, thin overlays in which the magnitude of the highest-order mode is always fairly close to the phase-matched value, significant off-axis loss will be present over a substantial wavelength range prior to phase-matching i.e. in low dispersion overlay devices. When the device possesses a highly dispersive overlay, the off-axis loss will be significant over a

much reduced wavelength range prior to phase-matching and a narrowing of resonance linewidth can be expected. This agrees with experimental observations.

A further result of coupling to off-axis overlay modes may be the asymmetrical nature of the resonances which occur in both the wavelength and index responses of the devices discussed in this chapter. This may be explained by the fact that after the phase-matching condition, no coupling to angularly degenerate modes can occur since no z-direction component of the highest order mode can be equal in magnitude to the fibre mode. Therefore, there is no significant off-axis loss on the high wavelength side of the phase-matching condition and rapid recovery of the transmitted power occurs as the wavelength is increased.

5.5.5 Device Insertion Loss

The device insertion loss is a combination of the loss induced in the fibre due to the presence of the polished fibre half-block and that caused by the presence of the overlay. Cutback measurements were made on the half-blocks ($\lambda = 1300$nm) with an air superstrate and found to be consistently less than 0.1dB, even for the high coupling strength half-blocks. The loss due to the overlay was determined by comparing the off-resonance device throughput with and without each oil overlay. The total insertion loss values, at off-resonance positions, for the devices incorporating the 95% and 12% coupling strength half-blocks (roc=22cm) are shown in Tables 5.12 and 5.13, respectively. There were noise limitations on the accuracy with which the loss measurements could be recorded but the general trend is that the loss increases as the overlay index decreases. The thicker overlays also tend to cause a greater loss. It is believed that this apparent loss is a result of incomplete decoupling of each successive overlay mode from the fibre mode prior to the next overlay mode becoming phase-matched. This effect depends on the spacing between the overlay modes, which is smallest for thick, low index waveguides. Hence the higher apparent loss for these devices. The effect of the coupling strength of the polished fibre half-blocks is clear from Tables 5.12 and 5.13. A dramatically increased insertion loss results when the 95% half-block is incorporated in the

Overlay Index	Insertion Loss (dB)	
	d=12μm	d=23μm
n_D=1.470	2.22	4.32
n_D=1.494	0.72	1.52
n_D=1.548	0.12	0.32
n_D=1.598	0.19	0.31
n_D=1.650	0.06	0.17
n_D=1.698	0.06	0.06

Table 5.12 : Insertion Loss of Devices with 95% Half-Block

Overlay Index	Insertion Loss (dB)	
	d=12μm	d=23μm
n_D=1.470	0.39	0.47
n_D=1.494	0.12	0.27
n_D=1.548	0.12	0.26
n_D=1.598	0.09	0.12
n_D=1.650	0.05	0.06
n_D=1.698	0.05	0.05

Table 5.13 : Insertion Loss of Devices with 12% Half-Block

devices which possess a low index overlay. Higher index overlay devices are less influenced. Referring to the explanation given above, significant coupling between the fibre mode and the overlay modes will occur over a broader wavelength range either side of the phase-matched wavelength when the higher coupling strength half-block is used. Therefore, the degree of decoupling will be reduced when compared with the 12% coupling strength half-block situation and an effective higher insertion loss will be observed.

5.6 Conclusions

Fundamental investigation of the basic fibre-overlay device structure has been carried out using oil overlay devices. The observed experimental results have established the basic trends in device behaviour with regard to variation of the fundamental overlay parameters, refractive index and thickness. Similarly, the effect of polished fibre half-block coupling strength (remaining cladding thickness) has also been determined. The spacing between resonances in the fibre wavelength-transmission response is clearly dependent upon the overlay mode structure (and, therefore, index and thickness) and can be theoretically calculated using the overlay eigenvalue equation. Trends in resonance linewidth have been shown to be closely related to the wavelength dispersion of the modes of the overlay waveguide while decreasing the half-block coupling strength has a beneficial effect on absolute values of resonance (channel) linewidth. Narrowest linewidths (3nm) were observed for devices which incorporated low coupling strength half-blocks and thick, high index overlays. Channel spacing was seen to vary between 43nm and 284nm.

The modulation depths (extinction ratios) of the wavelength-transmission resonances were found to be higher than expected (an advantageous effect) and this was attributed to the influence of a lateral loss mechanism. No clear trend relating modulation depth to the overlay parameters was identified. Off-resonance device insertion loss was also investigated and, for the devices possessing low coupling strength half-blocks, found to be <0.5dB. Devices with high coupling strength half-

blocks displayed only slightly higher loss except when thick, low index overlay waveguide were employed.

In addition to the study of the basic fibre-overlay device, a brief investigation of a switch structure was also conducted. A clear switch response was demonstrated via thermally-induced variation of the overlay (interlay) refractive index. Due to experimental difficulties, it was decided that further study of the switch structure would be restricted to solid-state overlay devices.

References

1. Refractive Index Liquids, R.P. Cargille Laboratories, Inc., N.J., cat #88103.

2. J. Wilson and J.F.B. Hawkes, *Optoelectronics: An Introduction*, Prentice-Hall, 1983.

3. D.L. Lee, *Electromagnetic Principles of Integrated Optics*, Wiley, 1986.

4. A. Yariv, *Optical Electronics*, Holt-Saunders, 3rd Ed., 1985.

5. D. Marcuse,"Investigation of coupling between a fiber and an infinite slab", J. Lightwave Technol., **LT-7**, pp122-130, 1989.

CHAPTER 6

Solid-State Devices

6.1 Introduction

After characterisation of the oil overlay devices, the next stage in the research programme was the development of practical, solid-state overlay devices. Several different materials were used in the role of the overlay/interlay waveguide: optical quality glass, dielectric thin films, Lithium Niobate and Silicon. The intention of using different waveguide materials was to gain the necessary fabrication expertise and knowledge of device behaviour prior to attempting to produce an active component. At the present time there are only a limited number of commercially-available, optically-active materials. However, this is likely to change in the near future due to research advances in the development of highly electro-optic organic[1] and thin-film dielectric[2][3] materials. In addition, previously unavailable crystalline materials possessing electro-optic coefficients orders of magnitude greater than $LiNbO_3$ are becoming commercially available e.g. Barium Strontium Niobate (BSN) r=1090pm/V and Barium Titanium Oxide ($BaTiO_2$) r=820pm/V. With a view to future device development, it is important to assess the compatibility of the device geometry with the required deposition/fabrication processes for these new materials. A variety of fabrication techniques are involved in the manufacture of the devices investigated in this chapter. These basic techniques are briefly described and subsequent device characterisation and performance are detailed together with notable modifications which were made to the fabrication techniques during the course of the experimental investigation.

6.2 Fabrication of Passive Polished Overlay Devices

Thicker overlay/interlay devices (5-50μm) were fabricated using optical quality glass and z-cut (to allow access to the largest electro-optic constant) Lithium Niobate

($LiNbO_3$). Three types of glass, refractive indices approx. 1.5, 1.65 and 1.77, were used. A thin sliver (1mm) of the required material was polished on one side to produce a flat, good optical quality surface. This surface was then bonded to a polished fibre half-block which was still mounted on the polishing jig used in its fabrication. Best possible parallelism of the overlay waveguide is ensured by adopting this approach rather than attempting to re-align a half-block on a different polishing jig. The lapping and polishing processes were similar to those described in Chapter 4, the only significant difference being in choice of polishing slurry. A number of different optically transparent glues were considered for use as the bonding agent. Important parameters were refractive index, viscosity (directly related to bond layer thickness), bond strength, resistance to solvents and absorption. The majority of suitable glues were low-medium viscosity Ultra-Violet curable with a cure time generally less than 10mins. A two-part epoxy (EPOTEK 301) was also used as the bonding agent and displayed high bond strength but had the disadvantages of high viscosity, thus producing thick bond layers, and slow cure times ($>$24hrs). It was essential that the half-block surface was completely free from any oils or solvents used in previous characterisation processes before application of the bonding agent. After curing, the exposed side of the bonded sliver was lapped and polished to $<30\mu$m to form a planar waveguide. The lapping process (cast-iron plate, 9μm and 3μm Al_2O_3/water slurry) was identical for glass and $LiNbO_3$ devices. However, the polishing process is of a mechanical/chemical nature and thus different polishing slurries (glass - 0.5μm Cerium Oxide, $LiNbO_3$ - silica suspension) were required due to the difference chemical composition of the two materials. Fabrication of a $LiNbO_3$ overlay device was considerably more difficult than a glass overlay due to its tendency to fracture or detach from the bonding layer when in the region of 20μm thick. A switch structure was formed by placing a second polished fibre half-block on the top surface of the overlay waveguide and ensuring appropriate alignment such that the power coupled from the input half-block could be collected. Important details of particular fabrication stages are described further in sections 6.6.

6.3 Fabrication of Active Polished Overlay Devices

The large linear electro-optic constant possessed by $LiNbO_3$ was the reason for its intended use as the overlay waveguide material. Application of an appropriate electric field causes a significant change in the material refractive index of $LiNbO_3$ and offers the possibility of actively tuning or modulating the mode structure of a $LiNbO_3$ waveguide. Obviously, the thinner the waveguide, the lower the applied voltage for the same field-induced index shift. The structure of a switch incorporating an electro-optic overlay is shown schematically in Figure 6.1. The glue and oil layers, present in a practical device, have been omitted. The device can be thought of as a basic intensity modulator if only the output from the transmitted arm is considered or as a bandpass filter if the wavelength response of the cross-coupled arm is considered. A transverse electric field can be developed across the active layer by forming a potential difference between the two Indium-Tin-Oxide (ITO) transparent electrodes. These electrodes were formed by rf magnetron sputtering of a pressed ceramic target of ITO (composition 90% In_2O_3 - 10% SnO_2) with Argon as the sputtering gas. Deposition conditions were similar to those outlined in section 6.1.2. The resistivity of the ITO was generally in the range 10^{-3}-$10^{-2}\Omega$cm, an order of magnitude higher than values quoted in the literature[4][5]. However, the resistivity values were deemed acceptable since the initial aim of the investigation is to determine the feasibility of the device structure. It was recognised that subsequent restrictions on device frequency response would, however, be severe. The use of y-cut $LiNbO_3$ and co-planar electrode structures similar to those used in Integrated-Optic $LiNbO_3$ devices[6][7] would allow high-frequency operation. There is no reason, in principle, why these electrode structures cannot eventually be incorporated in the device structure shown in Figure 6.1.

The fabrication of the active device (switch/modulator) overlays relied on the same techniques as outlined for the passive devices. However, the incorporation of the transparent ITO electrodes caused additional problems. In order to deposit the ITO onto the half-block surface, it was necessary to remove the block/steel pad

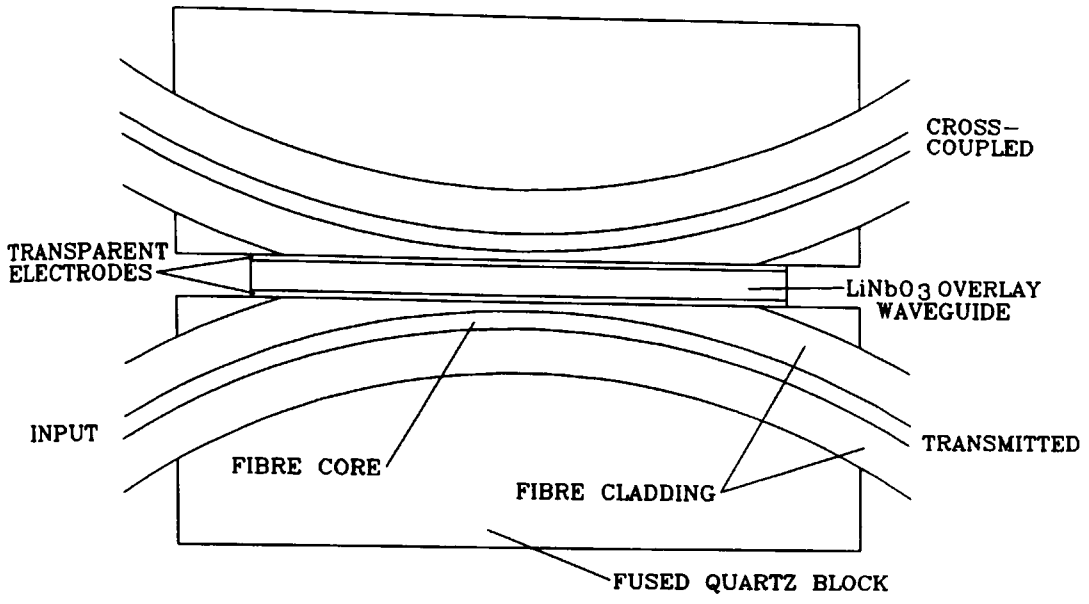

Figure 6.1 : Schematic of active switch structure

combination from the polishing jig for deployment in the vacuum chamber of the sputtering system. After deposition of the ITO layer, typically 25nm in thickness to keep the optical effect of the layer to a minimum, the block was then remounted onto the polishing jig for further processing. It was found that the dismounting and remounting procedure caused a slight misalignment of the half-block surface with the drive-ring of the polishing jig which was very difficult to correct. This meant that a slight wedging of the eventual polished overlay waveguide, and corresponding compromise of device performance, was unavoidable. The most sensitive waveguide parameter is its thickness and a change in waveguide thickness along the interaction region (as a result of a wedge or surface imperfections) produces a slight variation in the effective indices of the waveguide. Accordingly, there will be a range of wavelengths at which phase-matching of the fibre mode and an overlay mode can occur, thus broadening the resonances in the device wavelength response. The sharpness of these resonances can be related to drive voltage for an electro-optic overlay device and thus any wedging of the overlay is highly undesirable.

It was also found that a similar effect was caused by the parallelism and thickness

of the bonding layer between the polished fibre half-block surface and the $LiNbO_3$ overlay. A non-parallel or uneven glue line gives rise to a non-uniform refractive index distribution along the interaction length and thus the overlay effective indices will vary slightly from one end to the other. Again this will result in a slight broadening of the device resonances. Two UV-cured, optically transparent glues were eventually selected for use as the bonding agent. Best device performance was obtained when a low index (same as fused quartz), low viscosity UV-cured glue (LUXTRAX 000 1.46) was used since this allowed a very thin ($<1\mu m$), parallel layer to be produced. Unfortunately, the bond strength of this glue was not very high and the $LiNbO_3$ overlay would tend to disintegrate or detach from the half-block surface when it was polished to less than $30\mu m$. A stronger bonding layer could be obtained by using a slightly higher index ($n=1.5$), significantly higher viscosity glue (Norland 61) or the two-part epoxy. However, in these devices the eventual glue layer was believed to be in the range $3\text{-}5\mu m$ and it was extremely difficult to achieve even a reasonable degree of parallelism over the interaction length. It was possible though to polish the overlay to a thickness of $<10\mu m$, thus offering the advantage of a reduced drive voltage from the point of view of electrode separation. Some further fabrication details are described in section 6.7.

6.4 Fabrication of Thin Film Overlay Devices

A simple technique for the fabrication of solid-state overlay/interlay devices was by vacuum deposition of dielectric thin films directly onto the polished fibre half-block surface. Thin films were produced by both thermal evaporation and rf magnetron sputtering and were less than $3\mu m$ in thickness. Thermal evaporation of granular Zinc Sulphide ($n=2.28$) produced good optical quality thin dielectric films. Sputtered films of Indium-Tin-Oxide were fabricated using a standard ceramic sputtering target and Argon as the plasma gas and used as transparent electrodes in active devices. Devices comprising Silicon ($n=3.5$) as the overlay waveguide were also produced by using a standard Silicon wafer as the sputtering target. The temperature of the half-block was raised to approximately 120°C to promote adhesion of the thin films

to the polished fibre surface. Typical deposition conditions were:

Thermal Evaporation - vacuum $<2 \times 10^{-5}$mbar
substrate temp. 120°C
evaporation current 40A
Molybdenum boat
deposition rate 1-2nm/sec

RF Magnetron Sputtering - vacuum $<5 \times 10^{-6}$mbar
substrate temp. 120°C
power 100W
Argon pressure 8×10^{-3}mbar
deposition rate 25nm/min

The optical quality of the evaporated films was high and a good degree of parallelism was also achieved (gauged by observing the number of interference fringes across the interaction region). The sputtered films were of poorer quality but are likely to improve if better characterisation of the sputtering process is carried out. Switch or Bandpass filter structures were formed by contacting a second polished fibre half-block to the surface of the dielectric film with an oil incorporated at the interface to provide index matching and lubrication. Pressure was then applied to reduce the oil layer thickness to a minimum and the second half-block was translated laterally to obtain the necessary alignment.

6.5 Polished Glass Overlay Devices

Initial solid-state devices incorporated optical glass overlays, lapped and polished to a thickness generally less than 50μm. The main purpose of fabricating glass overlay devices was to gain experience of the necessary techniques before attempting a device incorporating $LiNbO_3$. Device failure would thus be less costly since optical

glass is considerably cheaper than optical grade $LiNbO_3$. The other reason for developing glass overlay devices was to assess their performance as wavelength selective elements e.g. channel-dropping filters. To this end, three different refractive index optical glasses were employed, n=1.515 (low index), n=1.650 (high index1) and n=1.77 (high index2). Parameters of interest are channel (resonance) spacing, FWHM linewidth and channel extinction ratio (related to modulation depth).

Prior to constructing an overlay directly on the surface of a polished fibre half-block, a number of cover blocks were fabricated. The cover blocks consisted of a polished fused silica block (same dimensions as standard half-block) onto which was bonded a slice of the lower index optical glass (the low index glass was found to be easier to process). The two-part epoxy mentioned in section 6.2 was used as the bonding agent to ensure good adhesion and the glass was lapped and polished in the standard manner. Early experiments then involved mating the cover blocks to a number of polished fibre half-blocks with an index matching oil present at the two polished surfaces. An oil index of n_D=1.456 was used as this was considered to be approximately equivalent to the fibre cladding index. The wavelength response of these devices was encouraging displaying similar behaviour to the oil devices discussed in Chapter 5. However, it was found that high modulation depth resonances could only be attained by using high coupling strength half-blocks. Figure 6.2 shows a section of the wavelength response of a device comprising a 98.7% coupling strength half-block mated to a 16μm glass (n=1.515) overlay cover block. Resonance spacing is 144nm while linewidths are 27.4nm and 31.6nm for the lower and higher wavelength resonances, respectively. Insertion loss was in the region of 0.5dB. The increase in linewidth with wavelength is expected from consideration of $dn_e/d\lambda$ which decreases as the mode order is reduced (each successive resonance corresponds to an decrement in the mode order). Note that the modulation depth also increases with wavelength. A wavelength scan of a highly multi-moded glass overlay (62μm) was also recorded (Figure 6.3) and produced resonance spacings in the region of 33nm with linewidths of 18nm (resonance close to 1300nm). The

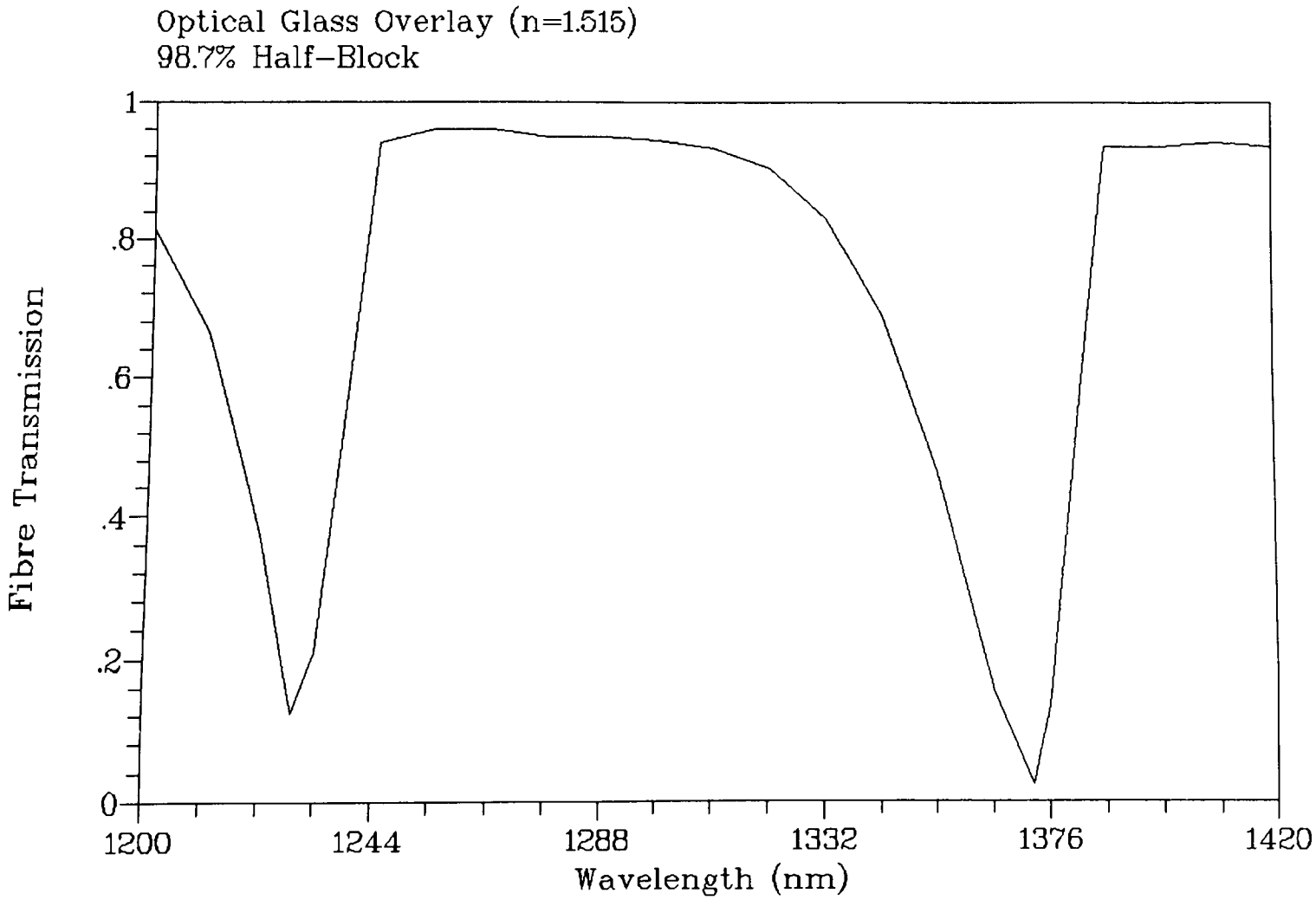

Figure 6.2 : Wavelength Response of Solid-State Device

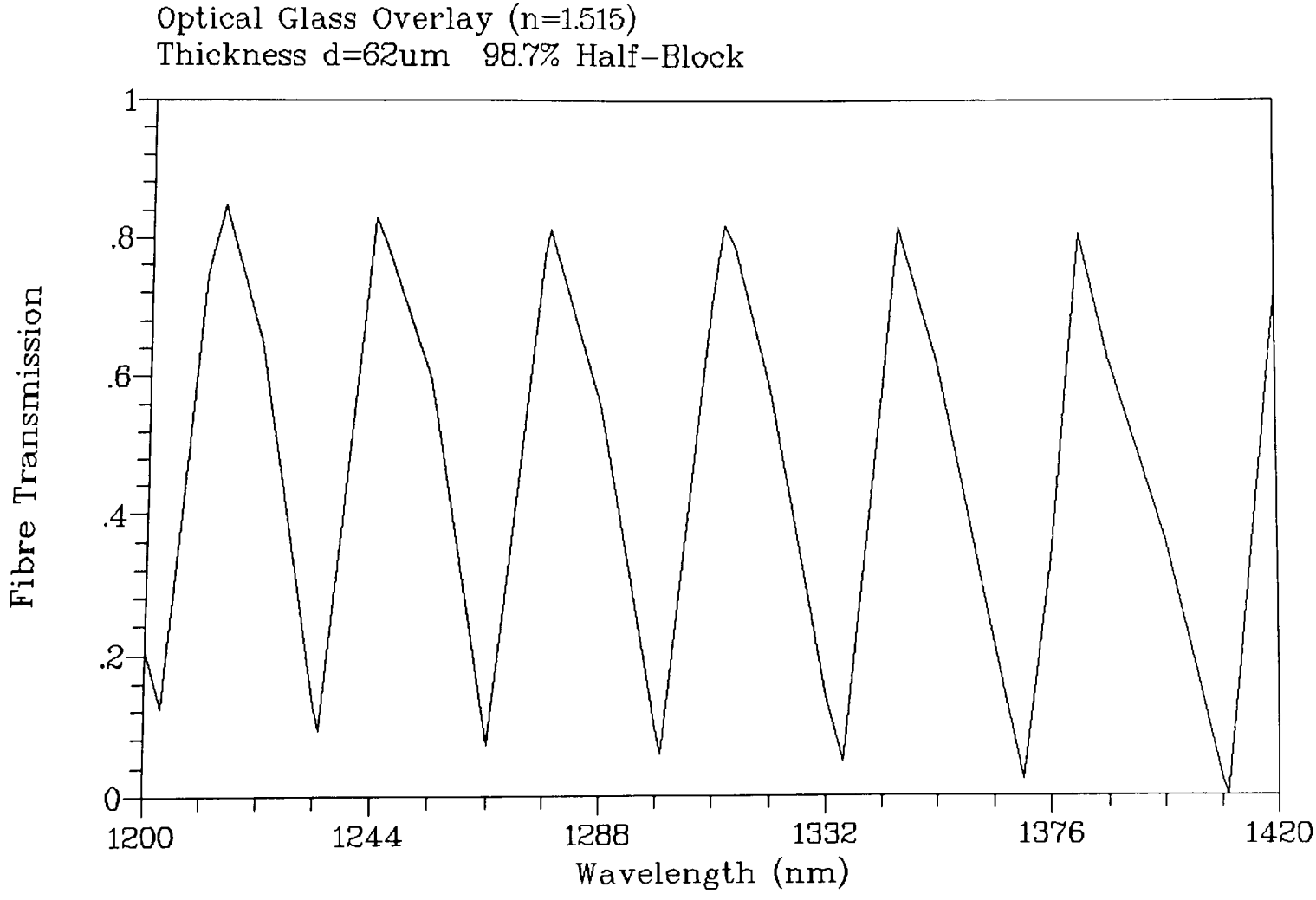

Figure 6.3 : Wavelength Response of Glass Overlay Device

highly multi-moded nature of the overlay meant that the mode spacing was very small and this led to incomplete decoupling between resonances. As a result, the insertion loss (<1dB) of the device was effectively increased. Note that again the modulation depth increases with wavelength. The broad resonances observed in both Figures 6.2 and 6.3 are believed to be a result of the high coupling strength of the half-block and wedged nature of the glass overlay (due to the epoxy bonding layer being non-parallel).

It was found that the choice of the index matching oil was significant. Using an oil with index less than or equal to the fibre cladding index meant that only high coupling strength half-blocks would produce useful results. It is believed that the oil layer was acting as extra cladding to the half-block and effectively reducing the coupling strength (increasing the fibre-overlay separation). Incorporating an oil with index above that of the cladding allowed the use of lower coupling strength half-blocks although a corresponding shift in resonance positions was observed. This indicated that the oil layer was acting as part of the overlay i.e. forming a compound oil/glass waveguide. As an example, mating the glass overlay with a 12% coupling strength half-block via $n_D=1.456$ index matching oil gave no resonant behaviour when wavelength scanned. However, using $n_D=1.512$ matching oil produced a wavelength response with resonances of $>80\%$ modulation depth. The spacing between the resonances was significantly less (122nm) than that observed from Figure 6.2, confirming that the oil layer/glass combination forms a thicker compound overlay. The modified linewidths were also reduced (20.3nm and 21.6nm for the corresponding resonances) as would be expected with the low coupling strength half-block. The inclusion of an index matching oil with index above that of the fibre cladding has useful implications with regard to tuning of device resonance positions i.e. variation of the oil layer thickness and/or index will effectively produce a new overlay with subsequent changes in the wavelength response. No extensive experimental investigation of the effect of different index matching oil layers was carried out due to time restrictions.

A number of attempts were then made to fabricate a thin, parallel, low index glass overlay directly on the surface of a polished fibre half-block. The parallelism of the bonding layer influenced the eventual parallelism of the overlay and could be assessed by illuminating the device with a monochromatic light source and observing the resulting interference fringe pattern. A large fringe spacing indicated that the glue line was fairly parallel. Several different types of optical glues were investigated and the low viscosity, low index UV-cured glue (mentioned in section 6.2) consistently produced the most parallel glue line. However, the device failure rate was high due to disintegration and detachment of the glass from the half-block surface when the thickness was less than about 30μm, particularly when the low viscosity glue was employed. Using the higher viscosity UV-cured glue (Norland 61) allowed the fabrication of thinner overlays and had the advantage of being closely matched in index to the low index glass, although the parallelism of the glue line was degraded. A device incorporating an 18% coupling strength half-block and a 7.6μm low index, glass overlay was successfully fabricated and tested. The wavelength response displayed a considerable polarisation sensitivity, as would be expected from the asymmetrical geometry of the overlay. Figure 6.4 shows the wavelength response for both TE and TM polarisations. The resonance spacings for TE and TM polarisations are 265nm and 255nm, respectively. Linewidth values of the sharper resonances are 16.5nm for TE and 17.5nm for TM. Slightly broader linewidths are expected for TM polarisation since the corresponding evanescent tail of the optical field extends further than in the TE case, producing a slightly greater coupling strength. The resonance spacing is greatly increased when compared with the corresponding values for the cover block devices. The reduced coupling strength of the half-block produced a clear improvement in linewidth despite the reduced overlay thickness. As before the linewidth of the device transmission resonances increases as the wavelength increases. Extinction ratio for both resonances is $>$ 18dB although the exact measurement was noise-limited and off-resonance insertion loss was approximately 0.2dB.

In an effort to produce solid-state devices with narrower channel-dropping filter

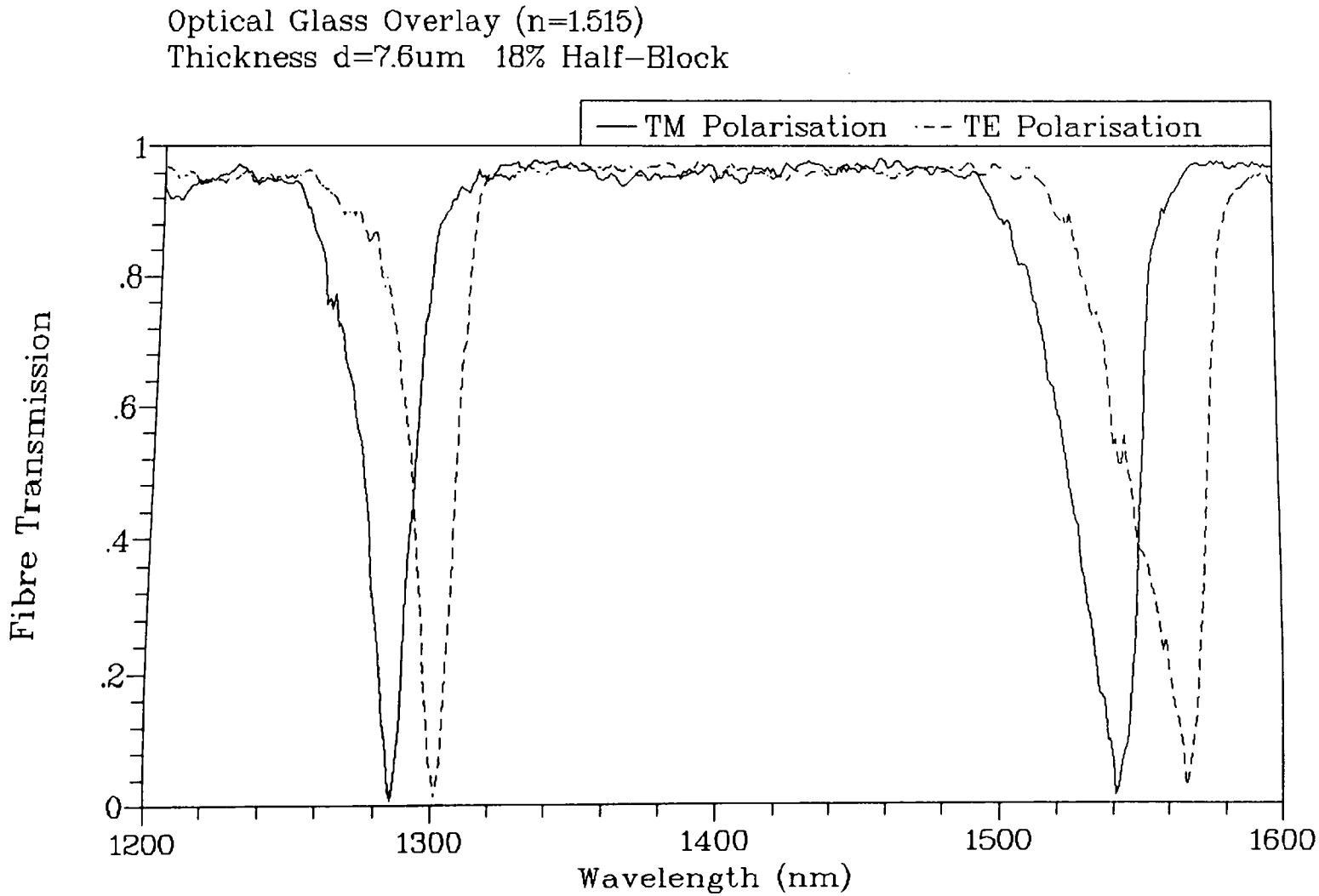

Figure 6.4 : Wavelength Response of Glass Overlay Device

responses, two higher index optical glasses were investigated (high index1 and high index2). Device fabrication proved significantly more hazardous compared with the low index glass devices. Bonding to the half-block surface and a good optical-quality polished surface finish were very difficult to achieve. The modified chemical composition and mechanical hardness of the higher index glasses was thought to be the major reason for the additional fabrication problems (the increased index is achieved by doping with appropriate elements). However, greater expertise in the necessary fabrication processes had been gained at this stage and the device failure rate had subsequently been reduced.

Two modifications to the original fabrication techniques contributed to the device success rate. The groove into which the fibre is bonded during fabrication of a polished fibre half-block was originally formed by a wire saw with wire diameter 200μm. This meant that a considerable amount of the epoxy used to hold the fibre in the groove was exposed on the finished half-block surface. Polishing rates for the epoxy and the fused silica block are unequal and this resulted in a slight difference in height along the edges of the groove. This could be observed by placing an optical flat in contact with the half-block surface and noting the resulting interference fringe under illumination from a monochromatic light source. It was observed that the interference fringes changed rapidly in the vicinity of the fibre groove, thus confirming a difference in level at this part of the surface. It is believed that this height difference was causing fabrication problems, particularly for the low viscosity glue, since along the groove region was always where the glass overlays would first detach from the half-block surface. A smaller diameter wire (130μm) was then used to form the groove so that the width was just greater than the actual fibre cladding diameter. This resulted in a much reduced amount of exposed epoxy and less of an irregularity in the surface flatness. Inspection with the optical flat confirmed an improvement in shape of the corresponding interference fringe pattern. The other process modification involved control of thickness of the glue line formed between the half-block surface and the glass overlay. When fabricating the initial devices, a substantial amount of pressure was applied to the overlay to produce a thin, parallel

glue line before curing (with the pressure maintained). It is believed that this caused the overlay to be mechanically stressed when bonded to the half-block. As the overlay was lapped/polished thinner, these internal stresses caused cracks and detachment from the glue/half-block surface. By applying a minimum of pressure to the overlay so that the glue line is relatively thick and allowing a lengthy settling period before curing, it was found that lapping/polishing to less than 20μm was possible with the low viscosity glue.

Two further points about this modified fabrication approach should be noted. The low index of the glue (matched to fused silica) meant that the glue line formed an extension of the remaining cladding on the polished fibre. Consequently, the effective coupling strength of the half-block was reduced by an unknown amount since the thickness of the glue line could vary for different devices. Therefore, higher coupling strength blocks were required for devices fabricated as outlined above (although the final coupling strength was likely to be low) to ensure good modulation depth. However, an advantage of this approach was that a compound waveguide of glue/glass did not result with the associated problems of index variation along the interaction region, etc.

The devices discussed in the following paragraphs were fabricated using the low viscosity, low index UV-cured glue. The improved process allowed the fabrication of a device with overlay parameters n=1.65, d=16.8μm and an initial half-block coupling strength of 55%. A best linewidth value of 9.5nm was recorded, significantly narrower than the low index glass device as expected. Resonance spacing was 65nm and 62nm for the TE and TM polarisations, respectively. The TE and TM resonance positions were separated by 9nm. A best extinction ratio of 11dB was observed, considerably lower than desired (increased extinction can be expected for a higher coupling strength half-block). A number of WDM/filtering applications require both narrow channel linewidth and spacing. Such a response can be potentially realised using the device structure investigated in this thesis if the overlay is of a high index material and sufficiently thick. A second device was fabricated

using high index1 glass as the overlay with an 85% coupling strength half-block. The overlay was lapped/polished to a thickness of 90μm and the device wavelength response recorded without the device being removed from the polishing jig. Resonance spacing was only 12.5nm for both polarisations although the extinction ratio was poor (6.5dB). This is believed to be due to the excessive thickness of the overlay combined with the effective coupling strength of the half-block (reduced by the presence of the low index glue). The resonance linewidths were as low as 2.4nm while the polarisation sensitivity was very small (a result of the high mode order). Further lapping/polishing was then performed on the device and the overlay thickness reduced by approximately half to 44μm. For highly multi-moded waveguides, reducing the thickness by half causes the mode spacing to double (this fact can be proved by simple manipulation of eqn 1.1 for the case of a highly multi-moded guide). Therefore, the expected resonance spacing is in the region of 25nm. A wavelength scan of the third device was performed and produced a best linewidth value of 3.3nm (TE polarisation) and a resonance spacing of 25nm. This agrees exactly with the simple analysis developed from the waveguide eigenvalue equation. Extinction ratio was improved (7.3dB) confirming that better modulation depth (extinction) can be expected from thinner overlays, as was indicated from the experimental results presented in Chapter 5 for oil overlay devices. Figure 6.5 compares the wavelength response of 90μm and 44μm high index1 glass overlay devices. Note that for the same wavelength range the number of resonances is halved when the overlay thickness is halved. The insertion loss (off-resonance) is slightly higher for the thicker overlay device. This can probably be attributed to the surface quality of the polished overlay being superior for the thinner waveguide i.e. scratches, surface indentations, etc., cause loss. This particular device was not polished thinner because it appeared likely to fail.

A third device incorporating the high index2 optical glass and a 55% coupling strength half-block was also fabricated to allow comparison of linewidths and extinction ratio. The lapping/polishing stage was continued until the overlay thickness was approximately the same as for the second high index1 device i.e.

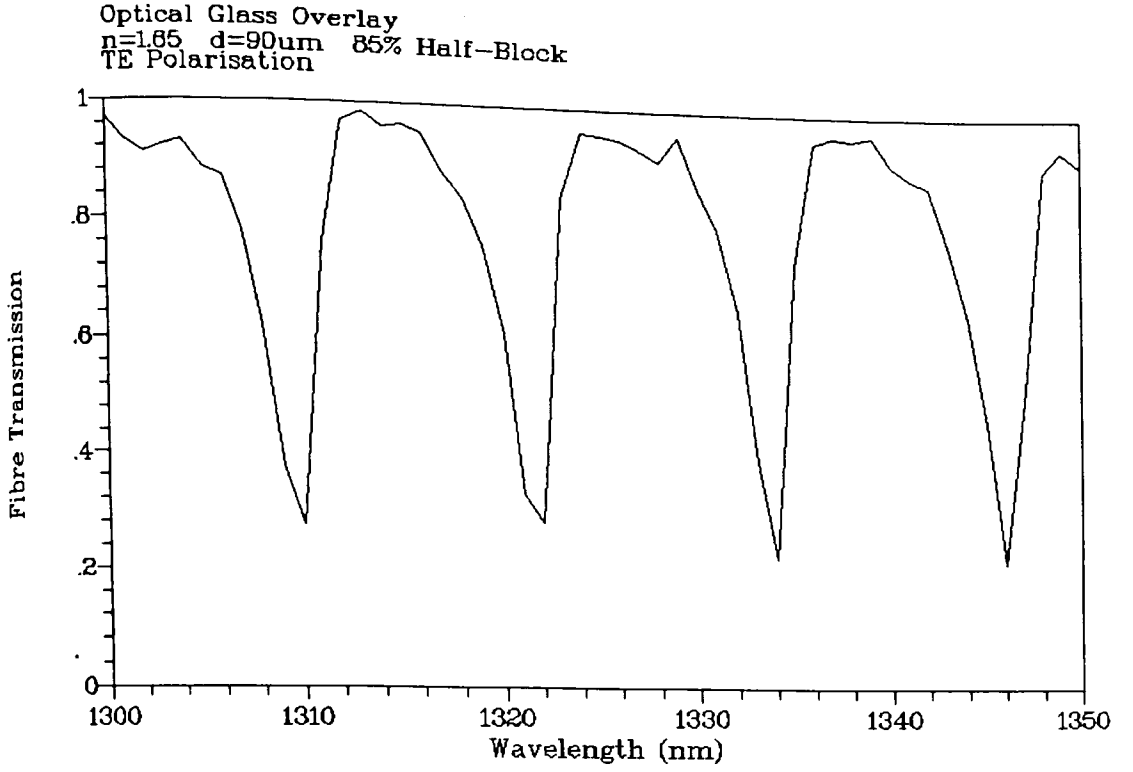

Figure 6.5(a) : Wavelength Response of Glass Overlay

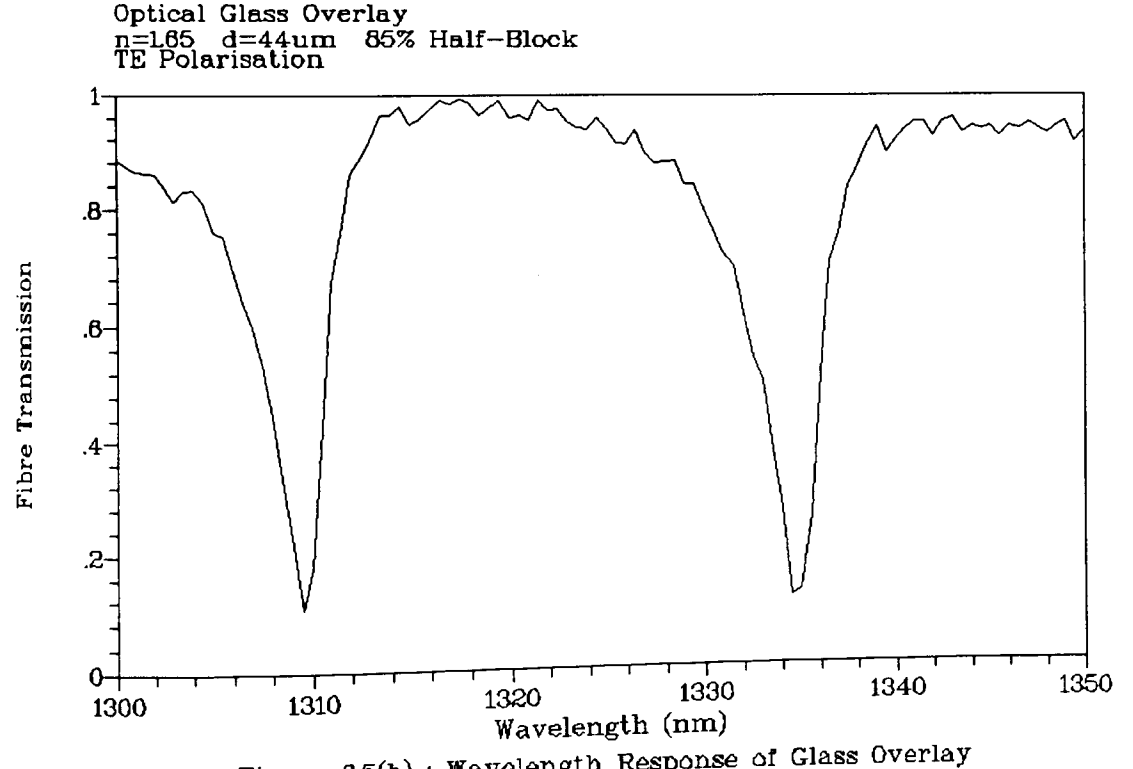

Figure 6.5(b) : Wavelength Response of Glass Overlay

44μm. A wavelength scan (1300-1350nm region) showed the resonance spacing to be 19nm and linewidth 2.8nm for the TE polarisation, an improvement on the corresponding high index1 device. The extinction ratio was also enhanced, with a best value of 9.3dB. Higher coupling strength half-blocks will produce higher extinction ratios although the corresponding resonance linewidths are likely to be slightly broadened. Using a higher index glue allows better control of the coupling strength (no reduction in original coupling strength) and probably extinction ratio but results in a compound overlay with increases in resonance spacing and linewidth. Restrictions on time prevented the fabrication and investigation of more glass overlay devices to extend the characterisation. However, the device structure shows promise for implementation as an in-line solid-state wavelength selective element possessing low insertion loss, variable channel linewidth and spacing and reasonably good extinction ratios.

6.5.1 Tuning of Resonance Positions

For the devices investigated above to be of practical use in areas such as optical signal processing, telecommunications and sensing, they must be capable of operating at desirable wavelengths e.g. 1310nm, 1550nm. It is possible to tune the transmission resonance positions of these devices in several ways. Variation of the overlay index or thickness produces a shift in the mode structure supported by the overlay and a consequent shift in the device resonance positions. For active (or dynamic) tuning, the overlay index can be altered via the electro-optic, acousto-optic or thermo-optic effect if it is composed of the appropriate material. Unfortunately, the number of commercially available, suitable electro- or acousto-optic materials is small. The thickness can be controlled by carefully continuing the overlay polishing process, terminating when the device displays a resonance centred on a desirable wavelength. This method of tuning is fairly time-consuming, requiring a tedious test/polish routine, but can provide a large tuning range. A simpler tuning technique is by variation of the overlay superstrate index and/or thickness which, in turn, produces a variation of the overlay mode structure and corresponding wavelength-transmission resonance positions. A practical method of achieving this index change

is by applying index oils to the top surface of the overlay. Again, the overlay mode structure is changed with a resultant shift in the device resonance wavelengths to higher values. The wavelength shift is obviously related to the refractive index of the "new" superstrate. Index and thickness of the overlay also have a major influence on the size of the wavelength shift induced by variation of the superstrate index. Figure 6.6 shows the experimental and theoretical relationship between resonance shift and superstrate refractive index for the low index optical glass device investigated earlier. Note the close agreement of theory and experiment. The shape of the graph in Figure 6.6 also agrees well with Figure 3.3 (theoretical cutoff wavelength) which would be expected since the resonance wavelength is always close to the cutoff wavelength for the overlay. The maximum shift for the lower resonance is 106nm for TM polarisation when an oil index of $n_D=1.456$ is applied (corresponding TE shift was 95nm). Notice that the resonance positions for each polarisation become closer together as the overlay is made more symmetric, i.e. superstrate index increased, and this agrees with theory developed in Chapter 3. Application of an oil with index greater than $n_D=1.456$ causes a dramatic broadening of the resonance linewidth and reduction in extinction ratio. The throughput of the device also reduces. There is no further shift from the position determined by the $n_D=1.456$ oil superstrate and the resonance eventually disappears as the superstrate index is increased. This is due to the overlay waveguide entering a "leaky mode" regime where the lower constraint on the values of effective index which the guided modes can possess is provided by the superstrate oil i.e. the index of the fibre cladding corresponds approximately to $n_D=1.456$. Partial coupling of the fibre mode to "leaky" modes of the overlay can occur while the superstrate index is still close to that of the fibre cladding and thus a resonant-like response persists initially when the overlay is only slightly asymmetric (or leaky).

For the devices investigated above, the tuning range was greater for the TM polarisation and the shifted resonance positions converged as the overlay became less asymmetric. This is expected from simple waveguide theory. The smallest tuning range was 5nm for the high index2, 44μm overlay device with TE Polarisation (the

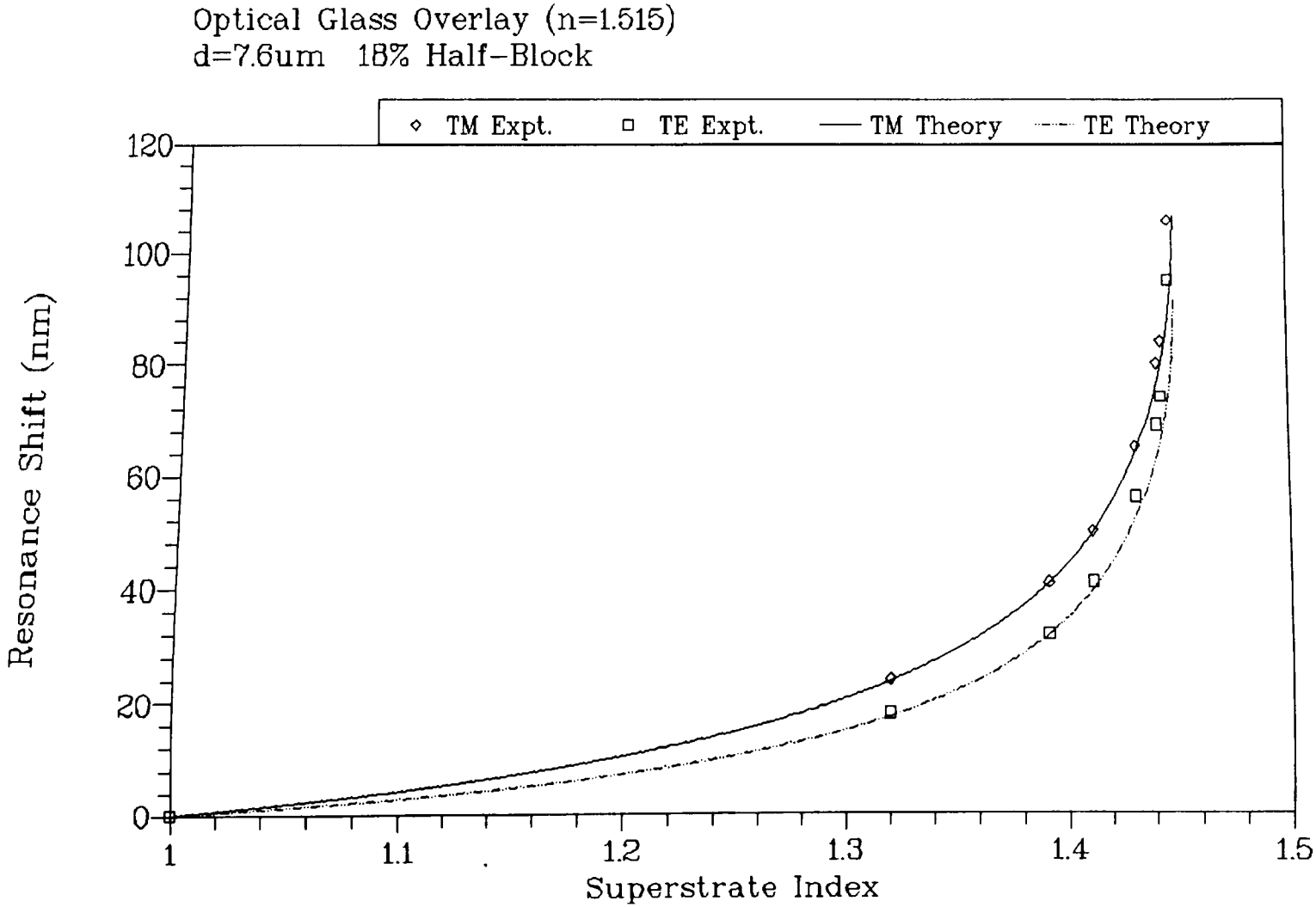

Figure 6.6 : Resonance Shift with Superstrate Index

high index1, 90μm device was not tuned) while the high index1, 16.8μm overlay device could be tuned a maximum of 15nm (TE), 24nm (TM). It is clear that the thickness of the overlay and, to a lesser extent, the index have a dramatic effect on the device tuning range. A very thin overlay (1-2μm) with index in the region of n=1.5 would allow a tuning range of >250nm but at the expense of broader resonance linewidths.

A further method of tuning the resonance response of a device is by deposition of thin, dielectric films onto the top surface of the overlay. The index of the dielectric film does not have to be less than the fibre cladding index provided it is very thin (100's of nm). If the index is greater than the fibre cladding then the film forms a compound waveguide with the original overlay. A film with index below that of the cladding forms a compound dielectric/air superstrate. In both situations, the original resonance positions are slightly shifted and the tuning range is small. The low index glass overlay device was used to test this tuning technique. A thin layer of Magnesium Fluoride (MgF_2) was built up on the overlay surface by repeated thermal evaporations. It has an index of approximately 1.38. After each deposition, the shifted resonance position was recorded for both polarisations. Figure 6.7 shows the resonance shift versus MgF_2 film thickness. The graph indicates that the resonance position shifts in an asymptotic manner towards the value it would have if MgF_2 was applied in bulk form as the superstrate. Notice that the shift is polarisation sensitive. Thin film values obviously result in an effective superstrate with an index intermediate between air and that of MgF_2. This method of tuning is suitable for small, permanent shifts. No evaluation of the tuning technique involving high index, thin dielectric films was carried out at this stage.

It appears that tuning of the channel positions can be readily accomplished via precise control of the overlay thickness or modification of the superstrate index and/or thickness. The drawback associated with tuning via superstrate modification with materials possessing an index less than the overlay index is a limited tuning range. An advantage of depositing thin, high index dielectric films (e.g. Aluminium

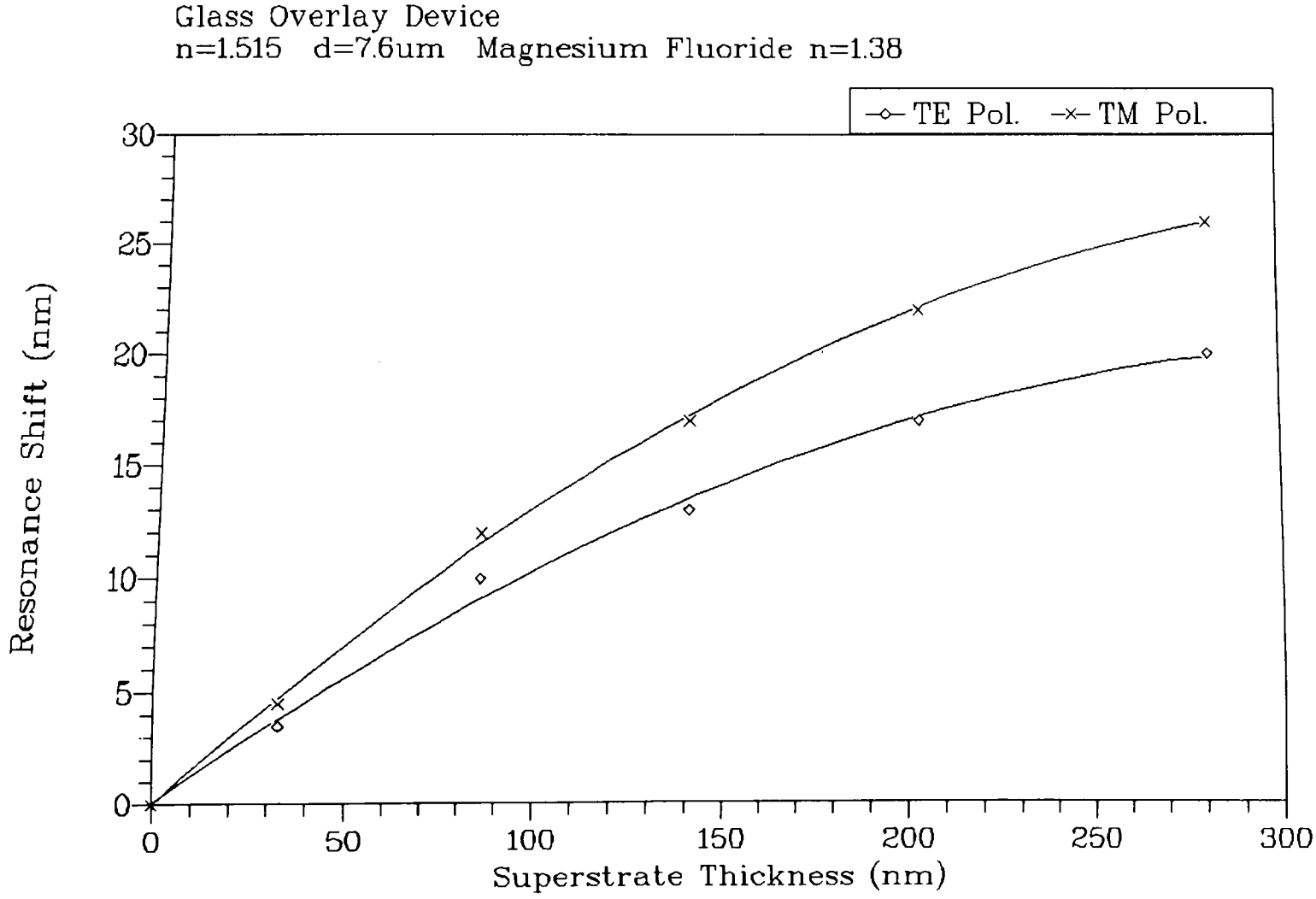

Figure 6.7 : Resonance Tuning via Thin Film Superstrate

Oxide n=1.7 approx.) is that a transmission resonance can be selected at any desired wavelength. If light of the desired wavelength is launched into the device and the transmitted output monitored as deposition of the dielectric film occurs[8], then the deposition process can be terminated when the transmitted signal is at a minimum. This will correspond to a transmission resonance at this wavelength.

6.5.2 Switch/Bandpass Structure with Glass Overlay

The low index glass overlay device investigated previously (n=1.515, d=7.6μm, 18% Half-Block) was also incorporated in a switch structure (Figure 3.3 with no electrodes present). A specially designed jig was used to hold the device stationary while a second half-block was brought into contact with the top surface of the glass overlay with the interaction regions as closely matched as possible. An index oil was used as a matching/lubrication layer between the two polished surfaces and pressure was applied to the second half-block to reduce the thickness (minimise the optical effect) of the oil layer. The second half-block was then translated laterally using micrometer screws until it appeared that the fibres of the two half-blocks were aligned. A matching/lubrication index oil with n_D=1.456 was used while the second half-block had coupling strength of 91.5% (roc=22cm). The wavelength response of the glass overlay device (throughput) was then recorded to determine the resonance positions. As would be expected, the resonance positions had shifted to higher wavelength values. Polarisation sensitivity was minimal due to the symmetry and relatively low index of the overlay (interlay) waveguide, and noise problems prevented separation of TM and TE resonance positions. Therefore, once on an apparent resonance minimum, the signal was reduced to a minimum using the polarisation controller and this polarisation state maintained during the experimental testing. The narrower resonance was now located at 1374nm (previously 1301nm for TE, 1286nm for TM) while the other resonance was located just above the wavelength scan range. Linewidth was 28.2nm, an increase when compared with the air superstrate measurement.

From Figure 6.6, an oil superstrate of n_D=1.456 shifted the corresponding resonance

to 1392nm and 1396nm for TM and TE, respectively. This suggests that the overlay "sees" a superstrate lower than $n_D = 1.456$, apparently closer to $n_D = 1.452$ (resonance at 1370nm for TM, 1374nm for TE). The input wavelength was then set to 1374nm and careful lateral adjustment (fine tuning) of the second half-block was carried out while the cross-coupled output arm of the switch was monitored. Power output from the coupled arm of the switch was zero initially but it was found that a maximum value of 20% of the off-resonance throughput could be achieved. The above procedure was repeated with several longitudinal adjustments made to the second half-block in an attempt to determine the effect of longitudinal offsets. No micrometer screws were available to perform this adjustment so the second half-block was demounted from its initial position and translated by approximately 1mm steps several times. It was found that this procedure had no effect on the resonance position. A maximum cross-coupled power of approximately 35% of the off-resonance device throughput was observed. Figure 6.8 shows the wavelength response of the switch structure (normalised to off-resonance throughput). Modulation depth has reduced to 91%, possibly due to the "loading" effect the second fibre has on the overlay which reduces the amount of light lost laterally. There appeared to be a longitudinal range of 2-3mm over which there was only a moderate reduction in cross-coupling efficiency. However, outwith this region a rapid loss of power coupling occurred. Repeating the experiment on different days produced similar results for power coupling efficiency but generally at a shifted resonance position. The wavelength range over which the resonance was located was 1274nm to 1292nm. This corresponds approximately to the $n_D = 1.450 - 1.456$ section of the curve in Figure 6.6 suggesting that temperature variations cause the index of the oil to decrease slightly with a corresponding index shift in the superstrate "seen" by the overlay. From a practical point of view, this is an undesirable effect but could be overcome by incorporating a matching layer possessing a much lower dn/dT.

To assess the effect of the index of the matching/lubrication layer, two other index oils were used, $n_D = 1.400$ and $n_D = 1.520$. A wavelength scan of the throughput for the $n_D = 1.400$ case produced a resonance at 1324nm which agrees with previously

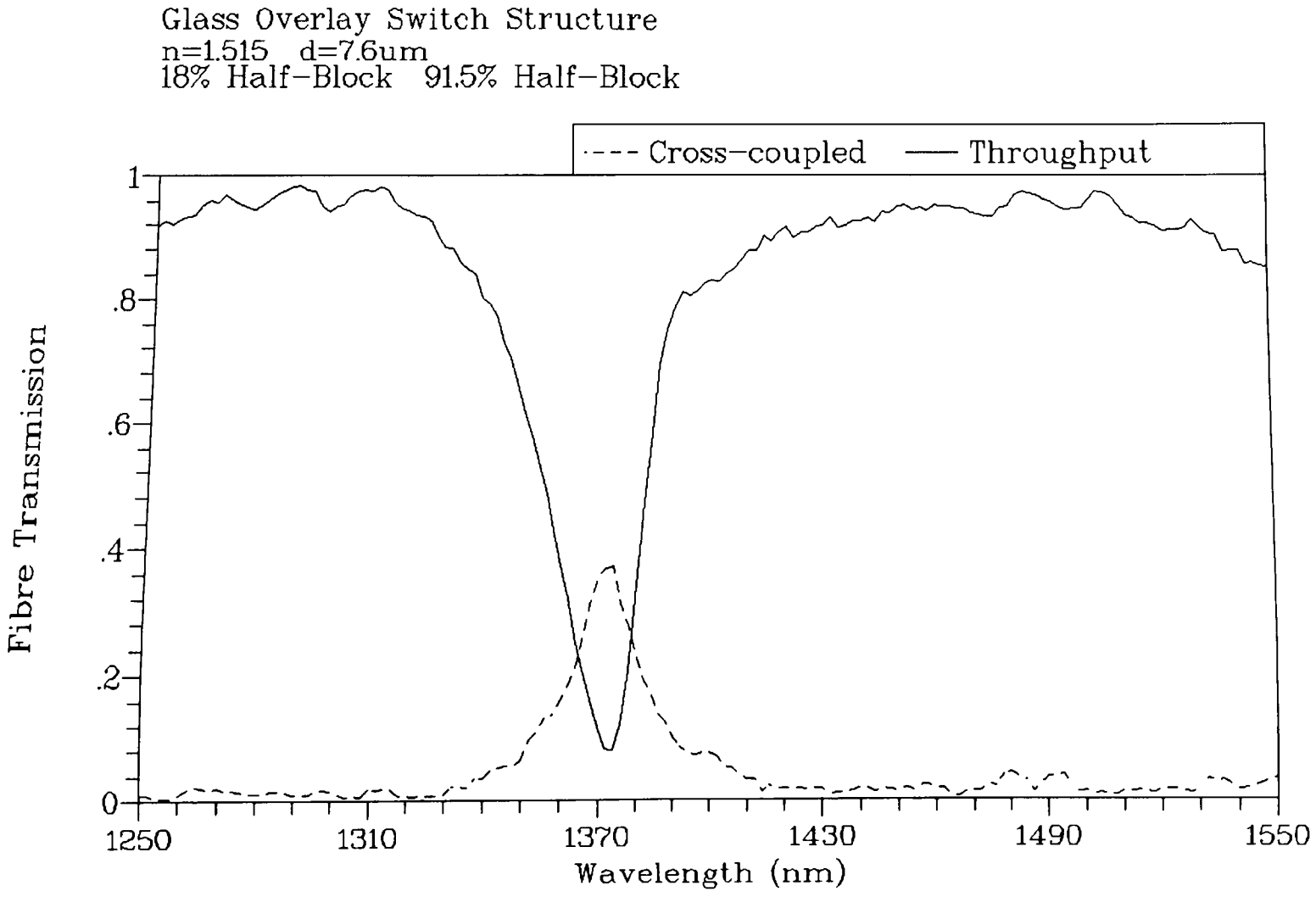

Figure 6.8 : Wavelength Response of Glass Overlay Switch

recorded tuned value from Figure 6.6. The switch was now found to be polarisation sensitive with the other resonance position at 1331nm. This reinforces the belief that the overlay "sees" the index of the oil layer as the superstrate and the effect of the index of the second half-block is minimal. The output from the coupled arm of the switch was then monitored as before but no power was detected despite extensive attempts to achieve cross-coupling. A possible explanation for this fact may be that the effective coupling strength of the second half-block was dramatically reduced due to the oil acting as an extended cladding. The "new" coupling strength of the half-block was then too low to allow significant power transfer in the interaction region available. The $n_D=1.520$ oil was then used as the matching layer. When applied to the overlay as a bulk superstrate there was a significant degradation of the device throughput as would be expected. However, when the second half-block was placed in position and pressure applied, the throughput signal recovered indicating that the oil and glass layers had formed a compound overlay. The polarisation sensitivity was negligible as would be anticipated from the overlay cladding indices now being equal. A wavelength scan revealed that the resonance position had shifted to 1398nm and that the shape of the resonance had changed. The maximum modulation depth was approximately 70% and the resonance now contained two dips thus producing a much larger linewidth (55.5nm). This was not a polarisation effect and may be due to the compound nature of the overlay producing a slight spread of phase-matching conditions.

Translation of the second half-block caused movement of the resonance position, a result of the oil layer thickness and, thus, the waveguide parameters varying. This presented some problems in achieving cross-coupling and continual monitoring of the resonance position was required. Despite the poor quality of the resonance, greater than 40% cross-coupling to the second fibre was observed but only at the higher wavelength dip on the resonance. Figure 6.9 shows the switch wavelength response. Note that the modified overlay has resulted in two resonance positions being located within the scan range. The amount of cross-coupled power is greater at the longer wavelength resonance, possibly as a result of stronger coupling coefficients, etc. The

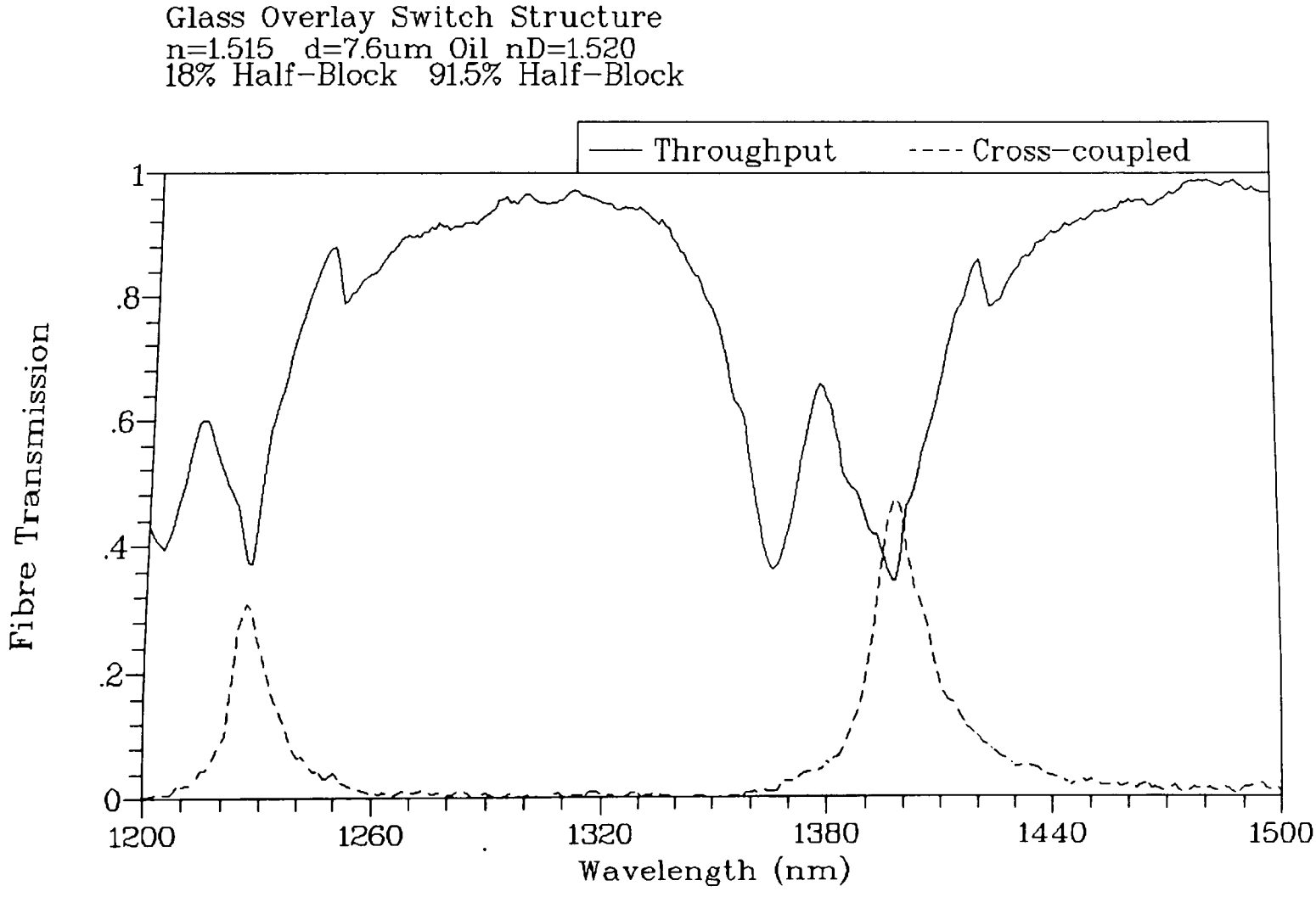

Figure 6.9 : Wavelength Response of Glass Overlay Switch

increased cross-coupling efficiency may be due to the fact that the second half-block coupling strength was not effectively reduced as before. A cut-back measurement was performed to determine the insertion loss of the switch and produced a value of 2dB, much higher than anticipated. However, when the switch was taken apart and the surfaces of the glass overlay and second half-block visually inspected using a microscope, there appeared to be a lot of surface damage (scratches, etc.). Light at 1300nm was then launched into the 91.5% Half-Block and it was found that applying an oil of index $n_D=1.456$ as a bulk superstrate caused the signal to increase significantly. Measurements indicated that the half-block had an insertion loss of 1.7dB for an air superstrate. Similarly, the glass overlay device was found to be slightly lossy for an air superstrate. It is believed that too much pressure was applied to the second half-block during the experiments with surface damage occurring as the half-block was translated laterally and longitudinally. A greater degree of cross-coupling can be anticipated for switch structures in which the components are not lossy. The broader resonances observed for the switch structure compared with the glass overlay device with an air superstrate may also have been a result of the surface damage.

6.6 Passive $LiNbO_3$ Overlay Devices

The next stage in the device fabrication schedule was the manufacture of passive $LiNbO_3$ overlay devices prior to the attempted realisation of active wavelength selective components. Similar fabrication techniques to those employed in the production of the glass overlay devices were appropriate (outlined in section 6.2) although a few additional problems were encountered. These were mainly related to the tendency of the $LiNbO_3$ overlay to scratch, fracture and disintegrate when thin, much more so than the optical glasses discussed earlier. This section details the successful fabrication and characterisation of passive WSEs and describes how the added fabrication problems were overcome.

The favoured approach to device fabrication was to use the low index, low viscosity

glue with a relatively high coupling strength polished fibre half-block (70-80%). It was anticipated that this glue would allow the fabrication of the most parallel overlay as well as provide the thinnest glue layer. The intended active device structures will employ transverse electrodes (see Figure 6.1) and, therefore, as thin a glue layer as possible is required to minimise drive voltages i.e. electric field is dependent upon the spacing between the electrodes. Initial attempts at device fabrication had a high failure rate due to the material properties of the $LiNbO_3$ differing from the optical glasses used for earlier devices. The $LiNbO_3$ is much more brittle than glass even when in wafer form (1mm thick) and also has a greater tendency to shatter when thermally shocked. This led to major problems when the $LiNbO_3$ overlay was lapped and polished to a thickness of $<30\mu m$. However, for eventual drive voltages to be realistic even for demonstration purposes, the thickness of the overlay had to be $<20\mu m$ (using $4.78V/\mu m$ calculated in Chapter 5). The $LiNbO_3$ source wafer (1mm thick) was generally cut into rectangular pieces of about 10mm x 15mm and lapped and polished to a thickness in the region of $800\mu m$ before being bonded to the half-block surface. Obtaining a unblemished polished surface on the $LiNbO_3$ slice was the first difficulty encountered. It was found that the corner areas of the slice would chip away as the polishing process was performed and be translated across the polished surface. This caused severe scratching of the sample. Rounding of the corners of the $LiNbO_3$ slice using a diamond file followed by ultrasonic cleaning to remove remaining fragments helped alleviate the problem. Surrounding the edges of the slice with UV-cured glue prior to polishing also reduced the number of scratches appearing on the sample but it was very difficult to completely prevent the appearance of scratches and other surface damage (indentations) on the eventual polished surface.

Before bonding to the polished fibre half-block, the $LiNbO_3$ was visually inspected using a microscope for both surface damage and cleanliness. The flatness of the sample was also observed by placing an optical flat in contact with the polished surface. It was found that the larger the surface area of the $LiNbO_3$ sample, the higher would be the degree of flatness in the centre region. It appeared impossible

to prevent edge-rounding of the sample. Good adhesion of the $LiNbO_3$ samples to the half-block surfaces seemed much more difficult to achieve than with the optical glass devices. In an effort to improve this situation, the bonding process was performed in a clean environment to prevent dust particles, etc. from getting caught in the glue layer. The $LiNbO_3$ slice was bonded to the half-block in the same manner as outlined for the optical glass devices with extreme care being taken to prevent air bubbles forming under the overlay. After curing, the overlay was surrounded by a higher viscosity "support" glue (Norland 61) to help reduce shear stress on the $LiNbO_3$ and also present a larger surface area to the lapping/polishing processes. The $LiNbO_3$/support glue combination was then reduced to a thin layer. During the polishing process, the likelihood of device failure could be assessed by observing the interference fringe pattern produced by the glue layer when illuminated by monochromatic light. If the overlay was beginning to detach from the half-block at a particular corner or area, the fringe pattern would be dramatically altered in that area, and as the polishing process was continued this area would spread before eventual device failure. The thinner the overlay, the greater the likelihood of this process occurring. Use of a more viscous glue as the bonding layer reduces but does not eradicate this problem. However, a more viscous glue produces other problems such as lack of parallelism, compound overlays, thick bonding layers. The fabrication of thin, parallel overlays of $LiNbO_3$ remains a major problem with the device geometry being investigated here.

Although the successful device yield was low, a device possessing an overlay of thickness approximately 20μm was successfully fabricated. The initial coupling strength of the half-block was 80%. The wavelength response was recorded (Figure 6.10a) and showed narrow linewidths (3nm for TE, 3.2nm for TM) and resonance spacing of approximately 22nm in the 1200-1250nm scan range. The TM and TE resonance positions were separated by 6nm. It was calculated that mode order for the TE and TM polarisations differed by a value of 3 (m=55 and m=52, respectively, for the lower resonance in the scan range). This is a result of the inherent material birefringence (n_{TE}=2.22, n_{TM}=2.15). Off-resonance insertion loss

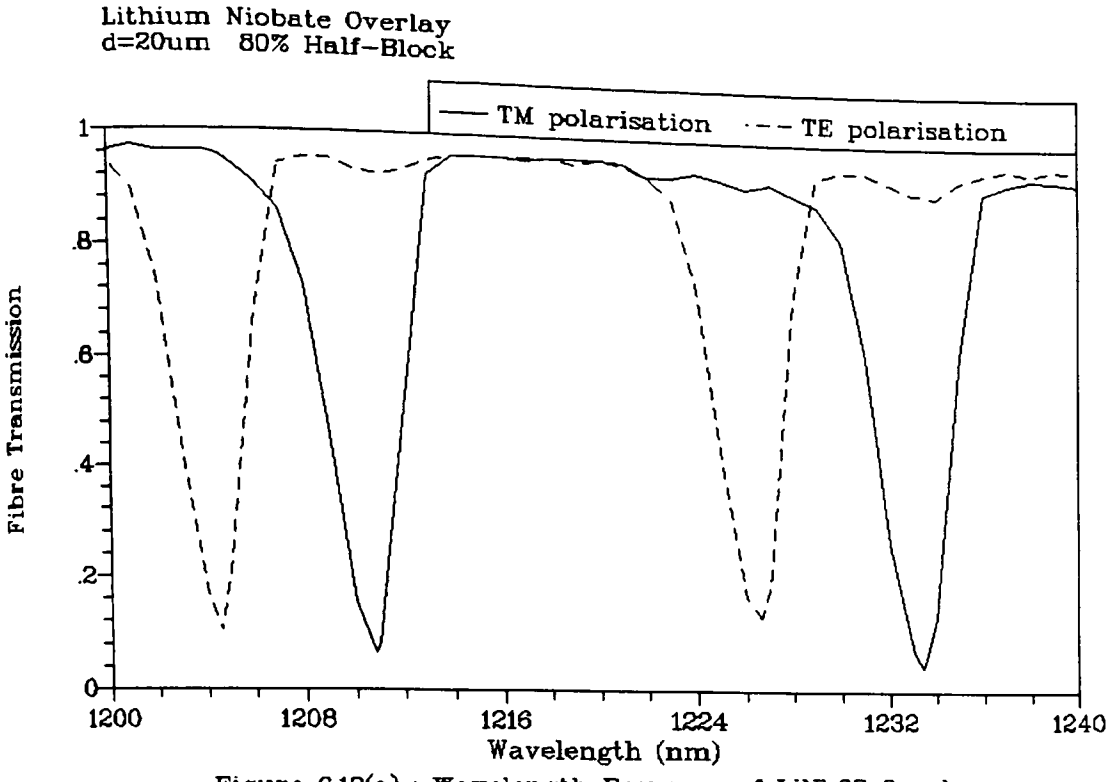

Figure 6.10(a) : Wavelength Response of LiNbO3 Overlay

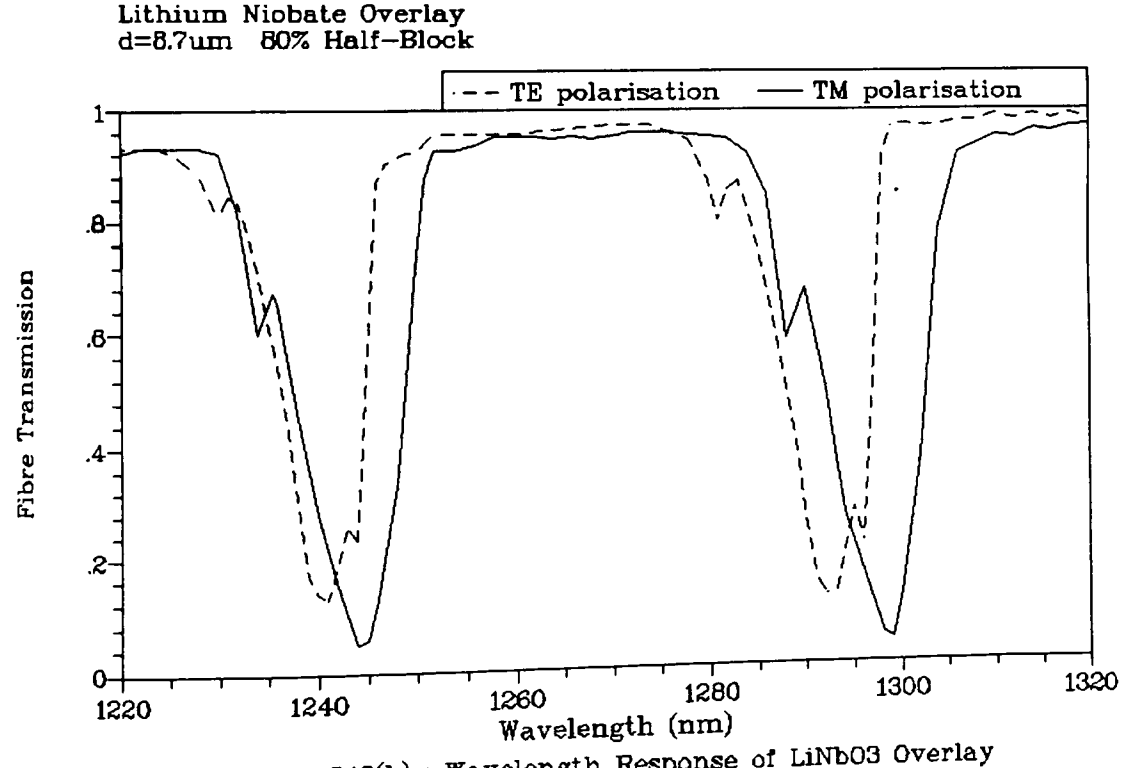

Figure 6.10(b) : Wavelength Response of LiNbO3 Overlay

was <0.2dB while the modulation depth was 95% (13dB) for TM polarisation and 89% (9.6dB) for TE polarisation. This is an improvement on the optical glass overlay devices in overall performance although the polarisation sensitivity may be a problem for practical applications. Unlike the glass overlay devices, the TE and TM polarisations cannot be made to converge by forming a symmetric overlay waveguide because of the material birefringence of $LiNbO_3$.

It is possible to use the response shown in Figure 6.10a to calculate a corresponding drive voltage to move on/off resonance for an active device (e.g. a modulator) possessing the same parameters. The wavelength variation, $\delta\lambda$, required to induce an intensity modulation of 10%-90% is 1.4nm (approximately the resolution limit of the equipment). This can be converted to an equivalent index variation using the relationship below which was derived, by simple differentiation, from the waveguide eigenvalue equation.

$$\delta n_o = -\frac{(n_o^2 - n_{eo}^2)}{\lambda n_o}\delta\lambda \qquad (6.1)$$

where n_o is the overlay material index, n_{eo} is the mode effective index and λ the resonance wavelength. The phase terms present in equation (1.1) have been neglected to ease the derivation since the mode order, *m*, is large. Using n_o=2.15 (the z-cut $LiNbO_3$ overlay results in the strongest electro-optic coefficient, r_{33}, operating on TM polarisation for transverse electrodes), $n_{eo}=n_f$=1.451 (the fibre effective index) and λ=1210nm, corresponding to the lower resonance, the calculated value of δn_o is 1.35×10^{-3}. Using equation (5.1), the corresponding required drive voltage is 176V or an electric field strength of 8.8V/μm. This value is considerably higher than drive voltages calculated earlier using oil overlay device results. Probable reasons for the higher calculated drive voltage are the optical quality of the polished surface and the parallelism of the $LiNbO_3$ overlay. Both these parameters influence the sharpness of the device transmission resonances. If the polished surface of the overlay is damaged or scratched above the fibre interaction region, then the

subsequent nonuniform thickness can cause an extension of the phase-matching condition and produce broader resonances. Similarly, an overlay which is not parallel will result in a spread of phase-matched wavelengths and again give a broadened device resonance response. The parallelism of the overlay becomes increasingly significant as the thickness decreases, an unfortunate occurrence since reduction of drive voltages depends on the attainment of thin overlay devices. Typically, for the oil results presented previously in Chapter 5, the resonance linewidth in terms of mode effective index $\delta n_{eo}=0.001$. This can be converted to a corresponding change in overlay thickness by using the expression below which was derived in a similar manner to equation (6.1).

$$\delta d = \frac{n_{eo} d}{(n_o^2 - n_{eo}^2)} \delta n_{eo} \qquad (6.2)$$

Letting $n_{eo}=n_f=1.451$, the thickness change, δd, to induce an effective index change, $\delta n_{eo}=0.001$ in a 20μm thick $LiNbO_3$ overlay is 11.5nm (using $n_o=2.15$). This means that to obtain a resonance with $\delta n_{eo}=0.001$ linewidth (in terms of mode effective index) for such a device requires that the deviation from absolute parallelism be less than 11.5nm (about $\lambda/100$) over the 1mm (typically) device interaction length. The stipulation on parallelism becomes more stringent as the overlay thickness is decreased. This degree of parallelism is difficult to achieve with the polishing processes and available equipment used to form the overlay and places a limit on achievable resonance linewidths.

However, despite the numerous fabrication limitations, a second device was produced which possessed an overlay with an approximate thickness of 8.7μm. Again, the initial coupling strength of the half-block was about 80% and the low viscosity, low index glue was used as the bonding agent. The wavelength response of the device, for both polarisations, is shown in Figure 6.10b. Narrowest resonance linewidths are 7nm and 10.7nm, respectively, for TE and TM polarisation, a considerable deterioration when compared with the 20μm thick overlay device. This

was believed to be mainly due to inferior surface quality and parallelism rather than the reduced thickness of the overlay, although this would contribute since the mode order has been approximately halved. The resonance spacing was 52nm (TE) and 55nm (TM). Device polarisation sensitivity was approximately the same as the first device, 3nm for the lower resonance, 6nm for the higher resonance. The birefringent nature of the $LiNbO_3$ overlay basically means that two quite separate eigenvalue equations result for TE and TM polarisations each incorporating the appropriate refractive index. Therefore, polarisation separation of the resonance positions will not necessarily increase as the overlay thickness is decreased, as would be expected for a non-birefringent overlay material i.e. only separation between TE and TM resonances with the same mode order can really be considered.

It is possible to again derive an equivalent drive voltage for a 10%-90% intensity modulation for the second $LiNbO_3$ device. The smallest wavelength change required to achieve the desired modulation was $\delta\lambda = 5.8$nm which gave, using equations (6.1) and (5.1), a drive voltage of 297V or an electric field strength of $34.1 V/\mu m$. This value is obviously much too high for a practical device with a similar device transmission response. However, the linewidth is particularly poor on this device and it should be possible, with existing fabrication processes, to produce resonance linewidths of < 4nm for overlay thickness $< 10\mu m$ which would allow a 10%-90% drive voltage in the region of 75V or less.

6.6.1 Resonance Tuning of $LiNbO_3$ Devices

The response of the $8.7\mu m$ thick $LiNbO_3$ overlay device to tuning with index oils as the superstrate was investigated. The resonance positions for both TE and TM polarisation for a range of superstrate indices are shown in Figure 6.11. Maximum resonance shifts were 27nm (TM) and 10.5nm (TE). Calculations indicate that their is a difference of 3 in the mode orders for the TE and TM resonances. Notice that there is a significant difference in the resonance positions even when the overlay is approximately symmetrical ($n_D = 1.456$) unlike the tuning of glass overlay devices. This is due to the material birefringence of $LiNbO_3$. No tuning was carried out via

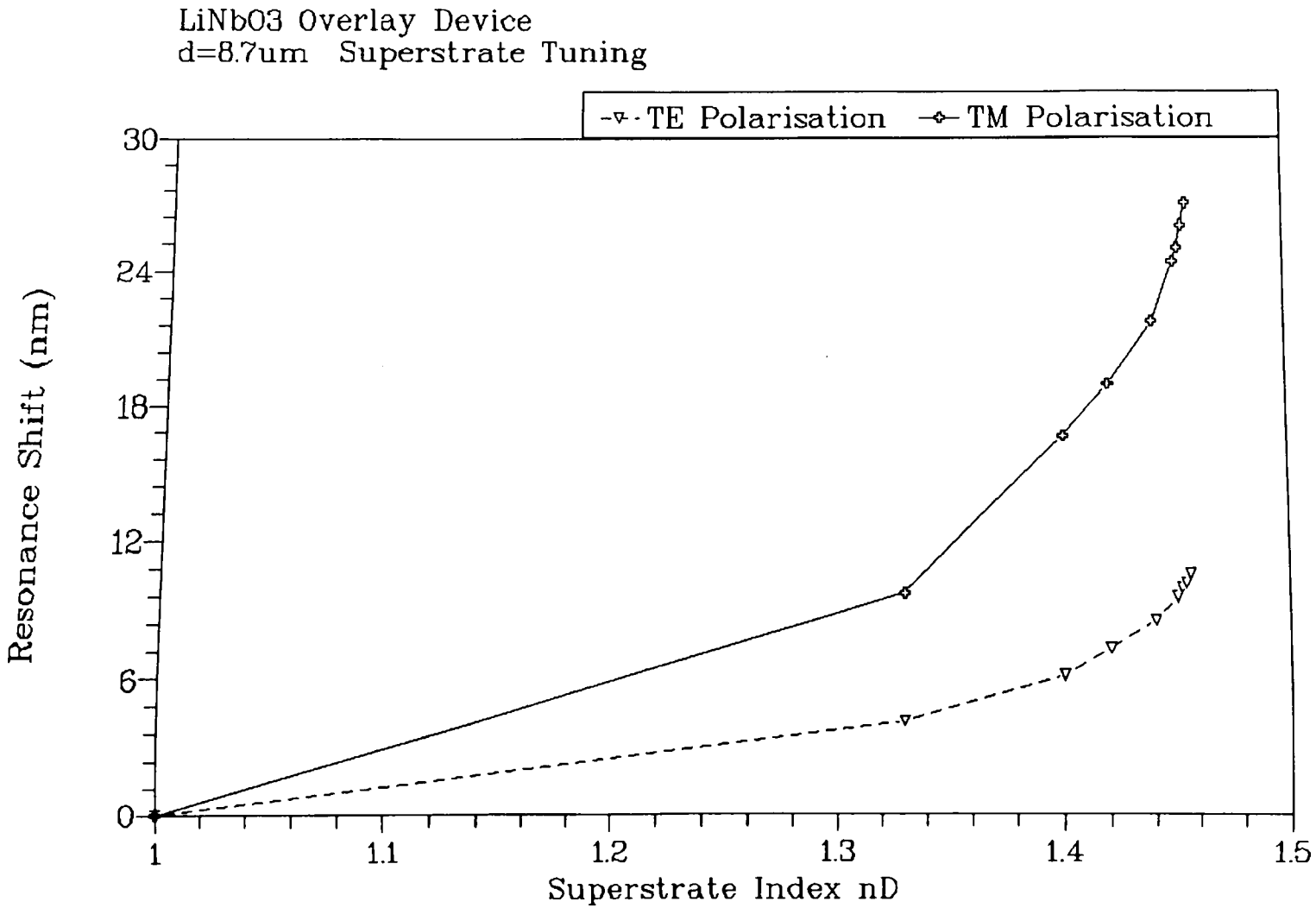

Figure 6.11 : Resonance Shift with Superstrate Index

deposition of thin films but a similar form of response to those recorded for glass overlay devices can be expected although the tuning range will be decreased.

6.6.2 Passive $LiNbO_3$ Overlay Switch/Bandpass Structure

The 8.7μm $LiNbO_3$ overlay device was also incorporated in a switch structure. A second half-block of 60% coupling strength (roc=22cm) was used to collect the power coupled out of the input half-block. The switch structure was constructed in a similar manner to that outlined for the optical glass overlay devices with an oil matching/lubrication layer of $n_D=1.456$. Slightly less pressure was applied to the second half-block in an effort to prevent damage to the adjacent optical surfaces of the overlay and half-block. The 60% coupling strength half-block was selected for use rather than the higher coupling strength half-blocks incorporated in other switches in an effort to reduce the linewidth of the cross-coupled resonance response. It was felt that the coupling strength was high enough to ensure strong cross-coupling. The switch structure was wavelength scanned in the 1200-1350nm region and the resonance positions recorded. TM polarisation was selected and the input wavelength was then set to a resonance minimum. It was believed that the greater modulation depths displayed by TM polarisation resonances would be more likely to result in efficient power transfer to the second fibre i.e. the maximum possible amount of light was available in the overlay at these wavelengths. Careful adjustment of the second half-block produced a maximum cross-coupled intensity of 88% of the off-resonance device throughput at a wavelength of 1325nm.

Figure 6.12 shows the wavelength switching characteristic of the device for TM polarisation. The power transfer occurs approximately periodically at each successive resonance minimum in the throughput signal. A similar switching characteristic (Figure 6.13) was obtained for TE polarisation although the maximum cross-coupling efficiency was reduced to 60%. The TE and TM wavelength responses are displaced by 12nm which is an increase on the separation recorded with an air superstrate. Again, this is due to the material birefringence of $LiNbO_3$ since the overlay is symmetrical in the switch structure. The successive resonance spacings are 51nm and

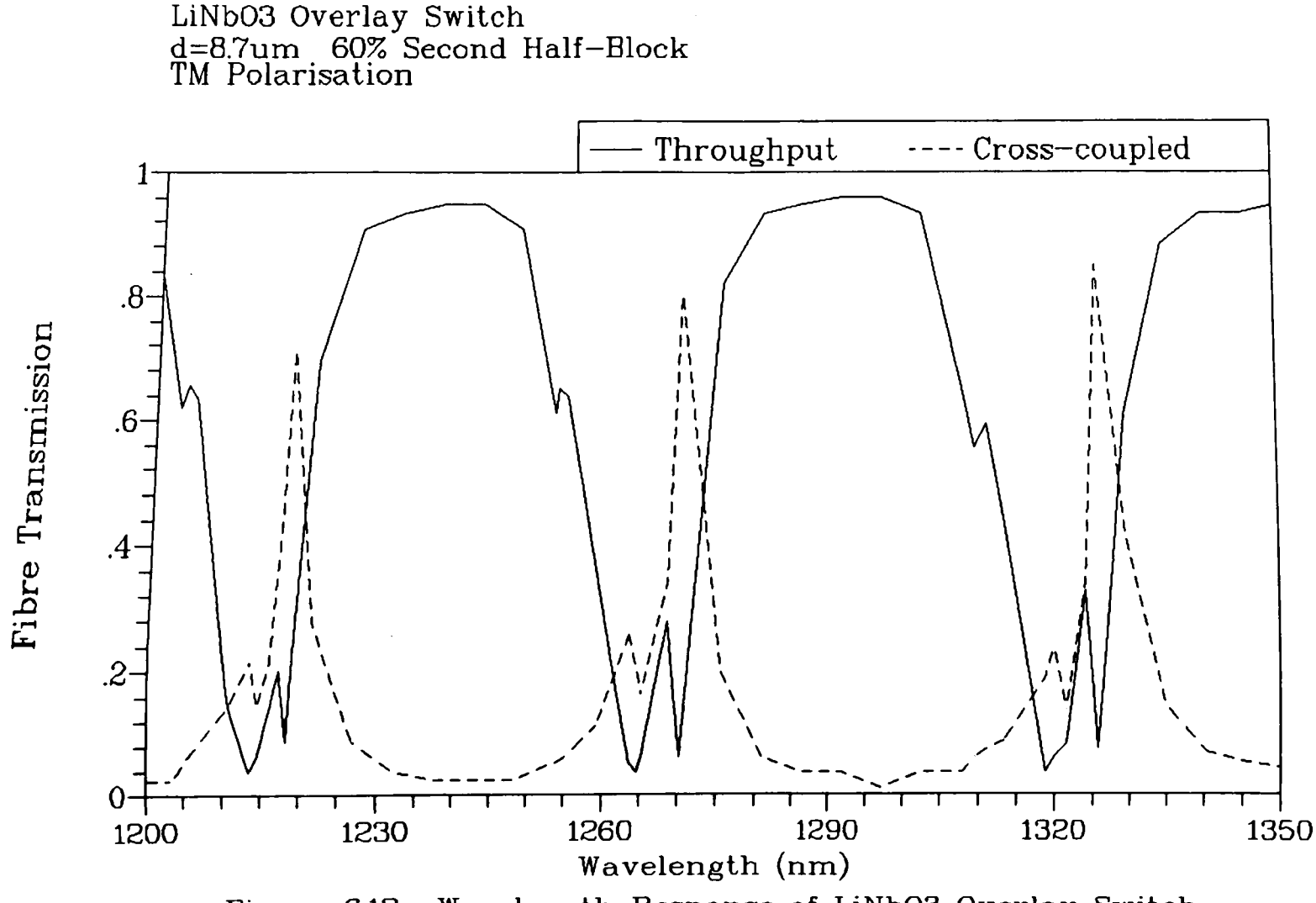

Figure 6.12 : Wavelength Response of LiNbO3 Overlay Switch

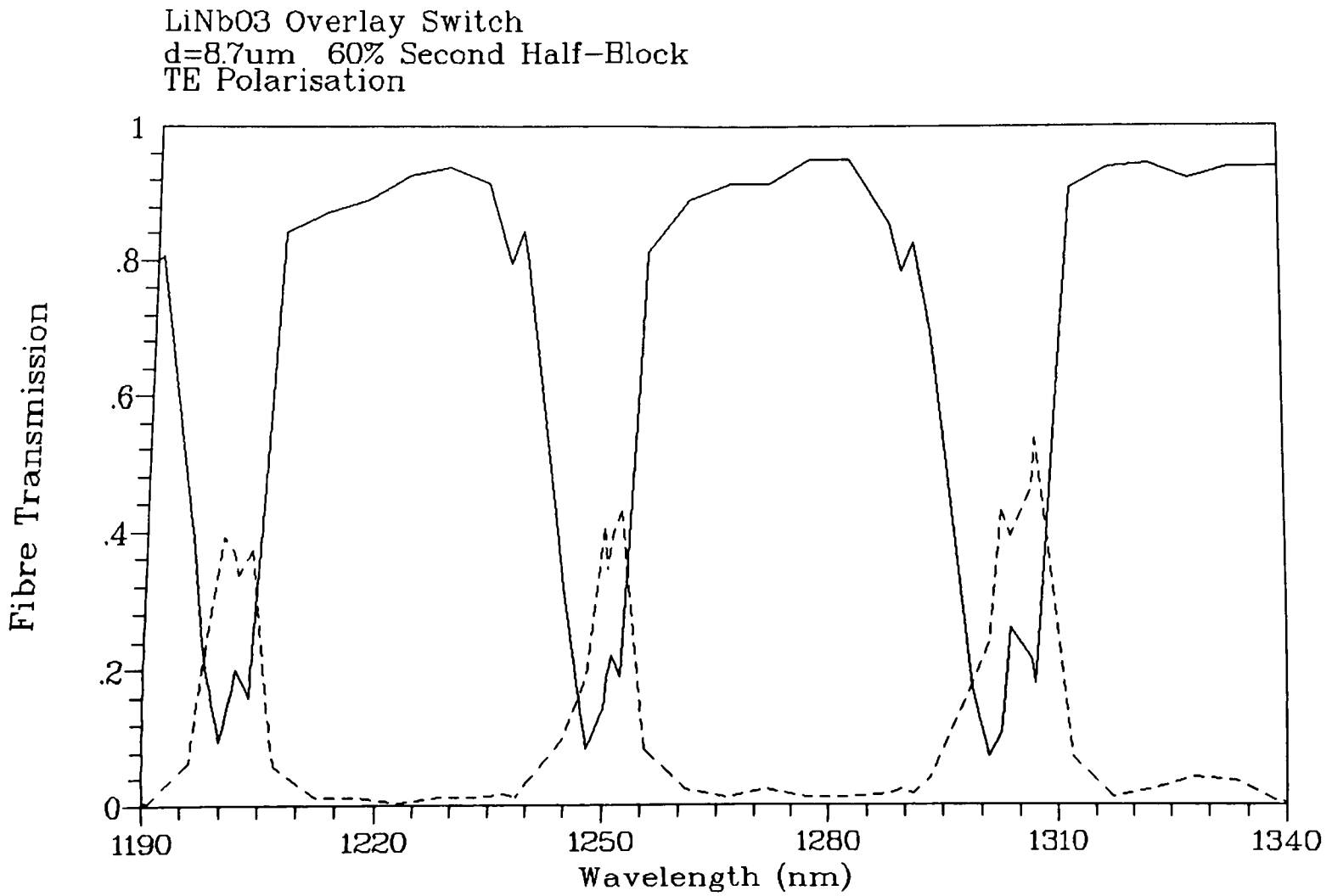

Figure 6.13 : Wavelength Response of LiNbO3 Overlay Switch

55nm for the TM polarisation and 48nm and 53nm for the TE polarisation. An increased resonance spacing is expected for the TM polarisation since the overlay index is less than for TE polarisation and thus results in wider overlay mode spacings. The shape of the resonances is considerably changed from those of the same device with an air superstrate. Several sharp dips have appeared within each resonance with a subsequent increase in the linewidth value. For TM polarisation, the best linewidth value is 12.5nm for the throughput intensity and 3.8nm for the cross-coupled intensity. The corresponding TE linewidth values are 10.9nm and 7.9nm. It appears that the presence of the second half-block degrades the shape and width of the resonances in the throughput intensity. Inspection of Figure 6.12 (or Figure 6.13) reveals that there is a high loss region on the low wavelength side of each resonance. Presumably the power is confined to the overlay at these wavelengths. The cross-coupled power then peaks on the high wavelength side of these lossy regions.

A qualitative description of the switch behaviour is difficult to obtain when considering coupled-mode theory. If the switch is considered as a multilayer structure, then a set of normal modes will be supported by the structure as outlined for the simpler fibre-overlay case in Chapter 3. However, three normal modes will be involved in the power transfer mechanism for the switch structure rather than the two considered for the fibre-overlay structure. Therefore, a more complicated situation exists in which the power oscillates (or beats) between the three guiding regions of the structure and a scenario where the majority of the power is located in the overlay, at the output of the interaction region, is possible. Further modelling of the switch as a multilayer structure should provide a better understanding of the exact power transfer mechanism.

From a switch performance point of view, the important device parameters are the power transfer efficiency to the coupled arm, ζ, the transmitted and coupled arm losses, α_1 and α_2, and the respective extinction ratios, ε_1 and ε_2. These values can be obtained from the wavelength response curves in Figures 6.12 and 6.13 and are

displayed in Table 6.1.

Polarisation	ζ	α_1	α_2	ε_1	ε_2
TM	90%	<0.5dB	<1dB	15dB	18dB
TE	60%	<0.5dB	<2dB	11dB	17dB

Table 6.1: Lithium Niobate 8.7μm Overlay Switch Performance Parameters

The lower cross-coupling efficiency for TE polarisation is possibly due to a longer coupling length than the TM polarisation as a result of the lower overlay index and smaller evanescent tail combining to produce smaller coupling coefficients. The minimum observed wavelength shift required to induce a 10%-90% modulation in throughput intensity was 6nm, a very slight increase on the equivalent measurement made with an air superstrate. The corresponding required drive voltage would be 301V or an electric field strength of 34.6V/μm. Therefore, by setting the input wavelength to the appropriate value, the throughput intensity could be effectively switched off while the cross-coupled intensity is switched to a maximum for application of a drive voltage of 300V. The cross-coupled arm of the switch requires less of a wavelength shift to produce a similar intensity modulation (10%-90%). An equivalent drive voltage of 135V can be calculated although the cross-coupled off state would also correspond to a throughput off state and, as such, does not allow a switching operation to be implemented. If the device overlay material was replaced by materials with higher electro-optic coefficients such as $BaTiO_3$ (n=2.2, r=820pm/V) or Barium Strontium Niobate (n=1.9, r=1090pm/V), the equivalent switching voltage would be reduced to 11.3V and 8.5V, respectively. Tuning of the switch resonance positions is best achieved by vacuum deposition of thin dielectric films as outlined in earlier sections. The formation of high index films is necessary since the overlay superstrate is essentially fixed (matching oil and second half-block). For a practical switch structure, the thickness of the top ITO electrode can be used to modify the device resonance positions.

6.7 Active $LiNbO_3$ Overlay Devices

The fabrication of active $LiNbO_3$ overlay devices employed the same techniques as those used for the passive device realisation (see sections 6.3. However, the incorporation of transparent electrodes in the device geometry and the problems of bonding to these electrodes had to be addressed. The electrodes were formed by the deposition of Indium-Tin-Oxide (ITO), an optically transparent conductor, as outlined in section 6.2. Although the ITO film had a refractive index greater than the cladding index ($n=1.9$-2.1 depending on deposition conditions), it was felt that the optical effect would be negligible if the film was kept very thin. The geometry of the overlay device (see Figure 6.1) is such that the ITO electrode is covered by a thin glue layer, even outwith the immediate area of the $LiNbO_3$ waveguide. For a basic modulator or channel-dropping filter structure (no second half-block) this presented only a minor problem since the glue could be carefully removed (using solvents) at one edge of the half-block without affecting the optical characteristics of the device. This then allowed straightforward electrical contact to be made via silver-loaded epoxy or conducting paint. The top electrode was then deposited on the $LiNbO_3$ top surface whilst ensuring no conducting path was formed to the bottom electrode. Similar contact to the top electrode could then also be made using silver-loaded epoxy. However, in the case of a switch structure, a second half-block with the same surface area as the lower half-block was to be placed in contact with the overlay top surface. This obviously meant that the surface topology of the overlay device had to be flat and, as such, areas of silver-loaded epoxy were undesirable.

Initially, extra grooves were cut in the half-block and copper wire secured in the grooves in the same manner as the optical fibre. When the half-block was lapped/polished, a section of the copper was left exposed at the half-block surface with the rest of the wire below the surface level. Contact to the ITO electrode deposited on the half-block surface could then be made using the copper wire. A similar set-up was envisaged for the second half-block although it was recognised that the matching oil layer would then be located between the electrodes and thus

contribute to the effective thickness of the overlay, an undesirable effect with regard to electric field strength considerations. Unfortunately, the contact between the copper wire and the ITO electrodes appeared to degrade as the lapping/polishing processes were performed on the $LiNbO_3$ overlay. It is believed that the mechanical stress applied to the overlay was transmitted to the ITO layer which then weakened along the edges of the groove in which the copper wires and the optical fibre were located. The degradation of the electrical contact was reflected by the increase in the resistance between copper wires located in separate grooves. By inserting two separate copper contact wires in the half-block, the continuity of the ITO electrode could be assessed. This was considered to be important since a number of early active devices, in which the ITO/copper contact could not be checked, unexpectedly displayed no electro-optic response. Possible reasons were thought to be fracturing of the ITO electrode in the vicinity of the device interaction region and therefore no electric field being developed in the required area of the overlay. To overcome this problem, the thickness of the ITO electrode was increased to about 100nm (rather than the initial 25nm). However, problems with the resistance of the copper/ITO electrode still persisted and it is uncertain whether the increased electrode thickness caused any difference.

Eventually, it was decided that the second half-block would have to be slightly reduced in size to allow contact to the ITO electrodes at the extreme edges of the lower half-block in the manner outlined for the modulator structure above. This approach required the fabrication of half-blocks with different dimensions and was, therefore, time-consuming and further complicated the alignment stage when switching experiments were being performed. However, it ensured better quality electrical contacts to the ITO electrodes and was adopted on this basis. The behaviour of ITO directly above the device interaction region remained uncertain. Certain modifications to the mechanical jig used for the switching experiments were also required due to the reduced dimensions of the second half-block. It was also decided that the top ITO electrode must be deposited directly onto the top surface of the $LiNbO_3$ overlay to ensure the maximum possible electric field was applied to

the $LiNbO_3$. Direct contact was then made to the edge of the top ITO electrode which was designed to extend beyond the width of the top (second) half-block (similar to the set-up for the modulator structure).

Good adhesion of the $LiNbO_3$ overlay to the ITO electrode proved to be extremely difficult to achieve, especially when the low viscosity glue was used. The high device failure rate at this stage prompted the use of the higher viscosity UV-cured glue (Norland 61) despite the drawbacks of wedged overlays, etc. and also the bond thickness which will reduce the electric field strength in the $LiNbO_3$ layer. Electro-optic modulation was first observed in a device which incorporated an 80% half-block and a $LiNbO_3$ thickness of $< 15\mu m$. The lower ITO electrode was 25nm, the bonding agent was Norland 61 and the top ITO electrode was 100nm. A wavelength scan of the device was performed and the best TM polarisation resonance linewidth was 13nm while the lowest resonance spacing was 59nm. Polarisation separation ranged from 10-26nm and the modulation depth for both polarisations was >95%. For a known overlay index, it is normally possible to determine the approximate thickness using the spacing between two resonances. Assuming that the overlay is composed entirely of $LiNbO_3$ gives a calculated thickness of $8.3\mu m$. If it is assumed that the overlay is composed entirely of glue ($n=1.51$), then the associated thickness using the recorded resonance spacing is $31.6\mu m$. Therefore, the actual thickness of the compound overlay (electrode separation) lies between these two extremes although it is more likely to be closer to the lower value. TM polarisation was established at the input to the device and 300V applied between the electrodes while another wavelength scan was recorded (the maximum electro-optic effect occurs for the TM polarisation and so only this polarisation is treated). The same procedure was repeated for an applied voltage of -300V. Figure 6.14 shows the shift in wavelength position for a resonance, located at 1435nm when 0V are applied to the device. The maximum shift in the wavelength response of the device is 2nm for 300V. Changing the polarity of the applied voltage reverses the direction of the wavelength shift which confirms that the electro-optic effect is the causing the shift. If the overlay was composed entirely of $LiNbO_3$ (thickness $8.3\mu m$), then the expected wavelength

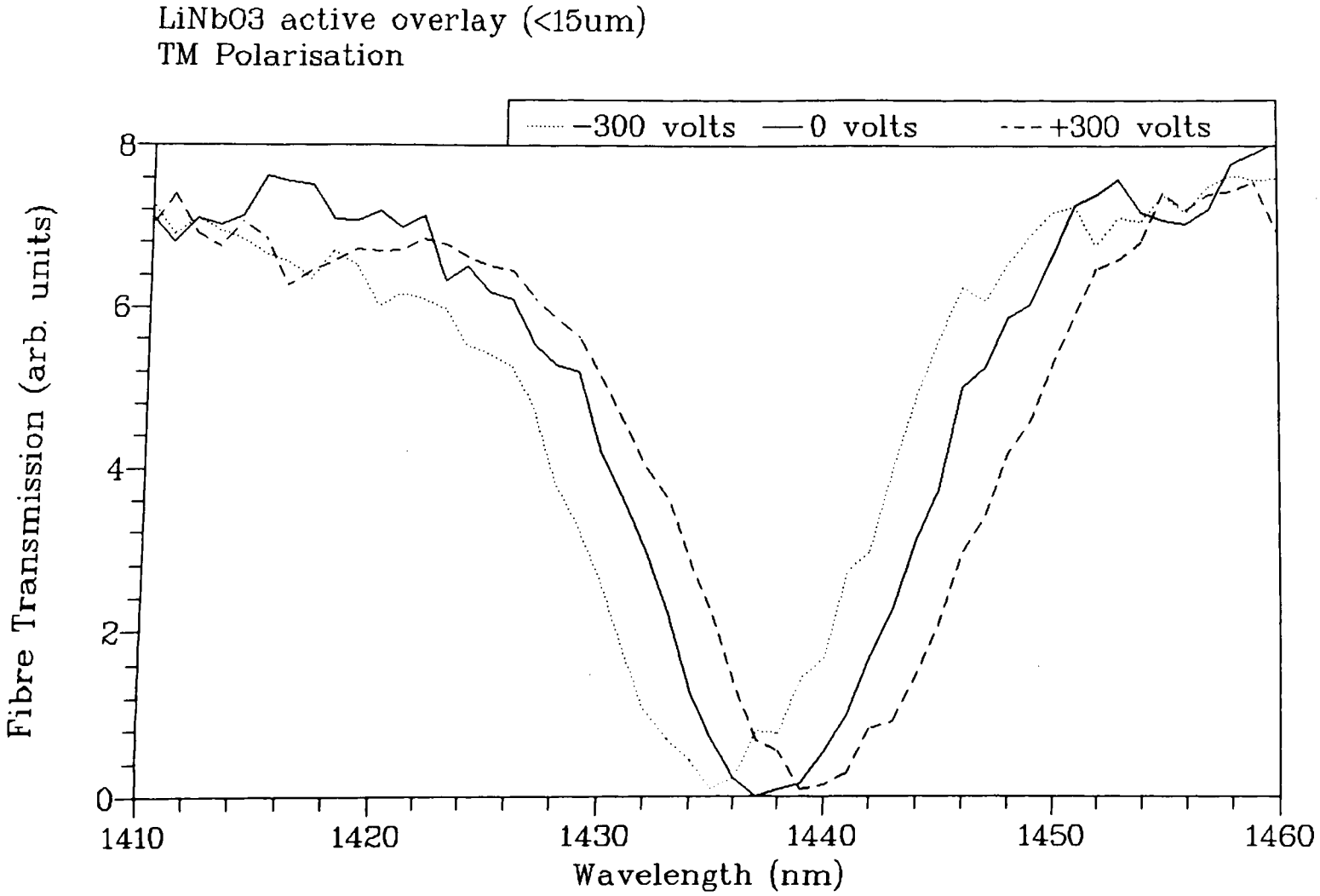

Figure 6.14 : Wavelength Shifts due to Applied Voltages

shift for application of 300V can be calculated using equations (5.1) and (6.1). For TM polarisation, the calculated shift is 6.8nm. Therefore, a much reduced electric field strength was obviously being developed in the $LiNbO_3$ part of the overlay almost certainly due to the substantial glue component of the overlay. This highlights one of the disadvantages of a device possessing a thick glue layer. In addition, the quality of the resonance was poor which meant that no more than about 30% intensity modulation was observed as a result of the 2nm shift. This was due to the top surface of the overlay which was not particularly well polished (the device appeared to be about to fail at the polishing stage) and also the high coupling strength of the half-block which was chosen to ensure good modulation depth.

A second active device was fabricated using the low viscosity glue. The $LiNbO_3$ overlay was about 16μm thick and the coupling strength of the half-block was initially 30%. Lower and upper electrode thicknesses were 40nm and 20nm, respectively. A wavelength scan of the device for TM polarisation is shown in Figure 6.15. Again, the resonance linewidths are broader than expected while the shape of the resonance is the reverse of the usual response. This is thought to be a result of damage to the polished surface of the overlay which causes increased loss as the overlay mode approaches cutoff. However, biasing the input wavelength to a sharp section of a resonance allowed approximately 50% intensity modulation for application of 350V. Figure 6.16 shows the wavelength shift for $\pm$350V. The maximum shift is $\pm$2nm, depending on the polarity of the voltage. This value can be used to back-calculate the exact voltage applied to the $LiNbO_3$. The corresponding index shift is 1.8×10^{-3} which translates to an electric field strength of 11.77V/μm. Since the bonding layer is index-matched to the fibre cladding, and assuming the optical effect of the ITO electrodes is negligible, then the resonance spacing can be used to provide a fairly accurate estimation for the $LiNbO_3$ thickness. The relevant resonance spacing is 32nm which gives a calculated thickness of 16.6μm. Therefore, the exact voltage applied to the $LiNbO_3$ was only 195.4V. A possible explanation is that a much higher proportion of the voltage is being dropped across the glue layer than was thought previously. This is almost certainly a result of the dielectric

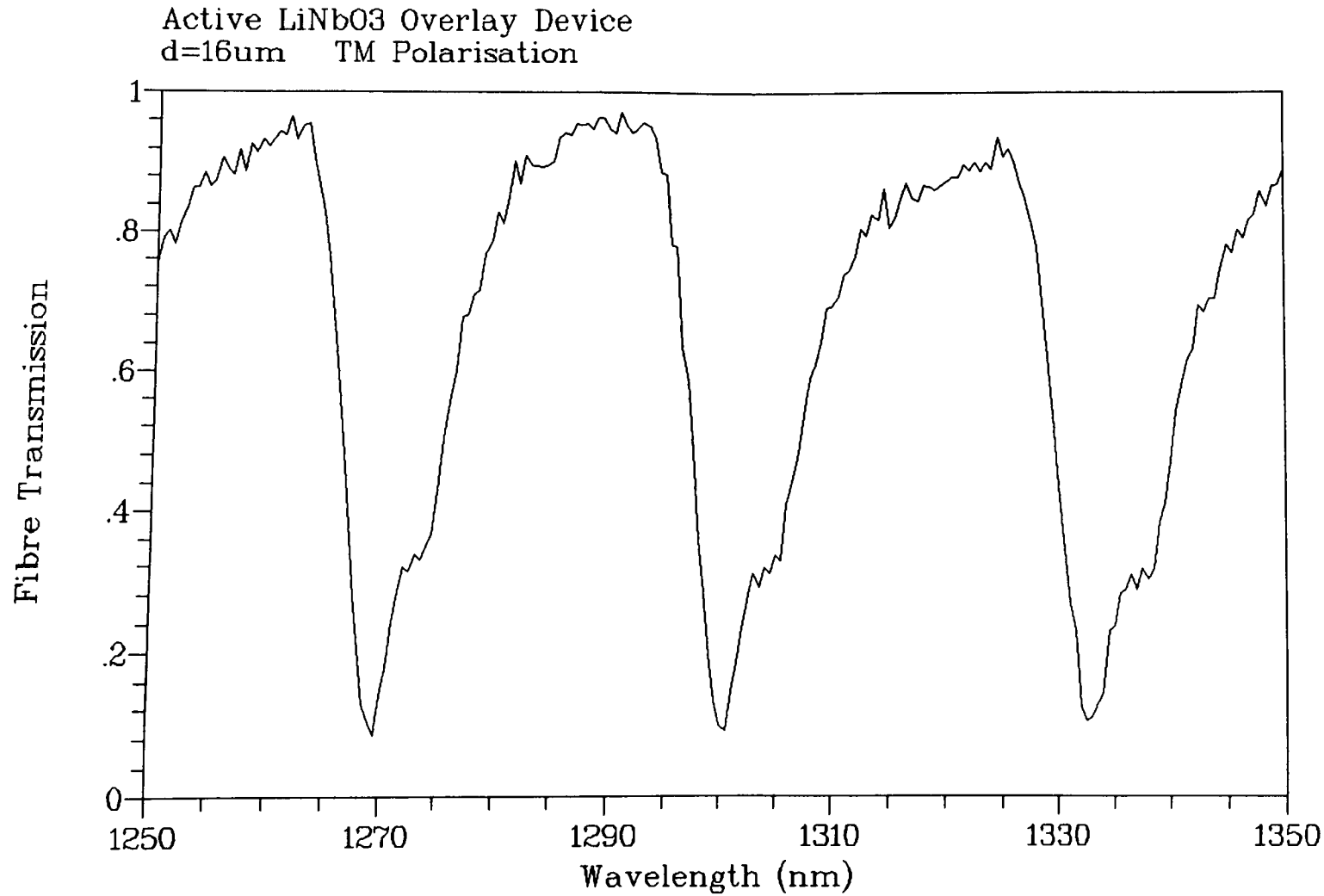

Figure 6.15 : Wavelength Response of Active Overlay

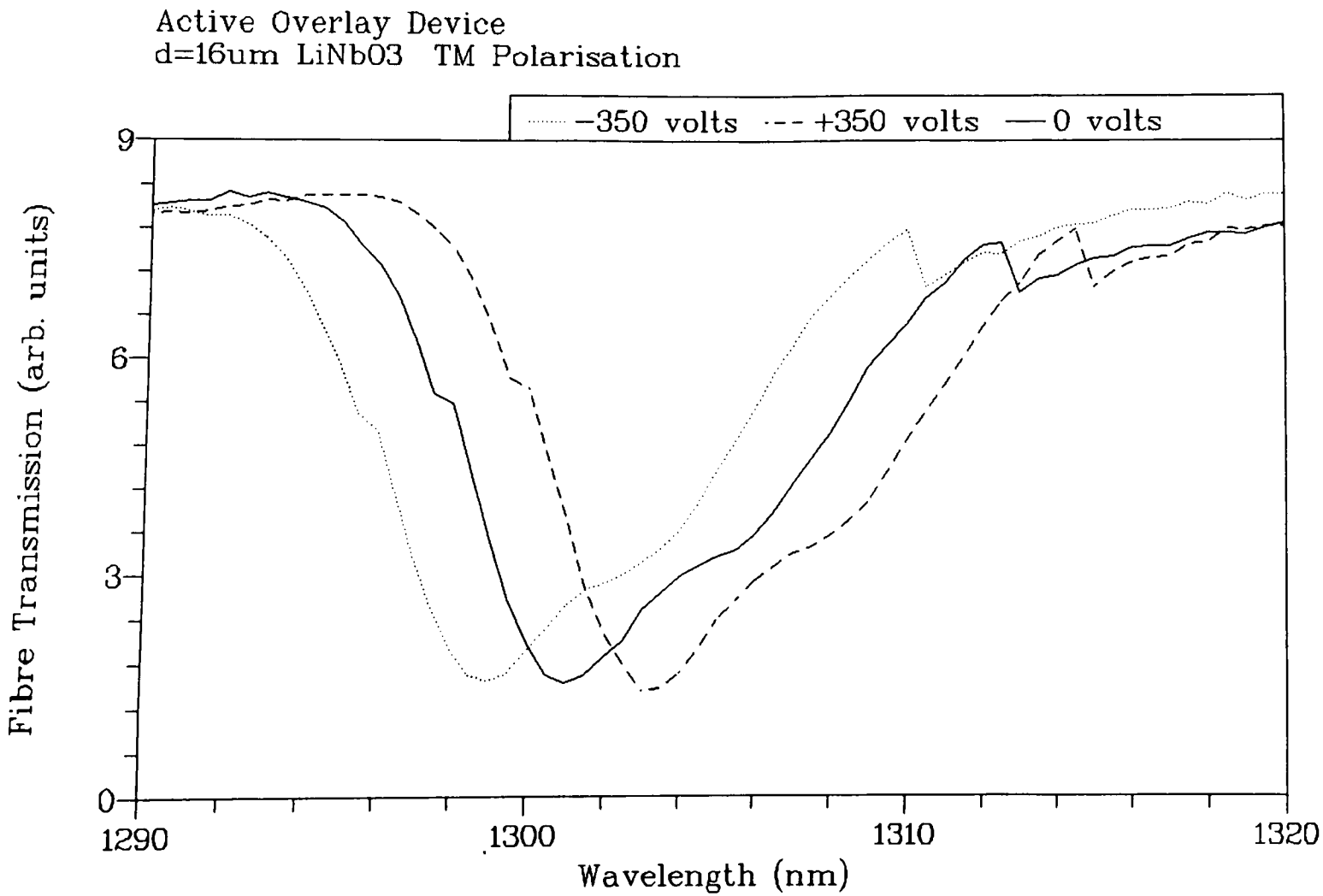

Figure 6.16 : Wavelength Shifts for Applied Voltages

strengths of the glue and $LiNbO_3$ layers being very different. Alternatively, if the presence of the ITO electrode (n=1.9-2.1) results in the glue layer behaving as part of the overlay, then the calculation of the thickness of the $LiNbO_3$ layer from the resonance spacing will produce an underestimation i.e. the resonance spacing will be increased due to the low index of the glue. In this case the observed 2nm wavelength shift may agree with theory.

6.7.1 Electro-Optic Switch/BandPass Structure

A third active device with an improved performance was also successfully fabricated. Again, the low viscosity glue was used and the $LiNbO_3$ thickness was approximately 18μm. Lower and upper electrode thicknesses were 20nm and 30nm, respectively. The device was incorporated in a switch structure with a 95% coupling strength second half-block and n_D=1.456 matching/lubrication oil. Maximum cross-coupled intensity was 70%. A section of the wavelength response of the switch for TM polarisation is shown in Figure 6.17. The modulation depth is only 88% and this probably limits the cross-coupling efficiency. Poor surface quality and too low coupling strength are the likely reasons for the lack of modulation depth. Although the presence of the second dip on the lower wavelength side of each resonance, the linewidth values are narrower than for the previous active devices (best value 6.8nm). The higher resonance spacing is 33.5nm. The input wavelength was set to a cross-coupled peak value and the cross-coupled arm of the switch was monitored while a voltage of $\pm$350V was applied. A maximum intensity modulation of 66% of the peak cross-coupled intensity was observed for 0V, dropping to a minimum for an applied voltage of 350V. Simultaneously, the device throughput was seen to shift from a minimum value to approximately 60% of the off-resonance throughput. This maximum switching action corresponds to the sharpest sections of the transmission resonance positions. Figures 6.18 and 6.19 show the wavelength shifts for the transmitted and cross-coupled arms of the switch, respectively, for different applied voltages. The maximum observed shift is 2.5nm for 350V. This corresponds to an electric field strength of 12.9V/μm in the $LiNbO_3$, assuming that the glue and ITO layers have no effect on the overlay parameters. Using the resonance spacing, the

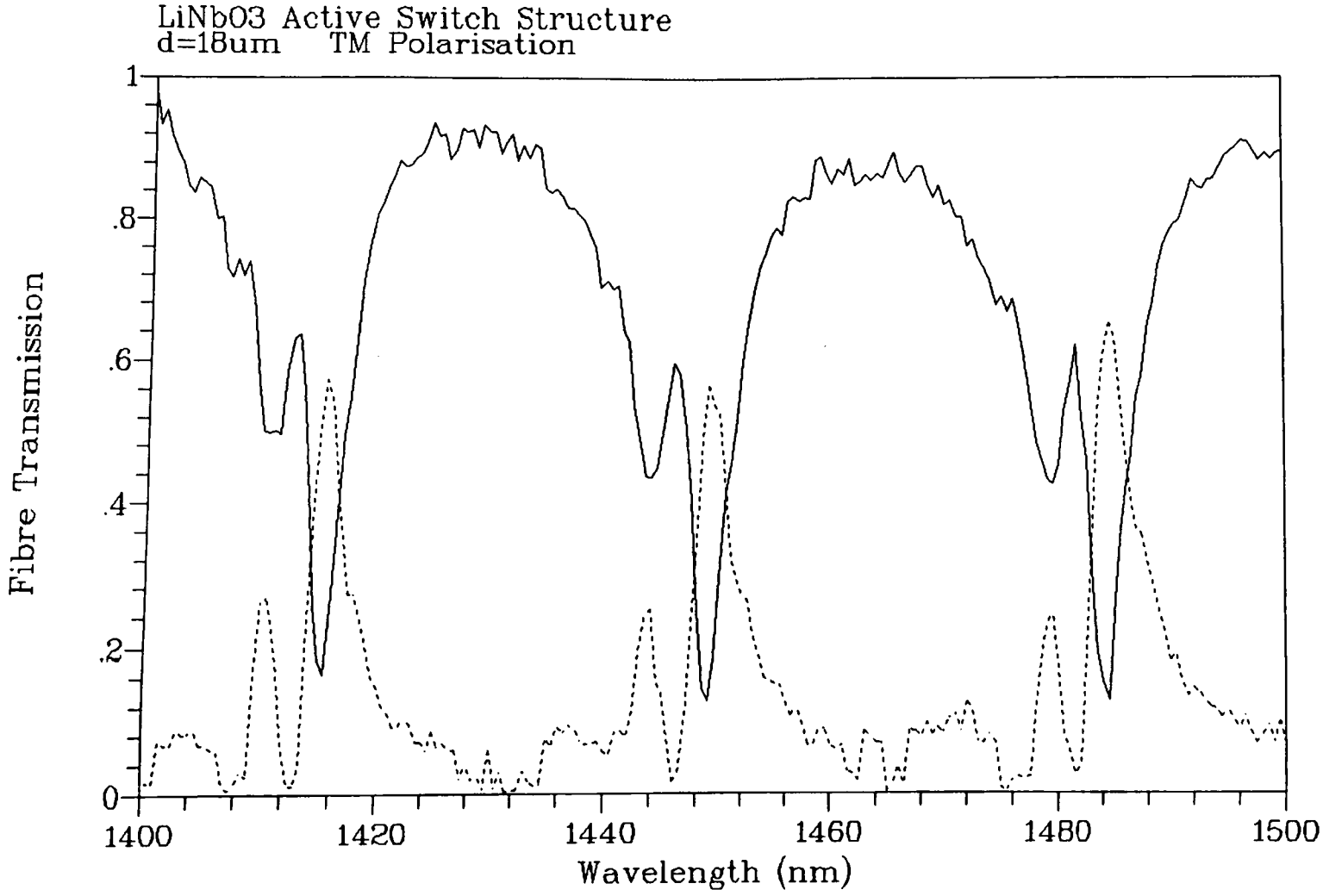

Figure 6.17 : Optical Fibre Switch Characteristic

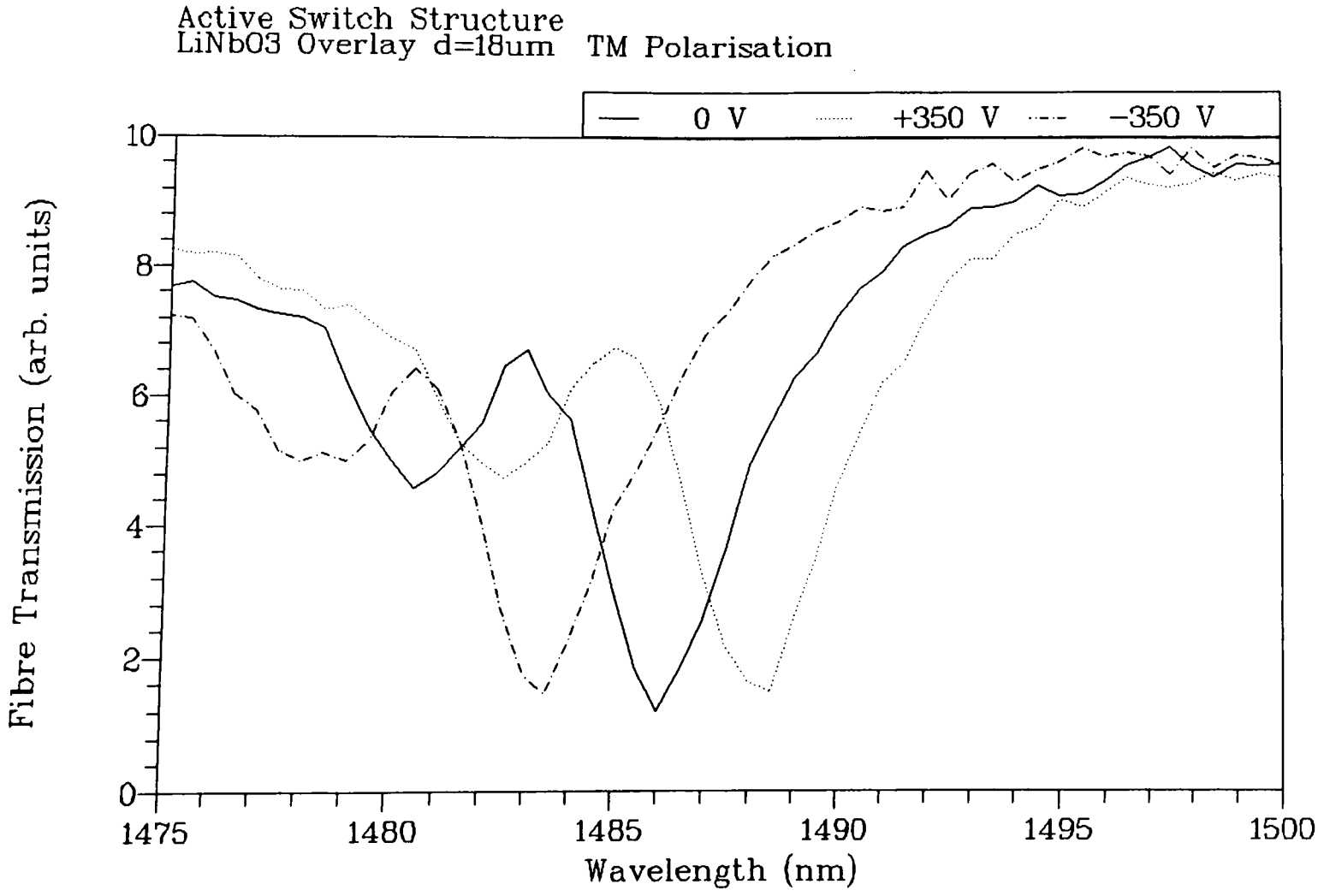

Figure 6.18 : Resonance Shifts for Applied Voltages

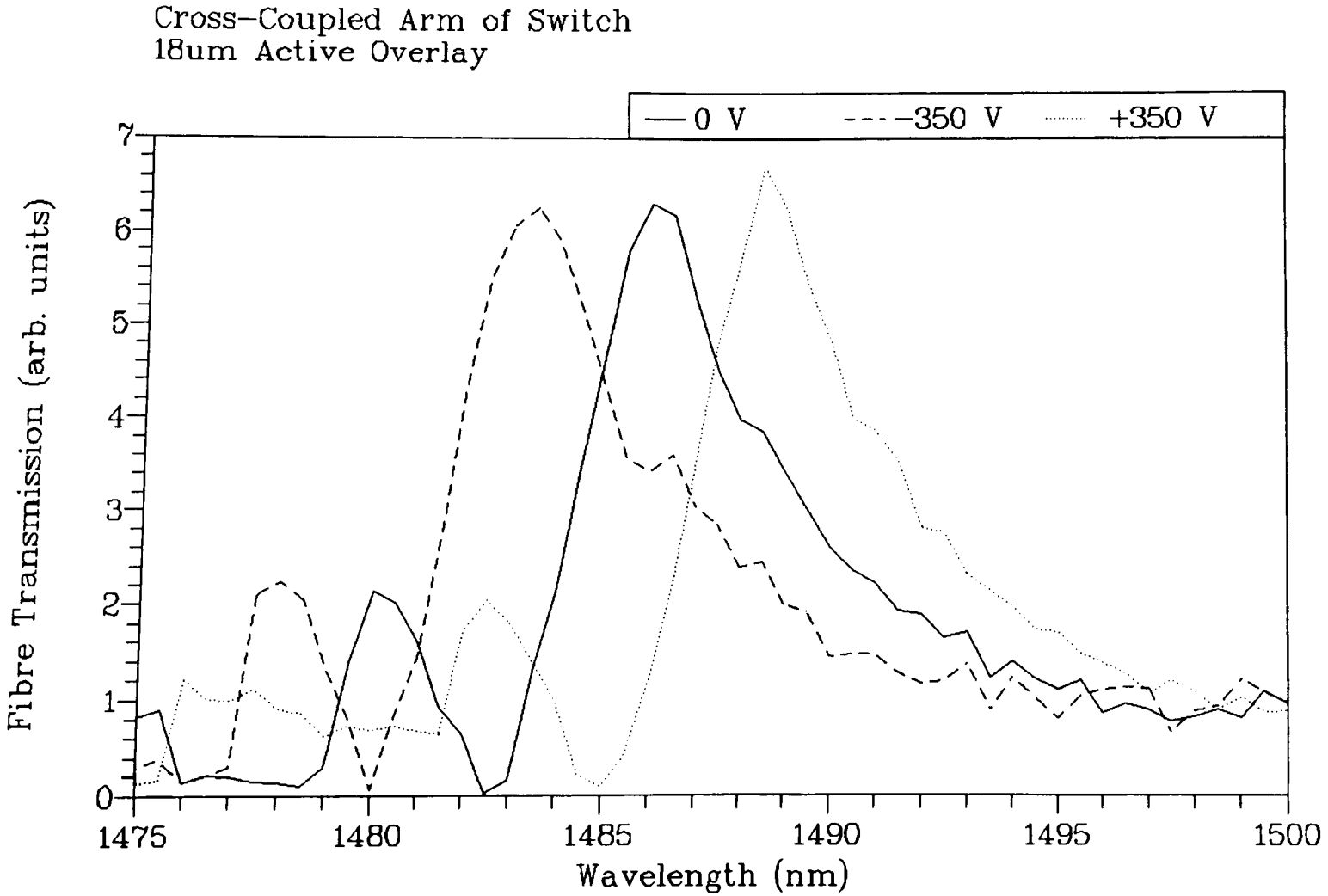

Figure 6.19 : Wavelength Shifts for Applied Voltages

calculated $LiNbO_3$ thickness is 18.8μm. Therefore, the voltage dropped across the $LiNbO_3$ layer is 242.5V. As with the second active device, a significant fraction of the applied voltage is not being developed across the $LiNbO_3$ layer. This leads to elevated drive voltages for significant directional switching to be achieved.

At this stage in the development of active fibre-overlay devices it is clear that low voltage operation is difficult to achieve. The combination of limited fabrication techniques and unavoidable bonding layer cause serious degradation of active device performance. Intensity modulation has been demonstrated to a limited extent but required high voltages ($>$300V). The principle of a tunable channel-dropping filter has also been established although the best device only displayed a tunability of 1nm shift for applied voltage of 150V. There are several fabrication difficulties to be overcome before the drive voltages approach realistic values. If $LiNbO_3$ is to be used as the active overlay, then a much reduced thickness is essential. However, with the available optical adhesives, a thickness much less than 10μm is very difficult to obtain with the present fabrication techniques. A stronger, low viscosity glue would enhance the possibility of producing a good device with a very thin overlay but there remains the problem of applying the external voltage directly to the $LiNbO_3$ layer. It appears that a transverse electrode configuration is undesirable due to the dielectric permittivity mismatch between the glue and $LiNbO_3$ layers. Unless the lower electrode can be deposited directly on the underside of the $LiNbO_3$ overlay and a suitable contact formed, a coplanar electrode configuration will be required (to reduce the interaction of the applied field with the bonding layer). This would demand several extra fabrication stages (photolithography) and slightly higher drive voltages (transverse electrodes produce the highest field strengths) but would allow the use of metal electrodes and the possibility of high frequency operation which is not possible with the ITO electrodes. However, it is anticipated that significant reduction in drive voltages for both intensity modulation and active wavelength tunability may be achieved through the use of improved fabrication techniques and higher electro-optic coefficient materials, even if a transverse electrode structure is retained.

6.8 Thin Film Vacuum Deposited Overlay Devices

An alternative method of forming high index planar multimode overlays on the surface of a polished fibre half-block is by vacuum deposition of appropriate materials. The immediate advantages of this approach to overlay fabrication are (i) 1-2μm overlay thicknesses are easily attainable (ii) the undesired bonding layers are removed and (iii) device fabrication is greatly simplified. However, electro-optic activity is difficult to achieve in films produced by vacuum deposition methods such as thermal evaporation and rf sputtering due to the inherent lack of crystallinity possessed by such films. Recent work[9] has seen improvements in this respect although elevated temperatures (400-600°C) and carefully selected substrates are generally required. An r-coefficient of 80pm/V has been observed in thin, rf sputtered films of Lanthanum modified Lead Zirconate Titanate (PLZT)[10] which, if possible for deposition on fused silica, promises extremely low voltage operation for the device architectures investigated in this thesis. Passive devices incorporating vacuum deposited overlays are also of interest for WDM/filtering applications and possess a number of advantages with regard to resonance tuning over their polished overlay counterparts.

6.8.1 Thermally Evaporated Zinc Sulphide Overlay Devices

Thermal evaporation was the simplest method of thin overlay fabrication and the general deposition conditions are outlined in section 6.4. Zinc Sulphide (ZnS) was selected as an appropriate overlay material due to ease of deposition and transparency in the infra-red wavelength region. The refractive index of evaporated ZnS is approximately 2.28 (at $\lambda = 1300$nm), reasonably similar to $LiNbO_3$. This allowed some performance predictions to be made on the assumption that $LiNbO_3$ overlays of similar thickness can be fabricated in the future, either by improved polishing techniques or evaporation/sputtering. Initial film deposition was performed with no heating of the polished fibre half-block and the optical quality of the overlays appeared satisfactory. However, tuning of the device resonance positions using index oils as the superstrate, with subsequent repeated solvent cleaning,

resulted in the film detaching from the half-block. Heating the half-block to approximately 120°C to promote adhesion of the film to the polished surface was then included in the fabrication procedure which allowed repeated tuning to be performed. A range of different coupling strength half-blocks were coated with the ZnS films to determine the effect on resonance linewidth. Film thicknesses were measured during the evaporation process via an in-situ monitor which calculated the thickness of the deposited layer based on a knowledge of the material density and acoustic impedance. However, it was found that an error of as much as 10% of the true value was common when the thickness was measured using a profilometer instrument. A thickness of greater than 2.5μm was difficult to achieve without repeated depositions but in general the films ranged in thickness from 0.5-1.5μm. The combination of high refractive index and small thickness meant that most devices possessed two or less transmission resonances within the normal wavelength scanning range (1200-1600nm) i.e. the resonance spacing was very large. For the case of two resonance positions, the approximate overlay thickness can then be calculated using the known refractive index and the resonance spacing, as was done for the $LiNbO_3$ devices in the previous section. The calculation is less accurate, however, since the overlay is not highly multi-moded in this instance. The wavelength response of a device incorporating a 26% coupling strength half-block and a ZnS overlay of approximately 1.2μm thickness is shown in Figure 6.20. The higher TE resonance is outwith the wavelength scan range due to the large polarisation separation associated with very thin, high index, asymmetric waveguides. Resonance spacing for TM polarisation is 344nm while the polarisation separation is 52nm for the lower resonances. The higher and lower TM resonances have linewidths of 17.3nm and 8.2nm, respectively, whereas the corresponding value for the TE resonance is 6.6nm. Modulation depth is greater for the TM polarisation (93%) but not as high as was expected considering the thickness of the overlay. Two more devices were fabricated with ZnS overlays of similar thickness but incorporating half-blocks possessing coupling strengths of 51% (Device2) and 85% (Device3) respectively. The resonance linewidths were measured for both TE and TM polarisation for both devices and are compared with the corresponding values

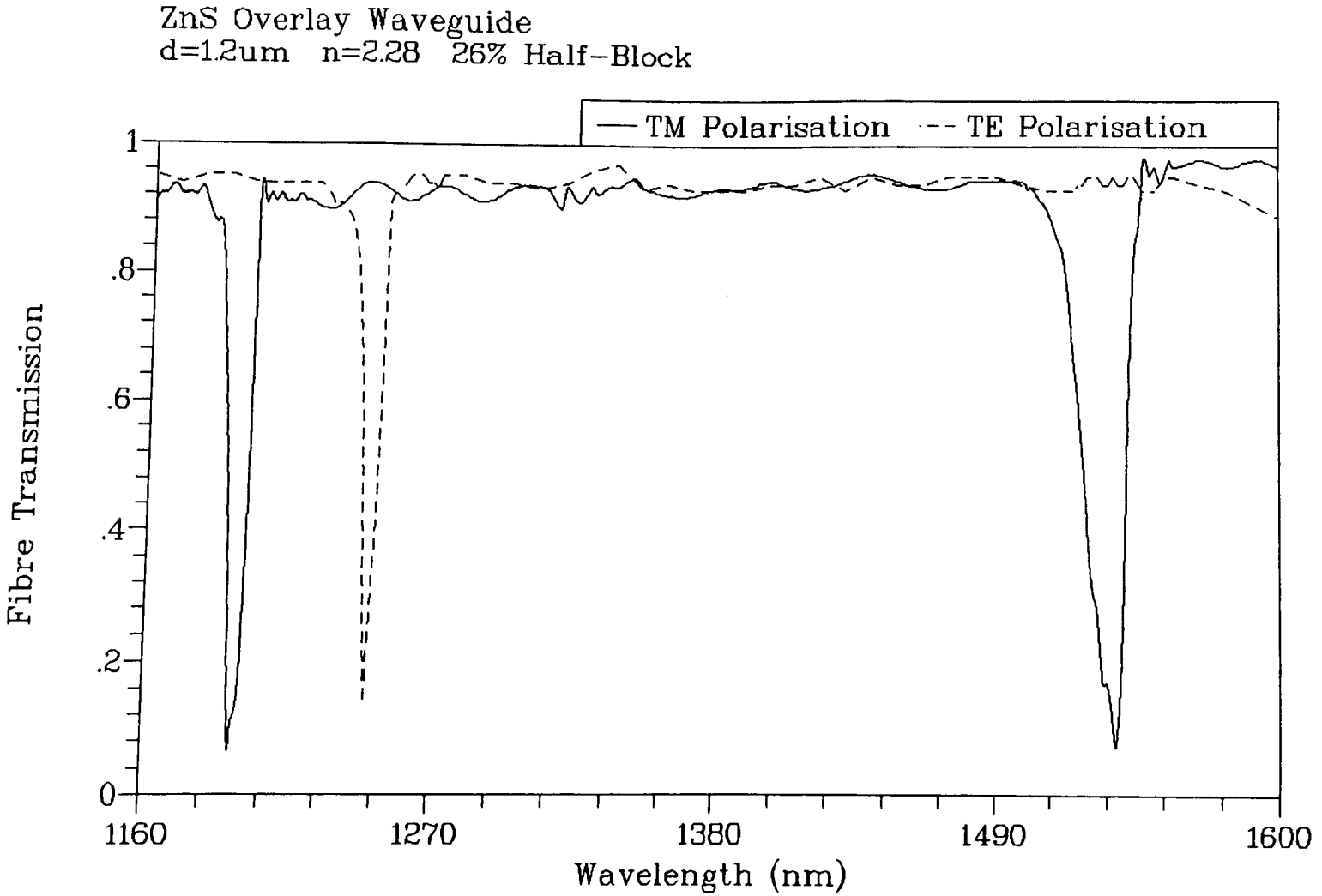

Figure 6.20 : Wavelength Response of ZnS Overlay Device

for the 26% coupling strength device (Device1) in Table 6.2.

Polarisation	Device1	Device2	Device3
	Linewidth	Linewidth	Linewidth
TE	6.6nm	12.6nm	19nm
TM	8.2nm	15nm	21nm

Table 6.2 : Resonance linewidths for different coupling strength devices

The data in Table 6.2 shows that a clear reduction in linewidth occurs for decreased half-block coupling strength. This agrees with results and theory developed earlier. In addition, the TM resonance is broader than the TE case as expected from greater evanescent field penetration which produces higher coupling coefficients, increased susceptibility to overlay surface imperfections, etc. The modulation depth increased as the coupling strength of the half-blocks increased reaching 99.3% (extinction ratio 21dB) for the 85% half-block. It is believed that the modulation depth measurements on the lower coupling strength devices were adversely affected by the limited dynamic range of the monochromator system. Subsequent measurements on a ZnS overlay device which possessed a transmission resonance corresponding to a laser diode wavelength indicated that the resonance extinction ratio was >34dB. The device had a ZnS overlay thickness of 0.6μm and 50% coupling strength half-block.

The minimum wavelength variation required to produce an intensity modulation (TM Polarisation) of 10%-90% was 5nm, recorded for device1 (sharp side of lower resonance). Assuming a similar device response for a $LiNbO_3$ overlay of the same thickness, equations (5.1) and (6.1) can be used to calculate an equivalent modulation or drive voltage. Taking the overlay thickness as 1.2μm gives a calculated voltage of 36.9V. Performing similar calculations based on a PLZT overlay (n=2.5, r=80pm/V)[10] gives a drive voltage of 12.8V. It is believed that the use of lower

coupling strength half-blocks and improved deposition techniques to improve film quality would allow further reductions in drive voltage.

6.8.2 Tuning of ZnS Overlay Devices

It was found that bulk superstrate tuning (using index oils) of the ZnS overlay devices resulted in large shifts in the wavelength response. For each device the resonance positions for TE and TM converged strongly as the waveguide became symmetrical. Figure 6.21 illustrates this point for device2 (51% coupling strength, $d=1.3\mu m$). With an air superstrate, the relevant TE and TM resonance positions are 1374nm and 1306nm, respectively. For a superstrate index of $n_D=1.456$, the TE resonance is located at 1432nm while the TM resonance is located at 1430nm. The largest wavelength shift was experienced by device3 with the TM resonance position moving 216nm. The corresponding TE resonance shift was 109nm with the polarisation separation having a minimum value (6nm) when the superstrate was $n_D=1.456$ i.e. symmetrical overlay. A larger tuning range was expected for device3 since it possessed the thinnest overlay, $<1\mu m$. No resonance tuning via deposition of low index dielectric superstrate films was investigated but the range is expected to be fairly large due to the sensitivity of the thin ZnS overlays to the bulk superstrate oils.

6.8.3 ZnS Overlay Switch/Bandpass Structure

A slightly thicker ZnS overlay ($2.5\mu m$ approx.) than those investigated previously was deposited onto the surface of a 30% coupling strength half-block for incorporation in a switch structure. The thicker overlay was selected to ensure at least two resonance positions. A second half-block of 60% coupling strength and matching/lubrication oil, $n_D=1.456$, were used to complete the switch structure. Cross-coupling appeared simpler to achieve than with the $LiNbO_3$ and optical glass switch structures, possibly because the reduced film thickness allowed greater interaction between the adjacent fibres. The maximum cross-coupled signal was 67% of the off-resonance device throughput and the polarisation sensitivity of the switch was negligible, which would be expected considering the results in the previous

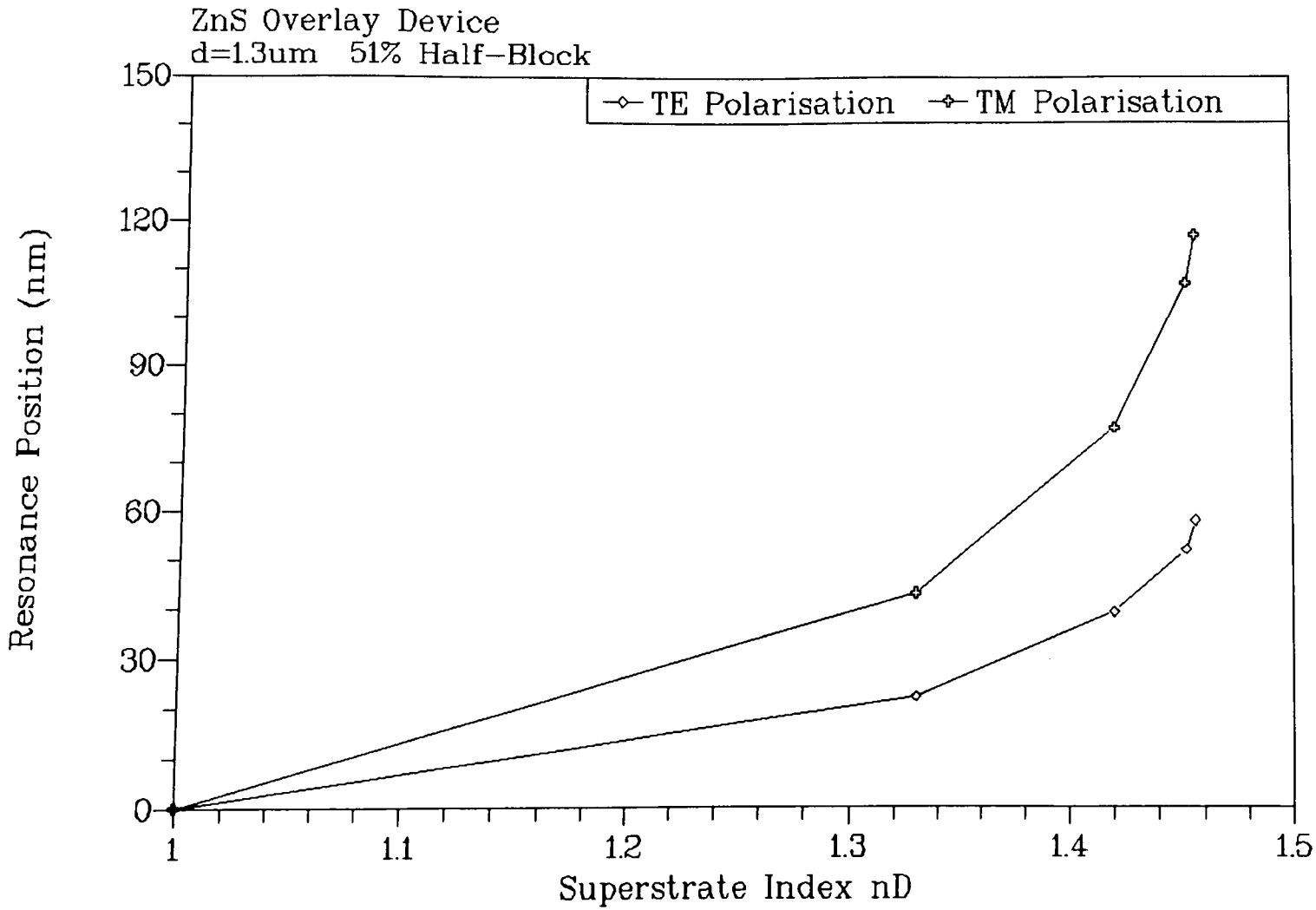

Figure 6.21 : Superstrate Tuning of ZnS Overlay Device

section. Figure 6.22 shows the wavelength response of the ZnS overlay switch structure. The lower and higher resonance linewidths are 21.5nm and 41.1nm, respectively, while the spacing is 205nm. A cutback measurement was performed to confirm the expected low-loss performance of the switch. An average value of 0.4dB was obtained for the off-resonance insertion loss for the throughput arm. For the cross-coupled arm, off-resonance cross-talk was in the region of -20dB. The resonance linewidths appear significantly broadened by the presence of the second half-block when compared with the values for an air superstrate (16nm and 22nm for TM polarisation). In addition, the shape of the resonances are degraded and similar to those observed for the $LiNbO_3$ switch structures i.e. multiple dips within each resonance. This confirms that the coupling characteristics of the switch structure are more complicated than the basic fibre-overlay device. Although the device transmission resonances are fairly wide, the inclusion of lower coupling strength half-blocks (5%) and better optical quality films may allow a reduction in resonance linewidths. Therefore, the possibility of vacuum deposited optically active thin films still suggests that a switch structure could operate at low drive voltages.

6.8.4 RF Magnetron Sputtered Silicon Overlay Devices

This method of thin film deposition is generally used for materials which possess high melting points and low vapour pressures. Sputtering is capable of more precise control of deposition rate and film quality than evaporation processes and widely utilised in the semiconductor industry. An immediate problem encountered with device fabrication using the sputtering process was the unavailability, at the time, of a substrate heater. As a result, no heating of the half-block could be performed during film deposition which prevented the formation of high optical quality films. However, the lower deposition rates associated with the sputtering process meant that to fabricate a device possessing an overlay of sufficient thickness to support several modes took in the region of 1.5-2hours and this caused the ambient temperature in the vacuum chamber to rise significantly. Whether this had any effect on film quality is uncertain. The transparency of Silicon in the infra-red wavelength region and the possibility of electro-optic effects[11] (e.g. via current injection) makes it an

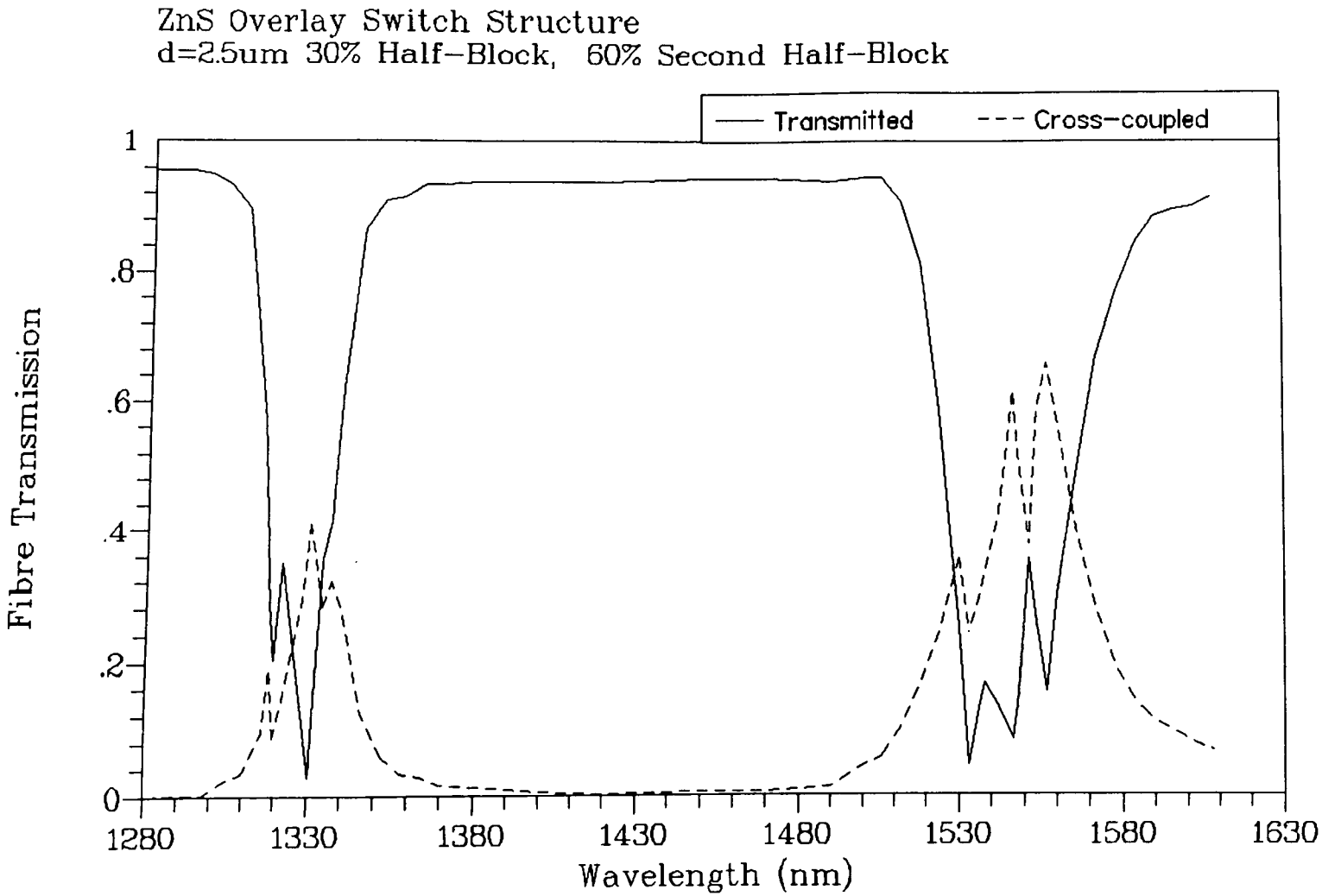

Figure 6.22 : Wavelength Response of ZnS Overlay Switch

interesting material with regard to fibre-overlay geometry. In addition, Silicon also has a high index (n=3.5 approx.) which allows a high mode order to be maintained when in thin waveguide form. No commercial Silicon sputtering target was available so a standard silicon wafer was used and a deposition rate of 12.2nm/min was achieved in test runs. The purpose of the experimental investigation was to determine whether coupling to the Silicon overlays could be achieved and estimate the refractive index of the sputtered material for comparison with the bulk value. The first device fabricated incorporated a Silicon overlay of 1.035μm (measured using profilometer) and a 98% coupling strength half-block. Resonant coupling was observed but the linewidth values were very wide (>100nm) suggesting that the coupling strength of the half-block was excessive and/or the film quality was poor. A second device was fabricated incorporating a 2.19μm Silicon overlay and a 35% coupling strength half-block. Three resonances were observed in the wavelength scan region 1200-1600nm for both polarisations although the response was not particularly good. Narrowest linewidth was 31.5nm with a modulation depth of only 66.5%. The TE resonance spacings were 126nm and 161nm for successive resonances while the corresponding TM values were 117nm and 152nm. Polarisation separation increased from 33nm to 51nm for the lowest and highest wavelength resonances. A cutback measurement was made and the off-resonance insertion loss found to be 1.9dB, significantly higher than previously recorded insertion losses for other devices. Again, film quality is believed to be the main reason for this higher loss. Since the thickness of the Silicon overlay was accurately measured using a profilometer to be 2.15μm, the recorded resonance spacings could be used to calculate the refractive index of the overlay. An average value of n=3.44 was obtained which agrees reasonably well with the index of bulk Silicon. The reduced modulation depth and broad resonance linewidths are also believed to be a result of poor film quality, probably due to unsuitable sputtering conditions. Characterisation of the process of sputtering thin films of Silicon will be required if the use of Silicon as an overlay is to be further investigated.

6.8.5 Tuning of Silicon Overlay Device

Although the device wavelength response was fairly unimpressive, tuning of the resonance positions was possible. Both the methods of tuning the device wavelength response via control of the overlay superstrate index and/or thickness were performed. The tuning curves for bulk superstrate variation and superstrate thickness variation are shown in Figures 6.23(a) and 6.23(b), respectively. Calcium Fluoride (CaF_2) was used as the thin dielectric overlay and has a bulk refractive index of 1.42. The maximum shift in resonance position was 48nm for TM polarisation and 23nm for TE polarisation, for bulk superstrate index variation. Polarisation separation of the resonance positions reduced as the overlay became more symmetrical (11nm with superstrate oil $n_D=1.45$). Less polarisation sensitivity was observed than for the ZnS overlay devices despite similar film thicknesses because the significantly higher index of Silicon meant the overlay supported several modes. In this case, the effect of the phase terms in the eigenvalue equation are less significant even though the overlay index is higher.

The fabrication of devices via vacuum deposition of the overlay waveguide appears relatively simple when compared with the lapping/polishing techniques used previously. In-situ monitoring[8] of the transmission resonance positions also allows simple tuning of the overlay parameters to operation at a desired wavelength. It is believed that further improvements in resonance linewidths, modulation depth, etc. will occur as greater experience of the deposition techniques and relevant parameters is obtained. The possibility of vacuum deposited, strongly electro-optic, thin films warrants further investigation of this method of device fabrication.

6.9 Conclusions

A range of solid-state overlay devices have been successfully fabricated and characterised via their wavelength-transmission response. Several different materials have been utilized as the overlay waveguide, ranging in refractive index from $n=1.515$ (optical glass) to $n=3.5$ (Silicon). A variety of techniques were used to

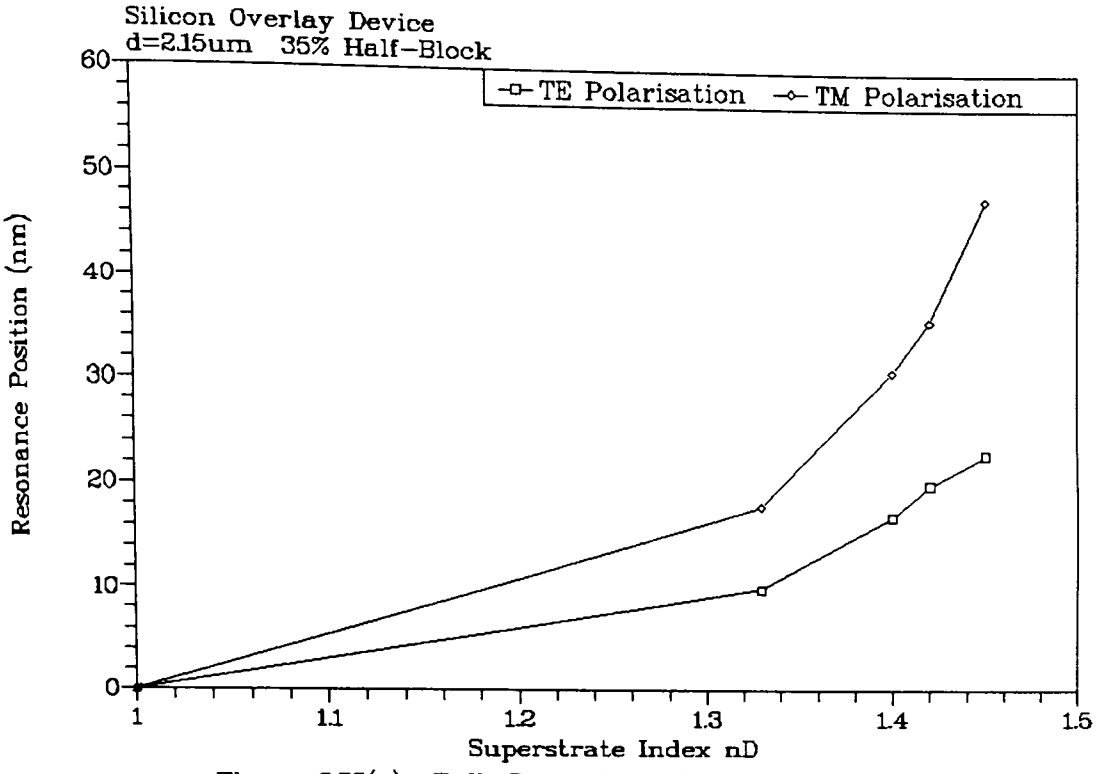

Figure 6.23(a) : Bulk Superstrate Tuning of Silicon Device

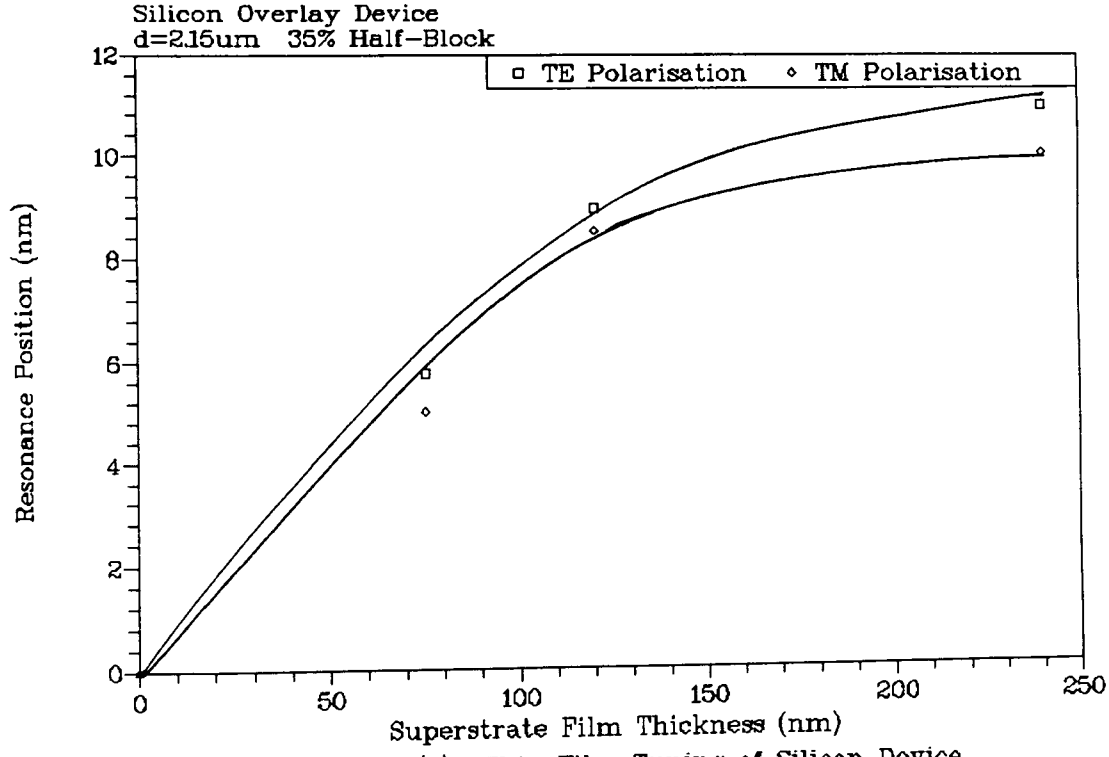

Figure 6.23(b) : Thin Film Tuning of Silicon Device

fabricate the solid-state overlays. These involved mechanical/chemical lapping and polishing of bulk materials to produce thin layers (glass and $LiNbO_3$ overlays) and thin film vacuum deposition methods; thermal evaporation and rf magnetron sputtering (ZnS and Si overlays). Passive device fabrication was reasonably straightforward using each of the techniques mentioned. However, active device fabrication was more difficult and restricted to the lapping/polishing method since bulk $LiNbO_3$ was the only available electro-optic material. A number of problems were encountered during the active device fabrication process and these prevented the realisation of a low voltage device.

6.9.1 Glass Overlay Devices

Initial experimental results were obtained for devices with glass overlay waveguides and confirmed the trends established in Chapter 5 as regards overlay index and thickness. Both channel (resonance) spacing and linewidth were observed to decrease as overlay index and thickness were increased. Narrowest channel linewidth (2.4nm) was recorded for a device with overlay index $n=1.65$ and thickness $d=90\mu m$. The corresponding channel spacing was 12.5nm. Highest recorded extinction ratio was $>18dB$ for a device with $n=1.515$ and $d=7.6\mu m$. Tuning of the wavelength-transmission response of the glass overlay devices was demonstrated by variation of the overlay superstrate index and/or thickness. The most extensive tuning ranges were observed for variation of the superstrate bulk index and it was found that the lower index glass ($n=1.515$), thin ($d=7.6\mu m$) glass overlay device could be tuned over a 106nm range (TM Polarisation). Fine tuning of channel positions could be achieved by vacuum deposition of a thin, low index dielectric film on the top surface of the overlay waveguide. The resultant compound dielectric/air superstrate then possesses an index value which ranges between air and the bulk index of the dielectric material, depending on the thickness of the dielectric film. A shift in channel position of 26nm was achieved for a vacuum deposited film of Magnesium Fluoride ($n=1.38$) with thickness 280nm. In addition to the basic channel-dropping filter glass overlay devices, a switch structure was also briefly studied. Wavelength-dependent cross-coupling of power was observed with a maximum power transfer

of approximately 40% (2.2dB crosstalk) of the off-resonance device throughput. It was shown that the index of the oil matching layer at the interface of the overlay surface and second polished fibre half-block had an influence on both the wavelength of the cross-coupled channel and the efficiency of the cross-coupling.

It appears that the glass overlay devices have potential application as rugged, low insertion-loss, continuous-fibre wavelength selective elements. Both channel-dropping (basic fibre-overlay structure) and bandpass (switch structure) filtering responses have been demonstrated. Furthermore, extensive tuning of the filter channel positions can be achieved by simple variation of the overlay waveguide superstrate index and/or thickness.

6.9.2 $LiNbO_3$ Overlay Devices

Several devices (passive and active) were fabricated with z-cut $LiNbO_3$ as the overlay waveguide. Wavelength-transmission responses displayed narrower linewidths (for the same overlay thickness) when compared with the previously-studied glass overlay devices. This was expected due to the significantly higher refractive index of $LiNbO_3$. Tuning of channel positions was again demonstrated using variation of the overlay superstrate bulk index. A smaller tuning range was observed (27nm for a device with overlay thickness 8.7μm and TM polarisation) when compared with the similar thickness glass overlay device mentioned above. This confirmed that large tuning ranges require thin, low index overlays. Further investigation of the switch structure was also carried out using $LiNbO_3$ overlay device. As with the glass overlay switch structure, wavelength-dependent cross-coupling was observed. Improved values of cross-coupling efficiency were achieved, as high as 90% (10dB cross-talk), with a narrowest channel linewidth of 3.8nm.

Active devices employing $LiNbO_3$ as the overlay in conjunction with transverse ITO electrodes were successfully fabricated but corresponding drive voltages were impractical (in the region of 300V). Device operation relied on shifting the wavelength-transmission response of the device by electro-optic variation of the

$LiNbO_3$ overlay index. The tunability of the wavelength response using this active method was low, with the best recorded value being 150V/nm. For modulator/switch implementation, the input wavelength should be biased to a resonance position. The sharpness of the resonance then determines the wavelength shift required to cause a significant change in transmitted intensity. Drive voltages of approx. 300V were required to induce a 4dB change in intensity for a device configured as a modulator. For a switch structure based on the same device, a corresponding 4.7dB change in intensity was observed in the cross-coupled arm for the same applied voltage.

The passive $LiNbO_3$ overlay devices exhibited useful filtering characteristics, both channel-dropping and bandpass, with fairly narrow channel linewidths and spacings. A drawback of the passive devices was inherent polarisation sensitivity due to the material birefringence of $LiNbO_3$. The realisation of active devices proved difficult and wavelength tuning, intensity modulation and directional switching could only be demonstrated for drive voltages in the region of 300V. However, the possibility of more practical devices exists if materials with higher electro-optic coefficients are incorporated as the overlay waveguide. High speed operation would, however, require the design and use of co-planar metal electrode structures.

6.9.3 Vacuum Deposited Overlay Devices

Thin film vacuum deposition was identified as an attractive technique for the overlay waveguide formation due to the relative simplicity and speed (when compared with the lapping/polishing approach). Devices with ZnS overlays in the region of 0.5-2μm were fabricated by thermal evaporation. Channel linewidths were as narrow as 6.6nm while corresponding extinction ratios (modulation depths) were in the region of 20dB (the best recorded extinction was 34dB). The channel spacing was generally very large (200-300nm) as was the channel tuning range (109nm for TE, 216nm for TM), a result of the reduced thickness of the overlay. A switch structure was also fabricated and a cross-coupling efficiency of 67% of the off-resonance device throughput was achieved. An attempt was also made to fabricate silicon overlay devices (channel-dropping) via rf magnetron sputtering. A limited degree of success

was achieved, although resonance linewidths were broader than expected (31.5nm narrowest linewidth). This was attributed to poor quality film deposition. The attraction of Si as the overlay waveguide is due to its high index (n=3.5) which could, potentially, result in thin-film overlay devices with narrow linewidths. Superstrate tuning of the resonance positions was again performed. Maximum wavelength shifts of 14nm for TE and 53nm for TM (for an overlay thickness, d=2.15μm) were achieved for tuning using bulk index oils. Vacuum deposition of Calcium Fluoride (n=1.42) as the superstrate produced a reduced tuning range, maximum shift was approximately (for both TE and TM polarisations) when a thickness of 240nm was deposited.

The advantages of simplified and rapid overlay waveguide fabrication make vacuum deposition techniques very attractive for device manufacture. Reasonably narrow linewidth channel-dropping filters and also a switch/bandpass filter have been demonstrated using these overlay fabrication techniques. Furthermore, monitoring (in-situ) of resonance (channel) positions during overlay formation can be used to fabricate devices to set specifications.

References

1. R.T. Bailey, F.R. Cruickshank, D. Pugh and J.N. Sherwood,"Organic electro-optic and nonlinear materials", Int. J. Optoelectronics, **5**, pp89-102, 1990.

2. H. Higashimo, H. Adachi, K. Setsune and K. Wasa,"High speed optical switches using sputtered PLZT thin films", Proc. Int. Conf. on Materials for Non-Linear and Electro-Optics, pp23-34, 1989.

3. J.R. Busch, S.D. Ramamurthi, S.L. Swartz and V.E. Wood,"Linear electrooptic response in sol-gel PZT planar waveguides", Electron. Lett., **28**, pp1591-1592, 1992.

4. S. Ray, R. Banerjee, N. Basu, A.K. Batabyal and A.K. Barua,"Properties of tin doped indium oxide thin films prepared by magnetron sputtering", J. Appl. Phys., **54**, pp3497-3501, 1983.

5. S. Ishibashi, Y. Higuchi, Y. Ota and K. Nakamura,"Low resistivity indium-tin-oxide transparent conductive films. II. Effect of sputtering voltage on electrical property of the films", J. Vac. Sci. Technol., **A8**, pp1403-1406, 1990.

6. R.L. Jungerman, C. Johnsen, D.J. McQuate, K. Salomaa, M.P. Zurakowski, R.C. Bray, G. Conrad, D. Cropper and P. Hernday,"High speed optical modulator for application in instrumentation", J. Lightwave Technol., **LT-8**, pp1363-1369, 1990.

7. S.K. Korotky, G. Eisenstein, R.S. Tucker, J.J. Veselka and G. Raybon,"Optical intensity modulation to 40Ghz using a waveguide electro-optic switch", Appl. Phys. Lett., **50**, pp1631-1633, 1987.

8. M. Iztkovich, M. Tur, A. Hardy and N. Croituro,"In-situ investigation of coupling between a fibre and a slab waveguide", Electron. Lett., **26**, pp1104-1105, 1990.

9. E.S. Ramakrishnan and W-Y. Howng,"Ferroelectric lead zirconate titanate thin films by radio frequency magnetron sputtering", J. Vac. Sci. Technol., **A10**, pp69-73, 1992.

10. H. Adachi and K. Wasa,"Sputtering preparation of ferroelectric PLZT thin films and their optical applications", IEEE Trans. Ultrason., Ferroelec. and Freq. Contr., **38**, pp645-655, 1991.

11. R.A. Soref and B.R. Bennett,"Electrooptical effects in Silicon", IEEE J. Quantum Electron., **QE-23**, pp123-129, 1987.

CHAPTER 7

Cut-Off Polished Fibre Device

7.1 Introduction

This chapter investigates a device with a similar geometry to those described in the preceding chapters but with one major difference. A modification of the original device geometry was made which allowed the realisation of a bandpass filter on a single-mode fibre i.e. a second half-block was not required to collect the filtered channel. Only limited characterisation of this device structure has been performed to date but initial results are encouraging. The bandpass filter has immediate applications in fibre-laser and amplifier systems for the purposes of linewidth narrowing, wavelength tuning and, potentially, mode selection. In addition, operation as a tunable filter in "broadcast and select" WDM architectures appears a definite possibility.

7.2 Device Geometry and Fabrication

As noted in Chapter 4, the coupling strength of a polished fibre half-block is dependent on the remaining cladding thickness on the polished side. By carefully continuing the polishing stage of the fabrication process, the coupling strength can be increased to 99.9% when virtually all the input light is tapped out of the fibre by application of a bulk overlay. At this coupling strength the remaining cladding thickness is very small and further polishing causes the fibre core to become exposed. When this occurs the optical field of the fibre mode becomes progressively "cutoff"[1] and the fibre exhibits high transmission loss, the attenuation increasing as the core size is decreased[2]. It was found that application of a bulk index oil with a refractive index similar to that of fused silica caused significant restoration of the input power. This behaviour has also been demonstrated elsewhere[2]. Figure 7.1 shows the response of a polished fibre "cutoff" half-block to a range of bulk

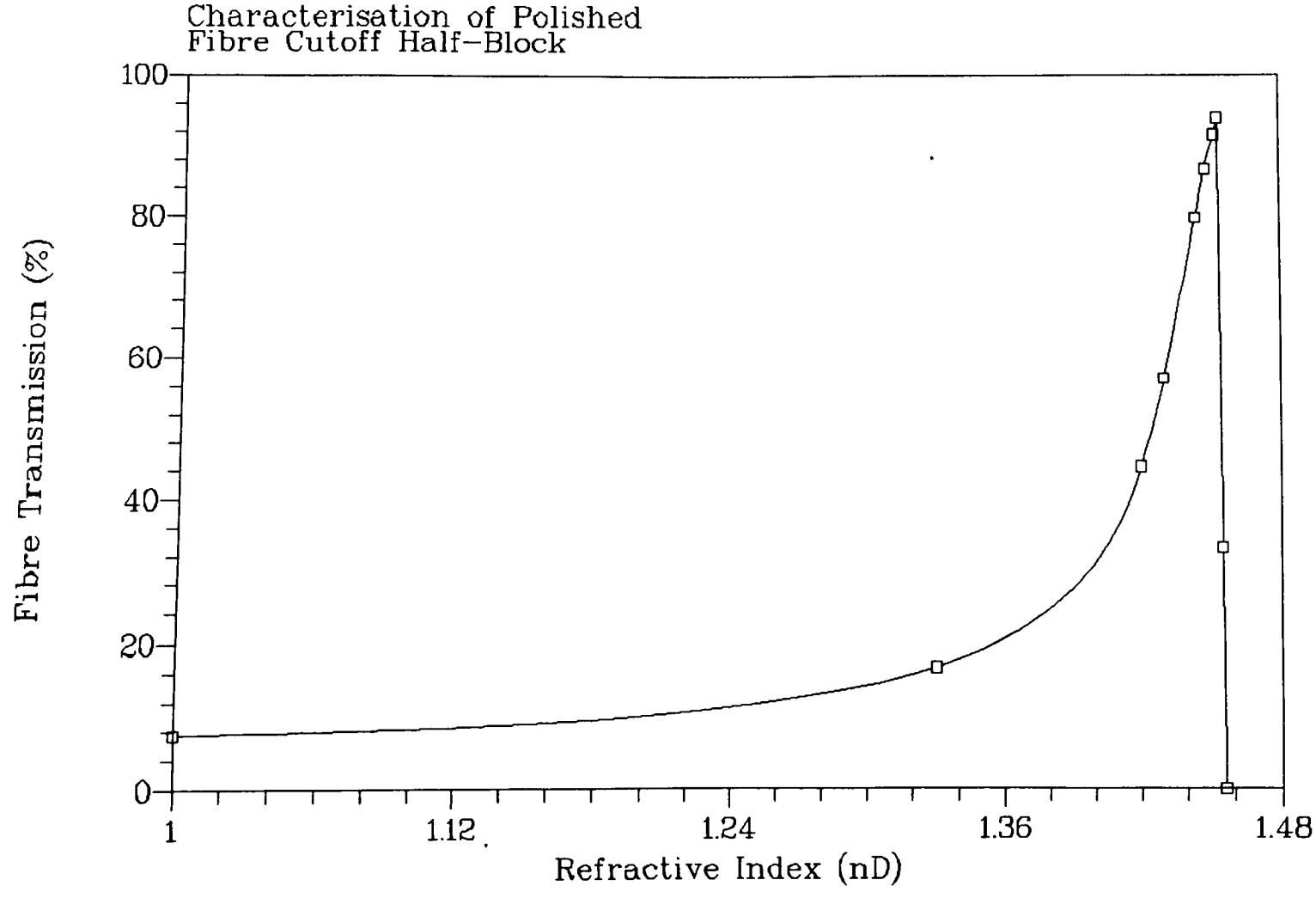

Figure 7.1 : Response of Cutoff Half-Block to Bulk Overlays

overlay indices. The fibre radius of curvature was the standard 22cm used for the earlier half-blocks. Typically, the difference between the maximum and minimum fibre throughput was in the 15-20dB range, with the maximum value being observed at a bulk overlay oil index of $n_D=1.452$. As would be expected, application of higher index oils caused the fibre throughput to fall to zero. A possible explanation of the behaviour observed in Figure 7.1 can be obtained by considering the slab waveguide analysis presented in Chapter 3. The concept of a "cutoff" wavelength for a guided mode was introduced and it was noted that the zero order mode of a symmetrical waveguide never cuts off. Once the remaining cladding on the polished fibre has been removed, the fibre can then be thought of as an asymmetric waveguide (air superstrate) which is single-moded below a cutoff wavelength. For high transmission loss, this cutoff wavelength is obviously below the 1300nm output from the test laser. Replacing the air superstrate with an oil of index approximately equal to the fibre cladding restores the symmetry of the waveguide and allows significant recovery of the input power.

The basic geometry of the cutoff polished fibre device is shown in Figure 7.2. A high index, multimode planar overlay waveguide was placed in optical contact with the surface of the cutoff polished half-block by an appropriate fabrication method. Initial device characterisation was performed on oil overlay devices fabricated as described in Chapter 5. A solid-state device was also constructed with z-cut Lithium Niobate as the overlay waveguide using the same fabrication procedures as described earlier in Chapter 6 for standard polished fibre overlay devices.

7.3 Device Characterisation using Oil Overlays

Variation of the input wavelength was again the simplest method of investigating the cutoff device structure shown in Figure 7.2. To assess the response of the device to variations in the overlay waveguide thickness and material index, initial experiments used Cargille refractive index oils, supported by Mylar spacers and a polished fused silica superstrate, in the role of the overlay. Spacer thicknesses of 12μm and 23μm

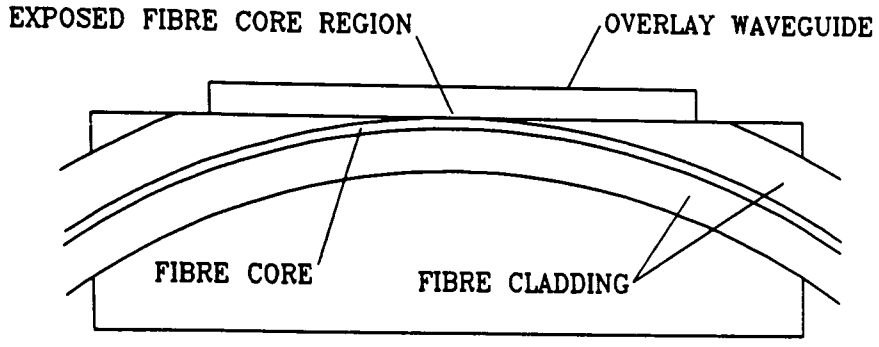

Figure 7.2 : Cutoff Polished Fibre Half-Block with Overlay

were used with 5 different oil indices, in the range n_D = 1.47 to n_D = 1.698. The intensity versus wavelength response for each device was then recorded using a Bentham Instruments scanning monochromator configured for use with optical fibre. A polariser and polarisation controller were also included in the set-up to establish a known polarisation at the input to the device. Typical intensity versus wavelength responses for the structure are shown in Figures 7.3 and 7.4 for overlays with n_D=1.65, d=23μm and n_D=1.494, d=12μm, respectively. For each combination of overlay thickness and index a periodic transmitted intensity response similar to Figures 7.3 and 7.4 were recorded. None of the devices displayed significant polarisation sensitivity due to the symmetry and multi-moded nature of the overlay. Tables 7.1 and 7.2 show the effect of overlay thickness, d, and refractive index, n_D, on channel spacing and linewidth, respectively. The figures were recorded for transmission channels close to λ=1300nm for each device. Inspection of Tables 7.1 and 7.2 indicate that high index, thick overlays produce the smallest channel spacing and narrowest linewidths. The figures for channel spacing can be compared with the theoretical values shown in Table 5.9 (Chapter 5) which were calculated using the overlay eigenvalue equation. Reasonably close agreement can be observed considering that the precise value of experimental overlay thickness is unlikely to exactly match the spacer thickness. A graphical representation of the experimental variation in channel linewidth with overlay index is shown in Figure 7.5. The linewidth is observed to decrease in an exponential-like fashion and Figure 7.5

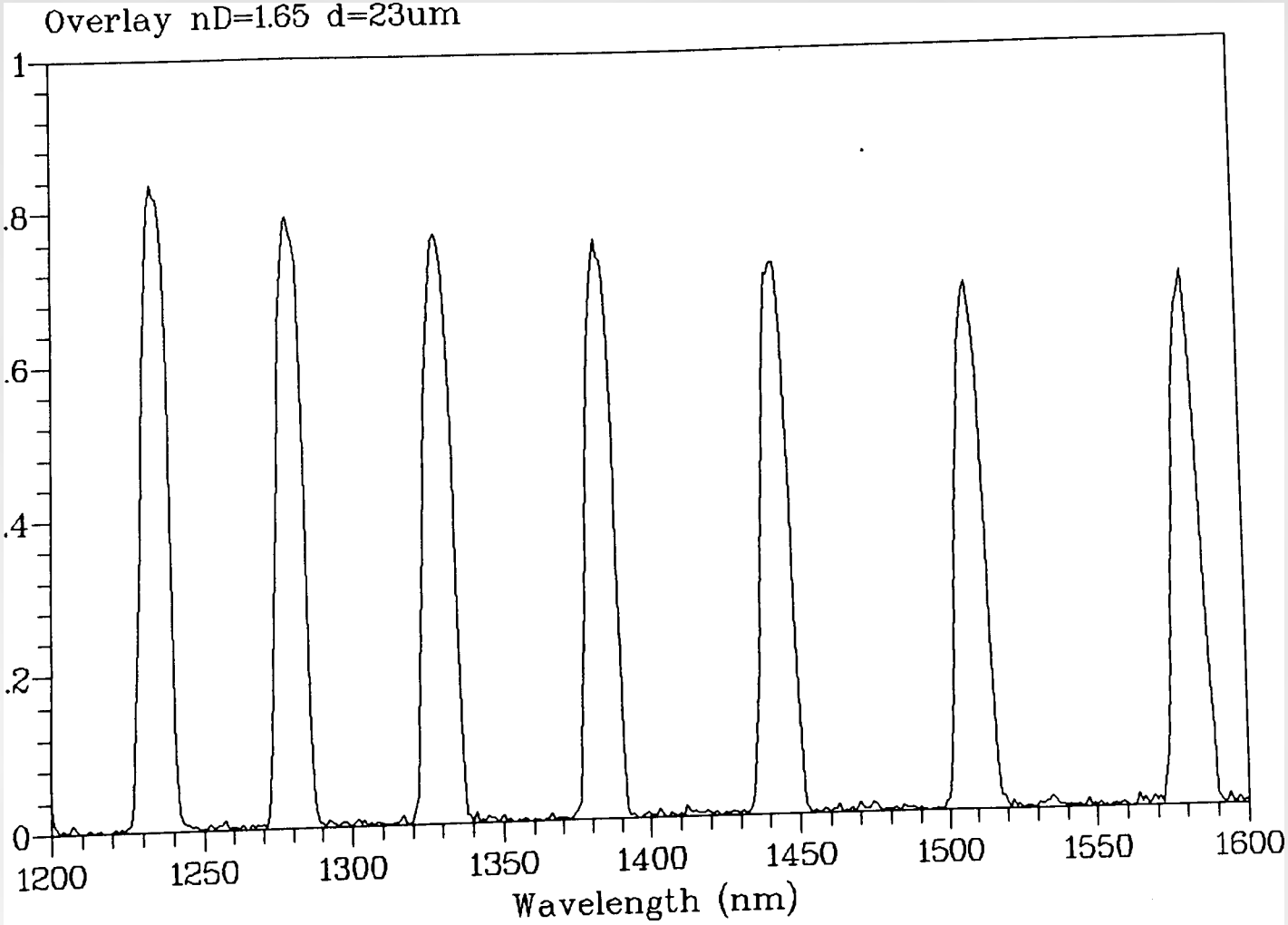

Figure 7.3 : Wavelength Response of Cutoff Fibre–Overlay Device

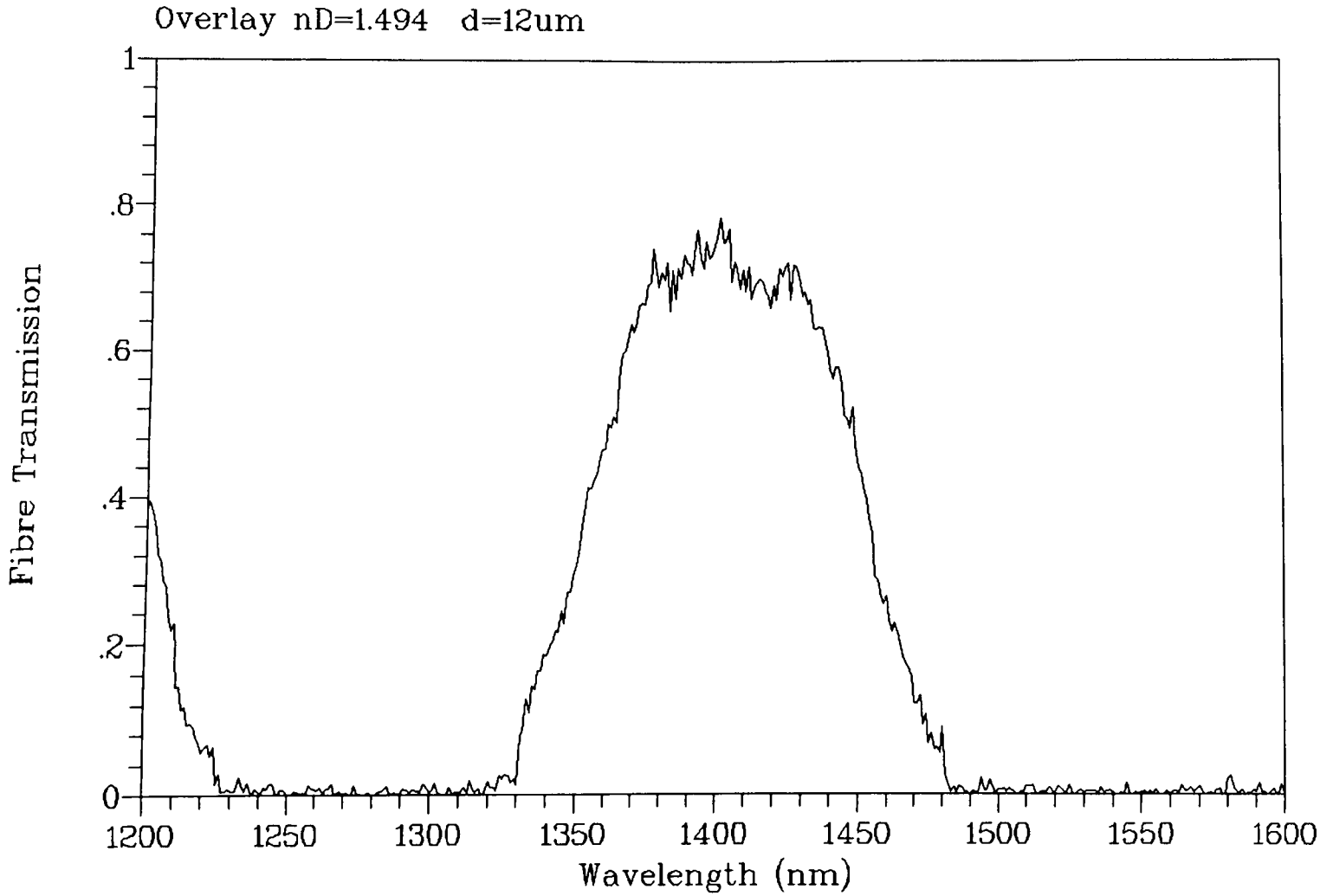

Figure 7.4 : Wavelength Response of Cutoff Device

Overlay Index	Channel Spacing	
	d=12μm	d=23μm
n_D=1.470	------	------
n_D=1.494	256nm	159nm
n_D=1.548	170nm	71nm
n_D=1.598	127nm	57nm
n_D=1.650	88nm	50nm
n_D=1.698	80nm	45nm

Table 7.1 : Channel Spacing with Overlay Index for two thicknesses

Overlay Index	Channel Linewidth (FWHM)	
	d=12μm	d=23μm
n_D=1.470	345nm	128nm
n_D=1.494	110.6nm	62.4nm
n_D=1.548	21.3nm	15nm
n_D=1.598	16.7nm	10.7nm
n_D=1.650	10.8nm	8.7nm
n_D=1.698	8.8nm	5.2nm

Table 7.2 : Channel Linewidth with Overlay Index for two thicknesses

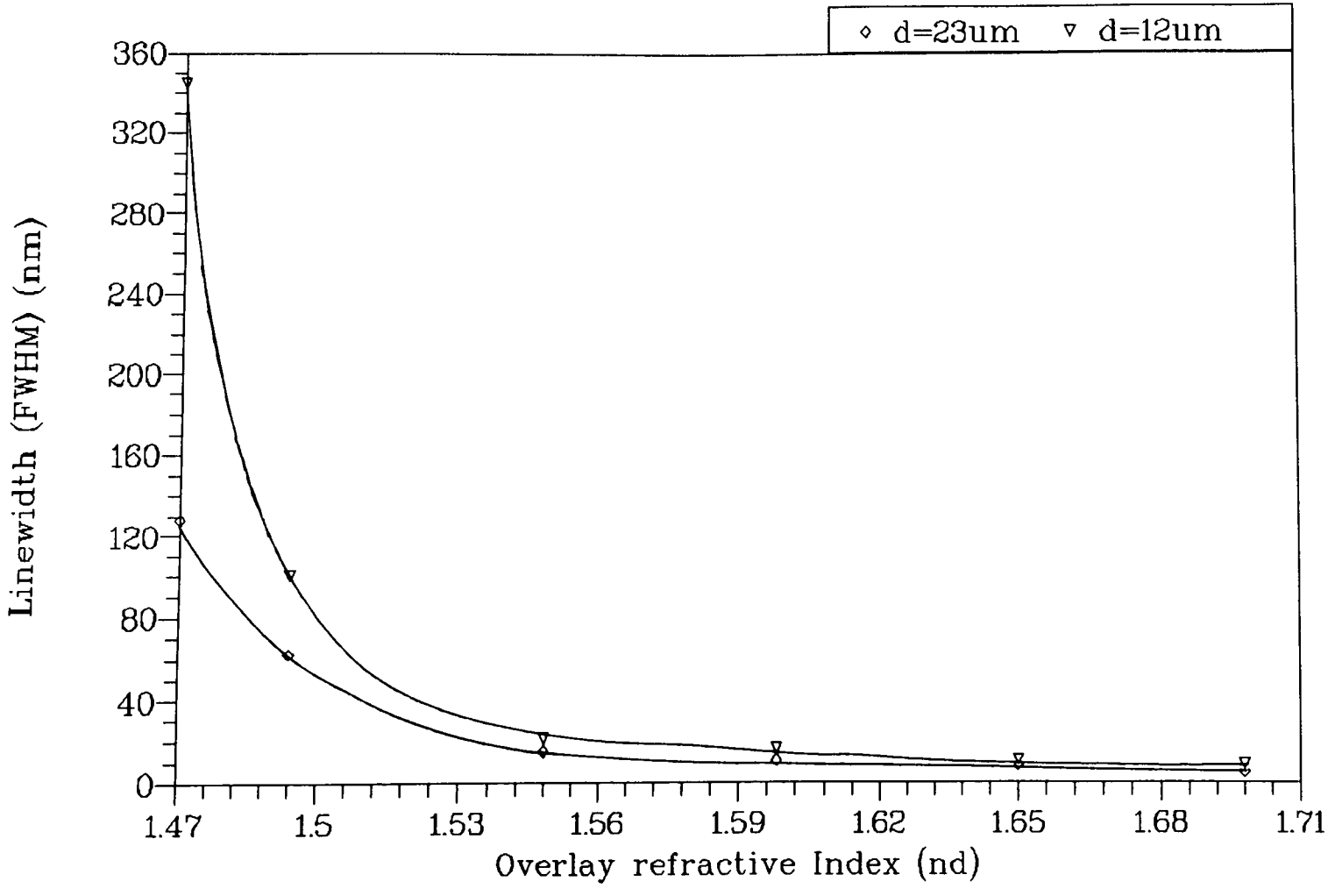

Figure 7.5 : Linewidth Response to Overlay Index and Thickness

compares favourably with Figures 5.10 - 5.11 and Figure 3.11 which apply for standard fibre-overlay devices. The resonance extinction ratio, in general, appeared to be in the region of 20dB although measurements were limited by the dynamic range of the instrumentation. Cut-back measurements performed on the oil overlay devices indicated that the insertion loss at the centre of a passband can be less than 0.5dB, although the loss tended to increase with wavelength. The increase in insertion loss as the wavelength is increased may be due to the fibre becoming "more cutoff" i.e. restoration of the input signal by application of a bulk overlay is reduced at longer wavelengths.

7.4 Device Operation

The precise mechanism governing device operation is uncertain. However, the similarity of Figures 7.5 and 5.10 - 5.12 which relate resonance linewidth to overlay index suggests that the cutoff device operation is closely connected to that of standard polished fibre half-block/overlay devices and, therefore, related to phase-matching between fibre and overlay modes. Additionally, calculated values of resonance spacing show a good match to experimental values recorded for the cutoff oil overlay devices. This reinforces the notion of device operation relying on a phase-matching condition in much the same manner as the standard polished fibre-overlay devices. A simple explanation of the device operation is proposed as follows. Outwith the exposed core region of the fibre the modes of propagation of the overlay waveguide can range in effective index, n_{eo}, from just greater than the index of the fibre cladding, n_c, to just below that of the overlay material, n_o. Phase-matching of the fibre mode (n_{ef}) and the highest order mode of the overlay can be achieved for the correct combination of overlay waveguide parameters (index, thickness or wavelength). When this phase-matching condition is established (by, for example, wavelength variation) strong directional coupling of power between the fibre and the overlay waveguide occurs[3]. Therefore, light launched into the input arm of the device couples to the highest order mode of the overlay, at the phase-matching condition, prior to reaching the "cut-off" region. The exposed core region of the

fibre has a "loading" effect on the overlay, due to the slight difference in core and cladding indices. This is thought to prevent or significantly reduce the lateral loss to off-axis overlay modes which strongly influences the standard polished fibre-overlay device operation. As a result, the coupled light traverses the exposed core region with low loss and is then recoupled to the fibre as it emerges from this region of the device. As each highest order overlay mode is tuned in and out of resonance with the fibre mode there is a corresponding peak in the fibre intensity transmission response. Outwith the phase-matching situation the fibre displays "cut-off" behaviour, resulting in a periodic bandpass filter response function. A much more detailed theoretical investigation of the cutoff fibre-overlay device is required to properly explain the operation of the device and should be part of any future work on the device structure. Based on the description given above, the resonance positions can be obtained from the eigenvalue equation (eqn. (1.1)) of the overlay waveguide. Inspection of eqn. (1.1) indicates that the thickness of the overlay waveguide (for a fixed material index) has a significant bearing on both the position of the transmission channels and also on the channel spacing (difference between adjacent resonance wavelengths). Thus, careful control of this parameter during device manufacture allows tailoring of the transmission response to produce channels at favourable wavelengths while also producing an appropriate channel spacing.

7.5 Solid-State Overlay Cut-Off Device

To further study the device structure, a solid-state device was fabricated. The device incorporated Lithium Niobate ($LiNbO_3$) as the overlay waveguide due to its high material index (n = 2.15) and potential for electro-optic applications. The device was fabricated using the standard procedures and the eventual $LiNbO_3$ thickness was approximately 7μm (giving a compound overlay composed of 2-3μm glue (n=1.5) and 7μm $LiNbO_3$). The wavelength response was then obtained and is shown in Figure 7.6 for both TE and TM polarisations. Channel spacing increases from 83nm to 113nm for TE polarisation while the corresponding TM polarisation values are 81nm and 107nm, respectively. This increase is expected from simple analysis of

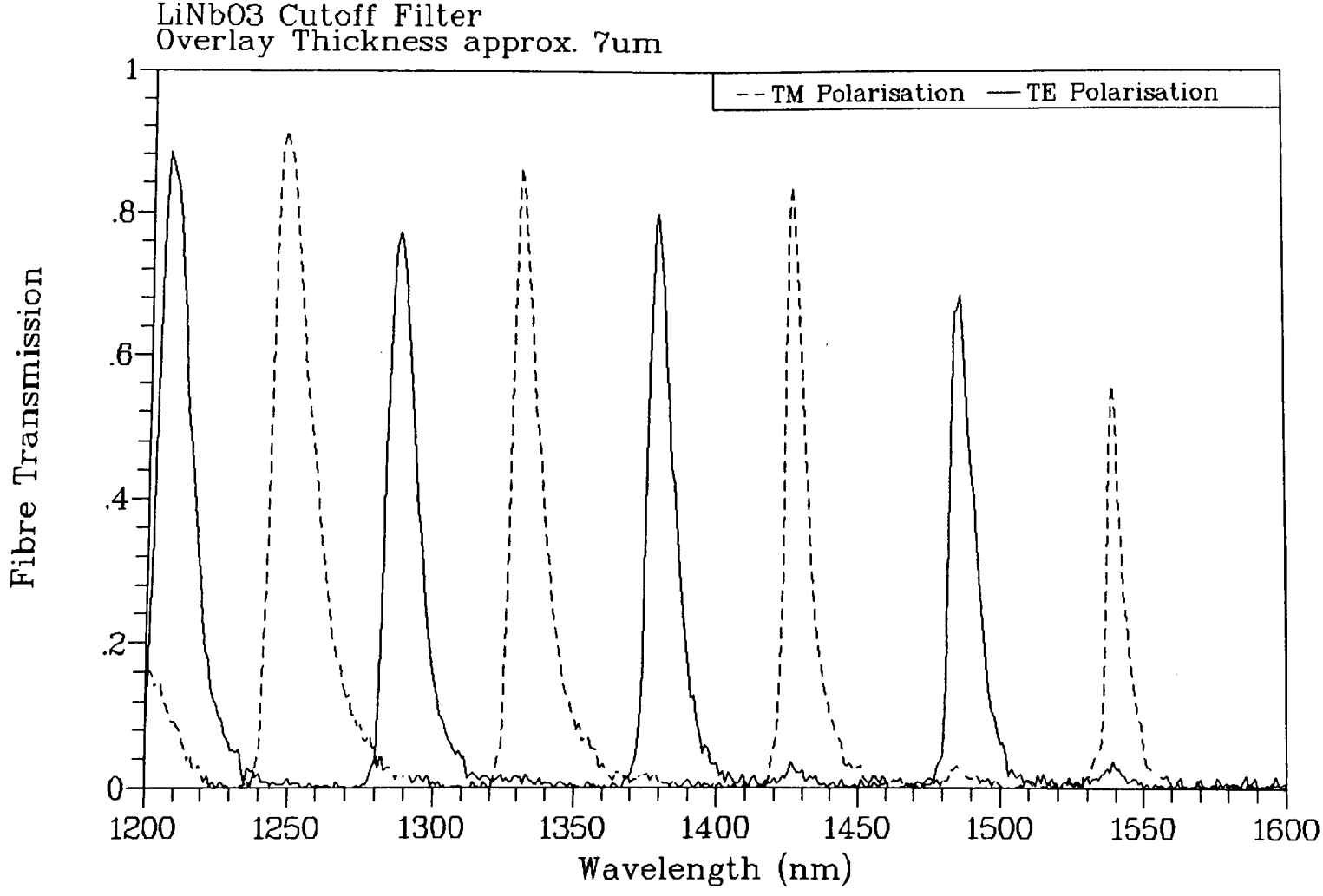

Figure 7.6 : Wavelength Response of Solid-State Cutoff Device

eqn. (1.1). The large polarisation sensitivity (41nm minimum separation for TE and TM channels) of the device is expected for a highly birefringent material such as $LiNbO_3$ (n_{TM}=2.15, n_{TE}=2.22). Extinction ratios (rejection) are around 20dB for both polarisations. The narrowest linewidth values were 8nm and 9.6nm for TE and TM polarisation, respectively, at the high wavelength section of Figure 7.6, although the loss on these channels was higher. The $LiNbO_3$ overlay device possessed an insertion loss range 0.5-2.5dB, depending on wavelength and polarisation. TM polarisation resulted in higher insertion loss which may be due to a larger evanescent tail. The optical quality of the overlay surface is believed to have a major effect on the device insertion loss since application of a bulk index oil to the top surface of the overlay reduced the insertion loss. This indicated that the polished top surface of the $LiNbO_3$ overlay was damaged and caused scattering loss and suggests insertion loss can be reduced by improved fabrication. Further experimental and theoretical investigation of the factors affecting insertion loss should also be part of future work.

7.5.1 Tuning of Channel Positions

Obviously, tuning of the wavelength response of the device is highly desirable, particularly for application in fibre laser systems. Incorporating electrodes into the device structure would, ideally, allow electro-optic tuning of the transmission channel locations by direct modulation of the overlay material index. However, the tuning range would be limited to a few nanometres either side of the passband centre wavelength depending on overlay thickness and the fixed value of electro-optic coefficient possessed by $LiNbO_3$. As discussed earlier in Chapter 6, this method of modulating/tuning the device response requires the development of materials with stronger electro-optic effects to allow practical realisation. However, the same methods of passive tuning described in Chapter 6 for standard polished fibre-overlay devices apply i.e. varying the overlay superstrate index and/or thickness. Two of the channel passbands (TM 1485nm and TE 1539nm) displayed by the $LiNbO_3$ cutoff device are of particular interest from a tuning viewpoint since they are located close to the gain region of an erbium-doped fibre laser system (approx. 1520-1560nm). For this reason, the tuning experiments were concentrated on these two wavelength

channels. A range of bulk index oils were used to form the overlay superstrate and the shifted resonance (channel) position recorded. Figure 7.7 shows the resulting tuning curves for each polarisation. The maximum tuning range was 45nm for TM polarisation and 19.5nm for TE polarisation. Thus, the TE polarisation passband located at a wavelength of 1539nm could be tuned across an appreciable section of the gain region in the fibre laser system mentioned above. It has been shown for standard fibre-overlay devices that the tuning range is highly dependent on the overlay material index and thickness. By producing a similar device with a different overlay index or thickness, the tuning range of an appropriately located channel could be extended to cover the entire gain region of the fibre laser. For example, an overlay of index 1.55 and thickness 3μm would result in a tuning range of >200nm.

7.6 Practical Application of Cut-Off Filter

To investigate the practical applications of the device described in the preceding paragraphs, it was incorporated in an experimental erbium-doped fibre laser system constructed by Physics Department at the University of Strathclyde. Figure 7.8 shows a diagram of the fibre laser system with the cut-off filter incorporated as an intra-cavity element.

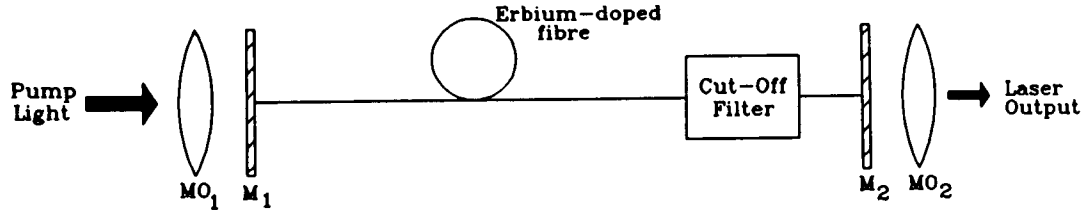

Figure 7.8 : Schematic of fibre laser system with cut-off filter incorporated

The pump source was a semiconductor diode laser operating at 1480nm. MO_1 and MO_2 are microscope objectives while M_1 and M_2 are high reflectivity mirrors. Since the gain of the system was greater than the nett cavity loss (3.5dB), including the insertion loss of the device (1.7dB), lasing was still possible with the device acting

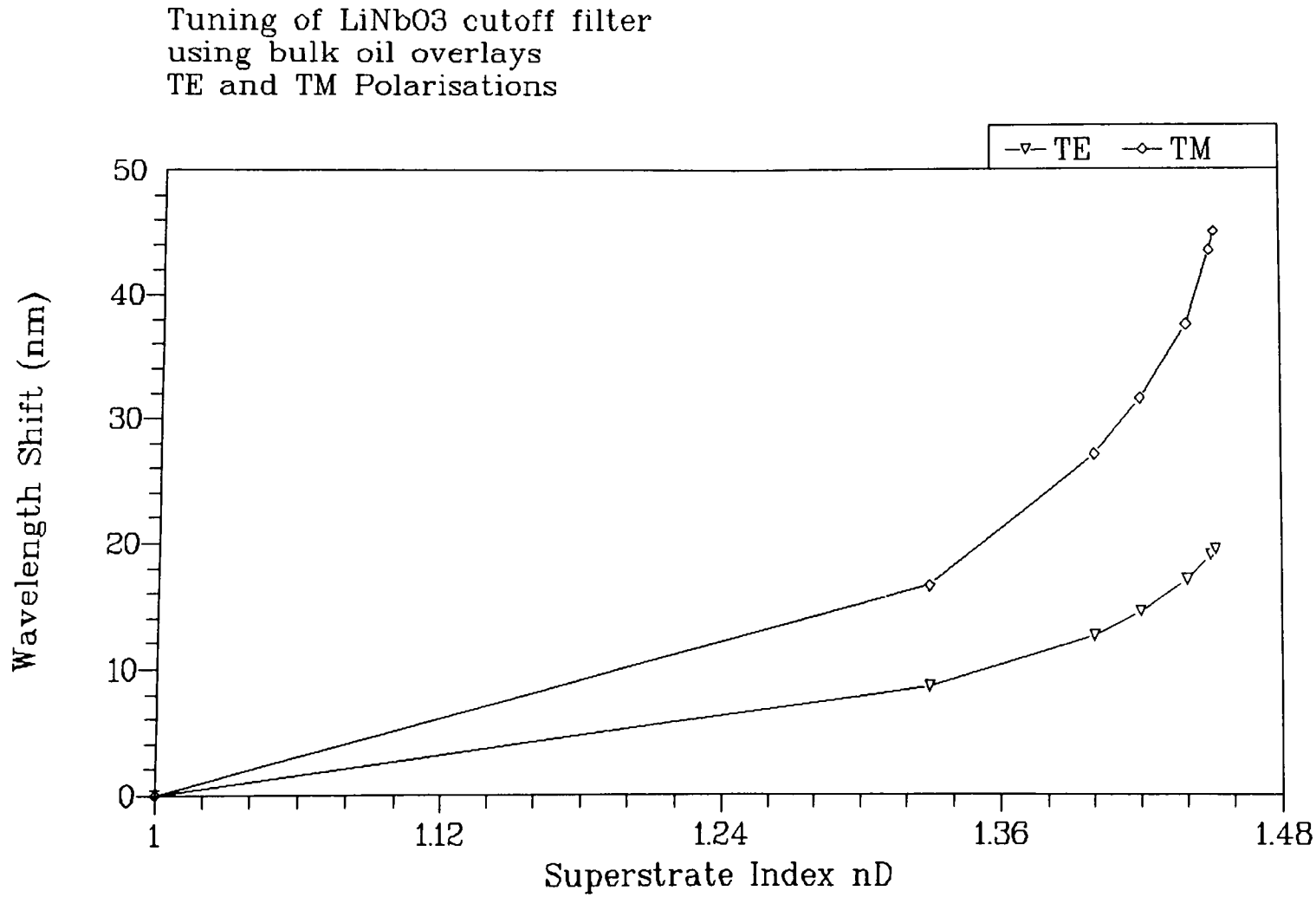

Figure 7.7 : Superstrate Tuning of Filter PassBand

as an intra-cavity element. A significant narrowing of the laser linewidth was observed when compared with the output in the absence of the filter. Figures 7.9a and 7.9b illustrate the effect of introducing the polished fibre cutoff filter into the laser cavity. The linewidth in Figure 7.9b is limited by the resolution (0.5nm) of the monochromator used to record the wavelength response of the fibre laser. Subsequent measurements have indicated that the linewidth (FWHM) is in the region of 0.03nm which is comparable with DFB laser performance. This significant narrowing is due to the multiple-pass nature of the laser system. Application of bulk oils as the overlay index allowed tuning of the centre wavelength of the fibre laser as expected, the maximum tuning range being 19.5nm for TE polarisation.

7.7 Conclusions

A highly desirable bandpass filtering function has been demonstrated using a novel "cut-off" polished fibre-overlay device. The device operation appears related to that of a standard polished fibre-overlay device in that the filtering function depends on the behaviour of the overlay waveguide mode structure. Initial experimental investigation concentrated on oil overlay devices in order to establish trends in device behaviour with regard to overlay index and thickness. Resonance (or channel) spacing was seen to range from 45nm for a high index (n_D=1.698), thick (23μm) overlay to 256nm for a low index (n_D=1.494), thinner (12μm) overlay. The corresponding resonance linewidths were 5.2nm and 110.6nm. Outwith the bandpass regions, the device throughput was reduced by about 20dB. A solid-state $LiNbO_3$ overlay device was also successfully fabricated and displayed a similar filtering response to the oil overlay devices but also a significant polarisation sensitivity. Best resonance linewidths of 8nm and 9.6nm, for TE and TM polarisations respectively. Narrowest channel spacing was 81nm for TM polarisation while the minimum polarisation channel separation was 41nm. On-resonance insertion loss was in the region of 1.7dB although measurements made for the oil overlay devices indicated insertion loss could be less than 0.5dB. Substantial tuning of the device wavelength-transmission channel positions could be achieved by application of bulk index oils

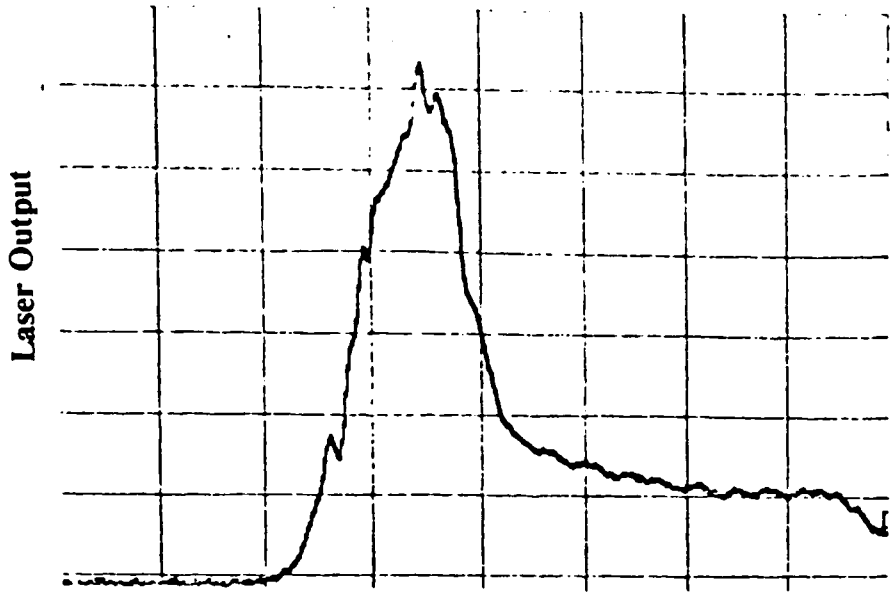

(a) Output of Laser with no intra-cavity elements

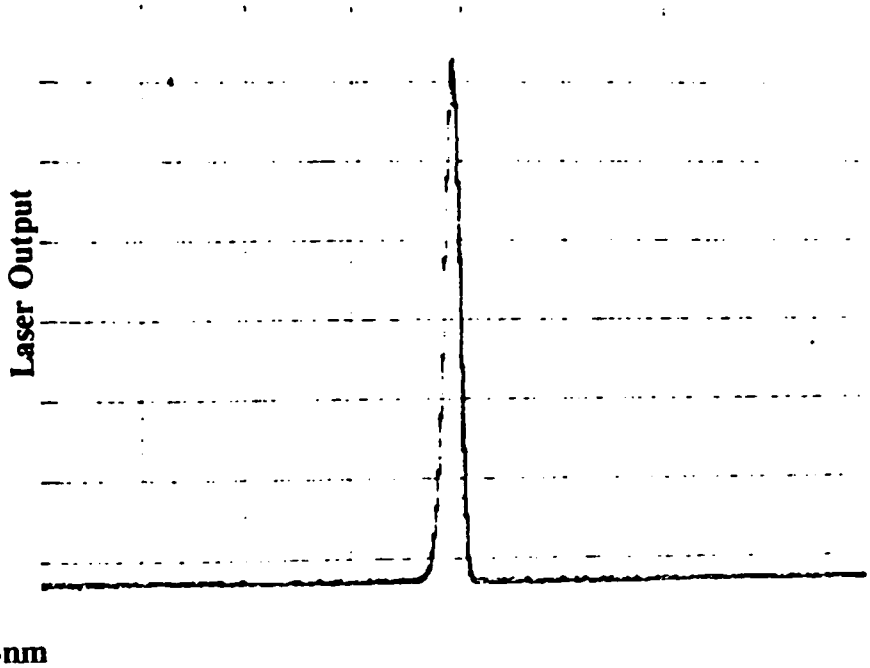

(b) Output of Laser with cut-off filter in cavity

Figure 7.9 : Effect of $LiNbO_3$ Cut-Off Filter on Fibre Laser Output

to form the overlay waveguide superstrate. A maximum range of 45nm was observed for TM polarisation while the corresponding TE polarisation range was 19.5nm. The solid-state device was incorporated in an erbium-doped fibre laser system with impressive results. A significant narrowing of the laser linewidth was observed (<0.03nm) while tuning over a maximum range of 19.5nm was possible (corresponding to TE polarisation). Employing electro-optic Liquid Crystals as the bulk superstrate would provide the means of an actively tuned fibre laser system.

References

1. J. R. Feth and C. L. Chang,"Metal-clad fiber-optic cutoff polarizer", Opt. Lett., **11**, pp386-388, 1986.

2. M.J.F. Digonnet, J.R. Feth, L.F. Stokes and H.J. Shaw,"Measurement of the core proximity in polished fiber substrates and couplers", Opt. Lett., **10**, pp463-465, 1985.

3. W. Johnstone, G. Thursby, D. Moodie, R. Varshney and B. Culshaw,"Fiber optic channel selector with high-resolution", Electron. Lett., **28**, pp1364-1365, 1992.

CHAPTER 8

Discussion and Conclusions

8.1 General Discussion

An extensive investigation of devices based on the interaction of a single-mode fibre, side-polished close to the core, and a high index planar multimode overlay has been undertaken. A range of different coupling strength and, therefore, remaining cladding thickness, polished fibre half-blocks were prepared using the standard lapping and polishing techniques outlined in Chapter 4. Two different fibre radii of curvature were also used to determine the importance of this parameter. Initial experimental devices incorporated oils of specified refractive index supported by plastic spacers as the overlay waveguide thus allowing repeated use of several polished fibre half-blocks. The majority of experimental results were obtained by recording the response of the fibre intensity transmission to variation of the device input wavelength (generally over the range 1200nm-1600nm). Typical wavelength responses yielded periodic-like resonance minima in the transmitted intensity (dropped or filtered channels). This provided a substantial amount of information on trends and patterns in device operation with regard to the fundamental overlay parameters (refractive index and thickness) and also half-block coupling strength. The coupling strength of the half-blocks was quickly identified as an important device design parameter with respect to channel (filter) linewidth and insertion loss whereas the fibre radii of curvature was found to be a less critical factor. Channel linewidth and spacing both reduced with increasing overlay refractive index and thickness (increasing waveguide mode order) while device insertion loss was seen to reduce. Dropped channel linewidth (FWHM) values ranged from 3nm to 205nm while channel spacing varied between 43nm and 284nm. These experimental results showed close agreement with predicted theoretical trends. The modulation depth or rejection ratio of the dropped (filtered) channel was also an important performance

parameter, particularly when considering the filtering capability of the device. For all the oil overlay devices, values of modulation depth were greater than 65% but no simple trend was observed for variation of overlay index or thickness. However, higher coupling strength half-blocks tended to produce greater modulation depths, consistently greater than 90% for devices with 12μm overlay thickness. Additionally, the larger radius of curvature half-blocks also resulted in devices which exhibited larger modulation depths (rejection ratios).

After establishing the fundamental principles of operation using oil overlay devices, further characterisation was performed on solid-state overlay devices. Initial experimental investigation concentrated on devices possessing overlays constructed from optical quality glass. Device fabrication involved the bonding of glass wafers to the surface of the polished fibre half-blocks followed by standard lapping and polishing techniques to produce the required overlay thickness. Again, variation of the input wavelength was the most practical method of device characterisation and similar wavelength versus fibre transmission responses to those of the oil overlay devices were obtained. Narrowest channel linewidth (2.4nm) was recorded for a 90μm thick glass overlay with a refractive index of 1.65. The corresponding channel spacing was 12.5nm although modulation depth was only 77%. An advantage of the glass overlay devices was the possibility of tuning the wavelength response by variation of the overlay superstrate (which was not possible with the oil devices). This was accomplished by either application of an index oil in bulk form or vacuum deposition of a thin film of appropriate refractive index. Extensive tuning ranges ($>$100nm), particularly for the low index glass overlay devices, were achieved which agreed well with theoretical calculations. In addition to characterisation of the basic fibre-overlay geometry, a switch structure (bandpass filter) was investigated in which a second polished fibre half-block was appropriately aligned on the top surface of the glass overlay. Significant cross-coupling of power at specific wavelengths was observed when the wavelength transmission response of the device was recorded. This demonstrated the feasibility of the device structure for operation as a directional coupler or bandpass filter (considering the transmission of the second fibre).

Tunability of this device structure was, however, less impressive and difficult to accurately control.

Fabrication of devices employing glass overlay waveguides served two purposes. Firstly, the viability of the basic device structure as a tunable wavelength selective element was demonstrated. Furthermore, the use of fairly inexpensive glass overlays allowed extensive investigation of the fabrication procedures involved in production of solid-state overlay devices. Factors such as choice of bonding agent, lateral dimensions of overlay waveguide for optimum device yield, thickness and parallelism of glue layer, and optical quality of overlay top surface were examined with regard to eventual device performance. This permitted the identification of the difficult and critical stages in the device fabrication.

The experience and expertise gained in the manufacture of glass overlay devices was then applied to the fabrication of solid-state devices incorporating $LiNbO_3$ overlays, (a much more expensive material). Interest in using $LiNbO_3$ in the role of the overlay stemmed from the relatively high linear electro-optic coefficient it possesses. This provided the possibility of realising an active component by varying the refractive index of the overlay waveguide, and thus wavelength-transmission response, via an appropriate control voltage. Initially, passive devices, which possessed no electrodes, were fabricated to investigate the behaviour of $LiNbO_3$ overlay devices in terms of linewidth, channel spacing, insertion loss, tunability, etc. From these values, predictions on active device performance could be made with the device structure configured as an intensity modulator and directional switch (this assumes biasing of the wavelength-transmission response to, and then operation about, a specific wavelength). Fabrication procedures were similar to those utilized for manufacture of the glass overlay devices although device yield was reduced due to a greater tendency of the $LiNbO_3$ to shatter during the lapping and polishing stages. However, narrow values of linewidth (3nm) were observed for passive $LiNbO_3$ overlay devices which, in turn, produced encouraging performance predictions for active devices in which a similar wavelength-transmission response

was assumed. Tuning of the channel positions was achieved by application of bulk index oils as the superstrate although tuning ranges were reduced when compared with those observed for glass overlay devices. Realisation of active devices utilizing $LiNbO_3$ overlays required that an appropriate electrode structure was included in the device architecture. Since the initial $LiNbO_3$ wafer was in a z-cut orientation, maximum index variation via the electro-optic effect could be achieved through the use of transverse electrodes i.e electrodes sandwiching the $LiNbO_3$ waveguide. With this configuration, the electrodes must be optically transparent since they then form part of a compound overlay waveguide. The most widely used optically transparent conductor is Indium-Tin-Oxide (ITO) and this was deposited by rf magnetron sputtering. The use of ITO electrodes which possessed relatively high resistance immediately compromised the frequency response of the subsequent active devices. However, the maximum electric field utilization provided by the transverse electrode configuration allowed a d.c. demonstration of device operation, which was the principal aim.

Unfortunately, a number of factors combined to push drive voltages up to several hundred volts. These factors included (1) an inability to successfully fabricate active devices with an overlay thickness of $< 15\mu m$ (2) a glue layer in the range 1-3μm and (3) broader resonance linewidth values than were expected for given overlay thicknesses. Since the electro-optic effect is a field-induced effect, it is obvious that the closer the electrodes the lower the required drive voltage for a specified electric field strength. As such, the desired active device overlay should be as thin as possible. However, difficulties were encountered when the fabrication of very thin overlays was attempted and no such device was successfully produced. This situation, therefore, put a limit on the lowest drive voltage required for active device operation. In addition, the voltage dropped across the glue layer was related to the dielectric constant of the glue as well as its thickness and was calculated to be a substantial fraction of the total applied voltage. This fraction was found to increase as the $LiNbO_3$ layer was reduced. Thus, elevated drive voltages were required to ensure a significant electric field strength within the $LiNbO_3$ layer and cause a

detectable shift in the wavelength-transmission response of the device. The third factor mentioned above, broadened resonance linewidths, was due to the increasing influence of waveguide nonparallelism as the overlay thickness is reduced. A wedged overlay results in a wider resonance response because the phase-matching condition is less clearly defined. This effect is enhanced when the overlay thickness is decreased. Subsequent drive voltages required to cause an on/off switching or modulation function were correspondingly higher. It was decided that the use of co-planar electrodes may overcome several of the drawbacks encountered with the use of transverse ITO electrodes and allow an improvement in active device performance. However, the feasibility of active components based on the device structure investigated in this thesis was demonstrated.

Alternative methods of overlay fabrication were also investigated, primarily vacuum deposition. The use of vacuum-deposited films as the overlay waveguide was immediately attractive since it removed several of the fabrication difficulties experienced with lapping/polishing techniques. There was no longer a requirement for an optically-transparent bonding layer, followed by laborious, wasteful, material removal to obtain the desired overlay thickness. Furthermore, in-situ monitoring of resonance positions provides a simple method of fabricating devices to given specifications, thus demonstrating an increased flexibility of this fabrication technique over those described earlier. Both thermal evaporation and rf magnetron sputtering were successfully used to produce overlay waveguides ranging from 0.5-3μm in thickness. Fairly narrow linewidth (6.6nm) channel-dropping filters and also a switch/bandpass filter device were fabricated and assessed. A result of the reduced overlay thickness (when compared with polished overlays) was substantial channel spacing ($>$300nm) while the extensive tuning range (maximum observed shift was 216nm for TM polarisation) of the channel-dropping filters identified as a very useful device characteristic. In general, the vacuum-deposited methods of overlay fabrication displayed great potential for repeatable, rapid, simple device manufacture.

A slight alteration of the basic polished fibre half-block geometry allowed the

realisation of devices which displayed a bandpass filter response without a requirement for a second fibre to access the filtered channel. By continuing the polishing stage of the half-block fabrication process, the core of the fibre was exposed and the fibre transmission greatly attenuated i.e. the fibre was then termed cut-off. It was found that placing an overlay waveguide in contact with the cutoff region of the fibre allowed wavelength-selective restoration of the transmitted intensity i.e. transmission resonances were observed. Both oil and solid-state overlays were formed on the cut-off fibre half-block and similar trends in wavelength response, in terms of resonance linewidth and spacing response to overlay parameter variation, to standard fibre-overlay devices were observed. Passband channel linewidths as narrow as 5.2nm were recorded while channel spacing ranged from 45nm to 256nm, for oil overlay devices. On-resonance insertion loss was not fully investigated but a best value of <0.5dB was observed. A $LiNbO_3$ overlay device was fabricated which allowed investigation of tuning of passband channel positions via bulk superstrate index variation. A maximum tuning range of 45nm was achieved for TM polarisation while the corresponding TE polarisation value was 19.5nm.

8.2 Conclusions

The research programme has resulted in the development of a number of potentially useful in-line fibre-optic device structures. The results presented in Chapters 5, 6 and 7 for the various device configurations suggest that the basic device structure can have a number of optical systems applications including: Wavelength Division Multi/Demultiplexing (channel-drop and bandpass filters), signal routing, and in-line modulation of semiconductor lasers. Several fabrication techniques (lapping/polishing, evaporation, sputtering) and materials (optical glass, $LiNbO_3$, ZnS, Si) have been shown to be compatible with the device architecture which allowed the realisation of various rugged, low insertion loss, passive and active components. The main thrust of the research programme was the investigation of the wavelength response of the basic device architecture. This involved the design, fabrication and assessment of a range of passive devices with varying overlay

thicknesses (0.5-35μm) and refractive indices (1.47-3.5).

8.2.1 Channel-Dropping Wavelength Selective Elements

The single polished fibre half-block passive components primarily display a bandstop or channel-dropping, almost periodic, filter wavelength response. A large number of these devices were fabricated and assessed during the course of the research project. A range of materials were used to form the overlay waveguide: index oils, three optical glasses, Lithium Niobate ($LiNbO_3$), Zinc Sulphide (ZnS) and Silicon. Channel linewidth was seen to range from as low as 2.4nm (glass overlay device) to as high as 100nm (low index oil overlay device) while channel spacing typically ranged from 10-200nm. Insertion loss is generally in the region of 0.1-0.5dB. The channel-dropping filters are the simplest device configuration to fabricate, are compatible with existing optical fibre systems and exhibit high mechanical stability. Relatively simple thin-film fabrication procedures such as evaporation and rf sputtering can be used to reduce device manufacture time. These devices have particular application in WDM systems where the dropped channel can be accessed from the overlay waveguide by a prism-coupling arrangement or a second fibre. Alternatively, the detector could be interfaced directly to the overlay to increase the compactness of the component. Precise control of the overlay waveguide thickness via in-situ monitoring (thin-film deposition techniques) or careful material removal (overlay fabrication by polishing) allows selection of the dropped-channel wavelength. Thus, devices can be manufactured to desired specifications in terms of wavelength response.

Extensive tuning ($>$200nm) of the wavelength-transmission response of the single half-block devices can be achieved by variation of the superstrate refractive index, particularly when the overlay waveguide is of low index (e.g $n=1.5$) and made thin (e.g. $d=1.5\mu$m). Electro-optic tuning of the dropped-channels was possible (variation of overlay material index) although the small wavelength shifts achieved for devices incorporating $LiNbO_3$ overlays required unrealistic drive voltages (150V/nm). However, the use of Barium Strontium Niobate ($r=1090$pm/V)[1] as the overlay

material would result in much reduced drive voltages (5V/nm). Furthermore, the choice of material for use as the overlay is not limited by the necessity for a refractive index similar to that of the fibre. Thus, a variety of material types ranging from polymers to exotic electro-optic crystals can be accessed, provided they can be arranged in thin-film form.

8.2.2 Switch/Modulator Structures

In addition to investigating the basic device structure as a wavelength selective element, switches (active and passive) and electro-optically activated in-line modulators utilizing the same fundamental device geometry were studied. The passive switch structure can operate as a fixed wavelength routing element or be considered as a bandpass wavelength filter capable of performing a demultiplexing function, in terms of the coupled arm response. Passive switch structures were successfully fabricated using oils, optical glass, $LiNbO_3$ and ZnS as the overlay (interlay) waveguide. The highest observed cross-coupling efficiency was approximately 90% for a $LiNbO_3$ device. Off-resonance cross-talk in the coupled arm was -18dB while an extinction of -15dB was observed in the input arm at the centre switching (resonance) wavelength. Narrowest linewidth for the cross-coupled (bandpass) channel was 3.8nm while the corresponding dropped-channel linewidth 12.5nm (input fibre response). Again, the wavelength response of the structure was tunable by varying the index-matching oil at the interface of the overlay and second half-block, although the range and ease was reduced when compared with single half-block channel-dropping WSEs. The bandpass filter response is of particular interest for broadcast-and-select style WDM architectures.

Material shortcomings and severe fabrication requirements prevented the realisation of a low voltage, high performance modulator or switch. Drive voltages of approx. 350V were required to induce an on/off ratio of 4.7dB in the cross-coupled arm for a corresponding on/off ratio of 4dB in the transmission arm. The major problems have arisen from the necessity for thin overlay waveguides to allow low drive voltages. Difficulties with adhesion and the mechanical integrity of the $LiNbO_3$

overlay combined to make device fabrication a hazardous undertaking and severely restricted the practical device performance. The $LiNbO_3$ overlay based switch can only be viewed as a demonstration of the feasibility of the device geometry. However, new bulk electro-optic materials and the possibility of vacuum deposition of thin optical quality films possessing high electro-optic coefficients removes several of the inherent fabrication difficulties associated with the active devices based on $LiNbO_3$ and promises low voltage operation. Calculations based on other bulk electro-optic materials (BSN r=1090pm/V) or vacuum deposited PLZT (r=80pm/V)[2] indicate that switching voltages in the region of 10V are achievable for extinction ratios around 20dB (based on passive device responses) without modification of the device geometry. These reduced voltage devices would retain the low insertion loss and compatibility with fibre systems which the devices investigated earlier have shown. Alternative methods of thin film deposition such as sol-gel processing[3] and spin-coating using organic materials[4][5] have also recently been used to produce thin films with high electro-optic coefficients and have the advantage of superior film quality. Similar reductions in drive voltage can be expected for devices based on these materials with the added advantages of simpler, faster fabrication techniques. The frequency response limitations of the switch/modulator devices, imposed by the use of ITO electrodes, can be improved by appropriate design of a coplanar metal electrode structure. Immediate applications of the modulator devices include external modulation of semiconductor diode lasers to avoid the problems/limitations associated with injection-current modulated methods and also active mode-locking of fibre lasers. Alternatively, the switch structure provides the possibility of active routing of optical signals.

8.2.3 Cut-Off Device Structure

The cut-off polished fibre half-block device (Chapter 7), which combines the bandpass filter function of the switch structure with the extensive tuning capability of the single half-block device geometry, shows much potential for application as a broadly tunable bandpass filter. Both oil and solid-state overlay ($LiNbO_3$) devices were fabricated and have shown the possibility of narrow linewidth (5nm), variable

channel spacing (10-200nm, typically) and low passband insertion loss (<0.5dB), while a useful tuning range, 45nm, has also been demonstrated by variation of the overlay superstrate index. Further applications for this device include the suppression of fluorescence in fibre amplifier systems or as a low-loss intra-cavity filter in fibre laser systems. Indeed, introducing the $LiNbO_3$ overlay cut-off filter, described in Chapter 7, into the cavity of a an erbium-doped fibre laser system resulted in a significant narrowing of the laser linewidth to <0.03nm and also allowed tuning of the lasing wavelength over a substantial portion of the laser gain spectrum.

8.3 Future Work

Future work on the device structures described in this thesis should be directed primarily at the design and manufacture of active components, with particular emphasis on the cut-off device structure. A number of previously unavailable highly electro-optic crystals are now becoming commercially accessible and may possibly be used as a direct replacement for $LiNbO_3$ in the role of the overlay waveguide. Alternatively, the use of thin-film deposition techniques has been identified as particularly suitable for overlay waveguide fabrication since it removes several laborious and time-consuming fabrication stages and provides a more clearly defined overlay. In addition, recent progress in active film deposition has been encouraging and the possibility of high electro-optic coefficients in conjunction with thin overlays promises low drive voltage, low insertion loss, mechanically stable, active devices. Therefore, in the longer term it would appear that thin-film deposition methods may be the key to successfully manufacturing low drive voltage, practical fibre-overlay devices. Consequently, investigation and optimisation of these methods, sol-gel processing in particular, should be one of the principal aims of future projects in this area of research.

References

1. A. Yariv, *Optical Electronics*, Holt-Saunders, 3rd Ed., 1985.

2. H. Adachi and K. Wasa,"Sputtering preparation of ferroelectric PLZT thin films and their optical applications", IEEE Trans. Ultrason., Ferroelec. and Freq. Contr., **38**, pp645-655, 1991.

3. J.R. Busch, S.D. Ramamurthi, S.L. Swartz and V.E. Wood,"Linear electrooptic response in sol-gel PZT planar waveguides", Electron. Lett., **28**, pp1591-1592, 1992.

4. M. Wilkinson, J.R. Hill and S.A. Cassidy,"Optical fiber modulator using electrooptic polymer overlay", Electon. Lett., **27**, pp979-981, 1991.

5. G. Fawcett, W. Johnstone, I. Andonovic, D.J. Bone, T.G. Harvey, N. Carter and T.G. Ryan,"In-line fiberoptic intensity modulator using electrooptic polymer", Electron. Lett., **28**, pp985-986, 1992.

Publications

A number of publications have resulted from the work presented in this thesis and are listed below:

Assessed Journals

K. McCallion, W. Johnstone and G. Thursby, "Investigation of an optical fibre switch using electro-optic interlays", Electron. Lett., **28**, pp410-411, 1992.

W. Johnstone, G. Thursby, D.G. Moodie and K. McCallion, "Fibre optic refractometer utilising multimode waveguide overlay devices", Opt. lett., **17**, pp1538-1540, 1992.

Conference Papers

W. Johnstone, G. Thursby, M. Gill, A. McDonach, S. Murray, D. Moodie, K. McCallion, G. Fawcett and B. Culshaw, "A multimode waveguide overlay approach to fibre optic sensors and components", Int. Congress on Optical Science and Engineering, Holland, March 1991.

K. McCallion and W. Johnstone, "An optical fibre switch using electro-optic interlays", SPIE Symposium OE/Fibres '91, Boston USA, 1991, SPIE Proc., **1580**, paper no. 27.

W. Johnstone, R. Varshney, D. Moodie, K. McCallion and B. Culshaw, "Wavelength selective optical fibre components using multimode waveguide overlays", SPIE Symposium OE/Fibres '91, Boston 1991, SPIE Proc. **1580**, paper no. 21.

G. Thursby, W. Johnstone, K. McCallion, D. Moodie and B. Culshaw, "A novel fibre optic refractive index sensor using resonance shift phenomena", OSA

Conference on "Optical Fibre Sensors", Monterey, California, USA, Jan. 1992.

W. Johnstone, G. Thursby, D. Moodie, K. McCallion, R. Varshney and B. Culshaw, "Fibre optic wavelength selective components using multimode waveguide overlays", OSA Conference on "Optical Communications", San Jose, California, USA, Feb. 1992.

W. Johnstone, D.G. Moodie, K. McCallion, G. Fawcett and G. Thursby, "Rugged tunable fibre optic wavelength selective elements with high resolution", Proc. of the "4th Bangor Communications Symposium", p12, 1992.

W. Johnstone, K. McCallion, D.G. Moodie, G. Fawcett and G. Thursby, "Active fibre optic components using solid state waveguide overlays", IOP Conference on "Applied Optics and Optoelectronics", Session Oe2, paper 4, 1992.

W. Johnstone, D.G. Moodie, G. Thursby, K. McCallion and G. Fawcett, "Tunable high resolution WDMs using the high index overlay approach", SPIE Proc., **1792**, paper no.12, 1992.

D.G. Moodie, W. Johnstone, G. Thursby and K. McCallion, "Refractive index sensors based on coupling to high index multimode overlays", SPIE Proc., **1796**, paper no. 7, 1992.

Submitted Articles (journals)

K. McCallion, W. Johnstone and G. Fawcett, "A tunable in-line fibre optic bandpass filter", Opt. Lett., 1993.

Filed Patent

W. Johnstone, K. McCallion and G. Fawcett, **Rugged Tunable All Fibre Laser**, Application No. 9313915, 6th July, 1993.